Investigation of MYC-driven Group 3 medulloblastoma using novel regulable cell based models

Shanel Jade Swartz

Thesis submitted in partial fulfilment of the requirements

for the degree of Doctor of Philosophy

Newcastle University

Faculty of Medical Sciences

Northern Institute for Cancer Research

December 2017

Declaration

I certify that no part of the material documented in this thesis has previously been submitted for a degree or other qualification in this or any other university. I declare that this thesis represents my own unaided work, carried out by myself, except where it is acknowledged otherwise in the thesis text.

Shanel Jade Swartz

December 2017

Acknowledgments

I would like to thank God for giving me the wisdom, patience and strength to achieve my goals. Also for placing the correct people in my life during this season, because each person's contribution has moulded me into a better scientist.

My sincerest thanks to my supervisors, Professor Steven Clifford and Professor Simon Bailey. Thank you for giving me the opportunity to do research in the field of medulloblastoma and for your continuous support and guidance throughout this project.

My deepest appreciation is extended to Dr Janet Lindsey. I would never have been able to achieve what I have without your wisdom, support and guidance. Thank you for going the extra mile beyond your duties and for comforting me during the difficult seasons of my studies. Thank you for believing in me.

I would like to thank my assessors Professor John Lunec and Professor Christine Harrison for their guidance and encouragement throughout my research.

I would like to thank Dr Daniel Williamson, Dr Matthew Selby and Dr Martina Finetti for your tremendous help, guidance and support.

Thank you to the Paediatric Brain Tumour research group and Leukaemia and Lymphoma research group for your support and encouragement.

I would like to thank EU-Saturn and Newcastle University whose financial support made this project possible.

Finally, I would like to thank my family and friends who encouraged and believed in me.

Abstract

Introduction: Medulloblastoma (MB) is the most common malignant brain tumour to occur in children, accounts for 10% deaths in children and has four distinct molecular subgroups. These subgroups are known as MB_{WNT}, MB_{SHH}, MB_{GRP3}, MB_{GRP4}. Patients with MB_{GRP3} have the worst outcome with an overall survival of ~ 50%. MB_{GRP3} patients commonly present with metastatic disease, large cell/anaplastic (LCA) histology and/or high *MYC* expression or gene amplification. MYC amplification is the strongest adverse prognostic factor, however MYC-dependent biology within MB_{GRP3} tumours remains poorly understood.

Method: Doxycycline (DOX)-inducible MYC silencing isogenic models (D425Med and HDMB03, two *MYC* amplified MB_{GRP3} cell lines) were generated and used to characterize MYC-dependent phenotypic changes by measurement of parameters including: cellular proliferation, cell cycle and induction of apoptosis. mRNAseq analysis was performed in these isogenic models to investigate the effect of MYC modulation on the transcriptional profile and to identify key downstream pathways which may highlight suitable therapeutic approaches.

Results: Silencing of MYC within D425Med resulted in a significant reduction in proliferation, G1 growth arrest and decreased apoptosis compared with controls. A less pronounced effect was seen in HDMB03. These results demonstrate that D425Med depends on and needs MYC for rapid proliferation. RNAseq analysis highlighted specific pathways and genes regulated by MYC and dysregulated in primary MB_{GRP3} such as the mTOR signalling pathway.

Conclusion: Transcriptome analysis in the DOX-inducible MYC silencing isogenic models identified key pathways and genes regulated by MYC and dysregulated in primary MB_{GRP3}. These pathways identified are those involved in cell cycle control, metabolism, differentiation and signalling pathways which could be therapeutically targeted.

List of Abbreviations

APC	Adenomatous polyposis
ATP	Adenosine triphosphate
BET	Bromodomain and extraterminal
BFB	Breakage-fusion-bridge
Bp	Base pair
CCNU	Lomustine
CDK	Cyclin dependent kinase
CGNP	Cerebellar granular neuron precursor
CMV	Cytomegalovirus
CNS	Central nervous system
CSF	Cerebrospinal fluid
CSRT	Craniospinal radiotherapy
CuO	Cumate operator
DMSO	Dimethyl sulfoxide
DNA	Deoxyribonucleic acid
DOX	Doxycycline
DSB	Double strand break
dsRNA	Double-Stranded RNA
E-box	Ehancer-box
ECL	Enhanced chemiluminescence
EFS	Event free survival
EGL	External granular layer
ERK	Extracellular receptor kinase
ES	Embryonic stem
EZH	Enhancer of Zest
FACS	Fluorescence-activated cell sorting
FBS	Fetal bovine serum
GFP	Green fluorescent protein
GSEA	Gene set enrichment analysis
GSK-3β	Glycogen synthase kinase

HART	Hyperfractionated accelerated radiotherapy
HAT	Histone acetyl transferase
HDAC	Histone deacetylase
HFRT	Hyperfractionated radiation therapy
HIV-1	Human immunodeficiency virus type 1
IPA	Ingenuity pathway analysis
IRES	Internal ribosomal entry sites
LB	Luria Bertani
LCA	Large cell anaplastic
LFS	Li-Fraumeni Syndrome
LTRs	Long terminal repeats
MB	Medulloblastoma
MBEN	Medulloblastoma with extensive nodularity
MB_{GRP3}	Medulloblastoma group 3
MB_{GRP4}	Medulloblastoma group 4
MB_{SHH}	Medulloblastoma SHH
MB_{WNT}	Medulloblastoma WNT
MCM	Minichromosome maintenance complex
Mins	Minutes
MOI	Multiplicity of infection
NS	Non-silencing
Nt	Nucleotide
ORC	Origin recognition complex
OS	Overall survival
P/C	Positive control
PACT	Protein (PKR)-activating protein
PBS	Phosphate buffered saline
PCA	Principal component analysis
PCR	Polymerase chain reaction
PFS	Progression free survival
PI	Propidium iodide

PI_3K	Phosphotidylinositol-3-OH kinase
PRC2	Polycomb repressive complex 2
pre-RC	Pre-replicative complex
PTCH 1	Patched 1
PVDF	Polyvinyl difluoride
RB	Retinoblastoma
RISC	RNA-induced silencing complex
RLU	Relative luminescence unti
RNA	ribonucleic acid
Rnase	Ribonuclease
ROS	Reactive oxygen species
RRE	Rev responsive element
RT	Room temperature
rtTA	Reverse transactivator
SDS	Sodium dodecyl sulfate
Ser62	Serine 62
SHH	Sonic hedgehog
shRNA	Short hairpin RNA
SIN	Self-inactivating
siRNA	Small interfering RNA
SMO	Smoothened
TBE	Tris/Borate/EDTA
TBST	Tris buffered saline
Tet	Tetracycline
TetR	Tet repressor
Thr58	Threonine 58
TRBP	TAR-RNA-binding protein
TRE	Tet responsive element
TRRAP	Transactivation transformation associated protein
Tta	Transactivator
UK	United Kingdom
VSV-G	Vesicular stomatitis virus-G

WNT	Wingless

Table of contents

DECLARATION ... I

ACKNOWLEDGMENTS ... II

ABSTRACT ... III

LIST OF ABBREVIATIONS ... IV

TABLE OF CONTENTS ... VII

LIST OF FIGURES ... XII

LIST OF TABLES ... XXVI

CHAPTER 1 INTRODUCTION ... 1

1.1 CANCER ... 2

1.1.1 Definition of cancer ... 2
1.1.2 Hallmarks of cancer ... 2
1.1.2.1 Sustaining proliferative signaling ... 3
1.1.2.2 Resisting cell death ... 3
1.1.2.3 Sustaining angiogenesis ... 4
1.1.2.4 Resisting growth suppressors ... 4
1.1.2.5 Activating invasion and metastasis ... 5
1.1.2.6 Enabling replicative mortality ... 5
1.1.3 Tumour suppressors and oncogenes ... 5

1.2. CANCER INCIDENCE AND MORTALITY IN THE UK ... 9

1.3 CHILDHOOD CANCER ... 10

1.3.1 Incidence and mortality of childhood cancer in United Kingdom ... 10

1.4 MEDULLOBLASTOMA ... 11

1.4.1 Histology of medulloblastoma ... 12
1.4.2 Risk stratification of medulloblastoma ... 13
1.4.3 Clinical presentation of medulloblastoma ... 16
1.4.4 Treatment of medulloblastoma ... 17
1.4.4.1 Surgery ... 17
1.4.4.2 Radiotherapy ... 17
1.4.4.3 Chemotherapy ... 18
1.4.4.4 Treatment for standard and high risk medulloblastoma patients ... 19
1.4.4.5 Treatment for infants and children less than 3 years of age ... 19
1.4.4.6 Treatment for relapse patients ... 19
1.4.5 Genetics aberrations of medulloblastoma ... 20
1.4.6 Advances in medulloblastoma genomics ... 22
1.4.7 Medulloblastoma subgroups ... 22

1.4.8 RECURRENT AND METASTATIC MEDULLOBLASTOMA 26
1.4.9 CHALLENGES OF GROUP 3 MEDULLOBLASTOMA 26
1.4.10 GENETIC ABERRATIONS IN GROUP 3 MEDULLOBLASTOMA 27
1.4.11 FUNCTION OF MYC IN GROUP 3 MEDULLOBLASTOMA 28

1.5 MYC 29

1.5.1 MYC AND ITS DEREGULATION IN CANCER 29
1.5.2 STRUCTURE OF MYC 31
1.5.3 TRANSCRIPTIONAL CONTROL BY MYC 32
1.5.4 MYC PROTEIN STABILITY 33
1.5.5 BIOLOGICAL FUNCTIONS OF MYC 33
1.5.5.1 ROLE OF MYC IN CELL CYCLE AND PROLIFERATION 33
1.5.5.2 ROLE OF MYC IN APOPTOSIS 34
1.5.5.3 ROLE OF MYC IN DIFFERENTIATION 34
1.5.5.4 GENOMIC INSTABILITY 35

1.6 THERAPEUTIC TARGETING IN CANCER 36

1.6.1 THERAPEUTIC OPTIONS FOR MYC DRIVEN CANCERS 36
1.6.2 THERAPEUTIC OPTIONS FOR GROUP 3 MEDULLOBLASTOMA 39

1.7 VIRAL VECTORS FOR GENE TRANSFER 39

1.7.1 INTRODUCTION TO LENTIVIRUS 40
1.7.2 INDUCIBLE LENTIVIRAL VECTORS 42
1.7.3 RNA INTERFERENCE 43

1.8 SUMMARY AND AIMS 44

CHAPTER 2 MATERIALS AND METHODS 47

2.1 CELL LINES 48

2.1.1 MAINTENANCE OF CELL LINES 48
2.1.2 CRYOPRESERVATION AND RECOVERY OF CELL LINES 49

2.2 PHENOTYPIC ASSAYS 49

2.2.1 PROLIFERATION ASSAY 49
2.2.2 CELL CYCLE ANALYSIS 50
2.2.3 APOPTOSIS 51

2. 3 MOLECULAR CLONING 52

2.3.1 PREPARATION OF PLASMIDS USED IN THIS STUDY 52
2.3.2 PREPARATION OF GLYCEROL STOCKS 53
2.3.3 PLASMID DNA EXTRACTION 54
2.3.4 TRANSFORMATION 54
2.3.5 SCREENING OF PLASMIDS AND POSITIVE CLONES 54
2.3.6 PRIMER DESIGN 55
2.3.6.1 PRIMER DESIGN FOR SEQUENCING 55
2.3.6.2 PRIMER DESIGN FOR DNA CLONING 55
2.3.7 SHORT HAIRPIN RNA DESIGN AND PREPARATION 56
2.3.8 POLYMERASE CHAIN REACTION 57

2.3.9 GEL ELECTROPHORESIS 58
2.3.10 POLYMERASE CHAIN REACTION PURIFICATION 58
2.3.11 GEL PURIFICATION 59
2.3.12 RESTRICTION ENZYME DIGEST 59
2.3.13 DNA LIGATION FOR MYC 60
2.3.14 LIGATION PROCEDURE FOR OLIGONUCLEOTIDES 60

2.4 LENTIVIRAL PROCEDURE 61

2.4.1 PACKAGING OF LENTIVIRUSES 61
2.4.2 LENTIVIRUS CONCENTRATION BY ULTRACENTRIFUGATION 61
2.4.3 PUROMYCIN KILL CURVE 62
2.4.4 TITERING OF LENTIVIRUS 62
2.4.4.1 TITERING METHOD FOR CUMATE VECTOR ONLY AND MYC/CUMATE CELLS 62
2.4.4.2 TITERING METHOD FOR THE PLKO-TET-ON SYSTEM 62
2.4.5 ANALYSING THE EFFECT OF DIFFERENT MULTIPLICITIES OF INFECTION 63
2.4.6 DETERMINING THE PERCENTAGE OF GFP POSITIVE CELLS BY FLOW CYTOMETRY ANALYSIS 63

2. 5 PROTEIN EXTRACTION AND QUANTIFICATION 63

2.6 SDS- PAGE AND WESTERN BLOT 64

2.7 NUCLEIC ACIDS 66

2.7.1 DNA AND RNA EXTRACTION 66
2.7.2 ASSESSING NUCLEI ACID CONCENTRATION AND QUALITY 66
2.7.3 CDNA SYNTHESIS 66

2.8 QUANTITATIVE REVERSE TRANSCRIPTION 67

2.8.1 PRIMER DESIGN FOR QUANTITATIVE REVERSE TRANSCRIPTION PCR (RT-QPCR) 67
2.8.2 RT-QPCR 68
2.8.3 RT-QPCR USING TAQMAN GENE EXPRESSION ASSAY 69
2.8.4 ABSOLUTE AND RELATIVE QUANTIFICATION 71
2.8.4.1 ABSOLUTE QUANTIFICATION 71
2.8.4.2 RELATIVE QUANTIFICATION 71

2.9 IMMUNOHISTOCHEMISTRY 71

2.9.1 CELL BLOCK PREPARATION 71
2.9.2 MYC ANTIBODY STAINING 72

2.10 STATISTICS 72

2.11 GENE EXPRESSION PROFILING 72

2.11.1 MRNA SEQUENCING 73

CHAPTER 3 GENERATION OF INDUCIBLE ISOGENIC MODELS OF MYC-DRIVEN GROUP 3 MEDULLOBLASTOMA 74

3.1 INTRODUCTION 75

3.1.1 SELECTION OF AN INDUCIBLE LENTIVIRAL SYSTEM 76

3.2 CELL LINE SELECTION 78

3.3 GENERATION OF INDUCIBLE MYC OVEREXPRESSION IN DAOY AND CHLA-259 82

3.3.1 Construction of MYC into the cumate inducible lentiviral vector 82
3.3.2 Determining optimum multiplicity of infection for DAOY 84
3.3.3 A time course analysis of MYC expression in DAOY MYC 86
3.3.4 Overexpression of MYC in CHLA-259 87

3.4 GENERATION OF INDUCIBLE MYC KNOCKDOWN IN D425MED AND HDMB03 88

3.4.1 Cloning of short hairpin RNA into the pLKO-Tet-On vector 88
3.4.2 Determining puromycin concentration for selection of positive clones in D425Med and HDMB03 90
3.4.3 Validating MYC knockdown in D425Med 90
3.4.4 Determining the multiplicity of infection for D425Med and HDMB03 92
3.4.5 Determining the minimum doxycycline concentration required to achieve maximum knockdown 95
3.4.6 Confirmation of reproducible MYC knockdown at the protein and mRNA level in D425Med and HDMB03. 99
3.4.7 Immunohistochemical staining of MYC in D425Med NS and D425Med MYC 2. 102

3.5 DISCUSSION 103

CHAPTER 4 IN VITRO ANALYSIS OF CELLULAR PHENOTYPES FOLLOWING MYC KNOCKDOWN 104

4.1 INTRODUCTION 105

4.2 ANALYSIS OF PHENOTYPIC EFFECTS OF MYC KNOCKDOWN IN D425MED 107

4.2.1 MYC knockdown significantly decreases proliferation in independent clones of D425Med MYC 2 and D425Med MYC 3. 107
4.2.2 MYC Knockdown in D425Med causes a G_1 cell cycle arrest 113
4.2.3 MYC knockdown increases expression of CDKN1A in D425Med MYC 2 and D425Med MYC 3 118
4.2.4 MYC knockdown decreases apoptosis in D425Med 119

4.3 ANALYSIS OF THE PHENOTYPIC EFFECTS OF MYC KNOCKDOWN IN HDMB03 122

4.3.1 Knockdown of MYC has adverse effects on HDMB03 proliferation . 122
4.3.2 Effect of MYC knockdown on HDMB03 cell cycle 124
4.3.3 MYC knockdown increases expression of CDKN1A in HDMB03 MYC 3 127
4.3.4 Effect of MYC knockdown on HDMB03 NS, HDMB03 MYC 2 and HDMB03 MYC 3 apoptosis 127

4.4 DISCUSSION 128

CHAPTER 5 GENE EXPRESSION PROFILING OF INDUCIBLE ISOGENIC MODELS OF MYC-DRIVEN GROUP 3 MEDULLOBLASTOMA 131

5.1 INTRODUCTION......132

5.2 RNA-SEQ ANALYSIS 134

5.2.1 SAMPLE PREPARATION......134
5.2.2 VALIDATING THE TRANSCRIPTIONAL EFFECT OF MYC KNOCKDOWN 134

5.2 MRNA-SEQ QUALITY CONTROL ANALYSIS......136

5.3 DIFFERENTIAL EXPRESSION BETWEEN DOX INDUCIBLE MYC KNOCKDOWN MODELS IN THE ABSENCE AND PRESENCE OF DOX 138

5.4 PRINCIPAL COMPONENT ANALYSIS (PCA) OF GENE EXPRESSION SIGNATURES FROM DOX INDUCIBLE MYC KNOCKDOWN MODELS INDICATES CONSISTENT GENE EXPRESSION CHANGES FOLLOWING MYC KNOCKDOWN. 139

5.5 MYC KNOCKDOWN LEADS TO CONSISTENT EXPRESSION CHANGES IN MEDULLOBLASTOMA CELL LINES......140

5.6 GENE SET ENRICHMENT ANALYSIS (GSEA) 145

5.6.1 GSEA CONFIRMS KNOCKDOWN OF MYC TARGET GENES AND CHANGES IN THE EXPRESSION OF GENES INVOLVED IN THE CELL CYCLE......145
5.6.2 MYC KNOCKDOWN DOWNREGULATES MTORC1 SIGNALLING PATHWAY.........147
5.6.3 MYC KNOCKDOWN UPREGULATES HYPOXIA AND EPITHELIAL MESENCHYMAL TRANSITION 148
5.6.4 MYC KNOCKDOWN UPREGULATES IL6-JAK-STAT 3 SIGNALLING PATHWAY ..149

5.7 INGENUITY PATHWAY ANALYSIS (IPA)......150

5.8 DISCUSSION 156

CHAPTER 6 CONCLUSION......158

6.1 LIMITATIONS......166

6.2 FUTURE WORKS......166

6.2.1 OPTIMIZATION OF HDMB03 DOX- INDUCIBLE MYC SILENCING ISOGENIC MODELS 167
6.2.2 PROTEOMIC PROFILING OF DOX- INDUCIBLE MYC SILENCING ISOGENIC MODELS 167
6.2.3 HIGH- THROUGHPUT FUNCTIONAL SCREENING OF DOX-INDUCIBLE MYC SILENCING ISOGENIC MODELS......167
6.2.4 METABOLIC PROFILING OF DOX-INDUCIBLE MYC SILENCING ISOGENIC MODELS 167
6.2.5 ASSESSMENT OF CANDIDATE THERAPEUTIC AGENTS WITHIN MOUSE MODELS ...168
6.2.6 KNOCKOUT OF MYC OR GENOME WIDE SCREEN BY CRISPR/CAS 9 168

6.3 FINAL CONCLUSION 168

CHAPTER 7 REFERENCES 169

List of Figures

Figure 1.1 The six original and the two emerging hallmarks of cancer, adapted from (Hanahan and Weinberg, 2011). The two emerging hallmarks indicated by * and enabling characteristics indicated by **. 3

Figure 1.2 Incidence and mortality statistics of the top 20 cancers in the UK in 2014. A) Top 20 common cancers diagnosed in the UK. B) Top 20 common cancers related deaths to occur in the UK. Figures adapted from Cancer Research UK. 9

Figure 1.3 Top 11 childhood cancers to occur in the UK (Children Cancer Statistics, Cancer Research UK). 10

Figure 1.4 Average number of new CNS tumour cases per year in the UK between 2012-2014 (figure adapted from (Cancer Research UK). 11

Figure 1.5 Medulloblastoma: T1-weighted sagittal MRI scan following gadolinium administration, showing tumour in the fourth ventricle (Pizer and Clifford, 2009). 12

Figure 1.6 Histopathological variants of medulloblastoma (taken from (Gajjar and Robinson, 2014). A) Classic MB variant is defined by masses of small cells. B) Microscopic image showing desmoplastic/nodular MB histology, this histology is characterized by nodules (N) and internodules (IN). C) Microscopic image showing MBEN histology, this variant is very similar to desmoplastic/nodular MB histology as it also contains nodules (N) and internodules (IN). However, MBEN has more nodules (N) in the tissue section and these regions are filled with a fusion of cells (indicated by the arrow). D) Anaplastic MB histological pattern displays an increased mitotic rate and increased cell death rates. E) Large cell MB histological pattern consists of enlarged and prominent nucleoli (Gajjar and Robinson, 2014). 13

Figure 1.7 The Wingless and Sonic Hedgehog signaling pathway in medulloblastoma. Stimulatory effects indicated by pointed arrows and inhibitory effects indicated by blunt arrows.*Mutations reported in specific proteins associated with pathway activation, taken from (Przer and Clifford, 2009). Frizzled (FRZ); dishevelled (DSH); adenomatous polyposis (APC); T cell factor/lymphoid enhancer factor-1 (TCF/LEF); patched (PTCH); smoothened (SMO); suppressor of fused (SUFU). . 21

Figure 1.8 Kaplan-Meier plot of overall survival curves between the different medulloblastoma subgroups. MBWNT, blue; MBSHH, red; MBGRP3, yellow; MBGRP4, green. Figure was adapted from (Kool et al., 2012). 27

Figure 1.9 Representation of MYC expression across a cohort of 240 primary medulloblastoma (Figure done by Dr Matthew Selby). 29

Figure 1.10 A systemic representation of the rearrangement of the chromosome by the non-homologous end joining repair system after chromothripsis. Taken from (Holland and Cleveland, 2012). 31

Figure 1.11 Structure of MYC and protein domains, adapted from (Aquino et al., 2013). 32

Figure 1.12 Processes involved in DNA replication and MYC's involvement. Taken from (Dominguez-Sola and Gautier, 2014). 36

Figure 1.13 Hexogram presentation of possible therapeutic strategies for targeting MYC. 38

Figure 1.14 Representation of the 1st, 2nd and 3rd generation of the HIV vectors, taken from (Sakuma et al., 2012). 42

Figure 1.15 Process of mRNA degradation through siRNA or shRNA. Taken from (O'Keefe, 2013). 44

Figure 1.16 Illustration showing the overview of the project. 45

Figure 2.1 Plasmid map for pcDNA3-cmyc (taken from Addgene). 52

Figure 2.2 Plasmid map for pLKO-Tet-On vector (taken from Addgene). 53

Figure 2.3 Plasmid map for SparQ all-in -one inducible lentiviral vector (taken from System Biosciences). 53

Figure 3.1 Mechanism of transcriptional control of cumate system (adapted from System Biosciences manual). A) The binding of the CymR repressor to the cumate operator (CuO) prevents MYC (represented by X) transcription from the CMV5 promoter. In the absence of cumate solution MYC is not overexpressed as shown by the cell line image that GFP has not been induced (-cumate). B) Addition of cumate solution changes the configuration of the CymR preventing if from binding to the CuO, as a result the CMV promoter stimulates expression of MYC as shown by the cell line image that GFP is induced (+ cumate) (NheI and BstBI are the restriction sites). 77

Figure 3.2 Mechanism of transcriptional control of pLKO-Tet-on, diagram adapted from (Wiederschain et al., 2009). A) In the absence of DOX the TetR (represented by the blue dots) binds to the TRE as a result the shRNA is not expressed (represented by X). B) Addition of Dox (represented by partial circle) binds to the

TetR, which prevents the TetR from binding to TRE as a result shRNA are expressed (Wiederschain et al., 2009). The AgeI and EcoRI are restriction sites... 78

Figure 3.3 Negative matrix factorization projection of subgroups specific metagenes derived from primary MB expression data onto cell line expression confidently assigns most cell lines to Group 3 with the remainder having no confident subgroup assignation. Plot shows selected cell lines (labelled diamonds) and primary samples of known subgroup (squares) (provided by Daniel Williamson). 79

Figure 3.4 MYC protein and mRNA expression in HDMB03, D452Med and DAOY cell lines. A) Western blot analysis of MYC expression in HDMB03, D425Med cell lines and DAOY. B) Densitometry analysis of MYC protein expression in HDMB04, D425Med and DAOY, results were normalised to beta-actin. C) RNA expression analysis of MYC in HDMB03, D425Med and DAOY. Beta-actin was used as a loading control.. 81

Figure 3.5 Overview of the cloning strategy of MYC into the inducible cumate lentivector. 83

Figure 3.6 Restriction enzyme digests analysis of selected colonies to confirm the MYC/ cumate vector construct.M: DNA marker, UC: uncut and C: Cut. Colonies were sequentially digested with NheI-HF then BstBI and separated on a 1% (w/v) agarose gel. The correct length insert was released in colonies 2,3,5,7,8,9,10 and 12. 83

Figure 3.7 The forward strand of MYC sequence inserted into the cumate inducible vector. Yellow represents the start codon and grey represents the stop codon. 84

Figure 3.8 Analysis of DAOY MYC either in the presence or absence of 1x cumate solution. In the absence of 1x cumate DAOY MYC MOI 3 had the lowest percentage of GFP positive cells. In the presence of 1x cumate, DAOY MYC MOI 3 had the lowest percentage of GFP positive cells and DAOY MYC MOI 5 and MOI 10 achieved the highest GFP positive cells.. 85

Figure 3.9 Analysis of MYC expression in DAOY MYC infected with different MOIs. A) Western blot analysis of DAOY MYC transduced with MOI 3, MOI 5 and MOI 10, cultured in the absence or presence of 1x cumate. DAOY parent cell line was included to serve as a negative control (N/C) and beta-actin served as a negative control. B) Densitometry results of the western blot analysis of DAOY MYC infected with MOI 3, MOI 5 and MOI 10, the results were normalised to beta-actin and quantified with respect to control (DAOY N/C) (grey, N/C – cumate; blue, – DOX; red, + DOX). 86

Figure 3.10 Western blot and densitometry of MYC protein expression in DAOY MYC in the absence or presence of 1x cumate. A) Western blot analysis of DAOY MYC harvested at different time points in the absence or presence of 1x cumate. The DAOY parent cell line was included and served as a negative control (N/C) and beta-actin as a loading control. B) Densitometry result of the western blot analysis of DAOY MYC harvested at different time points in the absence or presence of 1xcumate, the results were normalised to beta-actin and quantified with respect to control DAOY N/C (grey, N/C; blue, – DOX; red, + DOX).................................. 87

Figure 3.11 Cloning strategy for shRNAs into the pLKO-Tet-On vector. 88

Figure 3.12 XhoI restriction digest of selected shRNA/pLKO-Tet-On constructs. M: DNA marker, UC: uncut and C: Cut. A) XhoI restriction digest of NS, MYC-1 and MYC-2. B) XhoI restriction digest of MYC- 3. 89

Figure 3.13 Western blot and densitometry analysis of D425Med transduced with MYC 1, MYC 2 and MYC 3 lentiviral supernatant in the absence or presence of DOX. Western blot analysis of D425Med transduced with MYC 1 lentiviral supernatant in the absence (- DOX) or presence (+ DOX) of DOX. B) Densitometry analysis of D425Med transduced with MYC 1 lentiviral supernatant in the absence (blue, - DOX) or presence (red, + DOX) of DOX. C) Western blot analysis of D425Med transduced with MYC 2 lentiviral supernatant in the absence (-DOX) or presence (+ DOX) of DOX. D) Densitometry analysis of D425Med transduced with MYC 2 lentiviral supernatant in the absence (- DOX) or presence (+ DOX) of DOX. E) Western blot analysis of D425Med transduced with MYC 3 lentiviral supernatant in the absence (-DOX) or presence (+ DOX) of DOX. F) Densitometry analysis of D425Med transduced with MYC 3 lentiviral supernatant in the absence (- DOX) or presence (+ DOX) of DOX. In all three western blots beta-actin served as a loading control and densitometry results were normalized to beta-actin and quantified with respect to appropriate without DOX (- DOX) samples.. 91

Figure 3.14 Analysis of D425Med transduced with MYC 2 and NS lentivirus at MOI 1 and MOI 3. A) Western blot analysis of MYC protein expression in D425Med MYC 2 and D425Med NS at MOI 1 and MOI 3, in the absence (- DOX) or presence (+ DOX) of DOX. Beta-actin served as a loading control. B)

Densitometry result of the western blot analysis of D425Med NS and D425Med MYC 2 transduced with MOI 1, in the absence (blue, - DOX) or presence (red, + DOX) of DOX, the results were normalised to D425Med NS - DOX. C) Densitometry result of the western blot analysis of D425Med NS and D425Med MYC 2 transduced with MOI 3, in the absence (- DOX) or presence (+ DOX) of DOX, the results were normalised to D425Med NS - DOX. Densitometry results were normalized to beta-actin and quantified with respect to appropriate control (- DOX) samples. 93

Figure 3.15 Analysis of D425Med transduced with MYC 3 lentivirus and HDMB03 transduced with MYC 2 lentivirus at MOI 1 and MOI 3. A) Western blot analysis of MYC protein expression in D425Med MYC 3 infected with MOI 1 and MOI 3, in the absence (- DOX) or presence (+ DOX) of DOX. Beta- actin served as a loading control. B) Densitometry result of the western blot analysis of D425Med MYC 3 transduced with MOI 1 and MOI 3 in the absence (blue, -DOX) or presence (red, + DOX) of DOX, densitometry results were normalized to beta-actin and quantified with respect to appropriate control (- DOX) sample .C) Western blot analysis of MYC protein expression in HDMB03 MYC 2 infected with MOI 1 or MOI 3in the absence (- DOX) or presence (+ DOX) of DOX. Beta-actin served as a loading control. D) Densitometry result of the western blot analysis of HDMB03 MYC 2 transduced with MOI 1 or MOI 3 in the absence (blue represents - DOX) or presence (red represents + DOX) of DOX, densitometry results were normalized to beta-actin and quantified with respect to appropriate control (- DOX) sample. 94

Figure 3.16 Analysis of HDMB03 transduced with MYC 3 lentivirus at MOI 3. . A) Western blot analysis of MYC protein expression in HDMB03 MYC 3 infected with MOI 3in the absence (blue, -DOX) or presence (red, +DOX) of DOX. Beta-actin served as a loading control. B) Densitometry result of the western blot analysis of HDMB03 MYC 3 transduced with MOI 3 in the absence (-DOX) or presence (+DOX) of DOX, the results were normalised to HDMB03 parent cell line, which served as a positive control (grey) (P/C)... 95

Figure 3.17 Western blot and densitometry analysis of D425Med MYC 2 and D425Med NS treated with a range of DOX concentrations. A) Western blot analysis of D425Med NS cells in the absence DOX (- DOX) or in the presence of 0.1µg/ml, 1µg/ml, 3µg/ml, 5µg/ml and 10µg/ml DOX, beta- actin served as a loading control. B) Densitometry results of D425Med NS western blot analysis. C) Western blot analysis of D425Med MYC 2 in the absence (- DOX) or in the presence of 0.1µg/ml, 1µg/ml, 3µg/ml, 5µg/ml and 10µg/ml DOX. D) Densitometry results of D425Med MYC 2 western blot analysis. Densitometry results were normalized to beta-actin and quantified with respect to control (D425Med (P/C)). The colours represent the following DOX concentrations: blue, 0µg/ml; red, 0.1µg/ml; green,1µg/ml; purple, 3µg/ml; orange,5µg/ml; black, 10µg/ml. 97

Figure 3.18 Western blot and densitometry analysis of HDMB03 NS and HDMB03 MYC 2 treated with a range of DOX concentrations. A) Western blot analysis of HDMB03 NS cells in the absence DOX (- DOX) or in the presence of 0.1µg/ml, 1µg/ml, 3µg/ml, 5µg/ml and 10µg/ml DOX, beta actin was used as a loading control. B) Densitometry results of HDMB03 NS western blot analysis, results were normalised to beta-actin and quantified with respect to HDMB03 NS - DOX. C) Western blot analysis of HDMB03 MYC 2 in the absence (- DOX) or in the presence of 0.1µg/ml, 1µg/ml, 3µg/ml, 5µg/ml and 10µg/ml DOX. D) Densitometry results of HDMB03 MYC 2 western blot analysis, results were normalized to beta-actin and quantified with respect to HDMB03 MYC 2 - DOX. The colours represent the following DOX concentrations: blue, 0µg/ml; red, 0.1µg/ml; green,1µg/ml; purple, 3µg/ml; orange,5µg/ml; black,10µg/ml. 98

Figure 3.19 Analysis of MYC expression in D425Med NS, D425Med MYC 2 and D425Med MYC 3 in the presence or absence of DOX. A) Western blot analysis of MYC expression in D425Med NS, D425Med MYC 2 and D425Med MYC 3 in the absence (- DOX) or presence (+ DOX) of DOX. D425Med parent cell line was included as a positive control and beta- actin served as a loading control. B) Densitometry result of the western blot analysis of D425Med NS, D425Med MYC 2 and D425Med MYC 3 in the absence (blue, -DOX) or presence (red, + DOX) of DOX, (grey, P/C). Densitometry results were normalized to beta-actin and quantified with respect to control (P/C) C) MYC mRNA levels measured by real time qPCR and normalized for beta-2-microglobulin. The results are shown as mean ± SEM of three independent experiments and the significance was determined by unpaired Student’s t-test (*p< 0.05 and ****p< 0.0001 vs NS control). 100

Figure 3.20 Analysis of MYC in HDMB03 NS, HDMB03 MYC 2 and HDMB03 MYC 3. Western blot analysis of MYC expression in HDMB03 NS, HDMB03 MYC 2 and HDMB03 MYC 3 in the absence (- DOX) or presence (+ DOX) of DOX. HDMB03 parent cell line was included as a positive control (P/C) and beta- actin served as a loading control. B) Densitometry result of the western blot analysis of HDMB03 NS in the absence (blue, - DOX) or presence (red, + DOX) of DOX. C) Densitometry result of the western blot analysis of HDMB03 MYC 2 in the absence (blue, - DOX) or presence (red, + DOX) of DOX. D) Densitometry result of the western blot analysis of HDMB03 MYC3 in the absence (blue, - DOX) or presence (red, + DOX) of DOX. Densitometry results were normalized to beta-actin and quantified with respect to control (P/C). E) MYC mRNA levels measured by real time qPCR and normalized for beta-2-microglobulin. The results are shown as mean ± SEM of three independent experiments and the significance was determined by unpaired Student's t-test (*p< 0.05 and p< 0.0001 vs NS control). 101

Figure 3.21 Immunohistochemical staining of MYC expression in D425Med NS and D425Med MYC 2 in the presence or absence of DOX. A) Immunohistochemical staining of MYC expression in D425Med NS in the absence of DOX (- DOX). B) Immunohistochemical staining of MYC expression in D425Med NS in the presence of DOX (+ DOX). C) Immunohistochemical staining of MYC expression in D425Med MYC 2 in the absence of DOX (- DOX). D) Immunohistochemical staining of MYC expression in D425Med MYC 2 in the presence of DOX (+ DOX). The scale bar is 20mm. (Work done by Stephen Crosier, Yuru Grabovska and Halimat Popoola). 102

Figure 4.1 Effect of DOX inducible MYC silencing on proliferation in D425Med cells. A) A slight but significant difference in proliferation was observed in D425Med NS + DOX when compared to D425Med NS – DOX. (blue, – DOX; red, + DOX; y-axis, RLU, relative luminescence unit). B) No difference in proliferation was observed in D425Med NS + DOX (2nd) when compared to D425Med NS – DOX (2nd). C) No difference in proliferation was observed in D425Med NS + DOX (amalgamated data from both cell lines) when compared to D425Med NS – DOX. D) MYC knockdown in D425Med MYC 2 causes a significant reduction in proliferation when compared to the control (D425Med MYC 2 – DOX). E) MYC knockdown in D425Med MYC 2 (2nd) causes a significant reduction in proliferation when compared to the control (D425Med MYC 2 – DOX (2nd). F) MYC knockdown in D425Med MYC 2 (Both) resulted in significant inhibition of proliferation when compared to control (D425Med MYC 2 – DOX (Both). G) MYC knockdown in D425Med MYC 3 resulted in significant inhibition of proliferation when compared to control (D425Med MYC 3 – DOX). H) MYC knockdown in D425Med MYC 3 (2nd) resulted in significant inhibition of proliferation when compared to control (D425Med MYC 3 – DOX (2nd)). I) MYC knockdown in D425Med MYC 3 (both) causes a significant reduction in proliferation when compared to control (D425Med MYC 3 – DOX (Both). Proliferation was measured using the CellTiter-Glo luminescent assay as discussed in methods. The results are shown as means ± SEM of three to six individual experiments and the significance was determined by unpaired student's t-test (* p< 0.05, ** p<0.01, *** p<0.001, ****p<0.0001 vs control of the appropriate sample)..111

Figure 4.2 Phase contrast images of D425Med NS, D425Med MYC 2 and D425Med MYC 3 grown in the absence or presence of DOX at day 3 and day 5. The cell morphology of D425Med MYC 2 + DOX and D425Med MYC 3 + DOX has visibly changed at day 3, the cells were more adherent when compared to D425Med MYC 2 – DOX, D425Med MYC 3 – DOX respectively and D425Med NS ± DOX. This change in D425Med MYC 2 + DOX and D425Med MYC 3 + DOX was more evident at day 5. The scale bar is 400um and similar morphological changes were observed between replicates (images not shown)...112

Figure 4.3 DOX inducible silencing of MYC in the first D425Med clone induces a G1 cell cycle arrest. A) Cell cycle analysis of D425Med NS, D425Med MYC 2, D425Med MYC 3 grown in the absence or presence of DOX, cells were harvested after 3 days and detached by trypsin, fixed in 70 % ethanol and stained with PI as described in methods (2.2.2). A total number of 10 000 events per sample were counted. MYC knockdown in both D425Med MYC 2 + DOX and D425Med MYC 3 + DOX resulted in a significant increase in the number of cells in the G1 phase of the cell cycle and a significant decrease in the number of cells in the S phase of the cell cycle when compared to controls (D425Med MYC 2 – DOX, D425Med MYC 3 – DOX). There was no significant change in the cell cycle distribution for D425Med NS + DOX when compared to D425Med NS – DOX. The results are shown as means ± SEM of three individual experiments and the significance was determined by unpaired student’s t-test (** p<0.01, ***p<0.001 vs control of the appropriate sample). Dark grey represents G1 phase, red represents S phase and light grey represents G2 phase. B) Representative cell cycle profiles derived by by FlowJo V10 software (x axis = 585/42). 114

Figure 4.4 DOX inducible silencing of MYC in the first D425Med clone induces a G1 cell cycle arrest DOX inducible silencing of MYC in the second clone of D425Med induces a G1 cell cycle arrest. A) Cell cycle analysis of D425Med NS (2^{nd}), D425Med MYC 2 (2^{nd}), D425Med MYC 3(2^{nd}) grown in the absence or presence of DOX, cells were harvested after 3 days and detached by trypsin, fixed in 70 % ethanol and stained with PI as described in methods. A total number of 10 000 events per sample were counted. MYC knockdown in both D425Med MYC 2 + DOX (2^{nd}) and D425Med MYC 3 + DOX (2^{nd}) resulted in a significant increase in the number of cells in the G1 phase of the cell cycle when compared to controls (D425Med MYC 2 – DOX (2^{nd}), D425Med MYC 3 – DOX (2^{nd})). A significant decrease in the number of cells in the S phase of the cell cycle was seen in D425Med MYC 3 (2^{nd}) when D425Med MYC 3 – DOX (2^{nd}). There was no significant change in the cell cycle distribution for D425Med NS + DOX (2^{nd}) when compared to D425Med NS – DOX (2^{nd}). The results are shown as means ± SEM of three individual experiments and the significance was determined by unpaired student’s t-test (* p<0.05, **p<0.01 vs control of the appropriate sample). Dark grey represents G1 phase, red represents S phase and light grey represents G2 phase. B) Representative cell cycle profiles derived by by FlowJo V10 software (x axis = 585/42). 115

Figure 4.5 DOX inducible silencing of MYC in D425Med (both) induces a G1 cell cycle arrest. Cell cycle analysis of both D425Med NS, D425Med MYC 2, D425Med MYC 3 constructs. MYC knockdown in D425Med MYC 2 + DOX (Both) and D425Med MYC 3 + DOX (Both) resulted in a significant increase in the number of cells in the G1 phase of the cell cycle and a significant decrease in the number of cells in the S phase of the cell cycle when compared to controls (D425Med MYC 2 – DOX (Both), D425Med MYC 3 – DOX (Both). There was no significant change in the cell cycle distribution for D425Med NS + DOX (Both) when compared to D425Med NS – DOX (Both). The results are shown as means ± SEM of six individual experiments and the significance was determined by unpaired student’s t-test (** p<0.01, ***p<0.001, ***p<0.0001 vs control of the appropriate sample). Dark grey represents G1 phase, red represents S phase and light grey represents G2 phase. 117

Figure 4.6 Expression of CDKN1A in D425Med (both) grown in the absence or presence of DOX for 3 days (blue represents – DOX and red represents + DOX). MYC knockdown in both D425Med MYC 2 and D425Med MYC 3 caused an upregulation of CDKN1A expression when compared to D425Med NS - DOX (control). The expression of mRNA was normalised to GAPDH and D425Med NS – DOX was used as the calibrator. Data are presented as mean ± SEM of six individual experiments. Significance was determined by unpaired student's t-test and no significance was observed. 119

Figure 4.7 Effect of DOX inducible MYC silencing on apoptosis in D425Med cells. A) No significant difference was observed in D425Med NS + DOX when compared to control (D425Med NS – DOX) (blue, – DOX; red, + DOX; y-axis, RLU (relative luminescence unit)). B) MYC knockdown in D425Med MYC 2 causes a significant reduction in apoptosis at day 4 when compared to control (D425Med MYC 2 – DOX). C) MYC knockdown in D425Med MYC 3 resulted in a significant decrease in apoptosis at day 5 when compared to control (D425Med MYC 3 – DOX). D) No significant difference was observed in D425Med NS + DOX (2nd) when compared to control (D425Med NS – DOX (2nd). E) No significant difference was observed in D425Med MYC 2 + DOX (2nd) when compared to control (D425Med MYC 2 – DOX (2nd). F) No significant difference was observed in D425Med MYC 3 + DOX (2nd) when compared to control (D425Med MYC 3 – DOX (2nd). G) No significant difference was observed in D425Med NS + DOX (both) when compared to control (D425Med NS – DOX (both). H) MYC knockdown in D425Med MYC 2 (both) causes a significant reduction in apoptosis at day 4 and day 5 when compared to control (D425Med MYC 2 – DOX (both). I) MYC knockdown in D425Med MYC 3 (Both) resulted in a significant decrease in apoptosis at day 5 when compared to control (D425Med MYC 3 – DOX (Both). The results are shown as means ± SEM of three and six individual experiments and the significance was determined by unpaired student's t-test (* $p< 0.05$ vs control of the appropriate sample). 121

Figure 4.8 Effect of DOX inducible MYC silencing on proliferation in HDMB03 cells. A) No difference was observed in HDMB03 NS + DOX when compared to control (HDMB03 NS – DOX) (blue, – DOX; red, + DOX; RLU, relative luminescence unit). B) There was no difference in proliferation for HDMB03 MYC 2 + DOX when compared to control (D425Med MYC 2 – DOX). C) MYC knockdown in HDMB03 MYC 3 + DOX resulted in a significant reduction in cell number when compared to control (HDMB03 MYC 3 – DOX). Proliferation was measured using the CellTiter-Glo luminescent assay as discussed in methods (2.2.1). The results are shown as means ± SEM of three individual experiments and the significance was determined by the student's t-test (* p< 0.05, ** p<0.01, vs control of the appropriate sample). 123

Figure 4.9 Phase contrast image of HDMB03 MYC 3. HDMB03 MYC 3 cells cluster in neurophere like clumps, the scale bar is 100um. 124

Figure 4.10 DOX inducible silencing of MYC in HDMB03. A) Cell cycle analysis of HDMB03 NS, HDMB03 MYC 2 and HDMB03 MYC 3 in the presence or absence of DOX, cells were harvested after 3 days were detached by trypsin, fixed in 70 % ethanol and stained with PI as described in methods (2.2.2). A total number of 10 000 events per sample were counted. MYC knockdown in HDMB03 MYC 3 + DOX resulted in a significant decrease in the number of cells in the S phase of the cell cycle when compared to HDMB03 MYC 3 – DOX). There was no significant change in the cell cycle distribution for both HDMB03 NS + DOX and HDMB03 MYC 2 when compared to control (HDMB03 NS – DOX AND HDMB03 MYC 2 – DOX). The results are shown as means ± SEM of four individual experiments for HDMB03 NS ± DOX, three individual experiments for HDMB03 MYC 2 and two individual experiments for HDMB03 MYC 3 and the significance was determined by the student's t-test (** p<0.01 vs control of the appropriate sample). Dark grey represents G1 phase, red represents S phase and light grey represents G2 phase. B) Representative cell cycle profiles derived by by FlowJo V10 software (x axis = 585/42). 125

Figure 4.11 Expression of CDKN1A in HDMB03 NS, HDMB03 MYC 2 and HDMB03 MYC 3 cells grown in the absence or presence of DOX for 72 hours (blue represents – DOX and red represents + DOX). MYC knockdown in HDMB03 MYC 3 caused an upregulation of CDKN1A expression when compared to HDMB03 NS - DOX (control). The expression of mRNA was normalised to GAPDH and HDMB03 NS – DOX were used as the calibrator. Data are presented as mean ± SEM of three individual experiments and no significant changes was observed. Significance was determined by unpaired student's t-test. 127

Figure 4.12 Effect of DOX inducible MYC silencing on apoptosis in HDMB03 cells. A) No difference was observed in HDMB03 NS + DOX when compared to control (HDMB03 NS – DOX). B) MYC knockdown in HDMB03 MYC 2 causes a significant reduction in apoptosis at day 5 when compared to control (HDMB03 MYC 2 – DOX). C) MYC knockdown in HDMB03 MYC 3 resulted in a significant decrease in apoptosis at day 2 when compared to control (HDMB03 MYC 3 – DOX). Apoptosis was measured using Caspase-Glo 3/7 luminescent assay as discussed in methods (2.2.3). The results are shown as means ± SEM of three individual experiments and the significance was determined by the student's t-test (* p< 0.05 vs control of the appropriate sample). 128

Figure 5.1 Electropherogram of a typical sample showing the integrity and concentration of the RNA alongside the rRNA ratio. The red arrow represents the 18S fragment and the blue arrow represents the 28S fragment. 134

Figure 5.2 Expression of TRAP1 and RCC1 in D425Med and HDMB03 following growth in the absence or presence of DOX for 3 days (blue indicates - DOX and red indicates + DOX). A) MYC knockdown in both D425Med MYC 2 and D425Med MYC 3 caused a downregulation of TRAP1 expression when compared to D425Med NS - DOX (control). B) MYC knockdown in both D425Med MYC 2 and D425Med MYC 3 caused a downregulation of RCC1 expression when compared to D425Med NS - DOX (control). C) MYC knockdown in HDMB03 caused a downregulation of TRAP1 expression when compared to HDMB03 NS - DOX (control). D) MYC knockdown in HDMB03 caused a downregulation of RCC1 expression when compared to HDMB03 NS - DOX (control). The expression of mRNA was normalised to GAPDH and D425Med NS – DOX or HDMB03 NS - DOX were used as the calibrator. Data are presented as mean ± SEM of three or six individual experiments. 136

Figure 5.3 Overview of per base sequence quality for a typical sample. The y-axis shows the quality scores and the x-axis shows the position in the read (bp). The background of the plot shows three different colours: Green indicates good quality score, orange indicates a reasonable quality score and red indicates a poor quality score. 137

Figure 5.4 FastQC plot of the sample showing the sequence content of all bases for a typical sample. The y-axis shows the bases and the x-axis shows the position in the read (bp). Each nucleobase is represented by a different colour, thymine (T) is represented by red, cytosine (C) is represented by blue, adenine (A) is represented by green and guanine (G) is represented by black. A stable distribution of nucleotides occurs after the first 13 base pairs. 137

Figure 5.5 FastQC plot of a typical sample showing the per sequence GC content. The red line represents the GC count per read of sequencing data and the blue line represents the theoretical distribution curve. The GC count per read bell shape curve fits closely to the theoretical data which is an indication of good data. 138

Figure 5.6 Testing for differential expression between DOX inducible MYC knockdown models (D425Med and HDMB03) grown in the absence or presence of DOX. Scatter plot of log fold change versus mean of normalized counts. The red dots represent genes that are differentially expressed at a 10% FDR when a Benjamini and Hochberg correction is applied. The red dots at the upper or lower end of the scatter plot represents genes with either very low or high log fold change. 139

Figure 5.7 Supervised principal component analysis of gene expression signatures in DOX inducible MYC knockdown models. This PCA plot shows different biological samples. Replicates of the same condition are coloured the same and each dot is an individual replicate. A) D425Med cells expressing MYC (NS or –DOX) B) D425 cells following MYC knockdown (+DOX). C) HDMB03 cells expressing MYC (NS or –DOX) D) HDMB03 cells following MYC knockdown (+DOX). The x-axis is the second component (PC2 related to cell line identity) and the y axis the third component (PC3 related to MYC expression). 140

Figure 5.8 Heatmap of the top 100 significantly differentially expressed genes in D425Med NS, D425Med MYC 2 and D425Med MYC 3 grown in the absence and presence of DOX showing high reproducibility between replicates. Each row represents a gene and each column a sample. The light to dark blue colour represents genes that are downregulated and the light to dark orange colour represents genes that are upregulated. 142

Figure 5.9 Heatmap of the top 100 significantly differentially expressed genes in HDMB03 NS, HDMB03 MYC 2 and HDMB03 MYC 3 grown in the absence and presence of DOX. Each lane represents a gene (same gene set as shown in Figure

5.8) and each column a sample. The light to dark blue colour represents genes that are downregulated and the light to dark orange colour represents genes that are upregulated..143

Figure 5.10 Relative expression of selected differentially expressed genes in D425Med NS, D425Med MYC 2, D425Med MYC 3, HDMB03 NS, HDMB03 MYC 2 and HDMB03 MYC 3. A) Relative expression of genes that are downregulated in D425Med MYC 2, D425Med MYC 3 HDMB03 MYC 2 and HDMB03 MYC 3 grown in the presence of DOX. B) Relative expression of genes that are upregulated in D425Med MYC 2, D425Med MYC 3, HDMB03 MYC 2 and HDMB03 MYC 3 grown in the presence of DOX. The x-axis represents the sample names and the y-axis represents the variant stabilised transformed (VST) expression. Box plots shows median and quartile ranges....................................144

Figure 5.11 Selected hallmark GSEA enrichment plots of pathways positively or negatively enriched in either MYC knockdown or in MB_{GRP3} gene sets. The enrichment scores are the peaks occurring at the top or bottom of the plot, these peaks display the extent of which a gene is represented within the ranked list. The leading edge subset is represented by the vertical lines as these indicate the genes that contribute most to the enrichment scores. The ranking matrix is at the bottom of the enrichment plot. As you move down the rank list, the ranking matric values move from positive to negative. 146

Figure 5.12 Enrichment plots of MTORC1 signalling pathway which is negatively enriched in MYC knockdown and positively enriched in MB_{GRP3} primary tumours. The enrichment scores are the peaks occurring at the top or bottom of the plot, these peaks display the extent of which a gene is represented within the ranked list. The leading edge subset is represented by the vertical lines as these indicates the genes that contributes most to the enrichment scores. The ranking matrix is at the bottom of the enrichment plot. As you move down the rank list, the ranking matric values move from positive to negative..147

Figure 5.13 Enrichment plots of hypoxia and epithelial mesenchymal transition phenomenon, which is positively enriched following MYC knockdown and negatively enriched in MB_{GRP3} primary tumours. The enrichment scores are the peaks occurring at the top or bottom of the plot, these peaks display the extent of which a gene is represented within the ranked list. The leading edge subset is represented by the vertical lines as these indicates the genes that contributes most to the enrichment scores. The ranking matrix is at the bottom of the enrichment plot. As you move down the rank list, the ranking matric values move from positive to negative. 149

Figure 5.14 Enrichment plots of IL6-JAK-STAT 3 signalling which is positively enriched in MYC knockdown data and negatively enriched in MB_{GRP3} data. The enrichment scores are the peaks occurring at the top or bottom of the plot, these peaks display the extent of which a gene is represented within the ranked list. The leading edge subset is represented by the vertical lines as these indicates the genes that contributes most to the enrichment scores. The ranking matrix is at the bottom of the enrichment plot. As you move down the rank list, the ranking matric values move from positive to negative. 150

Figure 5.15 KEGG pathway analysis of phototransduction pathway. Genes that are differentially regulated in both MB_{GRP3} primary tumours vs medulloblastomas belonging to other subgroups and MYC knockdown vs control are highlighted in red. 153

Figure 5.16 GRK1 expression in MB_{GRP3} and in isogenic MB cell lines. A) Graph of GRK1 expression in MB_{GRP3} showing a negative correlation with MYC expression. The MYC amplified primary tumour samples (n=9) are within the rectangle. B) Relative expression GRK1 in D425Med and HDMB03 isogenic cell lines. MYC silencing causes upregulation of GRK1. The x-axis represents the sample names and the y-axis represents the variant stabilised transformed (VST) expression. Box plots shows median and quartile ranges.................................... 156

Figure 6.1 Schematic diagram showing potential therapeutic strategies directed at targeting MYC or its associated downstream effects. 160

List of Tables

Table 1: Examples of oncogenes commonly activated by mutation or chromosomal changes in human tumours (taken from (Kopnin, 2000) with a few adaptions) 7

Table 2: Examples of tumour suppressor genes commonly mutated or deleted in human tumours (taken from (Chial, 2008) with a few adaptions).. 8

Table 3: Chang staging system, taken from (Laurent et al., 1985) 14

Table 4: Medulloblastoma: currently accepted prognostic factors, adapted from (Pizer and Clifford, 2008) 15

Table 5: Summary of the most common integrated medulloblastoma diagnosis, with clinical correlations, taken from (Louis et al., 2016b) 16

Table 6: Summary of medulloblastoma subgroups showing clinical and molecular features, adapted from (Schroeder and Gururangan, 2014) (CGNP, cerebellar granular neuron precursor; EGL, external granular layer) 25

Table 7: Features of the four viral vectors (taken from (Howarth et al., 2010) 40

Table 8: Concentrations and preparations for cell cycle analysis reagents 51

Table 9: Constructs sequencing primers 55

Table 10: PCR primers for molecular cloning 56

Table 11: shRNAs targeting MYC and NS 57

Table 12: PCR components for amplification of MYC 57

Table 13: Thermocycler conditions for PCR amplification of MYC 58

Table 14: Components for XhoI restriction digest 59

Table 15:Transfection solution A for one replicate 61

Table 16:SDS-PAGE buffers and compositions 65

Table 17:Components for cDNA conversion 66

Table 18:Thermal cycling conditions for reverse transcription 67

Table 19: RT-qPCR primers 67

Table 20: RT-qPCR reagents for SYBR Green assay 68

Table 21:Cycling conditions for SYBR Green assay 69

Table 22: Reagents for Taqman gene expression assay 70

Table 23: Cycling conditions for Taqman gene expression assay 70

Table 24: Human medulloblastoma cell lines acquired by the Paediatric Brain Tumour Research group and subgrouped by metagene projection 80

Table 25:Human medulloblastoma cell lines selected for generation of isogenic models 81

Table 26: The effect of MYC knockdown in both independent clones of D425Med cell cycle distribution, results are shown as mean ± SEM 116

Table 27:The effect of MYC knockdown on D425Med cell cycle distribution, results are shown as mean ± SEM 118

Table: 28 The effect of MYC knockdown on HDMB03 cell cycle distribution, results are shown as mean ± SEM 126

Table 29:Top 5 ingenuity canonical pathways in primary MB_{GRP3} 152

Table 30: Top 5 Ingenuity canonical pathways for DOX inducible MYC knockdown models 154

Table 31:Selected upstream regulators for DOX inducible MYC knockdown models 155

Chapter 1 Introduction

1.1 Cancer

1.1.1 Definition of cancer

Cancer is a disease that is caused by uncontrolled cell division of abnormal cells (Cai and Jiang, 2014). Cancer occurs due to a gradual build-up of changes occurring in the genome (Forment *et al.*, 2012), changes such as mutations (Michor *et al.*, 2004) or chromosomal abnormalities (Forment *et al.*, 2012). Alteration of the genome leads to active oncogenes and inactive tumour suppressor genes (Hanahan and Weinberg, 2000; Forment *et al.*, 2012), leading to uncontrolled cell division (Forment *et al.*, 2012) and the accumulation of abnormal cells (Suzuki and Griffiths, 1976).

1.1.2 Hallmarks of cancer

In 2000, Douglas Hanahan and Robert A. Weinberg published a review describing six hallmarks that cells need to acquire in order for the cell to become cancerous. In 2011, they described two more hallmarks; these hallmarks are shown in Figure 1.1 and the first six hallmarks are described below (Hanahan and Weinberg, 2000; Hanahan and Weinberg, 2011).

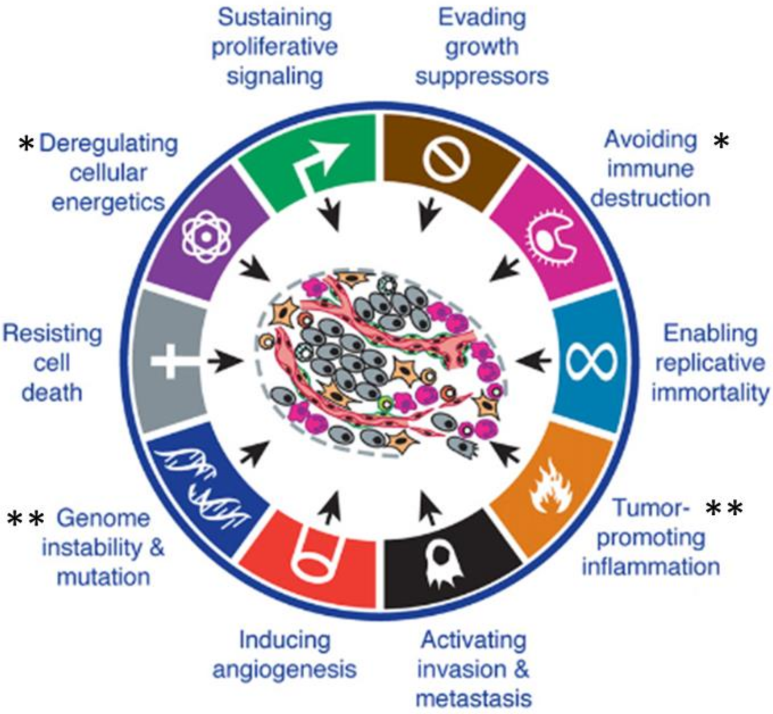
Sustaining proliferative signaling
Evading growth suppressors
Avoiding immune destruction *
Enabling replicative immortality
Tumor-promoting inflammation **
Activating invasion & metastasis
Inducing angiogenesis
** Genome instability & mutation
Resisting cell death
* Deregulating cellular energetics

Figure 1.1 The six original and the two emerging hallmarks of cancer, adapted from (Hanahan and Weinberg, 2011). The two emerging hallmarks indicated by * and enabling characteristics indicated by **.

1.1.2.1 Sustaining proliferative signaling

Cancer cells disrupt growth- promoting signals causing an imbalance in cell growth, cell death and the cell cycle. As a result, the most important feature of cancer cells arises and that is to continually undergo cell division, resulting in an accumulation of cell progeny. They achieve this through numerous mechanisms. Cancer cells can produce their own growth factor ligands, or they promote proliferation by triggering normal cells to produce different growth factors. Similarly, cancer cells can gain more receptors on their surface giving them advantageous access to growth factors, or they can activate growth factor receptors, eliminating the need for growth factors by stimulating downstream signaling pathways (Hanahan and Weinberg, 2011).

1.1.2.2 Resisting cell death

Cancer cells override apoptotic mechanisms due to various abnormalities within the cell. The most common abnormality is a defective *TP53* tumour suppressor gene. One of TP53's normal function is to trigger apoptosis, increasing NOXA and Puma BH3-only proteins in response to DNA damage. Another ability of cancer cells is to elevate anti-apoptotic proteins Bcl-2, Bcl-xL and survival proteins such as Igf 1/2 and decrease proapoptotic proteins such as Bax, Bim and Puma. During metabolic stress, the autophagy process can promote the survival of cancer cells (Mathew *et al.*, 2007; Hanahan and Weinberg, 2011). Lastly, the necrotic process initiates an inflammatory response that promotes tumour development because it aids in processes such as angiogenesis (Hanahan and Weinberg, 2011).

1.1.2.3 Sustaining angiogenesis

Tumour development and maintenance needs nutrients and oxygen and requires the ability to get rid of metabolic waste. These needs are met by cancer cells having the ability to activate angiogenesis. Angiogenesis is the genesis of new blood vessels from existing blood vessels, this process is stimulated by different factors that can either activate or inhibit angiogenesis. Proteins such as thrombospondin-1 protein are known to inhibit angiogenesis (Hanahan and Weinberg, 2011), whereas activating factors include the vascular endothelial growth factor-A (VEGF-A), which is stimulated during embryogenesis and postnatal development. It is also activated during physiological and pathological angiogenesis in adults (Maharaj *et al.*, 2006; Hanahan and Weinberg, 2011). Tumour angiogenesis can be promoted by an increase in *VEGF-A*, which can be caused by hypoxia and oncogenic signaling, and in addition by abnormal increases in fibroblast growth factors (FGFs) (Hanahan and Weinberg, 2011).

1.1.2.4 Resisting growth suppressors

Cancer cells also need to be able to overcome the growth suppressors that control cell growth and division. They are classified as tumour suppressors (discussed in 1.1.3), examples are the retinoblastoma-associated (RB) protein and the TP53 protein. The RB protein plays a role in cell cycle progression and cell growth (Hanahan and Weinberg, 2011), and can prevent the cell from entering the S- phase (Giacinti and Giordano, 2006). A defective RB protein will enable cancer cells to continually proliferate. In the case of TP53, if cell stress and genomic damage occurs, this protein stops the cycle cell so that these damages can be corrected, but if not repairable a apoptotic response will be activated (Hanahan and Weinberg, 2011).

1.1.2.5 Activating invasion and metastasis

Metastasis refers to cancer cells' ability to move from their primary location to other tissues and organs (Martin *et al.*, 2013), whereas invasion refers to the cells ability to pass their tissue barriers (Friedl and Wolf, 2003), The metastatic process occurs in a number of stages (Hanahan and Weinberg, 2011). The first stage is invasion, a result of cancer cells having lower cell-cell adhesion molecules and cellular matrix (Martin *et al.*, 2000; Cavallaro and Christofori, 2001). The second stage is known as intravasation, this stage refers to cancer cells entering the circulatory system, lymphatic system and spreading to a second site (Martin *et al.*, 2000; Hanahan and Weinberg, 2011). The third stage is extravasation, where cancer cells attach to endothelial cells, invade the endothelium and basal lamina and establish at a second site, (Martin *et al.*, 2000). The final stages of invasion and metastasis is the development of small tumours which progress to macroscopic tumours (Hanahan and Weinberg, 2011).

1.1.2.6 Enabling replicative mortality

Under normal conditions cells can only divide a certain number of times, this is due to protective caps at the end of their chromosomes known as telomeres. With each cell division telomeres shorten, until they become too short and unable to protect the ends of the chromosome, as a consequence crisis/apoptosis is triggered (Hanahan and Weinberg, 2011). The telomeric shortening can be prevented by telomerase, this DNA polymerase is responsible for adding the telomeric sequence (TTAGGG) to the end of the chromosomes, causing continued cell division (Shay and Wright, 2011). This enzyme is expressed at low levels or hardly traceable in somatic cells (Shammas, 2011), however in multiple cancers telomerase levels are imbalanced (Cesare and Reddel, 2013), which over time leads to genomic instability (Jafri *et al.*, 2016).

1.1.3 Tumour suppressors and oncogenes

As mentioned in section 1.1.1 and 1.1.2, the development of cancer is a multistep process. One of the first changes observed to cause tumourgenesis was gain of function mutations in proto-oncogenes, which then becomes oncogenes. Proto-oncogenes encodes for proteins involved in the signal transduction pathways that play a role in stimulating growth, proliferation and survival of cells (Collins *et al.*, 1997; Lee and Muller, 2010). Oncogenes can be activated by three mechanisms, the first of which is amplification (Pierotti *et al.*, 2003), which is an increase in copy number (Albertson, 2006) (the example of MYC amplification is discussed in 1.5.1). The second mechanism is mutational activation, which occur due to a structural change within the protein. In mammalian tumours the most common oncogenic mutation to occur is a point mutation, which is an alteration in a single amino acid within the encoded protein, for example in the RAS oncogenes (Pierotti *et al.*, 2003). The last mechanism is chromosomal rearrangement such as translocation (for example translocation involving MYC, which is discussed in 1.5.1) or inversion. These rearrangements creates gene fusions, which is the joining of two separate genes (Pierotti *et al.*, 2003). Oncogenes can be transcription factors, apoptosis regulators and growth factors or receptors (Table 1). Loss of function mutations in tumour suppressors have also been observed to promote tumourgenesis (Lee and Muller, 2010). However, for tumour suppressors to cause cancer, two mutations must be present; either two somatic mutations or one somatic and one germline mutation (Rice *et al.*, 2014). However, there are dominant negative mutations, for example in TP53 that can cause cancer (Rivlin *et al.*, 2011). Tumour suppressor genes encode proteins that are involved in activating cell cycle checkpoints, inhibiting the cell cycle, repairing DNA (Rice *et al.*, 2014) and stimulating apoptosis (Velez and Howard, 2015). Common tumour suppressors are listed in Table 2.

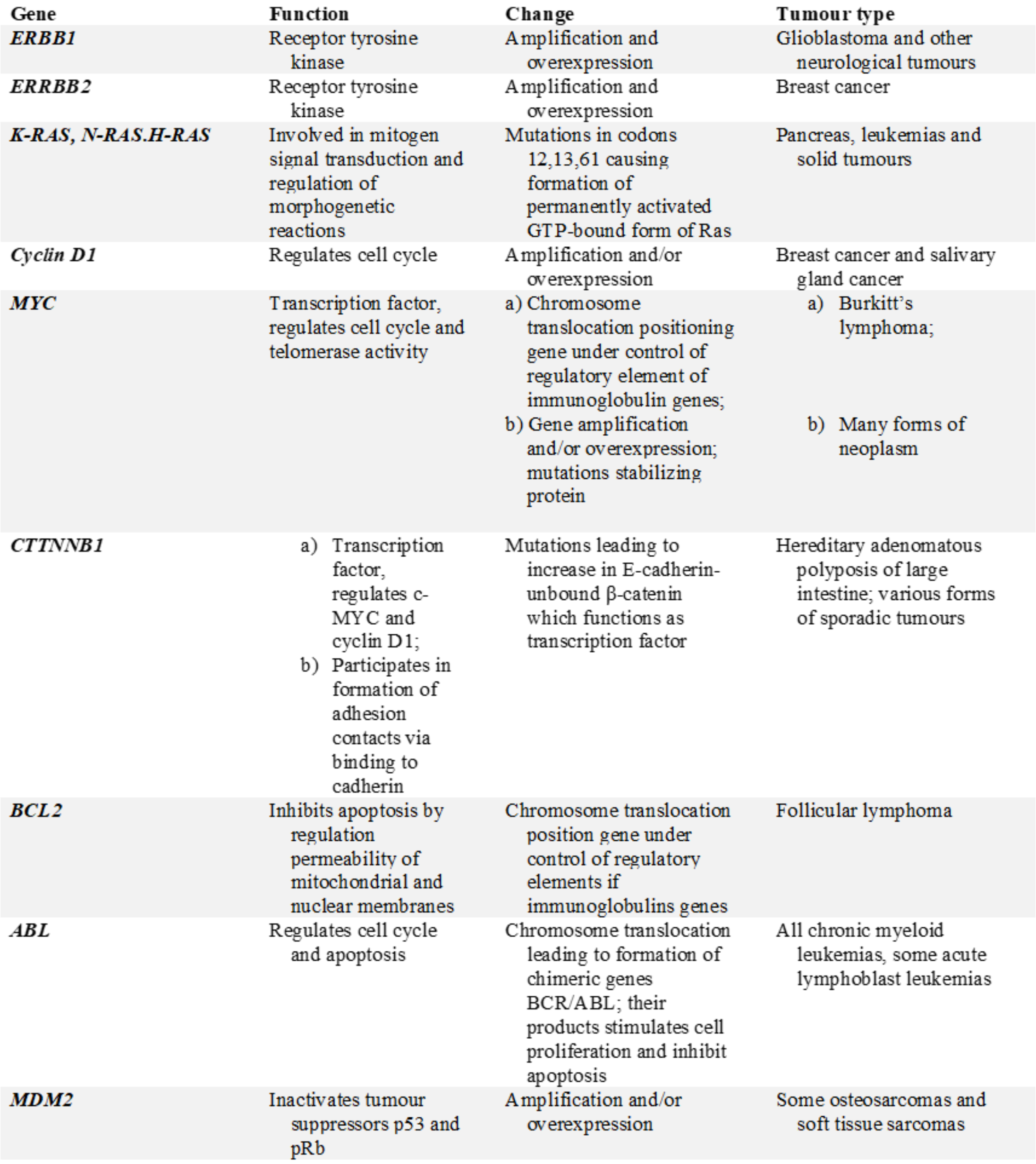

Gene	Function	Change	Tumour type
ERBB1	Receptor tyrosine kinase	Amplification and overexpression	Glioblastoma and other neurological tumours
ERRBB2	Receptor tyrosine kinase	Amplification and overexpression	Breast cancer
K-RAS, N-RAS.H-RAS	Involved in mitogen signal transduction and regulation of morphogenetic reactions	Mutations in codons 12,13,61 causing formation of permanently activated GTP-bound form of Ras	Pancreas, leukemias and solid tumours
Cyclin D1	Regulates cell cycle	Amplification and/or overexpression	Breast cancer and salivary gland cancer
MYC	Transcription factor, regulates cell cycle and telomerase activity	a) Chromosome translocation positioning gene under control of regulatory element of immunoglobulin genes; b) Gene amplification and/or overexpression; mutations stabilizing protein	a) Burkitt's lymphoma; b) Many forms of neoplasm
CTTNNB1	a) Transcription factor, regulates c-MYC and cyclin D1; b) Participates in formation of adhesion contacts via binding to cadherin	Mutations leading to increase in E-cadherin-unbound β-catenin which functions as transcription factor	Hereditary adenomatous polyposis of large intestine; various forms of sporadic tumours
BCL2	Inhibits apoptosis by regulation permeability of mitochondrial and nuclear membranes	Chromosome translocation position gene under control of regulatory elements if immunoglobulins genes	Follicular lymphoma
ABL	Regulates cell cycle and apoptosis	Chromosome translocation leading to formation of chimeric genes BCR/ABL; their products stimulates cell proliferation and inhibit apoptosis	All chronic myeloid leukemias, some acute lymphoblast leukemias
MDM2	Inactivates tumour suppressors p53 and pRb	Amplification and/or overexpression	Some osteosarcomas and soft tissue sarcomas

Table 1: Examples of oncogenes commonly activated by mutation or chromosomal changes in human tumours (taken from (Kopnin, 2000) with a few adaptions)

Gene	Function	Type of cancer
RB1	Cell division, DNA replication, cell death	Hereditary retinoblastoma and associated with many different cancers
TP53	Cell division. DNA repair, cell death	Hereditary Li- Fraumeni syndrome (Brain tumours, sarcomas, leukemia) and associated with many different cancers)
CDKN2A	Cell division, cell death	Hereditary melanoma and associated with many different cancers
MLH1, MSH2, MSH6	DNA mismatch repair, cell cycle regulation	Hereditary colorectal cancer (without polyposis) and associated with non-hereditary cancers such as colorectal, gastric, endometrial
APC	Cell division, DNA damage, cell migration, cell adhesion, cell death	Hereditary colorectal cancer (due to familial polyposis) and associated with many non- hereditary colorectal cancers
BRCA1, BRCA2	Repair of double-stranded DNA breaks, cell division, cell death	Hereditary breast and/or ovarian cancer and associated with rare non-hereditary cancers
WT1, WT2	Cell division, transcriptional regulation	Hereditary wilm's tumour
NF1, NF2	Ras-mediated signal transduction, cell differentiation, cell division, development processes	Hereditary nerve tumours (including brain)
VHL	Cell division, cell death, cell differentiation, response to cell stress	Hereditary kidney cancer

Table 2: Examples of tumour suppressor genes commonly mutated or deleted in human tumours (taken from (Chial, 2008) with a few adaptions)

1.2. Cancer incidence and mortality in the UK

In 2014 about 357,000 new cases were reported with most of diagnoses occurring in males (1.03:1). The most common cancers reported were breast (15%), prostate (13%), lung (13%) and bowel cancer (12%),with breast cancer being the most common cancer to occur in females and prostate cancer in males (Figure 1.2) (Cancer Incidence Statistics, Cancer Research UK). In 2014 cancer accounted for 163,000 deaths, with a higher death rate occurring in males than females (Cancer Mortality Statistics, Cancer Research UK).

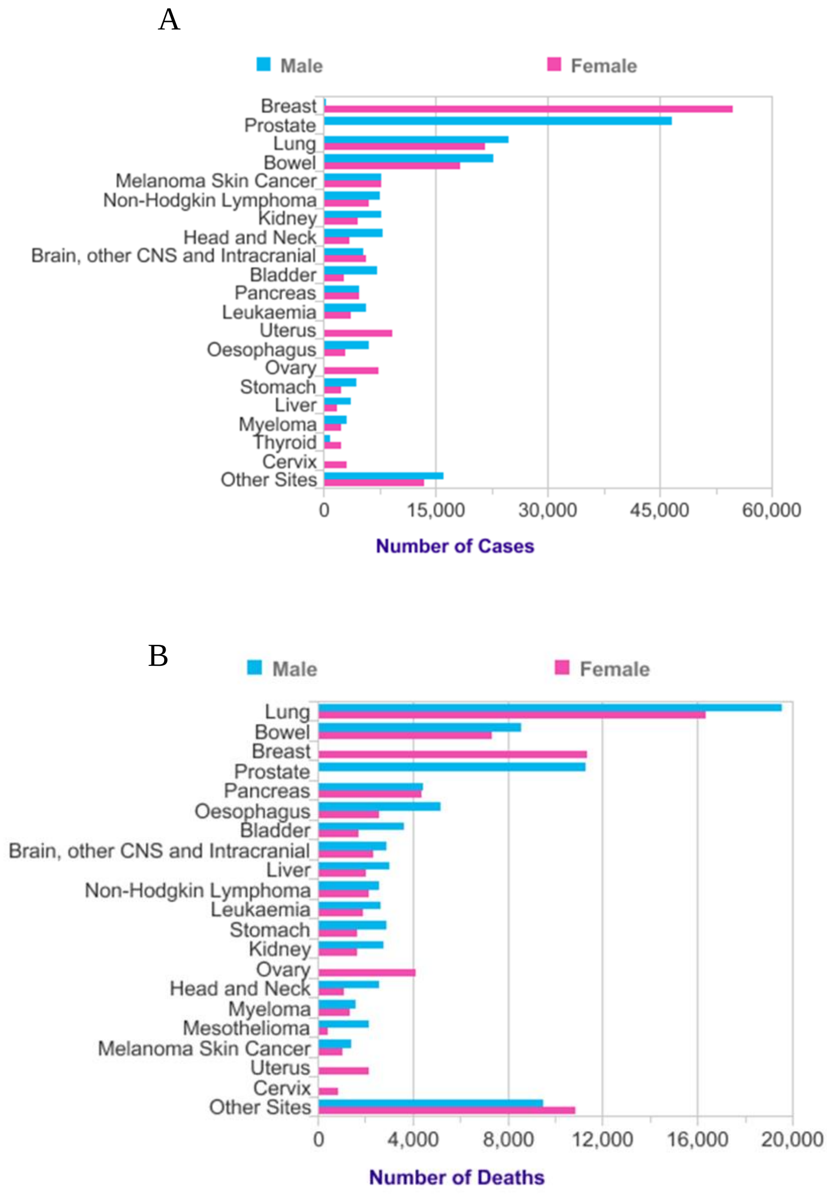

Figure 1.2 Incidence and mortality statistics of the top 20 cancers in the UK in 2014. A) Top 20 common cancers diagnosed in the UK. B) Top 20 common cancers related deaths to occur in the UK. Figures adapted from Cancer Research UK.

1.3 Childhood cancer

1.3.1 Incidence and mortality of childhood cancer in United Kingdom

Cancer in children (age less than 15 years) is rare, in the UK of the 1756 cases per year 257 children died of their disease. The most common cancers to occur in children are leukaemia, brain, other central nervous system (CNS) and intracranial tumours, lymphomas, soft tissue sarcoma and sympathetic nervous system tumours (SNS) (Figure 1.3) (Children Cancer Statistics, Cancer Research UK) . In CNS tumours the peak incidence rate in children was between 0-4 years in the period from 2012-2014 (Figure 1.4) (CNS Incidence Statistics, 2017). Medulloblastoma (MB) and other neuroectodermal tumours are responsible for 25% of all cases; MB accounts for the majority of these (15-20%) (Massimino *et al.*, 2016). The incidence of children with cancer has risen by 38% in the period from 1966-2000 in the UK, this increase is thought to be due to better diagnoses and reporting of cases. However, the five year survival rate for all paediatric cancers is 82%, even though the overall survival rate for brain cancers is 75% they are the leading cause of childhood cancer deaths (Children with Cancer UK, 2017).

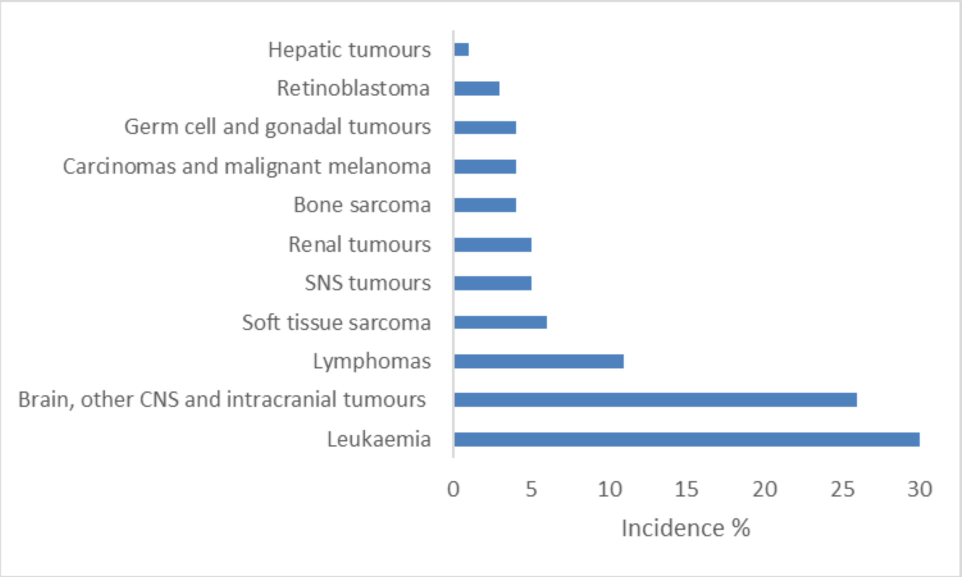

Figure 1.3 Top 11 childhood cancers to occur in the UK (Children Cancer Statistics, Cancer Research UK).

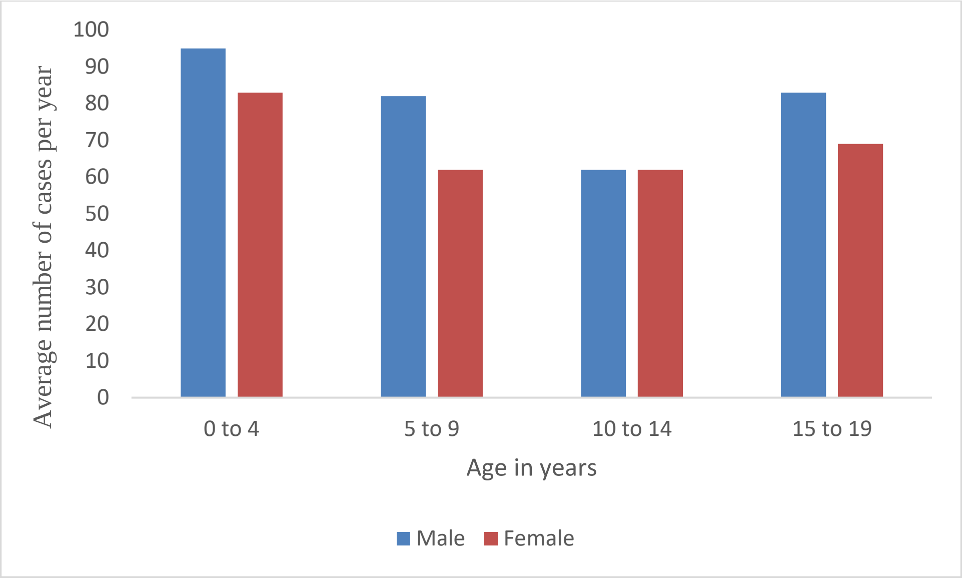

Figure 1.4 Average number of new CNS tumour cases per year in the UK between 2012-2014 (figure adapted from (Cancer Research UK).

1.4 Medulloblastoma

MB is the most common malignant brain tumour and is responsible for 10% of childhood cancer deaths (Pizer and Clifford, 2009; Caracciolo and Giordano, 2012; Jones *et al.*, 2012). It occurs more commonly in males (1.7:1) with a peak incidence between 4 and 7 years of age. MBs develop from the posterior fossa, usually arising in the roof of the fourth ventricle, located in the cerebellar vermis (Figure.1.5) (Pizer and Clifford, 2008; Pizer and Clifford, 2009). However, tumours may also arise from the cerebellar hemispheres. MB has the ability to metastasise, usually via the cerebrospinal fluid (CSF) pathways and metastases are found in approximately 35% of patients at diagnosis (Pizer and Clifford, 2008).

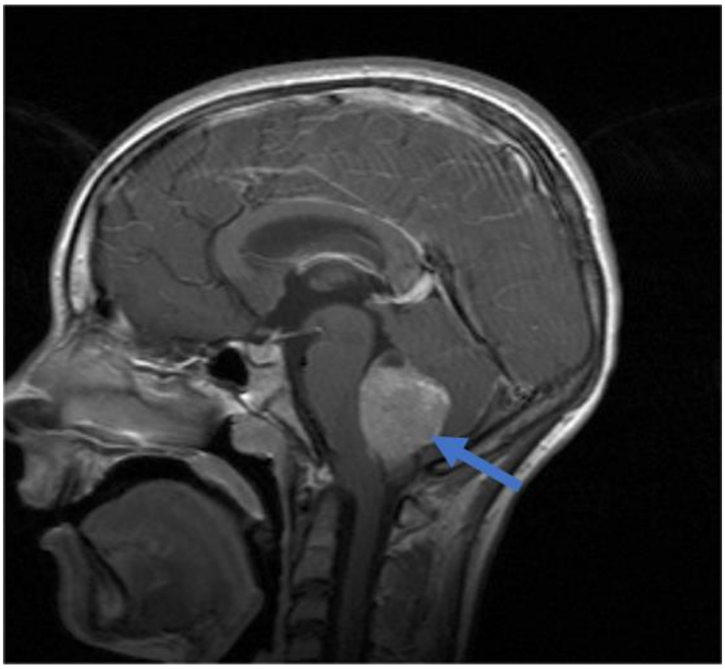

Figure 1.5 Medulloblastoma: T1-weighted sagittal MRI scan following gadolinium administration, showing tumour in the fourth ventricle (Pizer and Clifford, 2009).

1.4.1 Histology of medulloblastoma

MB is a heterogeneous tumour with five main histological subtypes; classic, desmoplastic/ nodular, MB with extensive nodularity (MBEN), large cell and anaplastic (large cell and anaplastic histology are normally grouped together and referred to as large cell anaplastic (LCA)) (Gilbertson and Ellison, 2008; Swartling *et al.*, 2010; Caracciolo and Giordano, 2012; Louis *et al.*, 2016b; Louis *et al.*, 2016a). Classical MB (80%) is defined by small cells with round to oval nuclei, an increased amount of chromatin found within the fibrillary matrix with minimal cytoplasm and with elevated and visible mitotic and apoptotic activity (Gilbertson and Ellison, 2008; Pizer and Clifford, 2008; Swartling *et al.*, 2010; Caracciolo and Giordano, 2012). Nuclear rosettes also referred to as Homer-Wright rosettes may be seen (Gilbertson and Ellison, 2008; Caracciolo and Giordano, 2012). The desmoplastic/ nodular subtype (15%) is defined by cells with a round appearance within pale nodules (Swartling *et al.*, 2010; Caracciolo and Giordano, 2012). Tumour cells in the nodules are less densely packed and pleomorphic than cells in the internodular/desmoplastic regions (Ellison, 2002). MBEN is defined by small neoplastic cells with distinct nodular structures and neuronal differentiation and occurs mainly in infants (Louis *et al.*, 2007; Caracciolo and Giordano, 2012). The LCA (17%) subtype consists of large cells with enlarged nuclei, nuclear pleomorphism increased mitotic rates and increased cell death rate (Figure. 1.6) (Ellison, 2010; Swartling *et al.*, 2010).

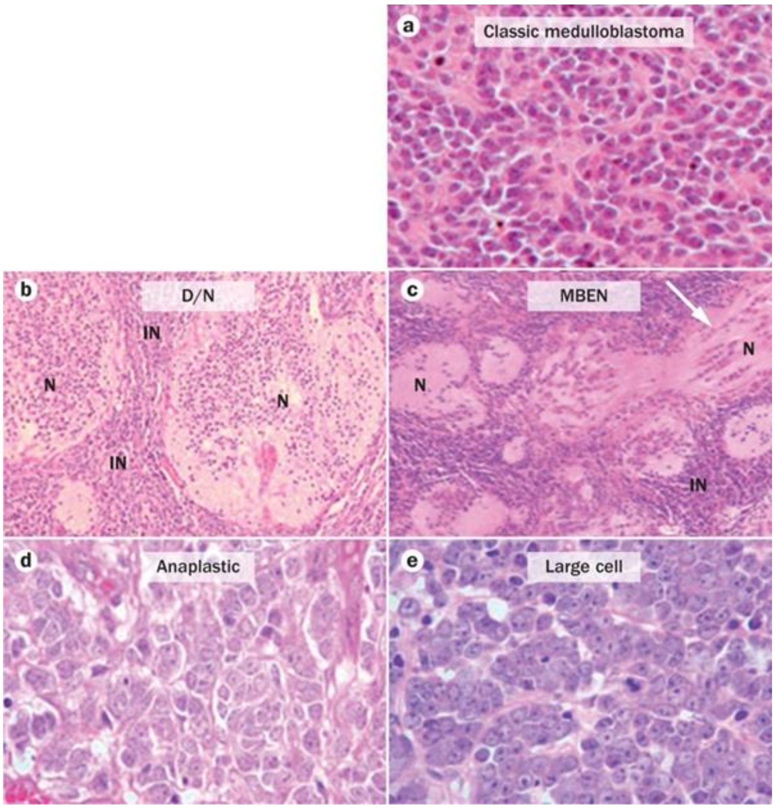

Figure 1.6 Histopathological variants of medulloblastoma (taken from (Gajjar and Robinson, 2014). A) Classic MB variant is defined by masses of small cells. B) Microscopic image showing desmoplastic/nodular MB histology, this histology is characterized by nodules (N) and internodules (IN). C) Microscopic image showing MBEN histology, this variant is very similar to desmoplastic/nodular MB histology as it also contains nodules (N) and internodules (IN). However, MBEN has more nodules (N) in the tissue section and these regions are filled with a fusion of cells (indicated by the arrow). D) Anaplastic MB histological pattern displays an increased mitotic rate and increased cell death rates. E) Large cell MB histological pattern consists of enlarged and prominent nucleoli (Gajjar and Robinson, 2014).

1.4.2 Risk stratification of medulloblastoma

The current risk stratification of MB is based on age, the extent of surgical resection, the presence of metastatic disease and the histological variant (Pei *et al.*, 2016). Metastatic disease is classified according to the modified Chang staging system; this consists of five stages M0, M1, M2, M3 and M4 (Table 3). MB patients over the age of 3 are either deemed standard risk or high risk. The standard risk group are those children diagnosed at 3 years of age or older with no metastatic disease at the time of diagnosis and with a tumour that is completely or near completely surgically resected (less than 1.5cm^2) (Pizer and Clifford, 2008; Dhall, 2009; Pizer and Clifford, 2009) and with no evidence of LCA histology (Hwang and Packer, 2013). The higher risk group are patients with either metastatic disease (M1 to M4) at diagnosis, residual tumour greater than 1.5cm^2 after surgery or have LCA histology (Table 4) (Pizer and Clifford, 2008; Dhall, 2009; Pizer and Clifford, 2009). Children less than 3 years of age at the time of diagnoses are also classified as high risk (Pizer and Clifford, 2008; Nikitovic and Golubicic, 2013). The World Health Organization describes the classification of MB using combined histological and molecular features that aids in prognostic and therapeutic approaches (Table 5) (Louis *et al.*, 2016a).

Staging	**Description**
M0	No evidence of gross subarachnoid or hematogenous metastasis
M1	Microscopic tumour cells formed in cerebrospinal fluid
M2	Gross nodular seeding demonstrated in cerebellar,cerebral subarachnoid space, or in the third or lateral ventricles
M3	Gross nodular seeding in spinal subarachnoid space
M4	Metastasis outside the cerebrospinal axis

Table 3: Chang staging system, taken from (Laurent et al., 1985)

Favourable risk	
Histology	Desmoplasia in patients <3 years old
Biology	Wnt/Wg pathway activation (β-catenin nuclear stabilisation)
Adverse risk	
Clinical/radiological	Age <3 years and non desmoplastic
	Metastatic disease
	Post-surgical residual disease >1.5 cm^2
Histology	Large-cell
	Severe and diffuse anaplasia
Biology	*MYC/MYCN* gene amplification

Table 4: Medulloblastoma: currently accepted prognostic factors, adapted from (Pizer and Clifford, 2008)

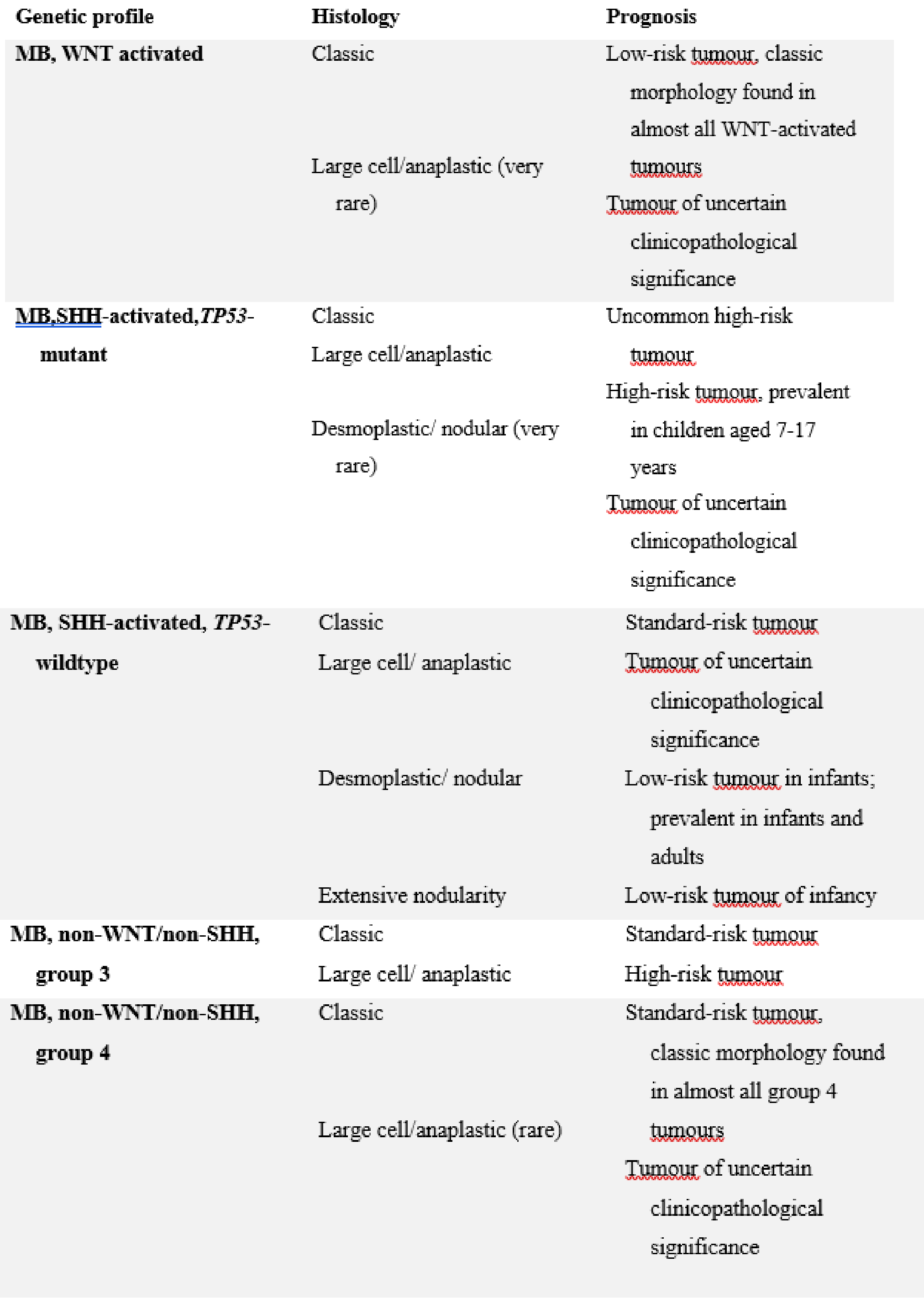

Genetic profile	Histology	Prognosis
MB, WNT activated	Classic	Low-risk tumour, classic morphology found in almost all WNT-activated tumours
	Large cell/anaplastic (very rare)	Tumour of uncertain clinicopathological significance
MB,SHH-activated,*TP53*-mutant	Classic	Uncommon high-risk tumour
	Large cell/anaplastic	High-risk tumour, prevalent in children aged 7-17 years
	Desmoplastic/ nodular (very rare)	Tumour of uncertain clinicopathological significance
MB, SHH-activated, *TP53*-wildtype	Classic	Standard-risk tumour
	Large cell/ anaplastic	Tumour of uncertain clinicopathological significance
	Desmoplastic/ nodular	Low-risk tumour in infants; prevalent in infants and adults
	Extensive nodularity	Low-risk tumour of infancy
MB, non-WNT/non-SHH, group 3	Classic	Standard-risk tumour
	Large cell/ anaplastic	High-risk tumour
MB, non-WNT/non-SHH, group 4	Classic	Standard-risk tumour, classic morphology found in almost all group 4 tumours
	Large cell/anaplastic (rare)	Tumour of uncertain clinicopathological significance

Table 5: Summary of the most common integrated medulloblastoma diagnosis, with clinical correlations, taken from (Louis et al., 2016b)

1.4.3 Clinical presentation of medulloblastoma

The majority of children present with signs and symptoms of raised intracranial pressure usually caused by obstruction to CSF flow at the cerebral aqueduct and/or fourth ventricle (Cassidy *et al.*, 2000; Pizer and Clifford, 2008). These signs and symptoms may include headaches (especially early morning), vomiting, lethargy, and drowsiness combined with swelling of the optic disc (papilloedema) (Pizer and Clifford, 2008) (Younas, 2011). Other symptoms may include double vision (diplopia) and uncontrolled movement of the eyes (nystagmus) (Cassidy *et al.*, 2000). Children may also present with in-coordination (ataxia) due to involvement of the cerebellum (ataxia) (Pizer and Clifford, 2008; Samano *et al.*, 2010). Younger patients may present with irritability, paralysis of upward gaze 'setting sun eyes' and an increase in head circumference (Piatt, 2004; Pizer and Clifford, 2008).

1.4.4 Treatment of medulloblastoma

The current treatment for MB involves surgical resection, radiotherapy and chemotherapy (Kool *et al.*, 2008; Northcott *et al.*, 2012b; Gerber *et al.*, 2014).

1.4.4.1 Surgery

Surgery remains the initial primary treatment for MB patients (Crawford *et al.*, 2007; Pizer and Clifford, 2008). The goals of surgery are to achieve total or near total resection of the primary tumour and to reestablish the CSF flow (Bartlett *et al.*, 2013; Gerber *et al.*, 2014). Studies have shown that total resection prolonged survival rates (Collange *et al.*, 2016). A number of complications can occur as a result of surgery which include aspetic and septic meningitis, bleeding, pseudomeningocele, CSF leakage and transient diabetes insipidus. In addition to these complications, posterior fossa syndrome occurs in 20-25% of all patients (De Braganca and Packer, 2013; Gerber *et al.*, 2014), the aetiology of which is not clearly understood. It normally manifests 24-48 hours after surgery, the predominant symptom being the patient's inability to speak. In addition ataxia, motor weakness, swallowing difficulties and mood disorders may occur and these symptoms may persist for months (Korah *et al.*, 2010; Bartlett *et al.*, 2013; Gerber *et al.*, 2014).

1.4.4.2 Radiotherapy

Craniospinal radiotherapy (CSRT) with a boost to the posterior fossa is given 4-6 weeks after surgery for average risk patients (Taylor *et al.*, 2004; Bartlett *et al.*, 2013; Taylor *et al.*, 2014(Mascarin *et al.*, 2015), if it commences >49 days after surgery it adversely influences the prognosis (Taylor *et al.*, 2004; Bartlett *et al.*, 2013; Taylor *et* *al.*, 2014). Side effects of radiotherapy include cognitive decline, hearing loss, growth impairment, cardiomyopathy, endocrine disorders and possible cataract development. Patients also have a higher risk of developing a second cancer (Fossati *et al.*, 2009; Anchineyan *et al.*, 2014). Radiotherapy is conventionally given daily from a Monday to Friday for up to 30 fractions. Hyperfractionated radiation therapy (HFRT) has been trialed in Europe, this form of treatment divides the total dose of radiation into two smaller dosages, allowing an increased dose to the tumour, but limiting the effects on healthy nervous tissue (Pizer and Clifford, 2008). Lannering *et al.* compared HFRT versus standard fractioned radiotherapy followed by the usual chemotherapy regimen (eight cycles of cisplatin, lomustine (CCNU) and vincristine). The results showed no difference in survival rate between the two methods (Lannering *et al.*, 2012). Radiotherapy alone combined with surgery results in a survival rate above 60% for standard risk patients (Carrie *et al.*, 2009). Hyperfractioned Accelerated Radiotherapy (HART) has been trialed in MB patients with metastatic disease. This type of treatment is administered twice per day in smaller doses. At the end of the study it was concluded that patients with high risk MB tolerated HART treatment with or without vincristine well (Taylor *et al.*, 2014).

1.4.4.3 Chemotherapy

Chemotherapy is used to treat all MB patients and is normally administered during and after radiation therapy. In infants, chemotherapy is used to postpone or avoid the use of radiation therapy (Ruggiero *et al.*, 2010; Bartlett *et al.*, 2013) or before radiotherapy in high risk MB patients (Verlooy *et al.*, 2006). The most common drugs used are cisplatin, vincristine, CCNU, cyclophosphamide and etoposide (Crawford *et al.*, 2007). Favorable results were shown by Packer *et al.* in a phase III trial, where treatment consisted of CSRT delivered at 23.4Gy and radiation therapy delivered to the posterior fossa at 55.8Gy. Patients also received vincristine during radiotherapy followed by either one of the two regimens, the first regimen consisted of vincristine, cisplatin and CCNU, and the second regimen consisted of vincristine, cisplatin and cyclophosphamide. These treatments achieved a 5 year event free survival (EFS) of ± 82% and overall survival (OS) of ± 87% for regimen A and for regimen B an EFS of ± 80% and OS of ± 85% (Packer *et al.*, 2006). The PNET 3 trail compared the use of chemotherapy before radiotherapy versus radiotherapy only, patients who received pre radiotherapy chemotherapy achieved a significantly better 3 year EFS of 78.5% whereas patients who only received radiotherapy EFS was 64.8% (Taylor *et al.*, 2003).

The pediatric oncology group (POG 9031) investigated whether pre or post irradiation chemotherapy would improve high risk patients EFS rates. The results showed very similar EFS (66% versus 70%) (Tarbell *et al.*, 2013).

1.4.4.4 Treatment for standard and high risk medulloblastoma patients

Standard risk patients receive 23.4 Gy of CSRT plus a boost to the posterior fossa, for a total of 54-55.8 Gy to the tumour bed. Chemotherapy is given after the completion of radiotherapy and in many cases during radiotherapy treatment (Pizer and Clifford, 2009; Gerber *et al.*, 2014). A number of regimens may be used, a common one forming the current European trials include vincristine, cisplatin and either CCNU (Packer regimen) or cyclophosphamide. In the PNET 4 trial this treatment regimen resulted in a 5 year progression free survival (PFS) and OS rate > 80% (Lannering *et al.*, 2012; Gerber *et al.*, 2014). Patients with high risk MB are treated with a number of protocols which usually involve higher dose of radiation (once daily or hyperfractionated) and high dose chemotherapy (Tabori *et al.*, 2010). Patients with high risk MB have a survival of 50-65% (Ramaswamy *et al.*, 2016).

1.4.4.5 Treatment for infants and children less than 3 years of age

Infants with MB remain a clinical challenge with a poorer survival rate than older children. The use of radiotherapy in the developing brain results in more severe radiation induced side effects and as a result CSRT is very rarely used in this age group (Dhall, 2009). Chemotherapy regimens are administered to infants and toddlers below the age of 3, which will either avoid the use of radiotherapy or use focal conformal radiotherapy (Gajjar and Pizer, 2010).

1.4.4.6 Treatment for relapse patients

Treatment strategies that have been tried for patients that relapse have involved surgery, radiotherapy and myeloablative chemotherapy with stem cell rescue (Dhall, 2009). Apart from infants who have not received previous radiotherapy the outlook for relapsed disease is poor (Hill *et al.*, 2015). The type of treatment strategies used are dependent on three factors, namely the age of the patient, the degree of the disease at the time of relapse and the treatment used in the first diagnosis (Dhall, 2009). Infants can be rescued by surgery and radiotherapy either with or without high dose chemotherapy, if they had a local relapse and were not previously irradiated (Pizer *et al.*, 2011), but in cases where patients have received craniospinal irradiation and relapsed, 95% do not respond to the conventional treatment and go on to die from their disease (Gajjar and Pizer, 2010).

1.4.5 Genetics aberrations of medulloblastoma

The first understanding of the genetics of MB was through two heritable congenital cancer syndromes, Gorlin and Turcot syndrome (Dhall, 2009; Northcott *et al.*, 2012b), another heritable cancer syndrome, Li-Fraumeni syndrome (LFS) has given further insight (Pfister *et al.*, 2010).

Gorlin syndrome, also referred to as nevoid basal cell carcinoma syndrome, is inherited in an autosomal dominant manner (Hahn *et al.*, 1996; Pomeroy *et al.*, 2002; Dhall, 2009), characterized by multiple abnormalities such as bone deformation, skin and neurological disorders (Shirisha Rani *et al.*, 2013; Singh *et al.*, 2014) as well as being a cancer predisposition syndrome in which 3 to 5% of patients develop MB (Dhall, 2009). It results from a mutation in the patched 1 (*PTCH1*) tumour suppressor gene located on chromosome 9q22.3 (Archer *et al.*, 2012; Northcott *et al.*, 2012b). The transmembrane protein PTCH1 has a function in the sonic hedgehog signaling pathway (Raffel, 2004; Archer *et al.*, 2012), a pathway which plays an important role in cerebellar genesis and maturation (De Luca *et al.*, 2016). In the presence of sonic hedgehog protein, smoothened (SMO) is released from its binding with PTCH1. Unbound SMO then triggers the release of the transcription factors, glioma-associated oncogene homologue (GLI1, GLI2, GLI3) which results in transcription of several genes (Huang and Yang, 2015). In MB defects found in the SHH pathway include mutations of *PTCH1*, *SUFU*, activating mutations of *SMO* (Pizer and Clifford, 2009) and amplification of *GLI1* and *GLI2* (Brugieres *et al.*, 2012) . Mutations in the SHH pathway occurs in about 25 % of sporadic MB cases (Ellison *et al.*, 2011).

Patients with Turcot syndrome have an increased risk of developing colorectal cancer and CNS tumours including MB (Dhall, 2009; Northcott *et al.*, 2012b). The adenomatous polyposis (*APC*) gene pathway which controls the levels of β-catenin is mutated in Turcot syndrome (Northcott *et al.*, 2012b). The cell membrane receptor known as frizzled controls the APC complex, the binding of fizzled to wingless causes the stimulation of the wingless pathway as well as the phosphorylation of the disheveled protein (Figure.1.7). Disheveled causes inhibition of proteins in the APC complex which increases the levels of cytoplasmic β-catenin, resulting in an increase in nuclear translocation where it stimulates transcription of numerous oncogenes (Dhall, 2009). *CTNNB1* (70-90% of WNT MB cases) (Li *et al.*, 2013) the gene coding for β-catenin and other genes involved in the wingless pathways, such as *APC* (2.5% of cases), *AXIN1(*2.5% of cases) and *AXIN2* (2.5% of cases) are found to be mutated in MB (Pizer and Clifford, 2009).

In addition, patients with Li-Fraumeni syndrome (LFS) have an increased risk of developing sonic hedgehog (SHH) MB (Pfister *et al.*, 2010; Kool *et al.*, 2014) . These patients have a germline *TP53* mutation, *TP53* is found to be mutated in 10% of MB cases (Roussel and Hatten, 2011). Inactive p53 tumour suppressor can lead to tumourgenesis due to its inability to initiate cell cycle arrest, DNA repair, senescence and cell death (Rivlin *et al.*, 2011; Rausch *et al.*, 2012). Patients with this mutation have an increased susceptibility to excessive toxicity from radiotherapy and DNA damaging chemotherapy (Schroeder and Gururangan, 2014).

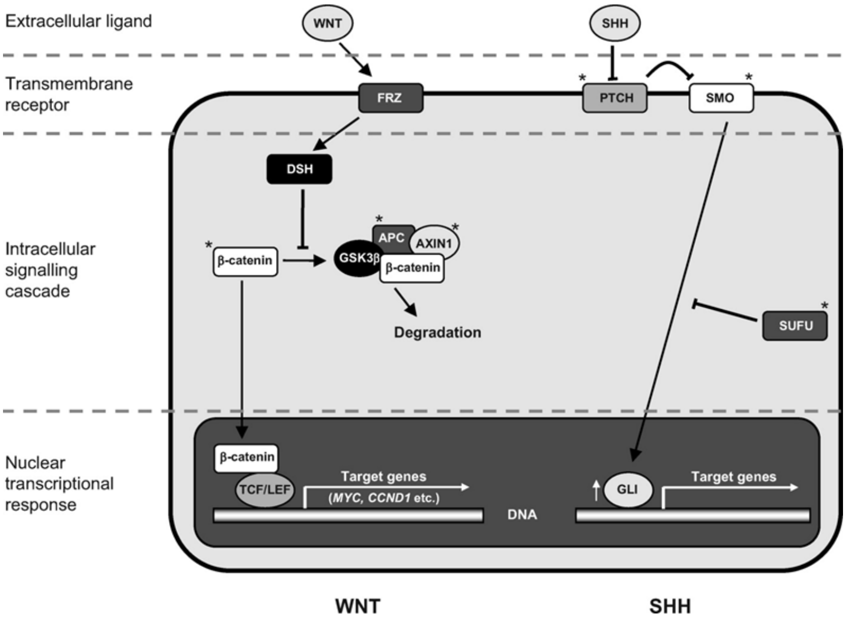
Extracellular ligand
Transmembrane receptor
Intracellular signalling cascade
Nuclear transcriptional response
WNT
SHH
FRZ
*
PTCH
SMO
*
DSH
*
APC
AXIN1
*
*
β-catenin
GSK3β
β-catenin
Degradation
SUFU
*
β-catenin
TCF/LEF
Target genes
(MYC, CCND1 etc.)
DNA
GLI
Target genes
WNT
SHH

Figure 1.7 The Wingless and Sonic Hedgehog signaling pathway in medulloblastoma. Stimulatory effects indicated by pointed arrows and inhibitory effects indicated by blunt arrows.*Mutations reported in specific proteins associated with pathway activation, taken from (Przer and Clifford, 2009). Frizzled (FRZ); dishevelled (DSH); adenomatous polyposis (APC); T cell factor/lymphoid enhancer factor-1 (TCF/LEF); patched (PTCH); smoothened (SMO); suppressor of fused (SUFU).

1.4.6 Advances in medulloblastoma genomics

The advancement in genomic, transcriptomic and methylomic profiling has led to the identification of MB subgroups (Thompson *et al.*, 2006; Kool *et al.*, 2008; Northcott *et al.*, 2011; Schwalbe *et al.*, 2011; Taylor *et al.*, 2012; Schwalbe *et al.*, 2013b). Researchers identified MB subgroups by means of gene expression profiling and subsequent algorithmic clustering (Thompson *et al.*, 2006; Kool *et al.*, 2008; Northcott *et al.*, 2011). DNA methylation profiling has identified the existence of four methylomic subgroups, which correlate with established MB subgroups (MB_{WNT}, MB_{SHH}, MB_{GRP3} and MB_{GRP4}) based on transcriptomic, molecular and clinic-pathological factors. This showed that DNA methylation allows for robust subclassification of MB subgroups in either formalin fixed or frozen biopsy material (Schwalbe *et al.*, 2013b). Hovestadt *et al*. have developed an effective and robust microarray assay that enables genome wide screening of CpG islands methylation (Hovestadt *et al.*, 2013). Northcott et al. have established an immunohistochemical assay that can identify MB subgroups using four novel antibodies; DKK1 (MB_{WNT}), SFRP1 (MB_{SHH}), NPR3 (MB_{GRP3}) and KCNA1 (MB_{GRP4}). Classification using this approach was possible in 98% of the formalin fixed biopsy material (Northcott *et al.*, 2011). Other approaches included a 13- gene mRNA expression signature assay that reproducibly identifies MB subgroups (Schwalbe *et al.*, 2011) and a nanostring technique using small amounts of RNA (Northcott *et al.*, 2012c).

1.4.7 Medulloblastoma subgroups

MB has been classified by consensus into four distinct subgroups each having their own demographics, DNA copy number aberrations, histopathology and clinical outcomes (Northcott *et al.*, 2011; Taylor *et al.*, 2012). These subgroups are known as WNT (MB_{WNT}), SHH (MB_{SHH}), Group 3 (MB_{GRP3}), and Group 4 (MB_{GRP4}). The MB_{WNT} and MB_{SHH} groups obtained their name through the involvement of these signaling pathways in their pathogenesis, MB_{GRP3} and MB_{GRP4} have generic names as the biology of these subgroups has yet to be fully classified (Taylor *et al.*, 2012). A summary of molecular and clinical features of each subgroup is presented in Table 6.

MB_{WNT} occurs equally in males and females and occurs at all ages but is rare in infants (Taylor *et al.*, 2012). Patients in this subgroup have a good prognosis compared to the other three subgroups, with a survival rate of approximately 90% (Taylor *et al.*, 2012; Roussel and Robinson, 2013). The majority of MB$_{WNT}$ subgroup patients have classic tumour histology (Northcott *et al.*, 2012b; Taylor *et al.*, 2012; Roussel and Robinson, 2013); however, few cases have been seen where patients have LCA histology (Taylor *et al.*, 2012; Li *et al.*, 2013). The characteristic abnormalities of these tumours are mutations in *CTNNB1*, intense nuclear staining for β-catenin on immunohistochemistry and a deletion of one copy of chromosome 6 (monosomy 6) (Clifford *et al.*, 2006; Taylor *et al.*, 2012). The mutation in *CTNNB1* leads to abnormal activation of the WNT pathway which results in an increase in nuclear β-catenin (Clifford *et al.*, 2006). Data from a MB$_{WNT}$ mouse model has suggested that these tumours develop from the lower rhombic lip of the cerebellum (Gibson *et al.*, 2010; Kawauchi *et al.*, 2012; Taylor *et al.*, 2012).

MB$_{SHH}$ subgroup tumours occur most commonly in infants between the age of 0-3 years and in those greater than 16 years of age with a male: female ratio of 1:1. (Taylor *et al.*, 2012; Roussel and Robinson, 2013). This subgroup's histology may be nodular desmoplastic, MBEN, LCA or classical (DeSouza *et al.*, 2014). The prognosis of the patients in this subgroup is intermediate; infants and younger children have a better outcome than adults (Schroeder and Gururangan, 2014). Metastatic disease is rare in this subgroup, but if present it is associated with other poor prognostic factors such as LCA and older age at diagnosis (Roussel and Robinson, 2013). Abnormal signaling occurs in the SHH pathway and mutations in *PTCH1*, *SMO*, *SUFU*, *TP53* and amplification of *GLI2* and *MYCN* and deletion of chromosome 9q is most frequently seen in this MB subgroup (Taylor *et al.*, 2012; Kijima and Kanemura, 2016) Mouse models have suggested that SHH subgroup tumours originate from the granule neuron precursor cells (Gibson *et al.*, 2010; Roussel and Hatten, 2011; Kawauchi *et al.*, 2012).

MB$_{GRP3}$ tumours exhibit classic and LCA histology, occur more frequently in males, and are found most commonly in infants and children and rarely in adults (Taylor *et al.*, 2012). This subgroup is associated with a poor prognosis and metastatic disease, and accounts for between 25 and 30% of MB (Roussel and Robinson, 2013). Group 3 is frequently *MYC* amplified (15% of cases) (Li *et al.*, 2013) , is likely to show chromosome 1q gain, and/or loss of chromosome 5q, 10q and isochromosome 17q (Taylor *et al.*, 2012). MYC-driven mouse models have been developed, there are two orthotopic transplantation models that were developed by either infecting inactive

Trp53 cerebellar stem or progenitor cells with Myc (Pei et al., 2012). The third model is a Glt1-tTA, TRE-MYCN/Luc transgenic mice model (Swartling *et al.*, 2010) . Even though *TP53* is not mutated in this subgroup, these models require a deficient p53 to develop the phenotype similar to human MB$_{GRP3}$. These mouse models serve as a useful tool to study the biology of this subgroup as well as to test potential therapeutic options (Northcott *et al.*, 2012b).

MB$_{GRP4}$ tumours exhibit classic and LCA histology, have an intermediate prognosis, are normally associated with metastatic disease and account for ~ 30% of MB cases. This subgroup has a higher incidence in males (Taylor *et al.*, 2012) and occurs mostly in children but may be found in adults (Roussel and Robinson, 2013). This subgroup may demonstrate amplification of *MYCN* and/or *CDK6*, and isochromsome 17q is observed in most cases. The loss of one X chromosome in females is also seen in this subgroup (Northcott *et al.*, 2012b; Min *et al.*, 2013; Schroeder and Gururangan, 2014). MB$_{GRP4}$ have overexpression of genes involved in neuronal differentiation and development; however, the causal link between these genes and the biology of this tumour has not yet been established. No known mouse models have yet been developed (Taylor *et al.*, 2012)

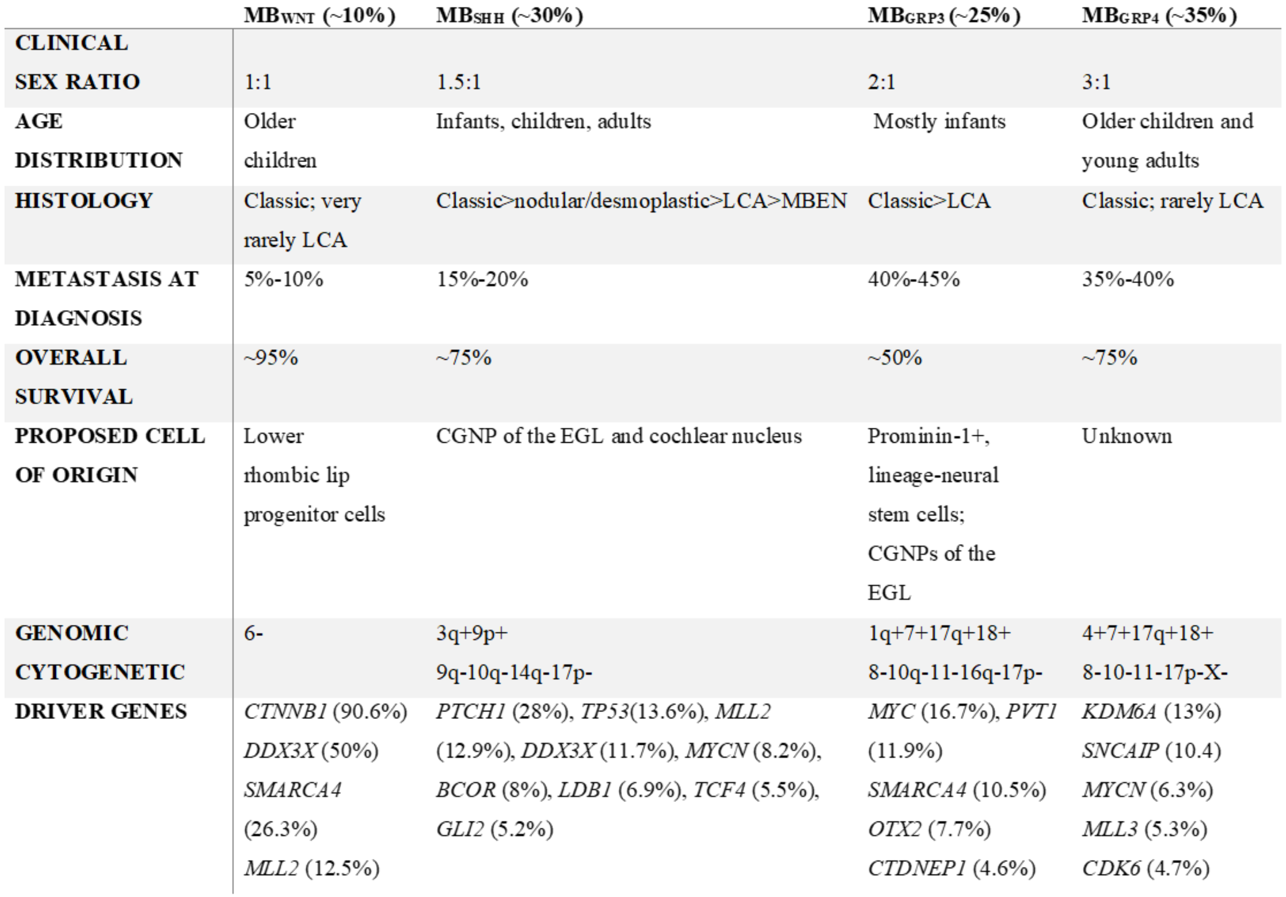

	MB_{WNT} (~10%)	MB_{SHH} (~30%)	MB_{GRP3} (~25%)	MB_{GRP4} (~35%)
CLINICAL				
SEX RATIO	1:1	1.5:1	2:1	3:1
AGE DISTRIBUTION	Older children	Infants, children, adults	Mostly infants	Older children and young adults
HISTOLOGY	Classic; very rarely LCA	Classic>nodular/desmoplastic>LCA>MBEN	Classic>LCA	Classic; rarely LCA
METASTASIS AT DIAGNOSIS	5%-10%	15%-20%	40%-45%	35%-40%
OVERALL SURVIVAL	~95%	~75%	~50%	~75%
PROPOSED CELL OF ORIGIN	Lower rhombic lip progenitor cells	CGNP of the EGL and cochlear nucleus	Prominin-1+, lineage-neural stem cells; CGNPs of the EGL	Unknown
GENOMIC CYTOGENETIC	6-	3q+9p+ 9q-10q-14q-17p-	1q+7+17q+18+ 8-10q-11-16q-17p-	4+7+17q+18+ 8-10-11-17p-X-
DRIVER GENES	*CTNNB1* (90.6%) *DDX3X* (50%) *SMARCA4* (26.3%) *MLL2* (12.5%)	*PTCH1* (28%), *TP53*(13.6%), *MLL2* (12.9%), *DDX3X* (11.7%), *MYCN* (8.2%), *BCOR* (8%), *LDB1* (6.9%), *TCF4* (5.5%), *GLI2* (5.2%)	*MYC* (16.7%), *PVT1* (11.9%) *SMARCA4* (10.5%) *OTX2* (7.7%) *CTDNEP1* (4.6%)	*KDM6A* (13%) *SNCAIP* (10.4) *MYCN* (6.3%) *MLL3* (5.3%) *CDK6* (4.7%)

Table 6: Summary of medulloblastoma subgroups showing clinical and molecular features, adapted from (Schroeder and Gururangan, 2014) (CGNP, cerebellar granular neuron precursor; EGL, external granular layer)

1.4.8 Recurrent and metastatic medulloblastoma

The survival rate for MB has improved over the years (Koschmann *et al.*, 2016) however, about 20-30% patients will relapse (Dunkel *et al.*, 2010). Relapsed patients whose initial treatment included radiotherapy has little chance of survival (Dunkel *et al.*, 2010) irrespective of re-treatment with surgery, radiotherapy, administering high dose chemotherapy with stem cell rescue (Ramaswamy *et al.*, 2013) or even enrolling the patient into phase I/II clinical trials (Ramaswamy *et al.*, 2013). When MB patients relapse the molecular subgroup at diagnosis is the same at relapse (Ramaswamy *et al.*, 2013; Hill *et al.*, 2015) regardless if it is a local recurrence or metastatic recurrence (Ramaswamy *et al.*, 2013). The relapse disease does behavior differently compared to disease at diagnosis (Kuzan-Fischer *et al.*, 2017), a study by Morrissy et al showed that the dominant clone at relapse differs to the dominant clone at presentation, therefore targeted strategies based on primary tumour is most likely to fail because the same targets might not be present (Morrissy *et al.*, 2016; Kuzan-Fischer *et al.*, 2017). A study by Hill *et al* showed that relapse patients acquires *MYC* gene family amplification along with P53 pathway defects. Relapsed patients with this combinational molecular defect has no chance of survival (Hill *et al.*, 2015). Treating recurrent MB patients is a challenge as there is no standard protocol (Wetmore *et al.*, 2014). Metastatic dissemination is responsible for a large proportion of deaths and treatment failures and at presentation metastatic dissemination occurs in about 30% of all patients. Metastases hardly occurs in MB_{WNT} however, it is found in 30% of $\text{MB}_{\text{SHH,}}$ 40-50% of MB_{GRP3} and 40% of MB_{GRP4}. MB metastases are understudied due to lack of samples because it is rarely biopsied (Kuzan-Fischer *et al.*, 2017).

1.4.9 Challenges of Group 3 medulloblastoma

MB_{GRP3} has the poorest 5 year survival rate ($\leq$ 50%) compared to the other subgroups (Figure 1.8) (Schroeder and Gururangan, 2014). It is unlikely that survival rates will be dramatically improved using current therapeutic strategies and, therefore, identification of novel therapeutic targets and molecular biomarkers are needed. An important feature of MB_{GRP3} is high levels of *MYC* expression and frequent *MYC* amplification (Henssen *et al.*, 2013; Roussel and Robinson, 2013; Morfouace *et al.*, 2014). The understanding of the phenotypic, genomic, transcriptomic and epigenomic effects of high levels of *MYC* expression in MB_{GRP3} may lead to identification of novel therapeutic strategies.

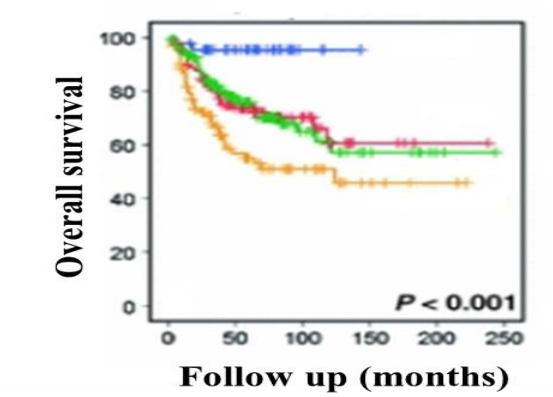

Figure 1.8 Kaplan-Meier plot of overall survival curves between the different medulloblastoma subgroups. MBWNT, blue; MBSHH, red; MBGRP3, yellow; MBGRP4, green. Figure was adapted from (Kool et al., 2012).

1.4.10 Genetic aberrations in Group 3 medulloblastoma

A few recurrent mutations for example *SMARCA4* (Jones *et al.*, 2012), *CTDNEP1* (Karajannis and Zagzag, 2015) were observed in this subgroup. However, MB_{GRP3} remains poorly defined unlike MB_{WNT} and MB_{SHH} (Northcott *et al.*, 2012a; Li *et al.*, 2013). In MB_{GRP3}, genes involved in controlling histone H3 lysine K27 trimethylation (H3K27me3), which is involved in the inhibition of gene transcription, have been found to be abnormally regulated (Li *et al.*, 2013). The polycomb repressive complex 2 (PRC2) controls H3K27me3 (Robinson *et al.*, 2012), and the methyltransferase known as enhancer of zeste (EZH) 2 is responsible for the maintenance of H3K27me3 marks and also form part of the PRC2 (Yoo and Hennighausen, 2012; Li *et al.*, 2013) and this plays a role in inhibiting gene expression (Yoo and Hennighausen, 2012). Both the lysine (K)-specific demethylase 6A (KDM6A) and KDM6B can reverse the inhibition of gene transcription (Li *et al.*, 2013). In MB_{GRP3} mutations have been found in 7 KDM family members; *KDM6A*, *KDM1A*, *KDM3A*, *KDM4C*, *KDM5A*, *KDM5B* and *KDM7A* (Robinson *et al.*, 2012; Li *et al.*, 2013). These mutations demonstrate that lysine demethylation is affected in this subgroup (Robinson *et al.*, 2012). In addition, *EZH2* overexpression and corresponding gain of chromosome 7q has been described in MB_{GRP3} by Robinson *et al*. Mutations have also been identified in *CHD7* and *ZMYM3* (Robinson et al., 2012*)* . It has thus been proposed that abnormal regulation of chromatin genes involved in histone methylation could play a major role in the development of MB$_{\text{GRP3}}$ (Li *et al.*, 2013).

1.4.11 Function of MYC in Group 3 medulloblastoma

MYC is overexpressed in many cancers and predominately associated with a poor clinical outcome. MB$_{\text{GRP3}}$ *MYC* expression is higher than in MB$_{\text{SHH}}$ and MB$_{\text{GRP4}}$ tumours but not than that in the MB$_{\text{WNT}}$ subgroup (Figure 1.9). High *MYC* expression in MB$_{\text{WNT}}$ subgroup is due to *MYC* being a downstream target of WNT signaling pathway (Roussel and Robinson, 2013). This increase in MYC expression happens when β-catenin translocate to the nucleus (process discussed in 1.4.5) it then binds to T-cell factor/lymphoid enhancer factor forming hetrocomplex that leads to increase of *MYC* transcription (Rogers *et al.*, 2009; Roussel and Robinson, 2013). The excellent prognosis of MB$_{\text{WNT}}$ despite high *MYC* expression remains unexplained, the influence of cellular context in which MYC expression occurs may be critical or MB$_{\text{GRP3}}$ may have additional defects which co-operate with MYC overexpression to drive an aggressive phenotype. Amplification of *MYC* occurs predominately in MB$_{\text{GRP3}}$ (10-17%) (Roussel and Robinson, 2013). Two Group 3 *MYC*- driven mouse models have been developed, the tumours which arise in these models are highly aggressive tumours with LCA histology (Pei *et al.*, 2012; Roussel and Robinson, 2013), and the removal of *MYC* causes the tumour to regress. LCA histology is frequently associated with *MYC* amplification (Stearns *et al.*, 2006). It has been proposed that this gene plays an important role in tumour initiation, development and maintenance (Roussel and Robinson, 2013).

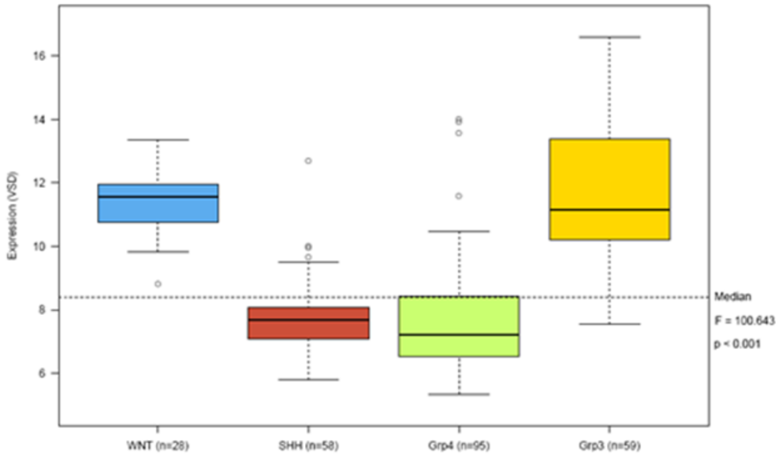

Figure 1.9 Representation of *MYC* expression across a cohort of 240 primary medulloblastoma (Figure done by Dr Matthew Selby).

1.5 MYC

1.5.1 MYC and its deregulation in cancer

This proto-oncogene *MYC* belongs to the *MYC* family of genes (MYC, MYCN, MYCL) (Dang, 2013). MYC was first identified through its relationship with the transforming gene (v-myc) in the avian myelocytomatosis virus MC29 (Nilsson and Cleveland, 2003; Valovka *et al.*, 2013). This transfactor regulates 10-15% of genes in the genome. MYC expression from transcription to a functional protein under normal conditions is tightly regulated (Tansey, 2014). For example MYC transcription is tightly regulated at the initiation and elongation step (Farrell and Sears, 2014) and translation is controlled and receptive to growth factor signaling (Farrell and Sears, 2014; Tansey, 2014), if failure occurs in any of these steps it could lead to tumourigenesis. For example, translocation in Burkitt's lymphoma, results in an increase in MYC production due to its coding sequences being regulated by the immunoglobulin µ heavy chain enhancer. This translocation is very rare in other cancers (Tansey, 2014), however a common abnormality observed in multiple cancers for example in breast, colorectal, lung is *MYC* amplification (Santarius *et al.*, 2010) and in MB overexpression and amplification of MYC occurs (Roussel and Robinson, 2013). Gene amplification is classified as a cellular process that causes an increase in copy number of a specific localized region of the chromosome arm (Albertson, 2006; Mukherjee and Storici, 2012; Matsui *et al.*, 2013). Amplicons can be identified either as intrachromosomal homogeneously staining regions or as extrachromosomal molecules known as double minutes (Mukherjee and Storici, 2012). Amplification has been proposed to occur through a mechanism that involves a double strand break (DSB) known as the breakage-fusion-bridge (BFB) cycle (Mukherjee and Storici, 2012) which occurs when the telomeres at the end of the chromosome erode and as a result the chromosomes fuse. During anaphase the two centromeres are pulled to opposite poles and break, the resulting chromosomes lack a telomere and can fuse again, leading to another dicentric chromosome, which again breaks during mitosis (Lo *et al.*, 2002; Albertson, 2006; Murnane, 2012). This cycle continues until the chromosome receives a telomere from a new chromosome by means of translocation (Albertson, 2006). Another process that can result in amplification of an oncogene is chromothripsis (Meyerson and Pellman, 2011; Korbel and Campbell, 2013). Chromothripsis can occur through many mechanisms, the micronucleus model is one of the proposed mechanisms. During this mechanism, the disintegration of a chromosome is thought to be a result of micronuclei production occurring due to errors in chromosome segregation during mitosis. DNA replication occurs at a slower rate in the micronucleus and when the chromosome is triggered to condense it breaks into small fragments (Forment *et al.*, 2012). Once chromothripsis occurs it is assumed that the cell triggers the DNA damage response (DDR) mechanism to rejoin the fragmented DNA pieces (Korbel and Campbell, 2013) primarily employing the nonhomologous end-joining repair system (Meyerson and Pellman, 2011; Holland and Cleveland, 2012). The new chromosome may have segments that are deleted, rearranged and the broken pieces can form circular double minute chromosomes (Figure 1.10) (Holland and Cleveland, 2012). Double minutes that contain an oncogene which has growth and survival advantages are retained by the cell and could become amplified (Forment *et al.*, 2012). Even though in cancer, amplification of an oncogene is the most frequent genetic change to occur, it does not always cause overexpression (Jia *et al.*, 2016).

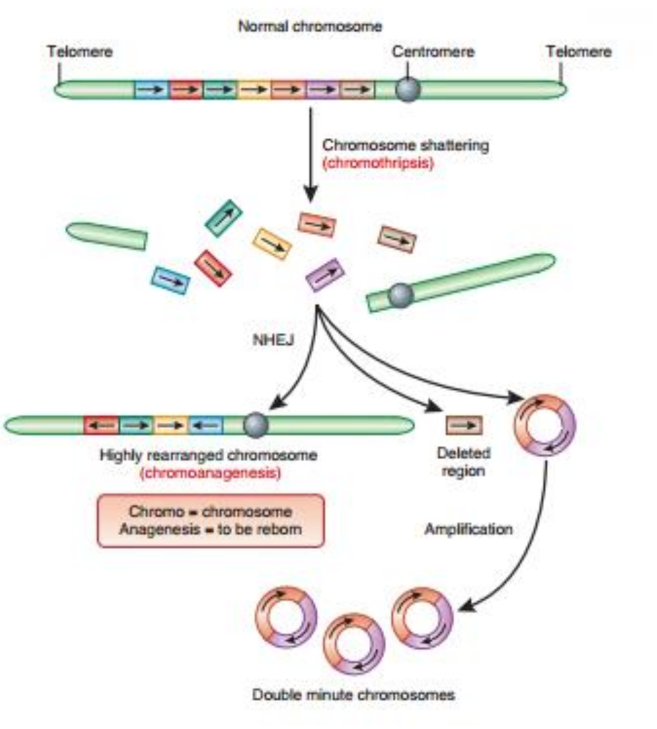
Normal chromosome
Telomere
Centromere
Telomere
Chromosome shattering
(chromothripsis)
NHEJ
Highly rearranged chromosome
(chromoanagenesis)
Chromo = chromosome
Anagenesis = to be reborn
Deleted region
Amplification
Double minute chromosomes

Figure 1.10 A systemic representation of the rearrangement of the chromosome by the non-homologous end joining repair system after chromothripsis. Taken from (Holland and Cleveland, 2012).

1.5.2 Structure of MYC

MYC is situated on chromosome 8q24 (Aquino *et al.*, 2013) and has one untranslated and two translated exons (Figure.1.11) (Facchini and Penn, 1998; Boxer and Dang, 2001; Buechner and Einvik, 2012). MYC has three different isoforms, one arising from a CUG start codon in exon 1, the second from a AUG start codon in exon 2 (Ryan and Birnie, 1996; Dang, 1999; Aquino *et al.*, 2013), and a third isoform which is 45kDa has been identified (Dang, 1999). The second isoform is 64kDa in size and is the most studied isoform, this isoform will be referred to as MYC (Facchini and Penn, 1998; Liao and Dickson, 2000) and responsible for many of MYC functional processes (Aquino *et al.*, 2013). Within the N-terminal region of MYC lies the transactivation domain (Ryan and Birnie, 1996; Andresen *et al.*, 2012) and two MYC boxes (I and II), the second MYC box plays an important role in many of MYC's cellular processes (Facchini and Penn, 1998; Tansey, 2014). Whereas the transactivation domain plays a role in transcriptional regulation (Ryan and Birnie, 1996; Andresen *et al.*, 2012). At the C- terminus lies the basic Helix-Loop-Helix/ Leucine Zipper (bHLH / Zip), which enables the binding of sequence specific DNA (Facchini and Penn, 1998; Tansey, 2014) (Figure 1.11).

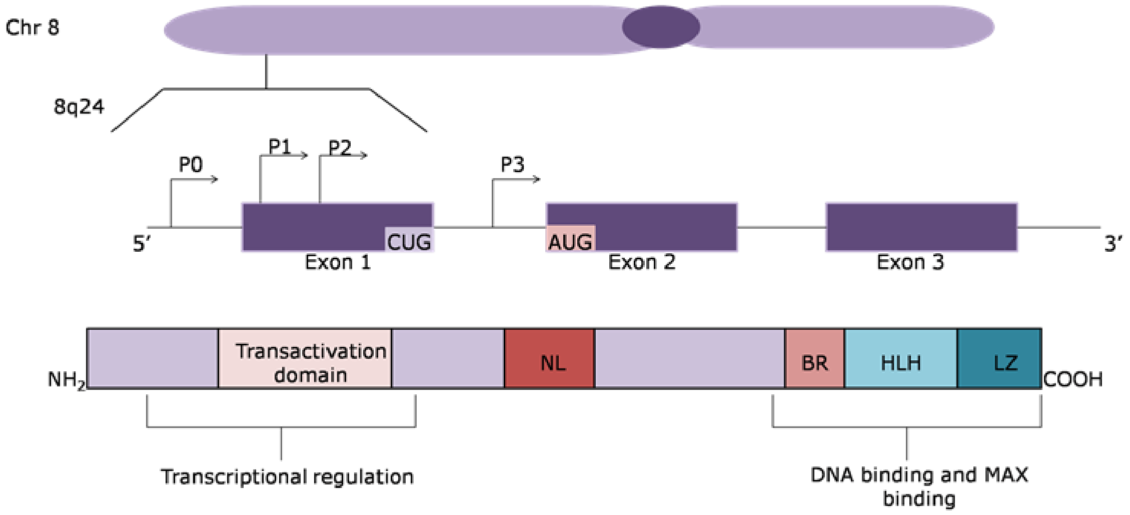

Figure 1.11 Structure of MYC and protein domains, adapted from (Aquino et al., 2013).

1.5.3 Transcriptional control by MYC

MYC binds to the transcription factor Max forming the MYC/ MAX complex that binds to Enhancer-box (E-box) regions which have a unique recognition DNA sequence - CACNNT (Buechner and Einvik, 2012; Lorenzin *et al.*, 2016); this interaction enables MYC to activate transcription. In contrast, MYC can also repress transcription through the ability of MAX to bind to MAD/MXI1 proteins. MYC can also suppress transcription through its binding with Miz-1. In addition, MYC can also regulate transcription through its interaction with two chromatin remodeling complexes, known as the ATP-dependent chromatin remodeling complex and the histone acetyl transferase (HAT) complex. The involvement with the HAT complex was through the discovery that MYC interacts with transactivation transformation associated protein (TRRAP), which is a member of two HAT complexes, known as STAGA and Tip60. Through this association MYC can also interact with individual members known as GCN5 which is part of the STAGA complex and Tip48/49 which is a member of the Tip60 complex (Amati *et al.*, 2001). MYC involvement with the ATP- dependent chromatin remodeling complex was identified through MYC's ability to interact with INI1, which is a member of the SWI/SNF complex (Amati *et al.*, 2001; Meyer and Penn, 2008).

1.5.4 MYC protein stability

MYC protein stability is controlled by various phosphorylation sites, two of them are situated within MYC box 1, known as Threonine 58 (Thr58) and Serine 62 (Ser62) (Vervoorts *et al.*, 2006). Upon mitogen stimulation and Ras activation, phosphorylation of S62 is initiated through the Extracellular Receptor Kinases (ERK) pathway, which leads to an increase in MYC protein stability. MYC protein stability is also increased by Ras inhibiting Glycogen Synthase kinase (GSK-3β) through the Phosphotidylinositol-3-OH kinase (PI_3K/AKT) pathway, thus preventing the phosphorylation of T58. GSK-3β is reactivated when the AKT signals decreases during the late G1 phase of the cell cycle (Adhikary and Eilers, 2005a) as a result phosphorylation of T58 is initiated as well as the removal of the phosphate residue from S62 by protein phosphatase 2A. The phosphorylated T58 is recognized by the E3 ubiquitin ligase SCF^{fbw7} which then stimulates MYC ubiquitination and prepares it for proteasomal degradation (Wang *et al.*, 2011).

1.5.5 Biological functions of MYC

1.5.5.1 Role of MYC in cell cycle and proliferation

Studies have shown that under normal conditions, MYC plays an important role in starting and regulating the progression of cells through the cell cycle (Dominguez-Sola and Gautier, 2014). Quiescent cells have very low levels of *MYC* expression but upon mitogenic stimulation MYC increases, moving the cells in to the cell cycle (de Alboran *et al.*, 2001; Pelengaris *et al.*, 2002). Expression levels then decrease to a level that still enables the progression of cells through the cell cycle (de Alboran *et al.*, 2001). Cells go into growth arrest when *MYC* levels are untraceable due to the removal of stimulation factors (Pelengaris *et al.*, 2002), in addition without growth factors quiescent cells can move into the cell cycle when MYC expression is enforced (Tansey, 2014). The ability of MYC to modulate the cell cycle is most likely due to MYC's ability to regulate genes involved in this process (de Alboran *et al.*, 2001), for example increased MYC can accelerate the cycling of cells through the G1 phase by upregulating the cyclin dependent kinases, such as cyclin D2, D3, E1 and E2 (Bretones *et al.*, 2015) and CDC25A, E2F1 and E2F2 (Meyer and Penn, 2008). MYC can restrain cell cycle progression by inhibiting P21$^{CIP1/WAF1}$, P27^{KIP1} (Bretones *et al.*, 2015), Gadd45 and Gas1 (Rohban and Campaner, 2015).

1.5.5.2 Role of MYC in apoptosis

The specific apoptotic pathway initiated by MYC is cell type dependent (Ryan and Birnie, 1996). MYC can drive apoptosis through cytochrome C release and via the alternative reading frame (ARF)/p53 pathway (Leone *et al.*, 2001) by causing an imbalance between proteins that are pro-apoptotic and anti-apoptotic. Studies have shown that MYC can simultaneously inhibit or stimulate the expression of members of the BH3-only category of the Bcl-2 family of proteins, for example during lymphomagenesis MYC simultaneously inhibit Bcl-2 and Bcl-X(L) while activating Bim. The release of Bim facilities the release of cytochrome C from the mitochondria and thereby initiates the apoptotic process. MYC can also stimulate Bax resulting in apoptosis through cytochrome C release and caspases (Tansey, 2014). As mentioned before MYC causes apoptosis through the ARF/p53 pathway by elevating p19^{ARF} expression (Eischen *et al.*, 2001). As a result it disables Mdm 2's ability to degrade p53 by interfering with Mdm 2 ubiqutin-ligase E3 and destabilization of p53 is prevented by Mdm 2 inhibition, leading to an increase in p53 and initiation of the cell death pathway (Tansey, 2014) (MYC's role in apoptosis is discussed in Chapter 4.1).

1.5.5.3 Role of MYC in differentiation

Research has shown that when MYC is deregulated, certain cells undergo differentiation (Facchini and Penn, 1998) but when MYC expression is overexpressed, differentiation is prevented in numerous cell types (Facchini and Penn, 1998; Meyer and Penn, 2008) including in murine embryonic stem (ES) cells (Eilers and Eisenman, 2008). In some cases, ectopic MYC expression can cause as well as inhibit complete differentiation, which was observed in myoblast differentiation. In primary keratinocytes differentiation was completed when MYC was constitutively overexpressed (Gandarillas and Watt, 1997; Facchini and Penn, 1998). Repressing MYC in the developing neural tube of a chick resulted in blocking differentiation (Iavarone and Lasorella, 2014) .

1.5.5.4 Genomic Instability

Elevated MYC expression can cause genetic instability by various mechanisms. Upregulated MYC expression leads to elevated mitochondrial biogenesis and metabolic activity causing a buildup of reactive oxygen species (ROS) and due to failure of the scavenging system (Rohban and Campaner, 2015), the accumulation of ROS leads to oxidative DNA damage (Kc *et al.*, 2006; Rohban and Campaner, 2015). Genomic instability can also a result from breakage-bridge-fusion cycles, due to MYC ability to regulate telomere activity (Louis *et al.*, 2005; Rohban and Campaner, 2015). Genomic instability has also been described as a result of elevated MYC promoting DNA replication stress (Dominguez-Sola and Gautier, 2014; Mazouzi *et al.*, 2014). The process of DNA replication starts by the formation of the pre-replicative complex (pre-RC) which occurs during the late mitosis or early G1 phase of the cell cycle. To form the pre-RC, the origin recognition complex (ORC) recruits Cdt1 and Cdc6 proteins to help with binding the minichromosome maintenance complex (MCM), this forms the inactive pre-RC complex (Dominguez-Sola and Gautier, 2014). In order for the pre-RC to turn into an active initiation complex it require the recruitment of CDKs as a result, Cdc45 and GINS are loaded onto the pre-RC complex which then becomes the cdc45-MCM-7-GINS (CMG) complex (Rohban and Campaner, 2015). DNA polymerase-α can then start the DNA replication process due to access to the unwound DNA as a result of role of the CMG complex (Dominguez-Sola and Gautier, 2014; Rohban and Campaner, 2015). MYC can interact with numerous steps throughout the DNA replication process (Figure 1.12), firstly CDKs play an important role during this process, as they are involved in activating the replication complex as well as inhibiting the replication complex from forming once DNA replication has started. As mentioned before MYC has the ability to affect CDKs' activity which could therefore affect the initiation of DNA replication as well as formation of the replication complex. Secondly the position of the ORC and function can be affected by MYC because MYC plays a role in histone and chromatin acetylation and interacts with many chromatins modifying enzymes and histone acetylation can affect the position and function of the ORC. Thirdly MYC regulates the loading of Cdc45 to the chromatin affecting the activation of DNA synthesis (Dominguez-Sola and Gautier, 2014).

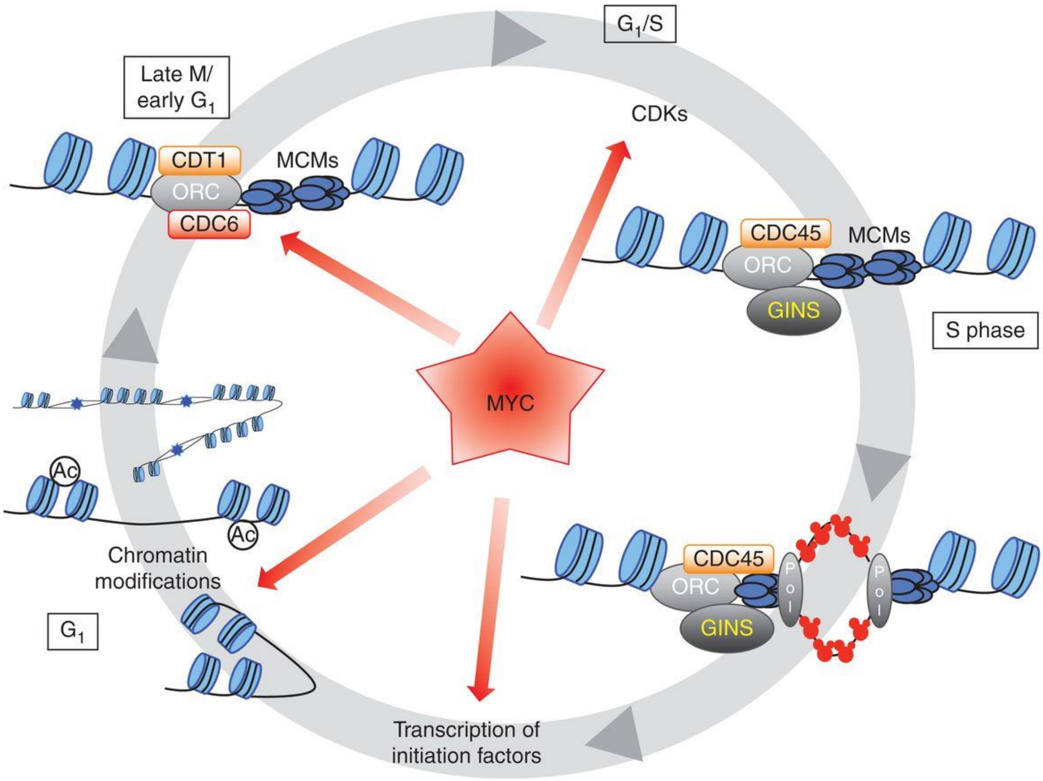
G$_1$/S
Late M/ early G$_1$
CDKs
CDT1
ORC
CDC6
MCMs
CDC45
ORC
MCMs
GINS
S phase
MYC
Ac
Ac
Chromatin modifications
G$_1$
CDC45
ORC
GINS
Pol
Pol
Transcription of initiation factors

Figure 1.12 Processes involved in DNA replication and MYC's involvement. Taken from (Dominguez-Sola and Gautier, 2014).

1.6 Therapeutic targeting in cancer

1.6.1 Therapeutic options for MYC driven cancers

The *MYC* oncogene plays a major role in the development of many cancers (Verdine and Walensky, 2007; Dang, 2012; Toyoshima *et al.*, 2012), but has not yet been successfully targeted by any drugs in the clinic (Toyoshima *et al.*, 2012; Roussel and Robinson, 2013). Much work has been done on attempting to target inhibition of MYC function (Figure 1.13), by either controlling the expression of the gene or by blocking its ability to bind to its partner proteins (Dang, 2012; Roussel and Robinson, 2013). MYC function could be inhibited by blocking the binding of MAX resulting in reduced transcription (Berg *et al.*, 2002; Dang, 2012). This has been tested by using small molecule inhibitors to affect the binding of MYC/MAX (Berg *et al.*, 2002; Kiessling *et al.*, 2006). Kiessling *et al*. showed that the binding of MYC/MAX can be affected by two small molecule inhibitors Mycro 1 and Mycro 2 (Kiessling *et al.*, 2006). Yin *et al*. identified a few small molecules that could affect the MYC-MAX complex, 10058-F4 is one of the inhibitors identified (Yin *et al.*, 2003; Fletcher and Prochownik, 2015).The challenge with some of these direct inhibitors is that it lacks the pharmacokinetics and pharmacodynamics required for *in-vivo* success (Zinzalla, 2016). In the initially in vivo testing of 10058-F4 it failed to meet the pharmacodynamics efficacy (Guo *et al.*, 2009; Zirath *et al.*, 2013) however, when tested again in a neuroblastoma model it showed promising results (Zirath *et al.*, 2013; Fletcher and Prochownik, 2015). This inhibitor can disrupt both the MYCN-MAX (Zirath *et al.*, 2013) and MYCL-MAX and is therefore able to disrupt all members of MYC (Fletcher and Prochownik, 2015). Due to its experimental success in neuroblastoma it could effective in MB_{GRP3} as well. Inhibition of the bromodomain and extraterminal (BET) - family bromodomain protein, specifically BRD4 has been targeted to suppress the transcription of MYC, by using small molecule inhibitors such as JQ1, i-BET and MMS417 (Koh *et al.*, 2016). This strategy has been tested in MB_{GRP3} which has shown to be successful in suppressing MYC (Bandopadhayay *et al.*, 2014). However, for such treatment to work, MYC transcription must be mainly regulated by BRD4 in addition BET also regulates the expression of other proteins as well (Koh *et al.*, 2016). This therapeutic strategy might not be effective in MB_{GRP3} because MYC amplification occurs in this subgroup (Roussel and Robinson, 2013). In addition, histone deacetylase (HDAC) inhibitors have shown promising results in a novel *MYC* amplified MB_{GRP3} cell line (HD-MB03) (Milde *et al.*, 2012; Roussel and Robinson, 2013), however MYC expression wasn't evaluated after treatment. The HD-MB03 cell line responded to treatment with histone deacetylase (HDAC) inhibitors administered either alone or in combination with radiation (Milde *et al.*, 2012; Roussel and Robinson, 2013). Another strategy to target MYC is through Aurora kinases A and B which are mitotic regulators. Aurora kinase inhibitors have been successful in many cancer cells with deregulated MYC (Horiuchi *et al.*, 2014a). There are several Aurora kinase inhibitors that are in clinical trials such as Barasertib (AZD1152), Alisertib (MLN8237) and AT9283 (Bavetsias and Linardopoulos, 2015). In neuroblastoma it has been shown that MYCN can be degraded by inhibiting the formation of the Aurora-A/MYCN complex using Aurora-A inhibitors MLN8054 and MLN8237 (Brockmann *et al.*, 2013). These Aurora-A inhibitors has shown to be effective in a transgenic model of MYCN driven MB (Hill *et al.*, 2015). As well as Aurora- B inhibitor (VX-680) has shown anti-tumourigenic effects in both *in-vitro* and *in-vivo* studies performed in MYC driven models (Fletcher and Prochownik, 2015). These studies indicate the possibility of using Aurora kinases A and B for treatment of MB_{GRP3}. Additional strategies to indirectly target MYC protein is by using mTOR inhibitors (Sabnis *et al.*, 2017) or

PI3K inhibitor (McKeown and Bradner, 2014) or dual mTOR and PI3K inhibitors (Sabnis *et al.*, 2017). One of the challenges is acquisition of resistance to PI3K-mTOR inhibitors, therefore targeting MYC through other indirect methods along with PI3K inhibitors might be required to overcome resistance (Tan and Yu, 2013). Pei *et al.* showed that a dual treatment of HDAC (LBH-589) and PI3K (BKM-120) inhibitors suppressed tumour growth in both in vitro and in vivo models of MYC driven MB, it was therefore suggested this form of treatment might be beneficial for patients with MYC driven MB (Pei *et al.*, 2016). Other indirect methods include cell cycle related kinases such as Polo-like kinases (Xiao *et al.*, 2016) or Chk1 (Horiuchi *et al.*, 2014a) or metabolic inhibitors such as glutaminase inhibitors have been tested to target MYC (Xiang *et al.*, 2015b). Xiao et al showed that inhibition of Polo-like kinase alone or in combination with Bcl 2 proves to be effective in neuroblastoma, small cell lung and MYC-overexpressing carcinomas (Xiao *et al.*, 2016). Inhibition of the Chk1 checkpoint which caused a reduction in proliferation in Myc driven pancreatic tumours (Murga *et al.*, 2011b; Horiuchi *et al.*, 2014a). Lastly another approach is the use of synthetic lethality screen of MYC driven tumours to identify druggable targets, which has identified sumoylation as an important factor for MYC tumour cell growth (Dang, 2012). These therapeutic strategies if not tested already could be tested to determine if they show efficacy in MB_{GRP3}.

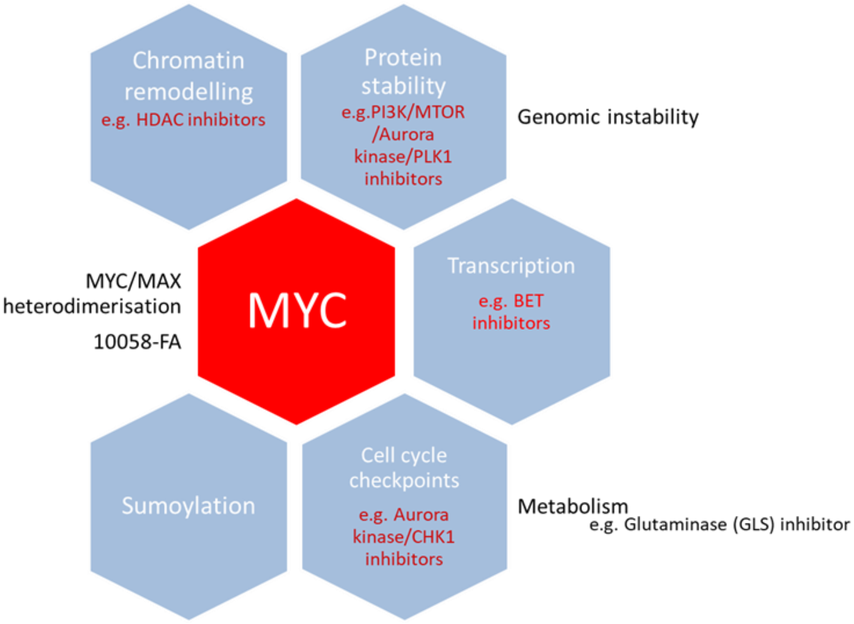
Chromatin remodelling
e.g. HDAC inhibitors
Protein stability
e.g.PI3K/MTOR /Aurora kinase/PLK1 inhibitors
Genomic instability
MYC/MAX heterodimerisation
10058-FA
MYC
Transcription
e.g. BET inhibitors
Sumoylation
Cell cycle checkpoints
e.g. Aurora kinase/CHK1 inhibitors
Metabolism
e.g. Glutaminase (GLS) inhibitor

Figure 1.13 Hexogram presentation of possible therapeutic strategies for targeting MYC.

1.6.2 Therapeutic options for Group 3 medulloblastoma

Currently there are no tailored therapeutic options for MB_{GRP3} patients but more effective options are being pursued. For example the use of inhibitors targeting EZH2 has been considered due to its high expression in MB_{GRP3} (Roussel and Robinson, 2013) and the successful use of these inhibitors in treating lymphomas (McCabe *et al.*, 2012; Roussel and Robinson, 2013). High throughput screens in MB_{GRP3} have identified gemcitabine in combination with pemetrexed to be effective in MYC driven MB (Morfouace *et al.*, 2014) as well as histone deacetylase inhibitors in combination with PIK3 inhibitors has shown promising results in MYC driven MB (Pei *et al.*, 2016; Sengupta *et al.*, 2017). Currently a clinical trial (SJMB12) is open to assess the use of gemcitabine, pemetrexed, vincristine, cisplatin and cyclophosphamide in high risk MB cases (Sengupta *et al.*, 2017). There has been two phase 1 studies to assess HDAC inhibitors in paediatric patients with relapsed/refactory CNS tumours (NCT01076530, NCT00994500). These studies revealed that vorinostat a HDAC inhibitor in combination with either temozolamide or bortezomib showed promising results (Hummel *et al.*, 2013; Muscal *et al.*, 2013; Gopalakrishnan *et al.*, 2015). Currently there is an ongoing clinical trial that is evaluating the use of vorinostat together with isotretinoin and chemotherapy in younger patients with embryonal tumours (NCT00867178) (Gopalakrishnan *et al.*, 2015).

1.7 Viral vectors for gene transfer

Gene transfer is a useful tool frequently used in in-vitro and in-vivo studies to gain understanding on the molecular biology of the gene of interest (Bouard et al., 2009). Many viral vector systems have been generated, each with its own negatives and positives (Howarth et al., 2010) (Table 7). The four main viral vectors commonly used are adenovirus, adeno-associated viruses, herpes simplex virus and retrovirus (Howarth et al., 2010). The retrovirus viral vector is the most frequently used system because of its high efficiency gene transfer (Walter and Stein, 2000) and its ability to stably integrate into the genome of the dividing target cell, which allows the gene of interest to be passed onto all daughter cells (Kurian et al., 2000) .

Vector	Entry	Immune response	Capacity (kb)	Location	Ease of production	Expression
Retrovirus	Fusion	Minimal	8	Integrates	10^8 **	Years
Adenovirus	Receptor	Brisk ***	36	Episomal	10^{12}*****	Weeks/months
AAV	Receptor	None	4	Integrates	10^8***	Years
HSV	Fusion	Brisk ****	30	Episomal	10^{10}****	Weeks

Table 7: Features of the four viral vectors (taken from (Howarth et al., 2010)

The asterisks indicate the level of ease, a higher degree of asterisks means a greater ease of production or immune response.

1.7.1 Introduction to lentivirus

Lentiviruses belongs to the *Retroviridae* viral family (Tomás *et al.*, 2013), lentiviral vectors were generated to be used as a gene transfer vector (Merten *et al.*, 2016). Lentiviruses are able to transduce differentiated, non-dividing and dividing cells (Manjunath *et al.*, 2009) making them a great tool for scientific research (Sakuma *et al.*, 2012), because their genetic materil can be inserted into the host genome (Ciuffi, 2008). The lentiviral vector was developed from the human immunodeficiency virus type 1 (HIV-1) (Sakuma *et al.*, 2012), for biological safety these vectors were further adapted into first, second and third generations (Figure 1.14). Safety modifications were made by separating only the necessary elements of the viral genome into 3- 4 plasmid vectors, which still enable stable integration into the host genome for expression of the gene of interest, but reduces the risk of replicating competent lentiviruses (Manjunath *et al.*, 2009). The first generation lentiviral vector is generated from three different plasmids; firstly, a packaging plasmid which constitutes all the necessary components to produce virions (viral particles) (Sakuma *et al.*, 2012). This plasmid contains two of the structural proteins (HIV Gag and Pol) and all the accessory proteins (Vif, Vpr, Vpu and Nef) and the regulatory proteins (Tat and Rev) (Sakuma *et al.*, 2012; Tomás *et al.*, 2013) regulated by a human promoter such as cytomegalovirus (CMV) (Sakuma *et al.*, 2012). The second envelope plasmid contains the glycoprotein most commonly the Vesicular Stomatitis Virus G glycoprotein (VSV-

G) instead of the HIV-1 glycoprotein(Sakuma *et al.*, 2012). The VSV-G glycoprotein enables entry into a broader range of species and cell types (Shaw and Cornetta, 2014). These plasmids were generated without the packing signal (ψ) and the long terminal repeats (LTRs) in order to reduce the risk of replicating competent lentiviruses during the viral production. Lastly, the third vector contains all the cis-acting components namely the LTRs, ψ and the Rev Responsive Element (RRE) and the transgene (Sakuma *et al.,* 2012). Even though the vector elements were separated into three plasmids the possibility of producing replicating competent lentivirus was still high because only three events of homologous recombination were needed (Tomás *et al.*, 2013). Therefore, a second generation of lentiviral vector was produced by eliminating the accessory proteins from the packaging plasmids and if replicating competent lentivirus was produced during production it wouldn't be infectious, however the number of events needed were the same as the first generation. To improve the biosafety of these lentiviral vectors a third generation was produced by removing the Tat and Rev from the packaging plasmid and placing the Rev on a separate plasmid. Both Tat and Rev are essential for HIV-1 replication, in order to make it a Tat free system either a CMV or rous sarcoma virus promoter was placed in the vector plasmid which replaced the U3 promoter of the 5'-LTR. To make this third generation even safer the U3 component of the 3' LTR in the vector plasmid was replaced with a self-inactivating (SIN) element. The SIN element reduces the probability of generating replication competent lentivirus by recombination with wild type viruses (Shaw and Cornetta, 2014). Separating the vector components into four plasmids increases the number of homologous events needed to produce replicating competent lentivirus. Even though the third generation is safer the viral titer is lower than the other two generations (Sakuma *et al.*, 2012).

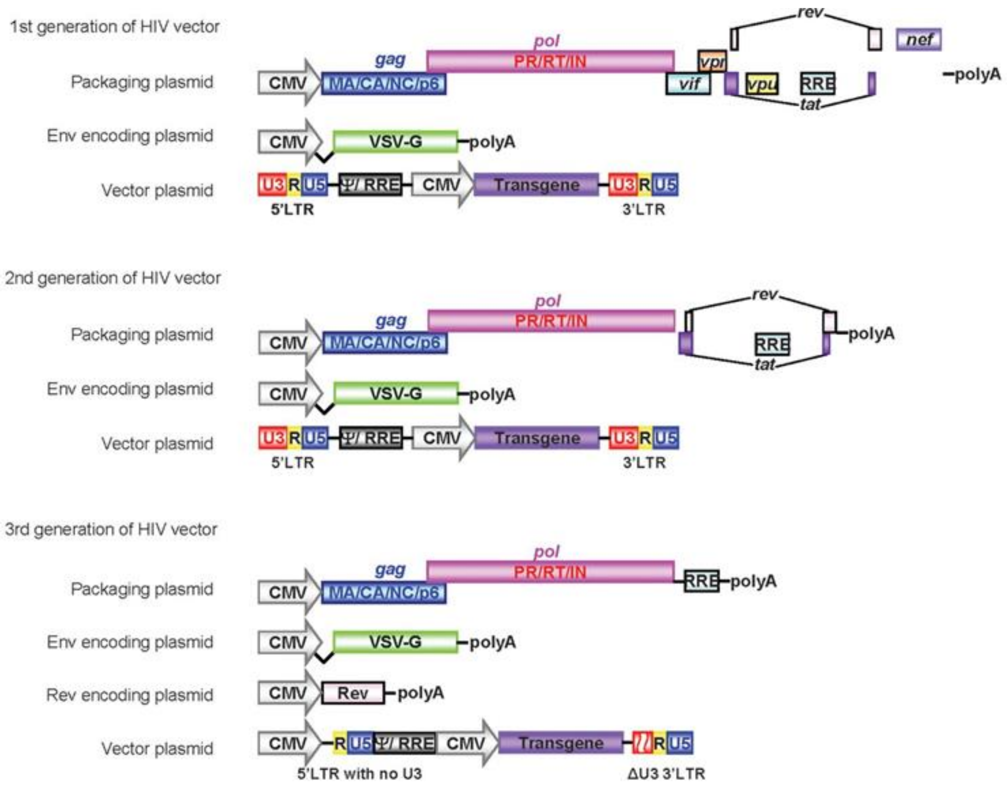
1st generation of HIV vector
Packaging plasmid
CMV
gag
MA/CA/NC/p6
pol
PR/RT/IN
vif
vpr
rev
vpu
RRE
tat
nef
polyA
Env encoding plasmid
CMV
VSV-G
polyA
Vector plasmid
U3 R U5
Ψ/ RRE
CMV
Transgene
U3 R U5
5'LTR
3'LTR
2nd generation of HIV vector
Packaging plasmid
CMV
gag
MA/CA/NC/p6
pol
PR/RT/IN
rev
RRE
tat
polyA
Env encoding plasmid
CMV
VSV-G
polyA
Vector plasmid
U3 R U5
Ψ/ RRE
CMV
Transgene
U3 R U5
5'LTR
3'LTR
3rd generation of HIV vector
Packaging plasmid
CMV
gag
MA/CA/NC/p6
pol
PR/RT/IN
RRE
polyA
Env encoding plasmid
CMV
VSV-G
polyA
Rev encoding plasmid
CMV
Rev
polyA
Vector plasmid
CMV
R U5
Ψ/ RRE
CMV
Transgene
R U5
5'LTR with no U3
ΔU3 3'LTR

Figure 1.14 Representation of the 1st, 2nd and 3rd generation of the HIV vectors, taken from (Sakuma et al., 2012).

1.7.2 Inducible lentiviral vectors

In basic translational research the most widely used inducible gene regulatory expression vectors are the tetracycline (Tet) systems (Naidoo and Young, 2012). The first vector generated was the Tet-OFF system, which is based upon the establishment of a ligand-regulated transactivator (tTA) to stimulate transcription from a promoter in the absence of Tet or its derivative DOX. The tTA was generated by binding the Tet-repressor protein with a herpes virus simplex viral protein 16 domain. The second vector generated was the Tet-ON system which depends on a reverse tTA (rtTA) to activate transcription when adding Tet or DOX. The establishment of the (rtTA) was due to the occurrence of random mutations within the tTA (Toniatti *et al.*, 2004; Benabdellah *et al.*, 2011). An advantage of an inducible vector system is the ability to control the level and time scale of the expression of the gene (Massie *et al.*, 2010). A disadvantages of an inducible system is the expression of the gene in the absence of the inducer "leakiness" (Gossen *et al.*, 1994) due to the promoter self-activation capabilities (Yang *et al.*, 2015) or the possibility of insertional mutagenesis be caused by transducing target cells with many vectors at high multiplicity of infection (MOI)

(Barde *et al.*, 2006; An *et al.*, 2017).To reduce leakiness a clone can be selected with minimal expression during the off state (Roney *et al.*, 2016) and the possibility of insertional mutagenesis could be reduced by using all-in-one inducible vector system which removes the multiple transduction steps (Barde *et al.*, 2006; An *et al.*, 2017).

1.7.3 RNA interference

RNA interference has proven to be a useful technology to investigate the function of genes by their silencing in human cell lines (Pushparaj *et al.*, 2008; Taxman *et al.*, 2010). Silencing of genes can be accomplished by either small interfering RNAs (siRNAs) or short hairpin RNAs (shRNAs) or initiated by microRNA (miRNA) (O'Keefe, 2013). Knockdown of protein achieved by miRNA is through translational inhibition of certain mRNAs (Manjunath *et al.*, 2009; O'Keefe, 2013) or through degradation of specific mRNAs triggered by either a chemically synthesised siRNA or through a shRNA expressed from a DNA vector (Taxman *et al.*, 2010) (Figure 1.15). Both siRNA and shRNA contains two oligonucleotides sequences (sense and antisense strands) that differs in base pair (bp) length) (O'Keefe, 2013). The shRNA complementary strands however, are joined by 4-11 nucleotides (nt) creating a loop sequence (Taxman *et al.*, 2010). The mechanism of protein silencing accomplished by siRNA or shRNA is very similar (Taxman *et al.*, 2010). Briefly once the long dsRNA is expressed in the cytoplasm it interacts with Dicer which is a ribonuclease (Rnase) III enzyme, due to the enzymatic reaction the long dsRNA is snipped into 21-23nt (Whitehead *et al.*, 2009; O'Keefe, 2013) with a 2 nt overhang at the 3' termini (O'Keefe, 2013).The siRNA is then loaded into a RNA-induced silencing complex (RISC), this complex contains Argonate-2 (Ago-2), Dicer and TAR-RNA-binding protein (TRBP) (Rao *et al.*, 2009; O'Keefe, 2013). Ago-2 is responsible for separating the double strand of the siRNA (Whitehead *et al.*, 2009) which enables the sense strand to leave the RISC. Once the sense strand exists the complex, Ago-2 then cleaves it (Rao *et al.*, 2009). The remaining strand in the RISC joins to identical mRNA sequences which cause mRNA degradation and therefore silencing of the protein. The cycle of mRNA degradation continues until the siRNA is either destroyed or the level of siRNA present in the cell is too low to continue the cycle (Whitehead *et al.*, 2009), therefore siRNA allows for a short term approach to induce protein knockdown. In contrast, shRNA allows for a more stable knockdown of protein (Manjunath *et al.*, 2009; Taxman *et al.*, 2010) because it gets integrated into the DNA of the cell (Taxman *et al.*, 2010). Once the shRNA is expressed in the nucleus it is transcribed by RNA polymerase (II or III). The transcript is then processed by an RNase III enzyme known as Drosha and DGCR8 which is a dsRNA binding protein. This process generates the pre-shRNA, which relocates to the cytoplasm via the help of Exportin 5. Once in the cytoplasm the loop structure in the pre-shRNA gets deleted through the cleavage of Dicer and TRBP/ protein R (PKR)- activating protein (PACT). Due to this a double stranded siRNA is generated with 2 nt overhangs at the 3' terminius. Once in this form silencing of protein occurs through the same mechanism as described for siRNAs (Rao *et al.*, 2009; O'Keefe, 2013). This technique has been used in many experiments to study knockdown of genes example the consequence of MYC knockdown has been studied in various cancers (Wang *et al.*, 2005; Wolfer *et al.*, 2010; Niu *et al.*, 2015). RNA interference technique has also been used in genetic screens(Moffat *et al.*, 2006) and drug screens (Zuber *et al.*, 2011; Mendes-Pereira *et al.*, 2012; Fellmann and Lowe, 2014).

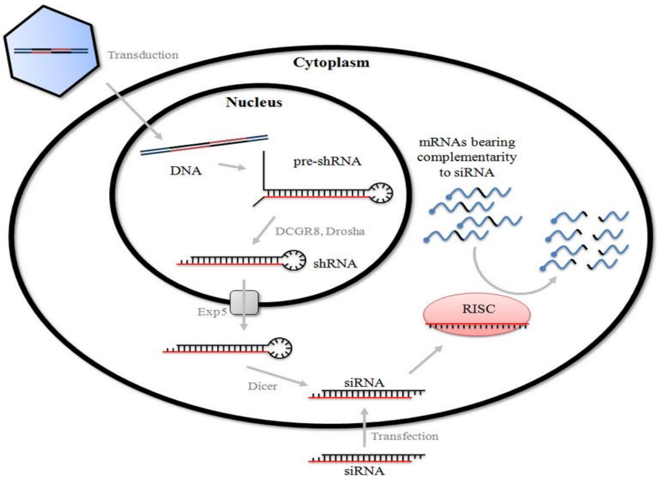

Figure 1.15 Process of mRNA degradation through siRNA or shRNA. Taken from (O'Keefe, 2013).

1.8 Summary and Aims

Currently MB_{GRP3} patients have a survival rate of ≤ 50%. High *MYC* expression/ amplification is predominately associated with MB_{GRP3} and is associated with poor outcomes, yet the role of *MYC* within MB tumorigenesis remains poorly understood. This project aims to gain an understanding of MYC biology within MB_{GRP3} and to use this understanding to identify potential novel therapeutic options for patients in this subgroup.

MYC expression will be modulated in a panel of MB$_{GRP3}$ cell lines by means of inducible lentiviral systems (cumate switch inducible vector and Tet-pLKO-puro). These cell models will be used to investigate the effect MYC overexpression and knockdown has on the phenotypic (proliferation, cell cycle and apoptosis) and functional properties of the cell, using methodologies such as RNA-seq.

Data collected from the functional study (RNA-seq which measure the expression of genes) will then be cross-referenced with datasets from primary tumour samples to identify therapeutic targets modulated by MYC and relevant to primary tumours. The identification of these targets could lead to the development of novel therapies for MB$_{GRP3}$ patients (Figure 1.16).

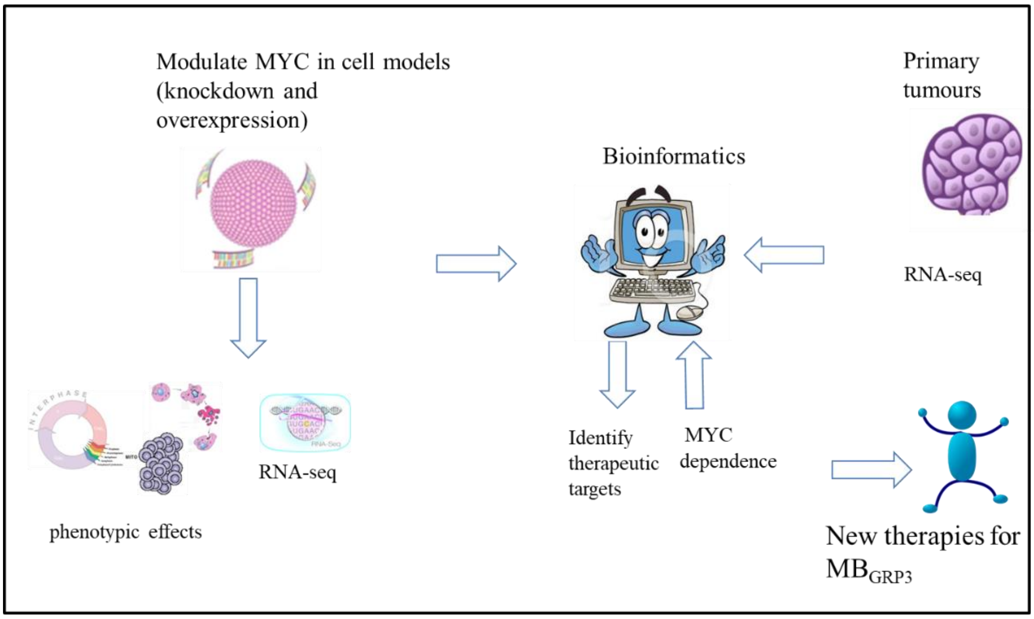
Modulate MYC in cell models (knockdown and overexpression)
Primary tumours
Bioinformatics
RNA-seq
RNA-seq
phenotypic effects
Identify therapeutic targets
MYC dependence
New therapies for MB$_{GRP3}$

Figure 1.16 Illustration showing the overview of the project.

This project aims to gain an understanding of MYC biology within MB$_{GRP3}$ and to use this understanding to identify potential novel therapeutic options for patients in this subgroup, with the following specific aims.

1. To establish MB$_{GRP3}$ cell lines with inducible expression of MYC through the cloning of *MYC* into the SparQ all-in-one inducible lentiviral vector to generate an overexpression model and to clone shRNAs targeting *MYC* into the pLKO-Tet-On vector to generate a knockdown model (Chapter 3).

2. These MYC dependent models of MB$_{GRP3}$ will be used to investigate the phenotypic changes associated with MYC modulation, by measurement of

parameters including cellular proliferation, cell cycle and induction of apoptosis (Chapter 4).

3. Investigation of the effect of MYC modulation on gene expression in the MYC dependent models of MB_{GRP3}. These cell lines will be profiled before and after modulation of MYC by RNAseq. Identification of important gene networks/ pathways will be assessed bioinformatically by analyses including Gene-set Enrichment Analysis (GSEA) and ingenuity pathway analysis (Chapter 5).

4. To cross-reference the gene expression profiles of the MYC dependent models of MB_{GRP3} with MB_{GRP3} primary tumour profiles to determine which are relevant in MYC amplified / overexpressing Group 3 human primary tumours and may represent clinically relevant druggable targets (Chapter 5).

Chapter 2 Materials and Methods

2.1 Cell lines

2.1.1 Maintenance of cell lines

D425Med (a gift from Dr Bigner, Duke University) (He *et al.*, 1991), DAOY (ATCC) (Jacobsen *et al.*, 1985) and HEK 293T (a gift from Dr Paul Sinclair, Newcastle University) (Shaw *et al.*, 2002) were maintained in Dulbecco's Modified Eagles's Medium (DMEM)(Sigma-Aldrich) supplemented with 10% (v/v) fetal bovine serum (FBS) (Gibco) and 1% (v/v) L-glutamine (200mM stock) (ThermoFisher Scientific). CHLA-259 (Children Oncology Group, Texas Tech University) was maintained in Iscove's Modified Dulbecco's medium (Sigma) supplemented with 20% (v/v) FBS, 2% (v/v) L-glutamine (200mM stock) and 1 % (v/v) insulin transferrin- selenium (100x) (ThermoFisher Scientific). HDMB03 (a gift from Dr Deubzer, German Cancer Research Center (DKFZ) (Milde *et al.*, 2012) was maintained in 1640 Roswell Park Memorial Institute (RPMI) medium (Sigma), supplemented with 10% (v/v) FBS, 1% (v/v) L-glutamine (200mM stock) and 1% (v/v) MEM Non- Essential Amino Acids Solution (100x) (ThermoFisher Scientific). For routine growth, cells were incubated at 37^{o}C in a 5% CO_2 incubator unless otherwise stated. Cells were passaged once they reached 80-90% confluency. Adherent cells were detached by treatment with a 1x solution of trypsin (Sigma-Aldrich Ltd, Gillingham, UK). Suspended cells were centrifuged at 335g for 5 minutes (mins), the supernatant was removed and the cells were resuspended in fresh media at a dilution of 1:3 to 1:6 for MB cell lines and 1:10 to 1:15 for HEK 293T.

To determine total cells/ml, a cell count was performed by mixing 10µl of sample with 10µl trypan blue (Bio-Rad) and then loading into a hemocytometer for manual counting or into a cell counting chamber slide (ThermoFisher Scientific) for automatic counting on the Countess II FL Automated Cell Counter (ThermoFisher Scientific). To determine cell number, the following formula was used:

Total cells/ml = total cells counted x dilution factor / number of squares counted x 10000 cells/ml.

Trypan blue stain is not absorbed by healthy viable cells but enters dead or damaged cells. Cell viability (%) was calculated as cells not staining with trypan blue/ total number of cells.

The *MYC* modulated knockdown cell lines (Chapter 3) were grown in the same conditions as the parent cell lines except tetracycline (Tet)- free FBS (Takara) was used instead of the normal FBS and 1µg/ml puromycin (Thermo Fisher Scientific) was added.

2.1.2 Cryopreservation and recovery of cell lines

Cell suspensions were centrifuged for 5 mins at 335g, supernatant was removed and ice cold FBS (500µl/per 1x10^6 cells) added to the pellet followed by an equal amount of freezing media (80% FBS + 20% dimethyl sulfoxide (DMSO) (Sigma) in a dropwise manner. One to five million cells in 1ml freezing media were transferred to a cryovial (Thermo Fisher Scientific). The cryovial was left for a few mins before being placed in a precooled (to -4^{o}C) Mr Frosty freezing container and placed in a -80 ^{o}C freezer for 24 hours, followed by transfer of the cryovials to liquid nitrogen for long-term storage. The same method was used for the *MYC* modulated cell lines except Tet-free FBS was used.

To recover cell lines, cryovials were removed from storage and placed immediately in a 37^{o}C water bath, but removed when a small amount of ice was left (to ensure the temperature of the mix remained below 0 ^{o}C) and placed on ice until completely defrosted. Once defrosted, the cell suspension was transferred to a Falcon tube (Corning) containing 1ml pre-cooled media and placed back on ice for a min for DMSO to diffuse slowly out of the cells. The Falcon tube was removed from the ice and 7-12mls of pre-warmed media was slowly added to the Falcon tube. The entire contents were either transferred to a T25 or T75 flask (Corning) and incubated overnight. On day 2, for adherent cells the media was removed and replaced with fresh media. For semi- adherent cells, the cell suspension was spun down at 335g for 5 mins and replaced with fresh media. On the 3rd day for the *MYC* modulated cell lines, the media was replaced with media containing 1µg/ml puromycin.

2.2 Phenotypic assays

2.2.1 Proliferation assay

To investigate the effect MYC modulation has on the proliferative capability of the cells, a luminescent assay (CellTiter-Glo (Promega)) was used. The luminescent signal correlates to the amount of adenosine triphosphate (ATP) present within the cells.

Cells were seeded in an opaque 96 well microtiter plate at a density of 6x10^3 cells/100µl and incubated for 8 hours in an incubator (as described in 2.1.1), before the addition of doxycycline (DOX) to induce MYC knockdown. A range of DOX concentrations (0.1, 1, 3, 5, 10µg/ml) were added to the cells to determine the concentration necessary to achieve maximum knockdown. Before taking a reading at 0, 24, 48, 72, 96 and 120 hours, the plate was equilibrated at room temperature (RT) for 30 mins following removal from the incubator. Next, 25µl of CellTiter-Glo reagent was added to the wells, followed by gently shaking for 2 mins by hand. The plate was then incubated for 10 mins before recording the luminescent reading using a FLUOstar Omega (BMG Labtech) plate reader. To maintain knockdown, DOX was refreshed every 48 hours, by adding DOX the appropriate wells to give a final concentration of 1µg/ml.

2.2.2 Cell cycle analysis

To analyze the effect MYC knockdown has on cell cycle distribution, a fluorescent dye (propidium iodide (PI) (Sigma)) was used to stain the DNA content of the cells and flow cytometric analysis was performed at Newcastle University Flow Cytometry Core Facility. Flow cytometry measures the light scattering and/or fluorescent properties after staining the DNA of a single cell to detect many features of the cell, such as size and granularity. To gather this information, a flow cytometry machine requires the following components; a fluidics system which uses sheath fluid and hydrodynamic focusing to transport an individual cell through the laser beam; an optical system which contains all the lasers to detect the light scattered by the cell as it passes through the laser beam. The light scattered is namely forward and side scatter, the forward scatter measures the size whereas granularity is measured by the side scatter. In addition, the fluorescent light can also be detected by the appropriate lasers if the cell is tagged with a fluorescent labelled antibody or dye. Lastly the photodetectors then convert the light signals into electrical signals, these electrical signals are amplified and transformed into digital signals. These digital signals are processed by the computer for analysis (Adan *et al.*, 2016). For this project cells were harvested in an appropriate manner; 1x10^6 cells were placed in a fluorescence-activated cell sorting (FACS) tube and pelleted by centrifugation at 149g for 5 mins. The supernatant was removed and the pellet was washed in 1ml ice-cold PBS and re-pelleted as before. The supernatant was removed and cells were fixed by vortexing the cells while slowly adding 1ml cold 70% ethanol. The samples were incubated at 4^{o}C for 30 mins or overnight. To remove the ethanol from the samples, samples were pelleted and washed twice in 1ml cold PBS and centrifuged. The pellet was resuspended in 1ml ice-cold PBS and RNA was digested by adding 50µl ribonuclease I (Rnase I) (Sigma). To stain the DNA and to lyse the cells, 250µl PI/ triton (1:10) mix was added to the cells. The samples were then analysed using the BD FACS Canto II and data analyses were done using flowjo 10 software (FlowJo, LLC). Concentrations and preparations for reagents shown in Table 8.

Reagent concentration	Preparation
50µg/ml PI	Prepared in phosphate buffered saline (PBS)
100µg/ml RNase I	Prepared in sterile distilled water and heated at 100°C for 10 mins
5% Triton	Prepared in in sterile distilled water

Table 8: Concentrations and preparations for cell cycle analysis reagents

2.2.3 Apoptosis

To assess apoptosis, the Caspase-Glo 3/7 (Promega) luminescent assay was used. This luminogenic substrate relies on the cleavage of DEVD peptide by the caspases 3 and 7 resulting in a luminogenic signal.

Cells were seeded in an opaque 96 well microtiter plate at a density of $6x10^3$ cells/100µl and incubated for 8 hours in incubator (as described in 2.1.1), before the addition of 1µg/ml DOX. Before taking a reading at 0, 24, 48, 72, 96 and 120 hours, the plate was equilibrated at RT for 30 mins. After equilibration, 25µl of reagent was added to the wells, followed by gently shaking for 2 mins. The plate was incubated for 30 mins before recording the luminescent reading using a FLUOstar Omega (BMG Labtech) plate reader. To maintain knockdown, DOX was refreshed every 48 hours by adding DOX to the appropriate wells.

2. 3 Molecular cloning

2.3.1 Preparation of plasmids used in this study

The expression vector pcDNA3-cmyc, a gift from Wafik El-Deiry (Addgene plasmid # 16011, Figure 2.1), and the empty backbone vector Tet-pLKO-puro, a gift from Dmitri Wiederschain (Addgene plasmid #21915, Figure 2.2), were supplied in bacterial hosts as agar stabs. To obtain a single colony, bacteria were streaked on a Luria Bertani (LB) plate (1% (w/v) Tryptone (Sigma Aldrich), 0.5% (w/v) Yeast extract (Sigma Aldrich), 1% (w/v) NaCl, 1.5%(w/v) agar (Sigma Aldrich) and double distilled H_2O) containing ampicillin (100µg/ml) and incubated for 12-18 hours at 37°C. The pcDNA3-cmyc, Tet-pLKO-puro, the all-in-one cumate switch inducible lentivector (System Bioscience plasmid #QM812B-1 Figure 2.3) and packaging plasmids psPAX2 and pMD2.G-VSVG were transformed into competent cells as described in 2.3.4. Glycerol stocks were made as described in 2.3.2 and plasmid DNA was isolated as described in 2.3.3.

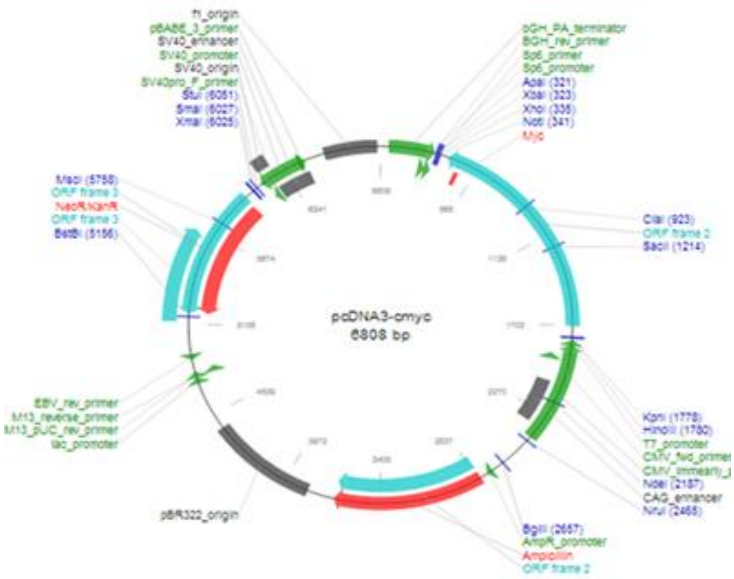
f1_origin
pBABE_3_primer
SV40_enhancer
SV40_promoter
SV40_origin
SV40pro_F_primer
StuI (6051)
SmaI (6027)
XmaI (6025)
MscI (5758)
ORF frame 3
NeoR/KanR
ORF frame 3
BstBI (5156)
EBV_rev_primer
M13_reverse_primer
M13_pUC_rev_primer
lac_promoter
pBR322_origin
pcDNA3-cmyc
6808 bp
bGH_PA_terminator
BGH_rev_primer
Sp6_primer
Sp6_promoter
ApaI (321)
XbaI (323)
XhoI (335)
NotI (341)
Myc
ClaI (923)
ORF frame 2
SacII (1214)
KpnI (1778)
HindIII (1780)
T7_promoter
CMV_fwd_primer
CMV_immearly_
NdeI (2187)
CAG_enhancer
NruI (2468)
BglII (2657)
AmpR_promoter
Ampicillin
ORF frame 2

Figure 2.1 Plasmid map for pcDNA3-cmyc (taken from Addgene).

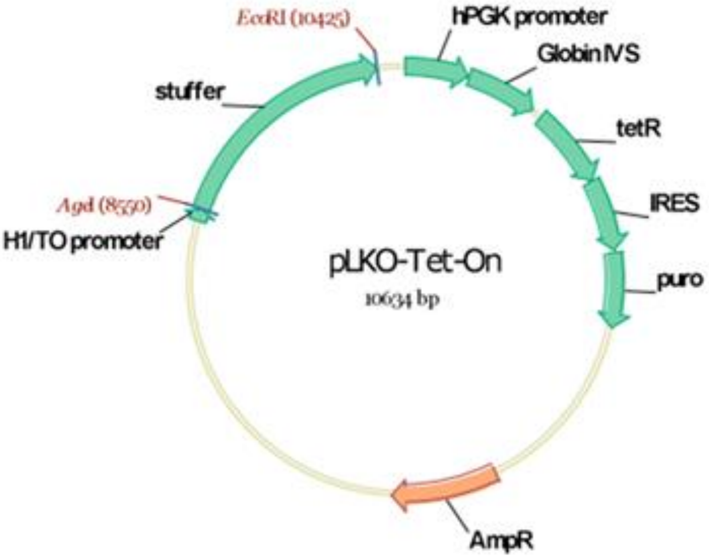
EcoRI (10425)
hPGK promoter
Globin IVS
stuffer
tetR
IRES
AgeI (8550)
H1/TO promoter
pLKO-Tet-On
10634 bp
puro
AmpR

Figure 2.2 Plasmid map for pLKO-Tet-On vector (taken from Addgene).

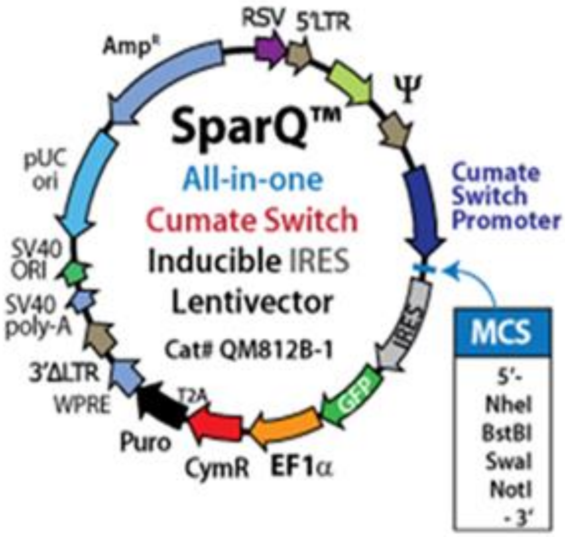
RSV
5'LTR
Amp^R
Ψ
SparQ™
All-in-one
Cumate Switch
Inducible IRES
Lentivector
Cat# QM812B-1
pUC ori
Cumate Switch Promoter
SV40 ORI
SV40 poly-A
MCS
5'-
NheI
BstBI
SwaI
NotI
-3'
IRES
3'ΔLTR
WPRE
T2A
GFP
Puro
CymR
EF1α

Figure 2.3 Plasmid map for SparQ all-in -one inducible lentiviral vector (taken from System Biosciences).

2.3.2 Preparation of glycerol stocks

A single colony was inoculated into 5ml LB media (1% (w/v) Tryptone (Sigma Aldrich), 0.5% (w/v) Yeast extract (Sigma Aldrich), 1% (w/v) NaCl and double distilled H_2O) containing ampicillin (100µg/ml) and incubated for 12-18 hours at 37^{o}C in a shaking incubator. After incubation, a bacterial stock was made by mixing a 1:1

dilution of cell suspension with 50% sterile glycerol (v/v) and followed by storage at –80°C.

2.3.3 Plasmid DNA extraction

Bacteria were cultured by inoculating a single colony into 5ml LB medium (100µg/ml ampicillin) and incubation for 12-18 hours at 37°C in a shaking incubator for small scale extraction (miniprep). For larger scale extraction (midiprep), a 5ml culture was incubated for 8 hours and then transferred to 100ml or 200ml LB (100µg/ml ampicillin) and incubated for a further 12-18 hours at 37°C in a shaking incubator. Plasmid DNA was isolated using the appropriate miniprep or midiprep kit (Qiagen) according to manufacturer's instructions.

2.3.4 Transformation

In order to store and replicate plasmids and ligation mixtures, DNA was transformed into Stbl3 chemically competent *E. coli* cells (Thermo Fisher Scientific) according to manufacturer's instructions (Thermo Fisher Scientific). Briefly, competent cells were thawed on ice and 1 to 5µl of DNA, 1µl of positive control pUC 19 and water as a negative control were added to 15-50µl of competent cells in separate Falcon tubes. The mixture was gently mixed by flicking the bottom of the tube and the Falcon tubes were incubated on ice for 30 mins. After incubation, cells were heat shocked for 45 seconds in a 42°C water bath without shaking and then immediately placed back on ice for 2 min. Next, 75-250µl SOC (Thermo Fisher Scientific) medium pre-warmed to 37°C was added to each tube and the tubes were shaken horizontally at 225rpm in a shaking incubator at 37°C for 1 hour. After incubation, 25-100µl of each transformation mixture was spread on a pre–warmed LB agar plate (37°C) containing 100µg/ml ampicillin. The agar plates were inverted and incubated overnight at 37°C.

2.3.5 Screening of plasmids and positive clones

The human MYC cDNA from the expression vector pcDNA3-cmyc was sequenced by DBS genomics (Durham) using SP6 and T7 primers (Figure 2.1). Clones were screened by doing a restriction digest (2.3.12) and clones which contained the correct size of insert were sequenced by DBS genomics or Eurofins mwg and aligned (https://blast.ncbi.nlm.nih.gov/Blast.cgi) against the known sequence to confirm the integrity of the cloned sequence (constructs sequencing primers shown in Table 9).

Primer name	**Sequence (5’-3’)**
Cumate reverse primer	TTCGGCCAGTAACGTTAGGG
Cumate forward primer	CACCTGGCCCGATCTGGCC
MYC forward primer	CCTACCCTCTCAACGACAGC
MYC reverse primer	TGAGAGGGTAGGGGAAGACC
pLKO shRNA reverse primer 1	TCTTTCCCCTGCACTGTACC
pLKO shRNA reverse primer 2	TGGATCTCTGCTGTCCCTGT

Table 9: Constructs sequencing primers

2.3.6 Primer design

2.3.6.1 Primer design for sequencing

Appropriate primers were designed using Primer 3 software; primers contained 18-21 nucleotides and had a GC content of 40-60%. All primers used were purchased from Sigma at 100µM and working stocks were made by diluting to 10µM in distilled H_2O. Primers were stored at -20^{o}C.

2.3.6.2 Primer design for DNA cloning

The restriction enzymes NheI (New England Biolabs) and BstBI (New England Biolabs) were used to remove the coding sequences of *MYC* from pcDNA3-cmyc for recloning into the all-in-one cumate switch inducible lentivector. NEBcutter V2.0(http://www.labtools.us/nebcutter-v2-0/) was used to confirm that NheI and BstBI restriction enzymes do not cut within the *MYC* coding sequence. The forward primer for amplifying the MYC coding sequence from the pcDNA3-cmyc plasmid was designed to contain 6 extra base pairs on the 5' end followed by the NheI (GCTAGC) restriction enzyme recognition sequence, and then the hybridization sequence which consisted of 21 base pairs; a kozak sequence was also included before the start codon (Table 10). The reverse primer contained 6 extra base pairs on the 5' end followed by the BstBI (TTCGAA) restriction enzyme recognition sequence and then the 21 base pair hybridization sequence (Table 10).

Primer name	**Sequence (5' - 3')**
pcDNA3-cmyc forward primer	GATAGAgctagcGATCCACCATGCCCCTCAACG
pcDNA3-cmyc reverse primer	TCGAGAttcgaaTTACGCACAAGAGTTCCGTAG

Table 10: PCR primers for molecular cloning

2.3.7 Short hairpin RNA design and preparation

Three shRNAs targeting *MYC* and a non-silencing (NS) shRNA were purchased from Sigma, these sequences were previously published (Table 11). Oligonucleotides were designed to contain EcoRI (New England Biolabs) and AgeI (New England Biolabs) restriction sites (position that each shRNA target is mentioned in 3.4.1). Oligonucleotides were reconstituted in ddH$_2$O to 0.1nmol/µl and were mixed and dissolved by vortexing for a few seconds, Equal amounts of two single complementary oligonucleotides were mixed in an PCR tube with 2.5µl 10x annealing buffer (1M NaCl, 100Mm Tris-HCI, pH7.4) and placed in a thermocycler. This was heated to 95^{o}C for 2 mins and then slowly cooled to 25^{o}C over a period of 45 mins followed by storage at 4^{o}C. In a sterile Eppendorf tube 1µl oligonucleotide was diluted 1: 400 in 0.5x annealing buffer; annealed and diluted oligonucleotides were stored at -20^{O}C.

Plasmid	Target sequence	Reference
MYC 1	5’CCGGATGTCAAGAGGCGAACACACCTCGAGGTGTGTTCGCCTCTTGACATTTTTT3’ 5’AATTAAAAAATGTCAAGAGGCGAACACACCTCGAGGTGTGTTCGCCTCTTGACAT 3’	(Guney *et al.*, 2006)
MYC 2	5’CCGGGATGAGGAAGAAATCGATGCTCGAGCATCGATTTCTTCCTCATCTTTTT 3’ 5’AATTAAAAACAACAAGATGAAGAGCACCAACTCGAGTTGGTGCTCTTCATCTTGTTG 3’	(Li *et al.*, 2010)
MYC 3	5’ CCGG CCTGAGACAGATCAGCAACAA CTCGAG TTGTTGCTGATCTGTCTCAGG TTTTT 3’ 5’AATTAAAAACCTGAGACAGATCAGCAACAACTCGAGTTGTTGCTGATCTGTCTCAGG 3’	(Raeder *et al.*, 2013)
NS	5’CCGG CAA CAA GAT GAA GAG CAC CAA CTCGAG TTG GTG CTC TTC ATC TTG TTG TTTTT3’ 5’ AATT AAAAA CAA CAA GAT GAA GAG CAC CAA CTCGAG TTG GTG CTC TTC ATC TTG TTG 3’	(Li *et al.*, 2010)

Table 11: shRNAs targeting MYC and NS

2.3.8 Polymerase chain reaction

The phusion High-Fidelity DNA polymerase (New England Biolabs) was used to perform the polymerase chain reaction (PCR). Genes of interest for DNA cloning and DNA inserts in clone constructs for screening were amplified by PCR. The PCR components are shown in Table 12 and the thermocycler conditions in Table 13.

Components	20µl reaction
Nuclease- free water	to 20 µl
5x Phusion HF or GC buffer	4µl
10mM dNTPs	0.4µl
10µM Forward primer	1µl
10µM Reverse primer	1µl
DNA template	Variable
Phusion DNA polymerase	0.2µl

Table 12: PCR components for amplification of MYC

* Negative controls (without DNA template) were included

Steps	**Time**	**pcDNA3-cmyc plasmid**	
		Temperature	**Cycles**
Initial Denaturation	5 mins	$98^{o}C$	1
Denaturation	10 seconds	$98^{o}C$	35
Annealing temperature	30 seconds	$65^{o}C$	
Extension	30 seconds	$72^{o}C$	
Final extension	10 mins	$72^{o}C$	1
Final hold		$4^{o}C$	

Table 13: Thermocycler conditions for PCR amplification of MYC

2.3.9 Gel electrophoresis

PCR products or digested DNA products were loaded onto a 0.7% to 2% (w/v) agarose gel. The agarose gel was prepared by melting agarose (Bioline) in 1x Tris/Borate/EDTA (TBE; 10.8g Tris (Sigma Aldrich), 5.5g Boric acid (Sigma Aldrich), 4ml 0.5M EDTA (pH 8) (Sigma Aldrich) made up to a 1L with distilled H_2O) buffer with the addition of 0.01% GelRed (Biotium). Each sample and an appropriate DNA ladder (Promega) were mixed with 5µl of 6x loading dye (Thermo Fisher Scientific) before loading into wells. 1x TBE buffer was used as the running buffer and the gel was run at 100 volts for 1 hour. DNA was visualized by an ultraviolet light source using the Syngene G box.

2.3.10 Polymerase chain reaction purification

PCR products and digested products required for downstream applications were purified using a PureLink® PCR Purification Kit (Invitrogen), according to manufacturer's protocol. Briefly, PCR products were mixed with the appropriate binding buffer and loaded into a spin column (Invitrogen). The double stranded DNA binds to the membrane allowing all impurities to be removed with washing buffer before eluting the DNA in elution buffer.

2.3.11 Gel purification

Gel purification for the digested recipient vectors was performed using a GeneJet^{TM} Gel extraction (Fementas) kit according to the manufacturer's protocol. Briefly, 1:1 volume of binding buffer was added to the gel slice containing the recipient vector DNA. The mixture was incubated for 10min at 50-60^{o}C, allowing the gel to dissolve before it was loaded into a column. After centrifugation, impurities removed with washing buffer before the purified DNA was eluted in 50µl elution buffer.

2.3.12 Restriction enzyme digest

To screen plasmids for positive clones and for directional cloning, target DNA, recipient vectors and constructs were digested with restriction enzymes. Briefly 2-3µg of the relevant PCR DNA product or 10µg of the cumate switch inducible lentivector DNA were first digested with 8-40 units of NheI-HF (New England Biolabs), and then with 8-40 units of BstBI (New England Biolabs) containing 1x NEBuffer and made up to the final volume with nuclease free H_2O. The reaction was incubated at 37^{o}C for 1 hour; after incubation the reaction was heat inactivated for 20 mins at 80^{o}C.The second enzyme was then added and the reaction incubated at 65^{o}C for 1 hour. A double digest was performed for the Tet-pLKO-puro vector (10µg) with EcoRI-HF (New England Biolabs) and AgeI-HF (New England Biolabs) (each 40 units) containing 1x NEBuffer and made up to the final volume with nuclease H_2O. The reaction was incubated at 37^{o}C for 2 hours. An XhoI (Promega) digest was performed to screen for positive shRNA clones as shown in Table 14; the reaction was incubated at 37^{o}C for 1 hour, and after incubation the reaction was heat inactivated for 15 mins at 65^{o}C.

Components	**Volume**
Plasmid DNA 1µg	-µl
XhoI (5 units)	0.5µl
10x buffer	2µl
BSA	0.2µl
Nuclease free H_2O to a final volume of	20µl

Table 14: Components for XhoI restriction digest

2.3.13 DNA ligation for MYC

The purified *MYC* cDNA was ligated into the cumate switch inducible lentivector using T4 DNA Ligase (Promega). The required amount of DNA insert (ng) was determined using this formula:

DNA insert= (ng of vector x insert length) / vector length x molar ratio of insert: vector.

The reaction contained the appropriate insert: vector molar ratios and 1x T4 DNA Ligase buffer, 6 units T4 DNA Ligase and was made up to a final volume with nuclease- free H_2O. Four controls were also included; control 1 contained T4 DNA ligase buffer, cumate vector DNA and nuclease-free H_2O up to 20µl; control 2 contained T4 DNA ligase buffer, cumate vector DNA, T4 DNA Ligase and nuclease-free water up to 20µl; control 3 contained T4 DNA ligase buffer, insert DNA and nuclease-free water up to 20µl and control 4 contained T4 DNA ligase buffer and nuclease-free water up to 20µl. The reactions were mixed gently. The cumate and *MYC* ligation reactions were incubated at RT for 4 hours. The ligation reactions were stored at –20 ^{o}C.

2.3.14 Ligation procedure for oligonucleotides

Oligonucleotides were ligated into the pLKO- Tet- On as shown.

Oligonucleotide dilution (1:400) (or 0.5x buffer as a negative control)	1µl
Gel-purified digested pLKO-Tet-On	1µl
10x ligase buffer	1µl
T4 DNA ligase (3 units)	1µl
Nuclease free water made up to	10µl

The ligation mixture was incubated at room temperature for 3 hours and stored at – 20 ^{o}C.

2.4 Lentiviral procedure

2.4.1 Packaging of lentiviruses

To produce lentivirus, the Calphos Mammalian Transfection kit (Clontech) was used. 293T cells were seeded at a density of $4x10^6$ cells/ 10ml in $10cm^2$ tissue culture plates in replicates of 5 and incubated for 16 hours (as described in 2.1.1). After incubation the transfection solution A was prepared as shown in Table 15 (volumes are per plate) and for solution B, 900µl 2x HEPES-buffered saline (HBS) was used per plate.

Components	Amounts
10µg Plasmid DNA	-µl
10µg psPAX2	-µl
5µg pMD2.G-VSVG	-µl
2M Calcium phosphate	112µl
H_2O made up to	900µl

Table 15:Transfection solution A for one replicate

A master mix was prepared for Solution A and B for all plates. Solution B was added to Solution A in a dropwise manner with continuous mixing. The transfection solution was incubated at room temperature for 15 mins. After incubation, the plate was gently moved back and forth while adding 1.8ml of transfection solution dropwise to the appropriate plate. The plates were incubated (as described in 2.1.1) for 8 hours and subsequently the transfection media was removed and replaced with fresh 10 ml media (DMEM with 10%FBS and 1% L-glutamine). Virus was harvested 48 hours later by collecting the media from the same plates into one tube and passing it through 0.45µM filter (Millipore). Aliquots were made and the viral stocks were stored at -80^{o}C or virus supernatant was concentrated (2.4.2).

2.4.2 Lentivirus concentration by ultracentrifugation

The centrifuge buckets, lids, adaptors (Beckman) and pots were thoroughly rinsed with 70% ethanol and left to air dry. The adaptor was placed in the bucket followed by the centrifuge pot. The centrifuge pots were filled with ~30ml supernatant and balanced. The centrifuge buckets were placed in the correct position within the SW32Ti rotor. The samples were centrifuged at 4^{o}C, 120000g for 2 hours. After the 2 hours the supernatant was removed. The pellet was resuspended in 300µl media, aliquots were made and stored at -80^{o}C.

2.4.3 Puromycin kill curve

Cells were seeded at a density of 5x10^{4}/2ml in a 6 well tissue culture plate and incubated for 24 hours. To the plate, a range of final puromycin concentrations (1µg/ml, 1.5 µg/ml, 2 µg/ml and 3 µg/ml) were added to the appropriate wells and a control (media only) was included. A cell count was done after 48 hours and the lowest puromycin to kill all cells were determined.

2.4.4 Titering of lentivirus

2.4.4.1 Titering method for cumate vector only and MYC/cumate cells

293T cells were seeded at a density of 5x10^{4}/2ml in a 6 well tissue culture plate. 24 hours later 8µg/ml polybrene (Santa Cruz Biotechnology, Inc) was added to each well and incubated for 20 mins. To the plate, the appropriate viral supernatant was added to give a concentration of 10$^{-3,}$ 10^{-4},10^{-5},10^{-6},10^{-7} and a control (media only) was included. The plate was incubated for 24 hours. After incubation, the media was removed and replaced with selection media (DMEM with 10%FBS and 1% L-glutamine and 1µg/ml puromycin). The plate was incubated for 7 days and selection media was changed every 2 to 3 days. The cumate vector only and MYC/cumate titer plate colonies were counted after 7 days and the average number of transducing particles/ml were calculated by multiplying the total number of colonies counted per well by the dilution factor.

2.4.4.2 Titering method for the pLKO-Tet-On system

Cells were seeded at a density of 5x10^{4}/1ml (D425Med) or 1x 10^{5}/1ml (HDMB03) in a 12 well tissue culture plate and incubated for 14-16 hours in an incubator. After incubation, 8µg/ml polybrene (Santa Cruz Biotechnology) was added to each well and followed by incubation for 20 mins; polybrene was not used for HDMB03 cells. To the plate, 1, 5, 10 or 20µl of viral supernatant was added to each well and a control well was included. The titer plate was incubated (as described in 2.1.1) for 14-16 hours and then the media was replaced with fresh media. The plate was incubated for a further 24 hours, after incubation each well was split into two and 1µg/ml puromycin was added to one well. The cells were removed with trypsin and counted after a further 48 hours of incubation. The average number of transducing particles/ml were calculated according to the following calculation:

Number of cells in well with puromycin/ number of cells in well without puromycin x 100 = % of cells that are infected.

A multiplicity of infection (MOI) of 1 usually equals 50% infectivity.

2.4.5 Analysing the effect of different multiplicities of infection

Cells were seeded at a density of 9 x 10^4/ 2ml in a 6 well tissue culture plate and incubated for 8 hours. After incubation, 8µg/ml polybrene was added to each well and incubated for 20 mins in the incubator (as described in 2.1.1). The appropriate amount of virus was added to each well to give a MOI of 1, 3, 5 or 10. The plate was placed back into the CO_2 incubator (as described in 2.1.1). The next day the media was removed and replaced with selection media.

2.4.6 Determining the percentage of GFP positive cells by flow cytometry analysis

The culture media was removed from the wells and washed with 1ml PBS. The PBS was removed and 0.5ml trypsin was added to each well followed by incubation for 5 mins. The trypsin was neutralized with 90% PBS and 10% FBS. The solution was placed in a Falcon tube and spun down at 300g for 5 mins. After centrifugation the supernatant was removed and the pellet was resuspended in PBS. The samples and control were analysed with BD FACS Calibur according to manufacturer's instructions.

2. 5 Protein extraction and quantification

Protein was extracted from 5x10^4 – 2x10^6 cells, 40µl of lysis buffer (2.5ml 0.5M Tris/HCl pH6.8, 0.4g sodium dodecyl sulfate (SDS), 2ml glycerol, 13.5ml H_2O) was added to the cells followed by heating at 100^{o}C for 10 mins. The samples were either stored at -20^{o}C or sonicated (Sonicator,Diagenode) for three cycles (of 10 seconds on / 10 seconds off). Protein was quantified using the BCA protein assay kit (ThermoFisher Scientific) according to manufacturer instructions. Briefly, diluted Albumin (BSA) standards were prepared and a working reagent (WR) was prepared by mixing 50 parts BCA reagent A with 1 part of BCA reagent B. 25µl of each standard and 1-5µl of sample were aliquoted into a clear 96 well plate. 200µl of WR was added to each well and mixed for 2 mins at RT. The samples were incubated for 30 minutes at 37°C before recording the absorbance (562nm) reading, using the FLUOstar Omega plate reader. Protein concentration was calculated by comparing the absorbance reading to a standard curve, the standard curve was generated by diluting Bovine Serum Albumin within a range of 20-2000µg/ml.

2.6 SDS- PAGE and western blot

Samples were prepared by mixing one volume of 5x loading dye (ThermoFisher Scientific) with 15-25µg protein and made up to a final volume with lysis buffer. The samples were heated for 10 mins at 99°C. The protein ladder (ThermoFisher Scientific) and samples were loaded into a 4-20% precast Amersham ECL gel (GE Healthcare Life Sciences). The run was performed at 160 volts for 1 hour in 1x running buffer. After the separation of proteins, the gel was transferred onto a polyvinyl difluoride (PVDF) membrane (ThermoFisher Scientific) and electrotransfer was performed at 100 volts in 1x transfer buffer (100ml 10x transfer buffer, 100ml methanol and 800ml distilled H_2O). After transfer, the blot was blocked in 1x tris-buffered saline – tween (TBST) containing 5 % skimmed milk, the blot was placed on a rocking platform for 1 hour at RT or overnight at 4°C without shaking. The blot was then placed in the MYC antibody (1:1000, isotope -synthetic peptide 408-438 of the human MYC) (ThermoFisher Scientific) for 60-90 mins. All antibodies used were made up in 1 X TBST containing 1% skimmed milk. After incubation the blot was washed, all blots were washed in 1x TBST for 5mins repeated twice followed by one 10 min wash. The membrane was then incubated in a horseradish peroxidase (HRP) conjugated secondary antibody (1:2500) HRP (Abcam) for 1 hour. After incubation the membrane was washed and the blot was exposed to enhanced chemiluminescence (ECL) (ThermoFisher Scientific) for 7 min followed by signal visualization using GBox Chemi XL1.4. After visualization, the blot was incubated in the TetR antibody (1:1000) (Clontech) for 60 mins. The same previously detailed procedure was performed with regard to washing, secondary antibody and signal visualization. After visualization of the TetR protein, the membrane was placed in 2ml stripping buffer (ThermoFisher Scientific) and incubated for 30 mins at 37°C. After incubation the blot was blocked overnight at 4° C in 1x TBST containing 5 % skimmed milk. The next day the beta-actin antibody (1:20000) (Abcam) was added to the blot, the blot was placed on a rocking platform for 1 hour at RT. After incubation, washing and signal visualization was performed. The composition of the buffers used are listed in Table 16.

Buffers	Compositions
10x Running buffer	0.3% (w/v) Tris base (Sigma Aldrich), 1.44% (w/v) Glycine (Sigma Aldrich), 0.1% (w/v) SDS (Sigma Aldrich)
10x Transfer buffer	1.44% (w/v) Glycine, 0.3% (w/v) Tris base
10x TBST	0.12% (w/v) Tris base, 0.29% Sodium chloride, 1% Tween 20 (Sigma Aldrich)

Table 16:SDS-PAGE buffers and compositions

2.7 Nucleic acids

2.7.1 DNA and RNA extraction

The DNeasy Blood and Tissue kit (Qiagen) was used to extract DNA. Trizol (ThermoFisher Scientific) or the Total RNA Purification kit (NORGEN Biotek) was used to extract total RNA. Trizol and kits were used according to manufacturer instructions.

2.7.2 Assessing nuclei acid concentration and quality

Nucleic acid concentration was measured using the Nanodrop spectrophotometer (NanoDrop 1000, ThermoScientific). The ratio between absorbances at the wavelengths A_{260nm} / A_{280nm} was used to determine the purity of DNA or RNA. For a more accurate measurement, the DNA concentration was quantified using the Qubit dsDNA BR assay kit (Invitrogen) according to manufacturer protocol and concentrations were read using the Qubit 2.0 fluorometer (Invitogen). To analyze integrity of RNA samples, the Agilent RNA 6000 Nano kit (Agilent Technologies) was used according to manufacturer instructions and the RNA chip was run on the Agilent 2100 Bioanalyser.

2.7.3 cDNA synthesis

cDNA was synthesized using the high capacity RNA-to-cDNA kit (ThermoFisher Scientific) according to manufacturer instructions; briefly, the reaction was set up according to Table 17 and thermal cycler conditions according to Table 18. Diluted cDNA was stored at 4ºC and cDNA was stored at -20ºC.

Component	**volume**
Sample	up to 9µl
2x RT buffer	1µl
20x RT enzyme mix	10µl
Nuclease- free H_2O	Made up to 20µl

Table 17:Components for cDNA conversion

Conditions	**Step 1**	**Step 2**	**Step 3**
Temperature (ºC)	37	95	4
Time	60 min	5 min	∞

Table 18:Thermal cycling conditions for reverse transcription

2.8 Quantitative reverse transcription

2.8.1 Primer design for quantitative reverse transcription PCR (RT-qPCR)

The primers used in this study were either obtained from the literature or designed using the NCBI primer designing tool (https://www.ncbi.nlm.nih.gov/tools/primer-blast/). To avoid amplification of genomic DNA, primers were designed to span an exon-exon junction. Primers were diluted and stored as described in section 2.3.6.1 and the primers used are listed in Table 19.

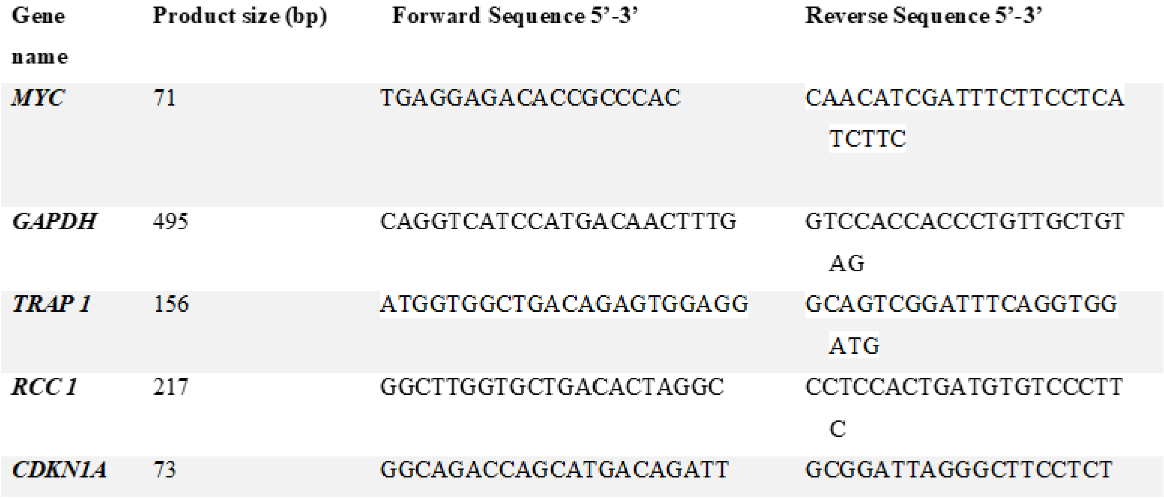

Gene name	**Product size (bp)**	**Forward Sequence 5’-3’**	**Reverse Sequence 5’-3’**
MYC	71	TGAGGAGACACCGCCCAC	CAACATCGATTTCTTCCTCATCTTC
GAPDH	495	CAGGTCATCCATGACAACTTTG	GTCCACCACCCTGTTGCTGTAG
TRAP 1	156	ATGGTGGCTGACAGAGTGGAGG	GCAGTCGGATTTCAGGTGGATG
RCC 1	217	GGCTTGGTGCTGACACTAGGC	CCTCCACTGATGTGTCCCTTC
CDKN1A	73	GGCAGACCAGCATGACAGATT	GCGGATTAGGGCTTCCTCT

Table 19: RT-qPCR primers

2.8.2 RT-qPCR

The Platinum SYBR Green qpcr Supermix-UDG with ROX (Life Technologies) was used to amplify 5ng cDNA. The SYBR Green dye produces a florescent signal as it binds to double stranded DNA. A 10µl reaction was set up according to Table 20 and 21 in a 384 well clear plate and the reaction was run on the ViiA7 machine (Applied Biosystems, UK). Samples were run in triplicate and the endogenous control *GAPDH* was used.

Components	Amount
DNA template (5ng) or nuclease free H_2O (control)	4µl
SYBR Green	5.1µl
Forward primer (10µM)	0.2µl
Reverse primer (10µM)	0.2µl
Nuclease free H2O	0.5µl

Table 20: RT-qPCR reagents for SYBR Green assay

Conditions	Temperature (ºC)	Time
Hold stage		
Step 1	50	2 min
Step 2	95	10 min
PCR Stage (40 cycles)	95	15 sec
Step 1	60	1 min
Step 2		
Melt Curve stage		
Step 1	95	15 sec
Step 2	60	1 min
Step 3	95	15 sec (Dissociation)

Table 21:Cycling conditions for SYBR Green assay

2.8.3 RT-qPCR using Taqman Gene Expression Assay

The Taqman Gene Expression assay (ThermoFisher Scientific) specific to *MYC* contained a Taqman MGB probe with a fluorescent dye FAM on the 5'position and a nonfluorescent quencher on the 3 position'. The endogenous control *B2M* contained the fluorescent dye VIC on the 5' end. Briefly, the appropriate Taqman probe binds to a specific region within *MYC* or *B2M,* when the probe is incorporated into a PCR product the polymerase cleaves the fluorescent dye from the quencher and as a result a fluorescent signal is produced. A 10µl reaction was set up according to Table 22 and 23 in a 384 well plate and the reaction was run on the ViiA7 machine.

Components	Amount
DNA template (5ng) or nuclease free H_2O (control)	4µl
Taqman Fast advanced master mix (Applied Biosystems)	5µl
Taqman probe	0.5µl
Nuclease free H_2O	0.5µl

Table 22: Reagents for Taqman gene expression assay

Conditions	Temperature (°C)	Time
Hold stage		
Step 1	50	2min
Step 2	95	10 min
PCR Stage (40 cycles)		
Step 1	95	15 sec
Step 2	60	1 min

Table 23: Cycling conditions for Taqman gene expression assay

2.8.4 Absolute and relative quantification

2.8.4.1 Absolute quantification

To determine primer pair efficiency a 10 fold serial dilution of cDNA was prepared and a real time assay was performed according to section 2.11.5. Primer efficiency was determined by the slope of the standard curve according to the following formula: $E= (10^{-1/m}-1) X 100$.

Primer sets with an amplification efficiency close to 100% or within a 5% difference were used.

2.8.4.2 Relative quantification

The relative quantification method was used to determine the change in gene expression between treated and control samples. The endogenous controls *GAPDH* or *B2M* were used as reference genes. To determine relative expression the following formula was used:

$$\Delta\ Ct = \text{Normalize } C_T \text{ (target gene) - } C_T \text{ (reference gene)}$$

$$\Delta\Delta Ct = \Delta C_T \text{ (test) - } \Delta C_T \text{ (control)}$$

$$\text{Relative expression} = 2^{-\ \Delta\Delta Ct}$$

2.9 Immunohistochemistry

2.9.1 Cell block preparation

A cell density between 4 to 6 x 10^6 cells were harvested in an appropriate manner. The supernatant was removed and 5ml 4% formaldehyde (Genta medical) was added to the pellet and mixed by inverting the tube for a few times. The samples incubated overnight at RT, after incubation cells were pelleted by centriguation for 10 mins at 335g. The supernatant was removed and pellet was resuspended in 1ml PBS and transferred to an Eppendorf tube. Cells were pelleted by centrifugation for 10 mins at 194g, the supernatant was removed and cells transferred to a PCR tube. Samples were incubated briefly at 65^{o}C; after incubation, cells were resuspended in 100µl of 2.5% agarose dissolved in PBS. To solidify the agarose, the samples incubated at 4^{o}C. Once solidified, the cone was removed with forceps and split into two with a scalpel. The two halves were placed into a tissue embedding and processing cassette and samples were paraffin embedded according to standard protocol.

2.9.2 MYC antibody staining

Briefly, the paraffin embedded slides were de-paraffinized in xylene and rehydrated in a descending range of 99-50% ethanol. 10mM Citrate buffer (Sigma Aldrich) (pH6) (2.1g Citric acid in 1L distilled water and pH adjusted with 2M Sodium hydroxide (Merck Millipore) solution (32g Sodium hydroxide in 400ml distilled water)) was used for antigen retrieval by heating the slides, and before chromogenic staining the slides were washed in H_2O and incubated for 20 minutes in 3% hydrogen peroxide. After incubation, slides were washed in washing buffer (TBS and tween (150mM Sodium chloride (Sigma Aldrich), 0.05% Tween 20 (Sigma Aldrich), 50Mm Tris-HCl buffer, pH 7.6 at 25 ^{o}C) for 5 mins, repeated 3 times. The slides were incubated in MYC antibody (1:300) for one hour at RT; after incubation slides were washed in washing buffer for 5 minutes, repeated 3 times. The Menapath X-Cell Plus HRP-Polymer kit (A. Menarini diagnostics) was used for antigen detection. Briefly, the slides were incubated for 30 min with the HRP polymer and washed once in H_2O before the slide was incubated for 2 mins with 3,3’ diaminobenzidine conc. Slides were then washed once with H_2O and immersed in haematoxylin (Gill No 3, Sigma Aldrich) for 30-60 seconds, then twice in acid alcohol (1% Hydrocholric acid (Sigma Aldrich) in absolute ethanol (Merck Millipore) and finally into Scott’s solution (5mM Magnesium sulfate heptahydrate (Sigma Aldrich), 0.2mM Sodium bicarbonate (Sigma Aldrich) dissolved in distilled water) for 2 mins. The slides were dehydrated and mounted using DPX and analyses were done using the Aperio softeware version 12.3.1.602 (Leica Biosystems). Processes involved in Immunohistochemistry were performed by Dr Stephen Crosier, Yura Grabovska, Halimat Popoola and Freya Hassall.

2.10 Statistics

Statistical analyses (Student’s t-test) were performed with GraphPad Prism (version 6.04) and $p<0.05$ was set as the threshold for statistical significance.

2.11 Gene expression profiling

High throughput technologies such as RNA was used to give insight into genome-wide gene expression profiles.

2.11.1 mRNA sequencing

RNA sequencing (RNA-seq) is a high throughput sequencing method used for determining gene expression levels, alongside the detection of alternative splicing, novel transcripts and gene fusions (Conesa *et al.*, 2016). RNA-seq has many advantages compared to other methods, Compared to microarrays, RNA-seq is more sensitive and has a larger dynamic range of quantification, with lower background noise.(Wang *et al.*, 2009). For this project, mRNA extraction was performed (as described in methods 2.7.1) and sent to the Genomics Core Facility at Newcastle University. For cDNA library preparation, the TruSeq Stranded mRNA kit (Illumina) was used according to the high throughput Truseq mRNA sample preparation protocol. Briefly, total RNA with a RNA integrity number ≥ 8 was purified for mRNA by selection of poly(A)-tailed RNA molecules using poly(T) oligonucleotides attached to magnetic beads. After enrichment, the mRNA was broken into smaller fragments followed by the synthesis of the first strand of cDNA by reverse transcription and random primers. After the second strand synthesis, a single nucleotide "A" was added to the 3' strand of the blunt cDNA, to prevent binding of the blunt ends during the ligation of index adaptors. The cDNA with adaptor molecules were then enriched by PCR, after enrichment samples were run on the NextSeq 500 machine. Analysis was performed by Dr Daniel Williamson; all samples were subjected to quality control using Fastqc, paired-end reads were mapped to the human genome hg19 using RNAstar (Dobin *et al.*, 2013). To quantify transcripts, expression the raw read counts for each sample were aligned to the Gencodev 17 library using HTseq (Anders *et al.*, 2015) and DEseq2 was used for variance stabilization, normalization and differential gene expression analysis (Love *et al.*, 2014).

Chapter 3 Generation of inducible isogenic models of MYC-driven Group 3 medulloblastoma

3.1 Introduction

Cell line models in which MYC expression can be modulated could give important insights into the role of MYC in MB, allowing assessment of the phenotype and subsequent functional consequences. A stable expression system was selected, whereby the genetic material is integrated into the host genome allowing the same cell line to be used in repeated experiments (Kim and Eberwine, 2010). An inducible expression system (discussed in 1.7.2) was chosen to allow both the level and period of overexpression or knockdown of the gene to be controlled. Some inducible expression systems require the addition of inducers such as heavy metals, steroid hormones or heat shock to regulate the expression of a gene (Gossen *et al.*, 1994; Mullick *et al.*, 2006); however, these systems may result in inconsistencies such as 'leakiness' (i.e. the expression of the gene in the absence of the inducer) which is caused by factors including the promoters being too active in the 'off' state and/or the initiation of pleiotropic activities caused by the inducing agents (Gossen *et al.*, 1994). It was therefore important to select an inducible expression system that has low basal activity in the 'off' state and no pleiotropic effects caused by the inducing molecule and to confirm this in any models developed. On this basis, an 'all in one' vector system was selected; a single vector containing all the essential elements for generation of the cell line models (Wiederschain *et al.*, 2009). The two inducible lentiviral systems selected are described in 3.1.1. The two inducible lentiviral systems selected are described in 3.1.1. The cumate vector is designed to facilitate regulatable expression of cDNA, whereas the pLKO-Tet vector was designed to allow regulatable shRNA expression. The promoters for the two vector systems differ as the cumate inducible lentiviral system for MYC overexpression uses a RNA pol II promoter (CMV), whereas the pLKO-Tet vector to knockdown MYC uses a RNA pol III promoter (H1).

The cell lines chosen to create the inducible systems were selected based on their *MYC* amplification and subgroup status (discussed in 3.2) as suitable for overexpression or MYC knockdown. There are 44 continuous (cell lines that have acquired genetic alterations that enables them to proliferate indefinitely (Masters, 2000) MB cell lines described in the literature, of which 18 have been assigned to a subgroup (Ivanov *et al.*, 2016). Although only a small percentage of primary tumours (approximately 5%) are $\mathrm{MB_{GRP3}}$ and have *MYC* amplification, the majority of the subgrouped cell lines belong to this tumour type, indicating that these tumours are more likely to establish growth *in vitro*, because of genetic changes that favour unlimited growth *in vitro*. MB cell lines that are classified into subgroups will be useful in developing targeted therapeutic approaches for patients and because MYC is a poor prognostic factor in $MB_{GRP3,}$ generating MYC inducible models will aid in developing targeted therapeutic options for MB_{GRP3} patients.

3.1.1 Selection of an inducible lentiviral system

To modulate the expression of MYC within MB_{GRP3} cell lines two inducible lentiviral systems were selected.

1)The cumate vector system (System Biosciences) was selected to overexpress MYC within selected cell lines. Briefly in the absence of the cumate solution the binding of the CymR repressor to the cumate operator (CuO) prevents transcription from the CMV5 promoter. Addition of cumate solution changes the configuration of the CymR, preventing it from binding to the CuO, as a result the CMV promoter stimulates expression of *MYC* (Figure 3.1) (Mullick *et al*., 2006). The Cumate vector system has a puromycin marker which allows for stable cell lines to be generated through positive selection. This system also allows for induction of overexpression of the gene of interest to be tracked by a green fluorescent protein (GFP) marker. The dual expression of *MYC* and *GFP* is mediated through an internal ribosomal entry site (IRES) which allows for simultaneous expression from the same promoter and because of its ability to be switched on and off, it is thus ideal for timed expression experiments (System Biosciences manual).

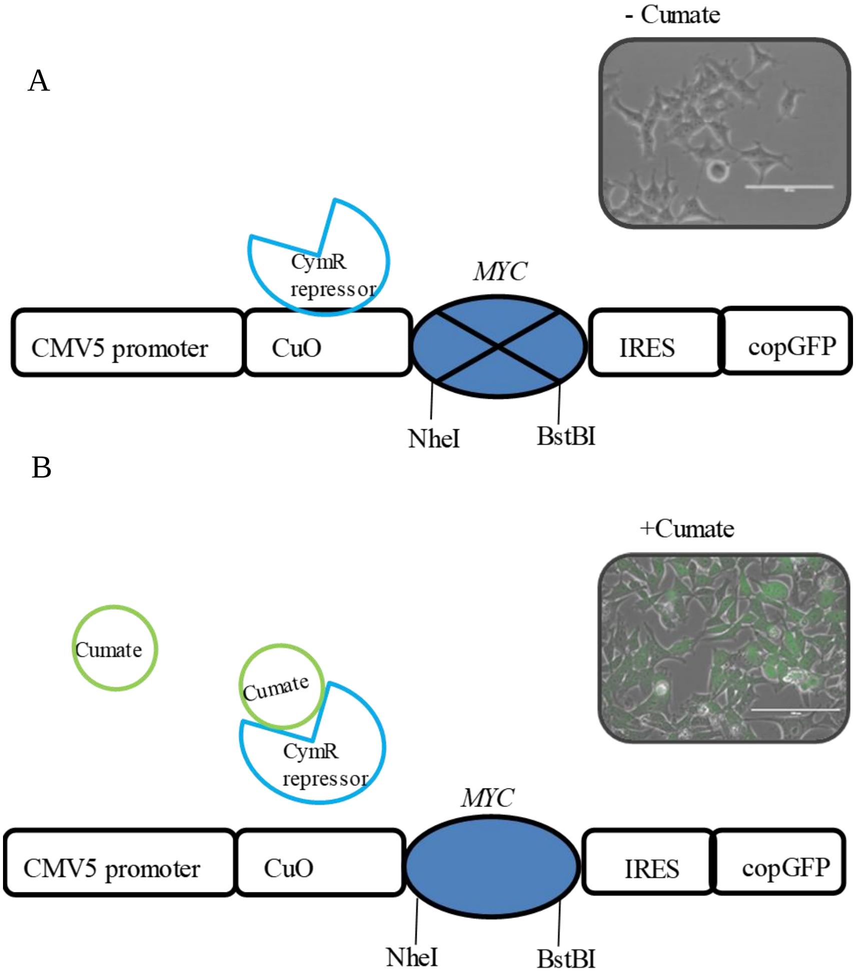
A
- Cumate
CymR repressor
MYC
CMV5 promoter
CuO
IRES
copGFP
NheI
BstBI
B
+Cumate
Cumate
Cumate
CymR repressor
MYC
CMV5 promoter
CuO
IRES
copGFP
NheI
BstBI

Figure 3.1 Mechanism of transcriptional control of cumate system (adapted from System Biosciences manual). A) The binding of the CymR repressor to the cumate operator (CuO) prevents *MYC* (represented by X) transcription from the CMV5 promoter. In the absence of cumate solution *MYC* is not overexpressed as shown by the cell line image that GFP has not been induced (-cumate). B) Addition of cumate solution changes the configuration of the CymR preventing if from binding to the CuO, as a result the CMV promoter stimulates expression of *MYC* as shown by the cell line image that GFP is induced (+ cumate) (NheI and BstBI are the restriction sites).

2) The pLKO-Tet-on system was used to knockdown MYC within selected MB cell lines. This system contains all the required components for a TeT inducible shRNA expression system. The pLKO-Tet-on system contains the H1 promoter which has two Tet responsive elements (TRE) on each side of the TATA box and regulates the expression of the shRNA. The Tet repressor (TetR) is downstream from the polymerase II hPGK promoter. The IRES allows for simultaneous expression of TetR and puromycin from the hPGK promoter. The TetR binds to TRE which prevents expression of the shRNA. Addition of Dox binds to the TetR, which prevents the TetR

from binding to TRE as a result the shRNA are expressed (Figure 3.2) (Wiederschain *et al.*, 2009). Stable inducible cell lines can easily be generated because of the puromycin selection marker (Wiederschain *et al.*, 2009).

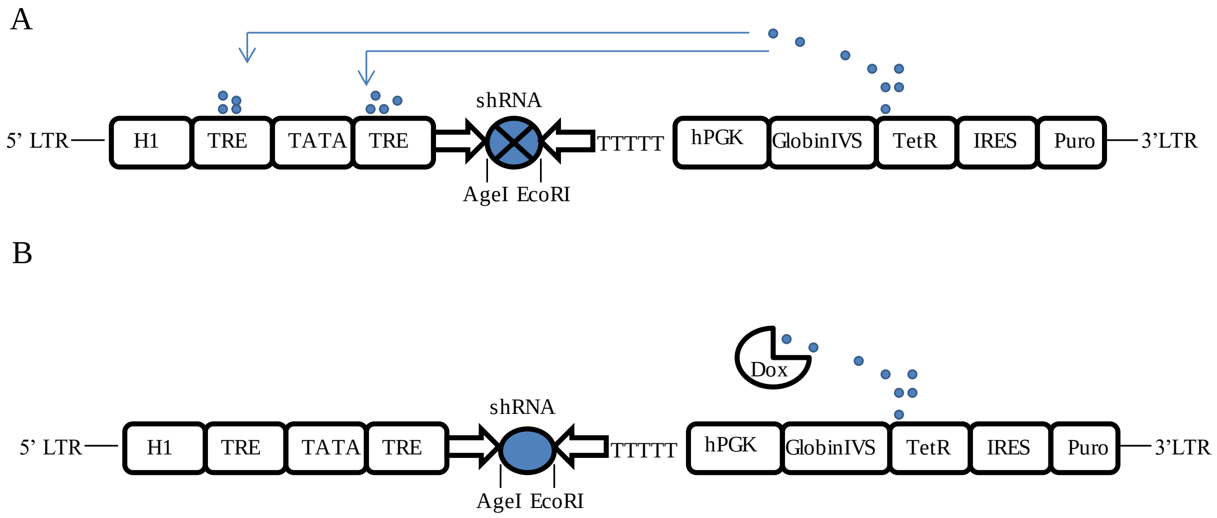

Figure 3.2 Mechanism of transcriptional control of pLKO-Tet-on, diagram adapted from (Wiederschain *et al*., 2009). A) In the absence of DOX the TetR (represented by the blue dots) binds to the TRE as a result the shRNA is not expressed (represented by X). B) Addition of Dox (represented by partial circle) binds to the TetR, which prevents the TetR from binding to TRE as a result shRNA are expressed (Wiederschain *et al*., 2009). The AgeI and EcoRI are restriction sites.

3.2 Cell line selection

MB cell line subgroup status (Table 24) was assigned by the projection of four subgroup specific metagenes derived from primary MB methylation data (Schwalbe *et al.*, 2013a) using non-negative matrix factorization (NMF) onto the methylation profiles of 14 medulloblastoma cell lines (analysis performed by Daniel Williamson). NMF projection of subgroup-specific metagenes derived from primary MB expression data onto cell line expression data gave confirmatory results (Figure 3.3) (Schwalbe *et al.*, 2013a). The cell lines selection for this study were based on the *MYC* and subgroup status of the cell line. Cell lines selected were MB$_{\text{GRP3}}$ with either non- amplified or amplified *MYC* status alongside a non MB$_{\text{GRP3}}$ cell line (DAOY) which was used as a control (Table 25). DAOY (non MB$_{\text{GRP3}}$) and CHLA-259 (MB$_{\text{GRP3}}$), two non-amplified cell lines with low *MYC* expression were selected to generate the isogenic cumate inducible MYC overexpression models. CHLA-259 was selected because it is the only MB$_{\text{GRP3}}$ cell line with non-amplified *MYC* status and with low *MYC* expression. DAOY was selected to optimize the cumate inducible lentivector system because it is adherent, robust and grows quickly. DAOY also has low MYC protein and mRNA expression (Figure 3.4 A-C) and therefore is an ideal cell line to be used for optimization. CHLA-259 is the only MB$_{\text{GRP3}}$ cell line investigated without amplification or gain of the *MYC* locus. HDMB03 and D425Med are the MB$_{\text{GRP3}}$ cell lines selected to generate the isogenic DOX inducible MYC knockdown models. These two cell lines were selected because they are robust and grows quickly. These two cell lines have *MYC* amplification which leads to an increased protein and mRNA expression (Figure 3.4 A-C) and therefore represent suitable models for MYC knockdown.

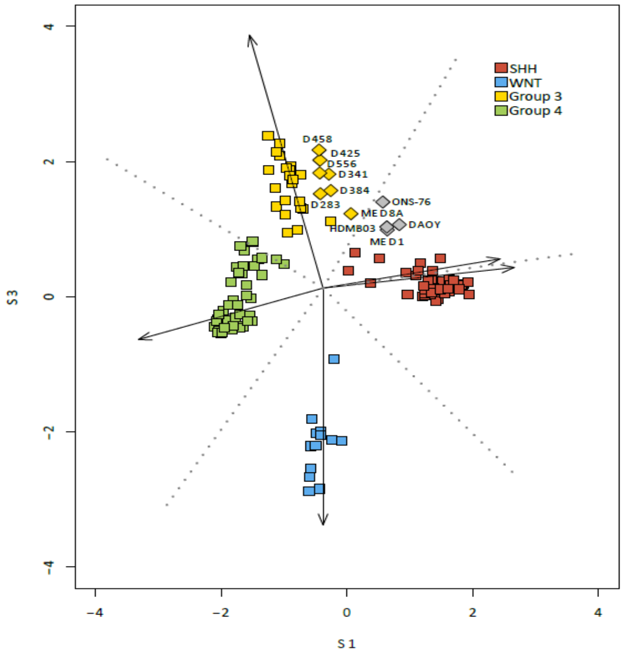

Figure 3.3 Negative matrix factorization projection of subgroups specific metagenes derived from primary MB expression data onto cell line expression confidently assigns most cell lines to Group 3 with the remainder having no confident subgroup assignation. Plot shows selected cell lines (labelled diamonds) and primary samples of known subgroup (squares) (provided by Daniel Williamson).

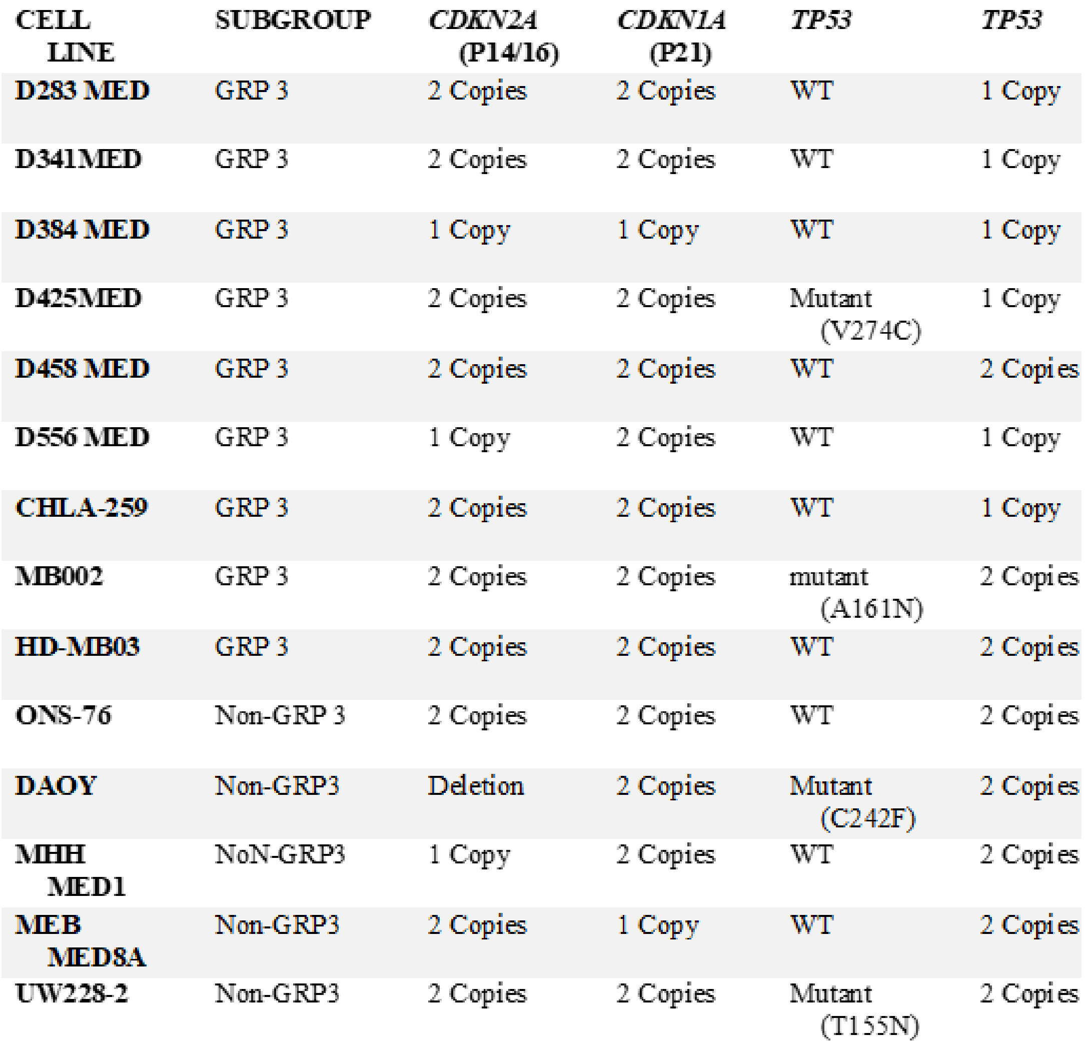

CELL LINE	SUBGROUP	*CDKN2A* (P14/16)	*CDKN1A* (P21)	*TP53*	*TP53*
D283 MED	GRP 3	2 Copies	2 Copies	WT	1 Copy
D341MED	GRP 3	2 Copies	2 Copies	WT	1 Copy
D384 MED	GRP 3	1 Copy	1 Copy	WT	1 Copy
D425MED	GRP 3	2 Copies	2 Copies	Mutant (V274C)	1 Copy
D458 MED	GRP 3	2 Copies	2 Copies	WT	2 Copies
D556 MED	GRP 3	1 Copy	2 Copies	WT	1 Copy
CHLA-259	GRP 3	2 Copies	2 Copies	WT	1 Copy
MB002	GRP 3	2 Copies	2 Copies	mutant (A161N)	2 Copies
HD-MB03	GRP 3	2 Copies	2 Copies	WT	2 Copies
ONS-76	Non-GRP 3	2 Copies	2 Copies	WT	2 Copies
DAOY	Non-GRP3	Deletion	2 Copies	Mutant (C242F)	2 Copies
MHH MED1	NoN-GRP3	1 Copy	2 Copies	WT	2 Copies
MEB MED8A	Non-GRP3	2 Copies	1 Copy	WT	2 Copies
UW228-2	Non-GRP3	2 Copies	2 Copies	Mutant (T155N)	2 Copies

Table 24: Human medulloblastoma cell lines acquired by the Paediatric Brain Tumour Research group and subgrouped by metagene projection

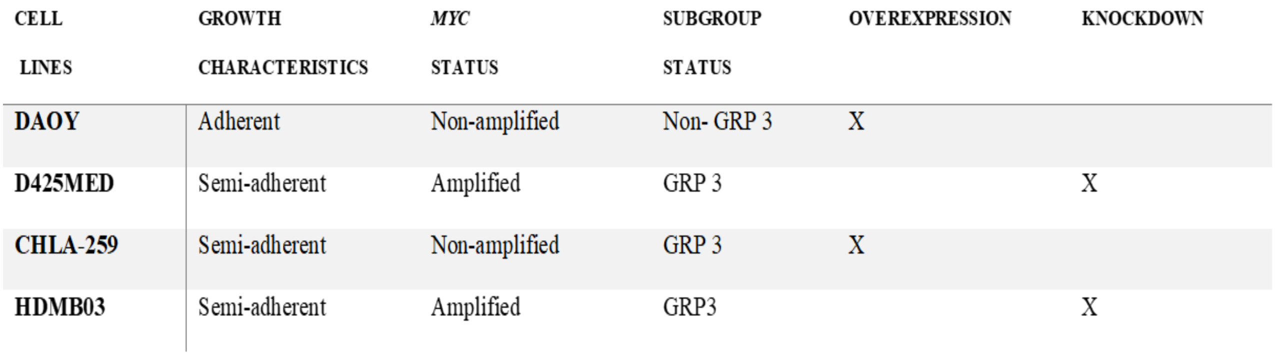

CELL LINES	GROWTH CHARACTERISTICS	*MYC* STATUS	SUBGROUP STATUS	OVEREXPRESSION	KNOCKDOWN
DAOY	Adherent	Non-amplified	Non- GRP 3	X	
D425MED	Semi-adherent	Amplified	GRP 3		X
CHLA-259	Semi-adherent	Non-amplified	GRP 3	X	
HDMB03	Semi-adherent	Amplified	GRP3		X

Table 25:Human medulloblastoma cell lines selected for generation of isogenic models

X denotes the intended manipulation for each cell line

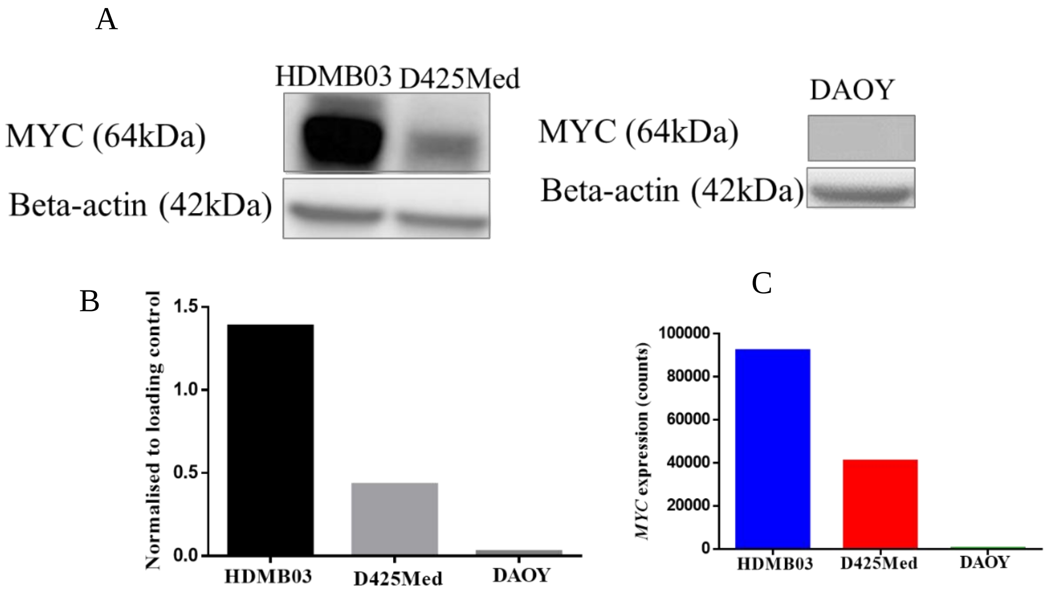

Figure 3.4 MYC protein and mRNA expression in HDMB03, D452Med and DAOY cell lines. A) Western blot analysis of MYC expression in HDMB03, D425Med cell lines and DAOY. B) Densitometry analysis of MYC protein expression in HDMB04, D425Med and DAOY, results were normalised to beta-actin. C) RNA expression analysis of *MYC* in HDMB03, D425Med and DAOY. Beta-actin was used as a loading control.

3.3 Generation of inducible MYC overexpression in DAOY and CHLA-259

3.3.1 Construction of MYC into the cumate inducible lentiviral vector

To overexpress MYC within MB cell lines, a region of DNA (1320bp) encompassing the *MYC* coding sequence was cloned into the cumate inducible lentiviral vector (Figure 3.5). Once the correct *MYC* sequence in its plasmid of origin (pcDNA3-cmyc, Figure 2.1) was verified by Sanger sequencing, composite primers containing 5’ tags with recognition sites for the appropriate restriction enzymes were designed and used to PCR amplify the region containing the sequence for MYC (primers listed in methods, Table 10). To test the *MYC* sequence was successfully amplified, 1µl of PCR product was separated on an agarose gel and visualized as described in methods (2.3.9) (result not shown). The cumate vector and gene insert (amplified product) were each sequentially digested with NheI- HF restriction enzyme followed by BstBI restriction enzyme (methods, 2.3.12). Both insert and vector were purified and then ligated at different ratios (vector: insert, 1:3, 1:5 and 1:8). The ligation mixtures were transformed into Stbl3 competent cells and DNA from ampicillin resistant colonies was purified and sequentially digested with NheI-HF then BstBI to release the insert, followed by separation on an agarose gel and visualization. DNA from bacterial colonies containing the desired construct are shown in figure 3.6 (colony: 2, 3, 5, 7, 8, 9, 10 and 12). The *MYC* cumate constructs were verified by sequencing both the forward (Figure 3.7) and reverse strand. After sequence verification lentivirus was produced and viral titer was determined (see methods, 2.4.4.1 and 2.4.1).

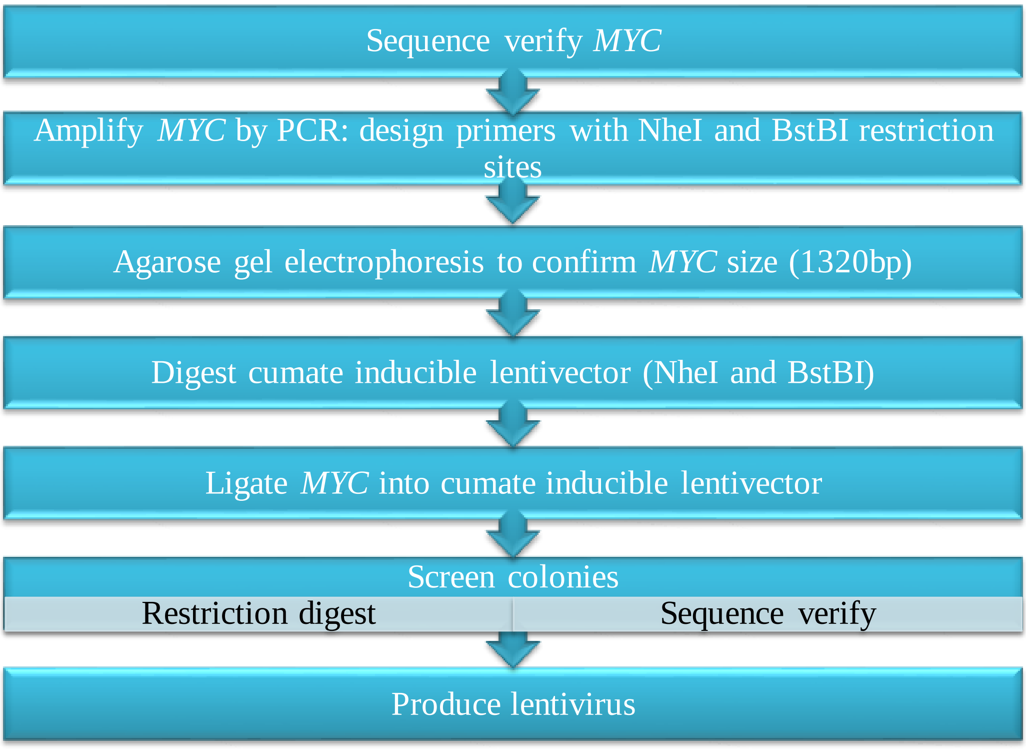
Sequence verify MYC
Amplify MYC by PCR: design primers with NheI and BstBI restriction sites
Agarose gel electrophoresis to confirm MYC size (1320bp)
Digest cumate inducible lentivector (NheI and BstBI)
Ligate MYC into cumate inducible lentivector
Screen colonies
Restriction digest
Sequence verify
Produce lentivirus

Figure 3.5 Overview of the cloning strategy of MYC into the inducible cumate lentivector.

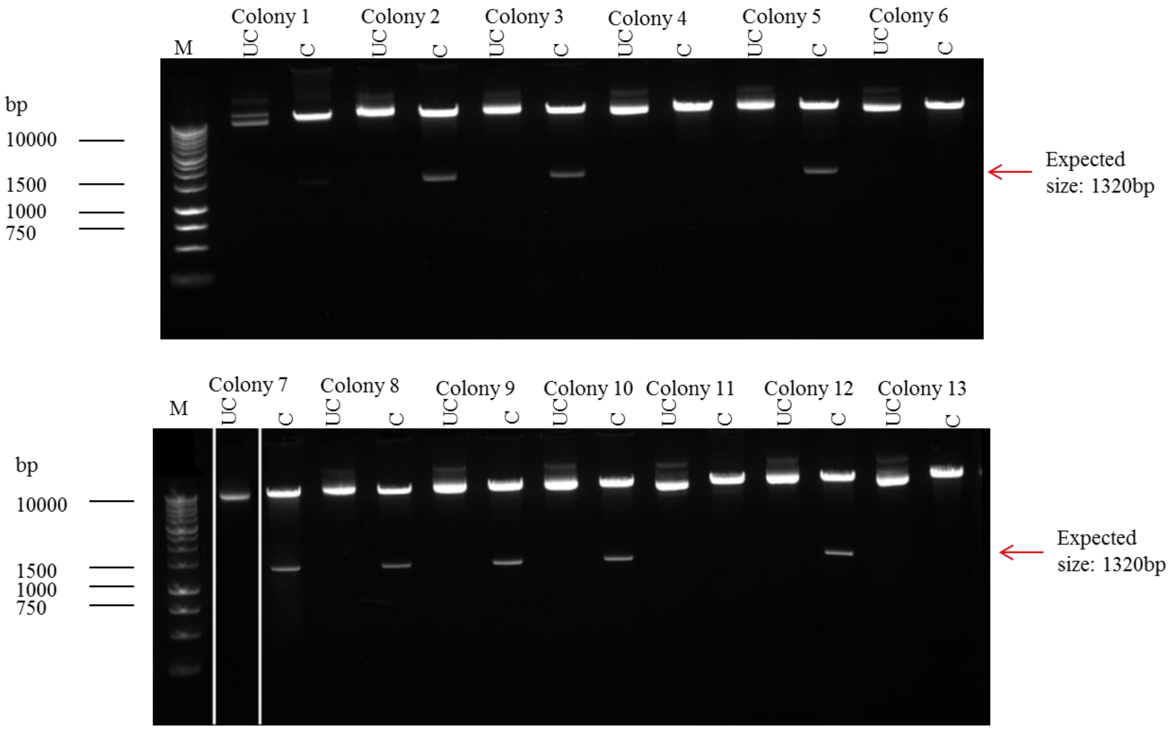
Colony 1
Colony 2
Colony 3
Colony 4
Colony 5
Colony 6
M
UC
C
bp
10000
1500
1000
750
Expected size: 1320bp
Colony 7
Colony 8
Colony 9
Colony 10
Colony 11
Colony 12
Colony 13
M
UC
C
bp
10000
1500
1000
750
Expected size: 1320bp

Figure 3.6 Restriction enzyme digests analysis of selected colonies to confirm the MYC/ cumate vector construct.M: DNA marker, UC: uncut and C: Cut. Colonies were sequentially digested with NheI-HF then BstBI and separated on a 1% (w/v) agarose gel. The correct length insert was released in colonies 2,3,5,7,8,9,10 and 12.

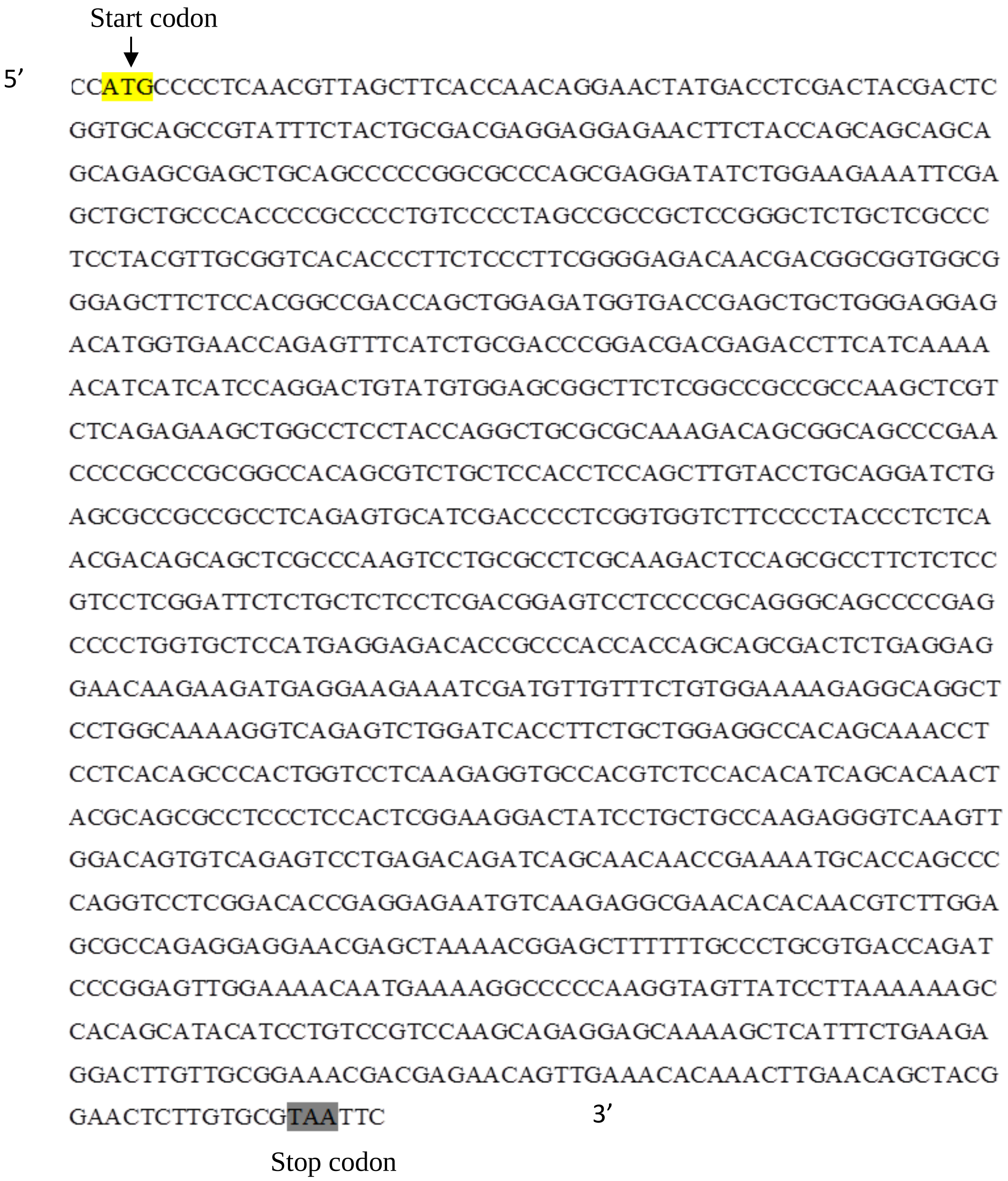

Start codon

5′ CCATGCCCCTCAACGTTAGCTTCACCAACAGGAACTATGACCTCGACTACGACTC
GGTGCAGCCGTATTTCTACTGCGACGAGGAGGAGAACTTCTACCAGCAGCAGCA
GCAGAGCGAGCTGCAGCCCCCGGCGCCCAGCGAGGATATCTGGAAGAAATTCGA
GCTGCTGCCCACCCCGCCCCTGTCCCCTAGCCGCCGCTCCGGGCTCTGCTCGCCC
TCCTACGTTGCGGTCACACCCTTCTCCCTTCGGGGAGACAACGACGGCGGTGGCG
GGAGCTTCTCCACGGCCGACCAGCTGGAGATGGTGACCGAGCTGCTGGGAGGAG
ACATGGTGAACCAGAGTTTCATCTGCGACCCGGACGACGAGACCTTCATCAAAA
ACATCATCATCCAGGACTGTATGTGGAGCGGCTTCTCGGCCGCCGCCAAGCTCGT
CTCAGAGAAGCTGGCCTCCTACCAGGCTGCGCGCAAAGACAGCGGCAGCCCGAA
CCCCGCCCGCGGCCACAGCGTCTGCTCCACCTCCAGCTTGTACCTGCAGGATCTG
AGCGCCGCCGCCTCAGAGTGCATCGACCCCTCGGTGGTCTTCCCCTACCCTCTCA
ACGACAGCAGCTCGCCCAAGTCCTGCGCCTCGCAAGACTCCAGCGCCTTCTCTCC
GTCCTCGGATTCTCTGCTCTCCTCGACGGAGTCCTCCCCGCAGGGCAGCCCCGAG
CCCCTGGTGCTCCATGAGGAGACACCGCCCACCACCAGCAGCGACTCTGAGGAG
GAACAAGAAGATGAGGAAGAAATCGATGTTGTTTCTGTGGAAAAGAGGCAGGCT
CCTGGCAAAAGGTCAGAGTCTGGATCACCTTCTGCTGGAGGCCACAGCAAACCT
CCTCACAGCCCACTGGTCCTCAAGAGGTGCCACGTCTCCACACATCAGCACAACT
ACGCAGCGCCTCCCTCCACTCGGAAGGACTATCCTGCTGCCAAGAGGGTCAAGTT
GGACAGTGTCAGAGTCCTGAGACAGATCAGCAACAACCGAAAATGCACCAGCCC
CAGGTCCTCGGACACCGAGGAGAATGTCAAGAGGCGAACACACAACGTCTTGGA
GCGCCAGAGGAGGAACGAGCTAAAACGGAGCTTTTTTGCCCTGCGTGACCAGAT
CCCGGAGTTGGAAAACAATGAAAAGGCCCCCAAGGTAGTTATCCTTAAAAAAGC
CACAGCATACATCCTGTCCGTCCAAGCAGAGGAGCAAAAGCTCATTTCTGAAGA
GGACTTGTTGCGGAAACGACGAGAACAGTTGAAACACAAACTTGAACAGCTACG
GAACTCTTGTGCGTAATTC 3′

Stop codon

Figure 3.7 The forward strand of MYC sequence inserted into the cumate inducible vector. Yellow represents the start codon and grey represents the stop codon.

3.3.2 Determining optimum multiplicity of infection for DAOY

To determine the optimal multiplicity of infection (MOI) for infecting DAOY, cells were infected with the cumate inducible lentiviral system expressing MYC at a range of MOIs (Figure 3.8, Figure 3.9 A and B). The GFP marker was used to monitor induction of cells, infected with MYC lentivirus in the presence or absence of 1x cumate solution. In the absence of 1x cumate, MOI 3 gave the lowest percentage of GFP positive cells (Figure 3.8). In the presence of 1x cumate, MOI 5 and MOI 10 gave a slightly higher number of GFP positive cells compared to MOI3 (Figure 3.8). MYC protein expression for the different MOIs were analysed by immunoblotting using an antibody against MYC (method described in 2.6). In the presence of 1x cumate DAOY infected with MOI 3 MOI 5 and MOI 10 achieved similar levels of MYC overexpression (Figure 3.9 A and B), the overexpression of MYC isn't as strong as the amplified cell lines (Figure 3.13). For further optimization of this system we selected DAOY infected with the MYC inducible lentiviral system at a MOI 3 as the stable cell line to use. MOI 3 was selected because in the absence of 1x cumate solution it had the lowest percentage of GFP positive cells indicating that it has a lower basal background expression; less 'leaky' compared to MOI 5 and MOI 10. Western blot analysis showed that MOI 3 achieved comparable MYC overexpression to MOI 5 and MOI 10. Therefore, DAOY infected at MOI 3 was selected as the stable cell line, henceforth this cell line will be referred to as 'DAOY MYC'.

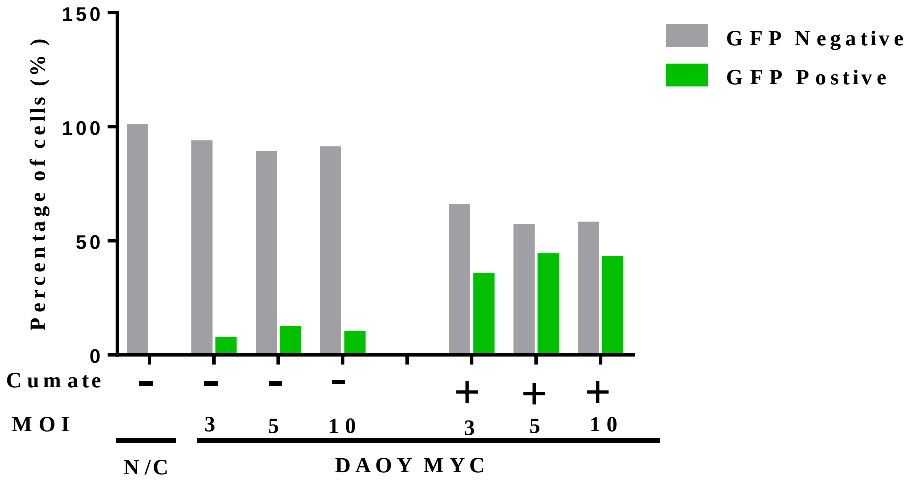

Figure 3.8 Analysis of DAOY MYC either in the presence or absence of 1x cumate solution. In the absence of 1x cumate DAOY MYC MOI 3 had the lowest percentage of GFP positive cells. In the presence of 1x cumate, DAOY MYC MOI 3 had the lowest percentage of GFP positive cells and DAOY MYC MOI 5 and MOI 10 achieved the highest GFP positive cells.

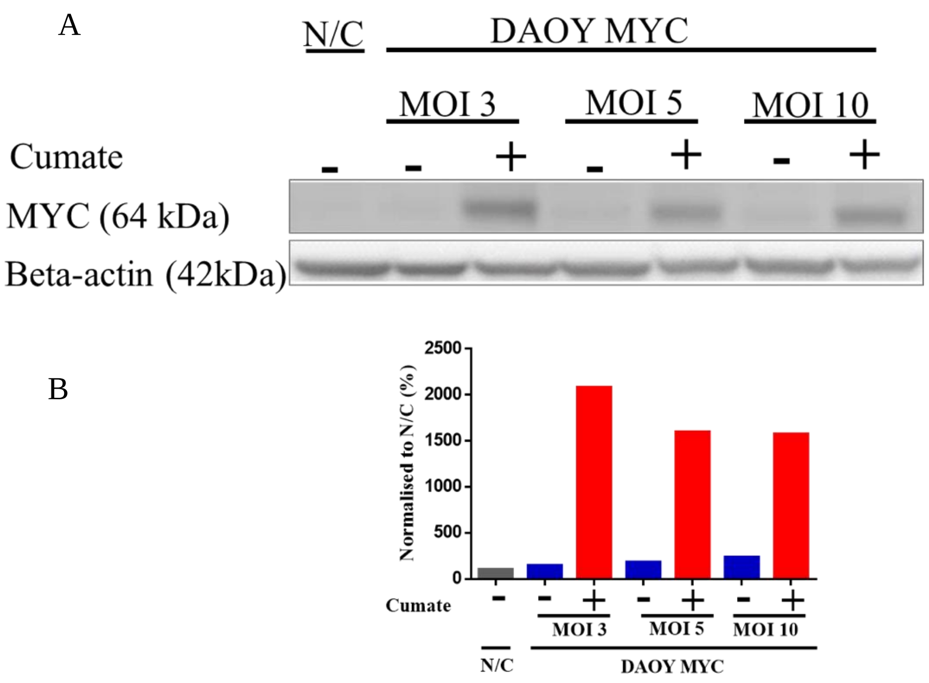

Figure 3.9 Analysis of MYC expression in DAOY MYC infected with different MOIs. A) Western blot analysis of DAOY MYC transduced with MOI 3, MOI 5 and MOI 10, cultured in the absence or presence of 1x cumate. DAOY parent cell line was included to serve as a negative control (N/C) and beta-actin served as a negative control. B) Densitometry results of the western blot analysis of DAOY MYC infected with MOI 3, MOI 5 and MOI 10, the results were normalised to beta-actin and quantified with respect to control (DAOY N/C) (grey, N/C – cumate; blue, – DOX; red, + DOX).

3.3.3 A time course analysis of MYC expression in DAOY MYC

To determine the optimal time point for MYC overexpression following the addition of 1x cumate to the culture media, DAOY MYC cells were seeded and incubated for 8 hours before the addition of 1x cumate and, as a control, cells were cultured in the absence of 1x cumate. After 24, 48, 72 and 96 hours, cell pellets were harvested and MYC protein expression was analyzed by immunoblotting using a MYC antibody. In DAOY MYC at 48 hours, MYC overexpression was seen (Figure 3.10 A and B) in the presence of 1x cumate. A similar increase was seen at 72 hours, with greatest increase achieved at 96 hours (Figure 3.10 A and B). However, at 96 hours in the absence of 1x cumate, MYC was also overexpressed compared to the negative control and other time points (Figure 3.10 A and B). This indicates that at 96 hours in the absence of 1x cumate, the promoter activity is too high causing expression leakage.

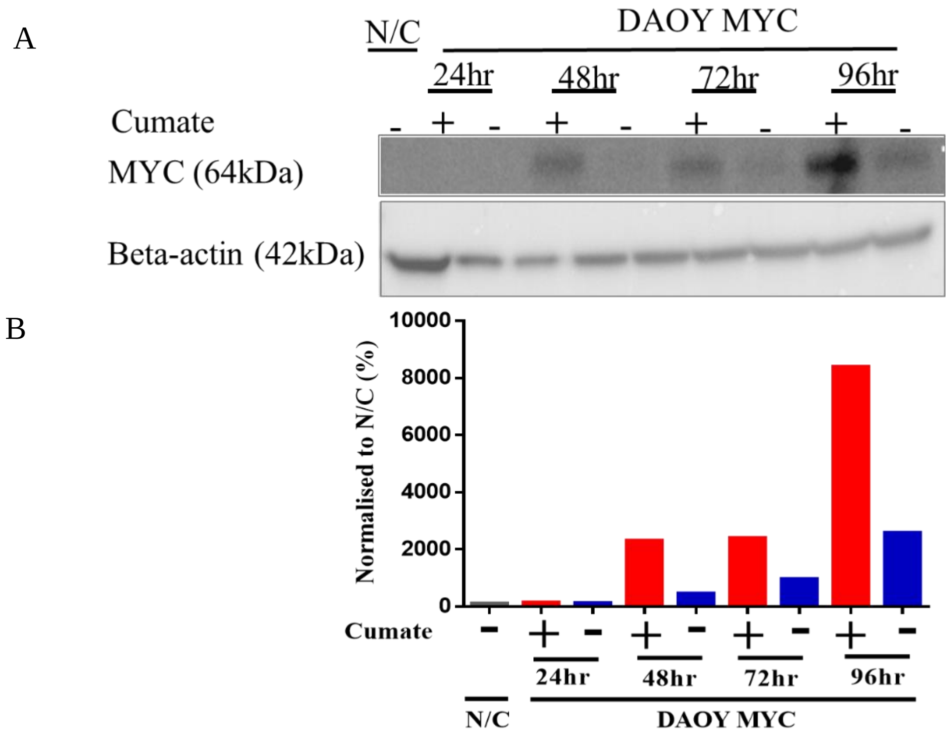

Figure 3.10 Western blot and densitometry of MYC protein expression in DAOY MYC in the absence or presence of 1x cumate. A) Western blot analysis of DAOY MYC harvested at different time points in the absence or presence of 1x cumate. The DAOY parent cell line was included and served as a negative control (N/C) and beta-actin as a loading control. B) Densitometry result of the western blot analysis of DAOY MYC harvested at different time points in the absence or presence of 1xcumate, the results were normalised to beta-actin and quantified with respect to control DAOY N/C (grey, N/C; blue, – DOX; red, + DOX)

3.3.4 Overexpression of MYC in CHLA-259

Following successful transduction of the non MB_{GRP3} cell line DAOY with the cumate vector system, attempts were made to generate an inducible version of the MB_{GRP3} cell line CHLA-259. Unfortunately, this cell line was unable to be transduced. CHLA-259 is a semi adherent cell line, with a slow doubling time (96 hours) and grows in neurosphere-like clusters. Despite numerous attempts at optimization, any puromycin resistant clones generated were found not to contain the construct and ultimately transduction of CHLA-259 was unsuccessful.

3.4 Generation of inducible MYC knockdown in D425Med and HDMB03

3.4.1 Cloning of short hairpin RNA into the pLKO-Tet-On vector

To knockdown MYC within MB cell lines, three shRNAs targeting *MYC* and a NS control were cloned into the pLKO-Tet-On vector (Figure.3.11). The pLKO-Tet-On vector was double digested with AgeI and EcoRI and subsequently gel purified. The shRNA oligos: designated MYC-1, MYC- 2, MYC-3 and NS were ligated into the pLKO-Tet-On vector. The shRNA oligos: MYC- 1 (128752642-12753447), MYC-2 (128752642- 128753204), MYC- 3(128752642-128753201) (Genome Reference Consortium GRCh37) all target the third exon of *MYC* at different positions. The ligation mixtures were transformed into Stbl3 competent cells and DNA from ampicillin resistant colonies were purified and sequentially digested with XhoI to release the insert. Successfully colonies were identified by release of two products below 200bp for the NS, MYC-1, MYC-2 (Figure 3.12 A) and for MYC-3 (Figure 3.12 B). The shRNA pLKO-Tet-On constructs were sequenced verified (sequences are the same as in Table 9) and after sequence verification lentivirus was produced and viral titer was determined.

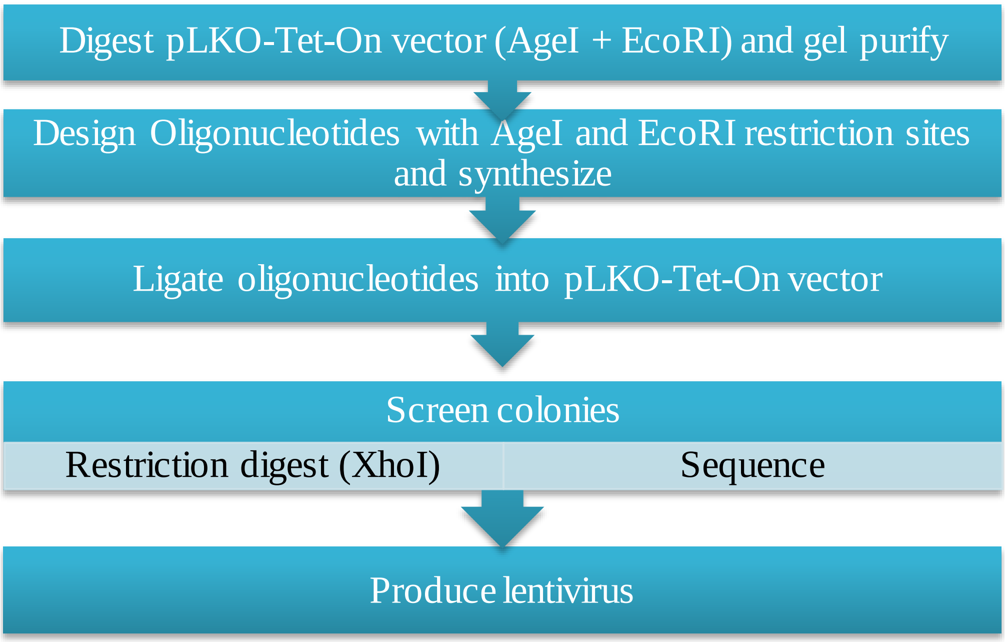
Digest pLKO-Tet-On vector (AgeI + EcoRI) and gel purify
Design Oligonucleotides with AgeI and EcoRI restriction sites and synthesize
Ligate oligonucleotides into pLKO-Tet-On vector
Screen colonies
Restriction digest (XhoI)
Sequence
Produce lentivirus

Figure 3.11 Cloning strategy for shRNAs into the pLKO-Tet-On vector.

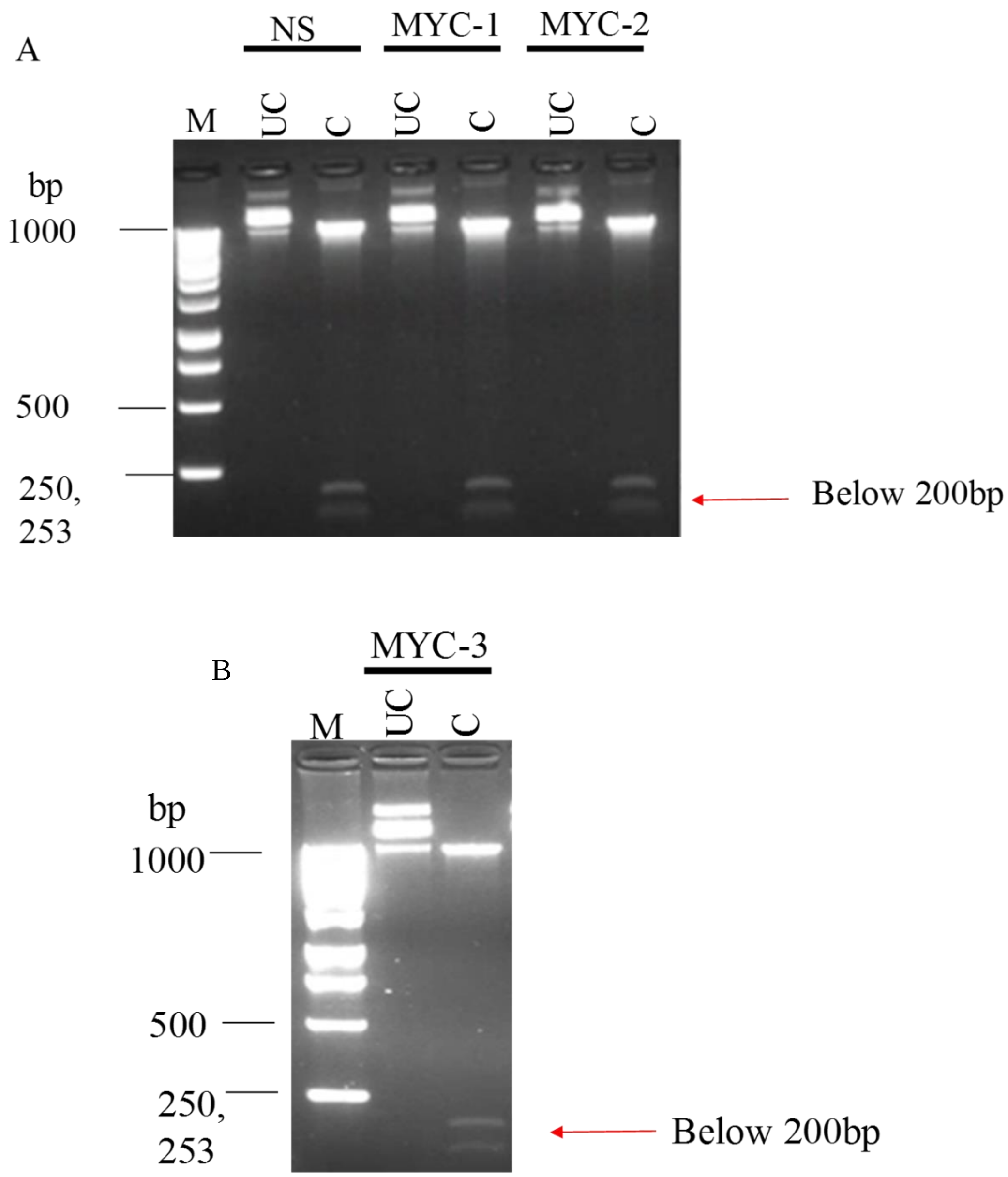
A
NS
MYC-1
MYC-2
M
UC
C
UC
C
UC
C
bp
1000
500
250,
253
Below 200bp
B
MYC-3
M
UC
C
bp
1000
500
250,
253
Below 200bp

Figure 3.12 XhoI restriction digest of selected shRNA/pLKO-Tet-On constructs. M: DNA marker, UC: uncut and C: Cut. A) XhoI restriction digest of NS, MYC-1 and MYC-2. B) XhoI restriction digest of MYC- 3.

3.4.2 Determining puromycin concentration for selection of positive clones in D425Med and HDMB03

The puromycin concentration for positive selection was determined for D425Med and HDMB03. D425Med and HDMB03 were dosed with a range of puromycin (1µg/ml, 1.5µg/ml, 2µg/ml) and after 48 hours a cell count was done and the lowest concentration that killed all cells was determined to be 1µg/ml of puromycin (result not shown).

3.4.3 Validating MYC knockdown in D425Med

To determine if each shRNA targeting *MYC* could knockdown MYC in the presence of DOX, D425Med was infected with the MYC-1, MYC-2 and MYC-3 lentiviral for 24 hours, after incubation the media was replaced with selection media (recipe described in 2.1.1). The cells were grown until they reached 80% confluency before the addition of DOX to the appropriate wells. Cell pellets were harvested after 72 hours and the protein expression analysed by immunoblotting using antibodies against MYC, TetR and beta-actin (method described in 2.6). The presence of TetR protein confirmed the successful transduction of cells with the beta-actin protein used as a loading control. In the presence of DOX shRNA, MYC -1 did not achieve MYC knockdown (Figure 3.13 A and B). However, shRNA MYC-2 and shRNA MYC-3 achieved approximately 88% and 65% MYC knockdown in the presence of DOX (Figure 3.13 C -F). The NS-shRNA has no effect on MYC protein (results not shown). The generation of stable cell lines was thus optimized using shRNA MYC-2 and shRNA MYC-3.

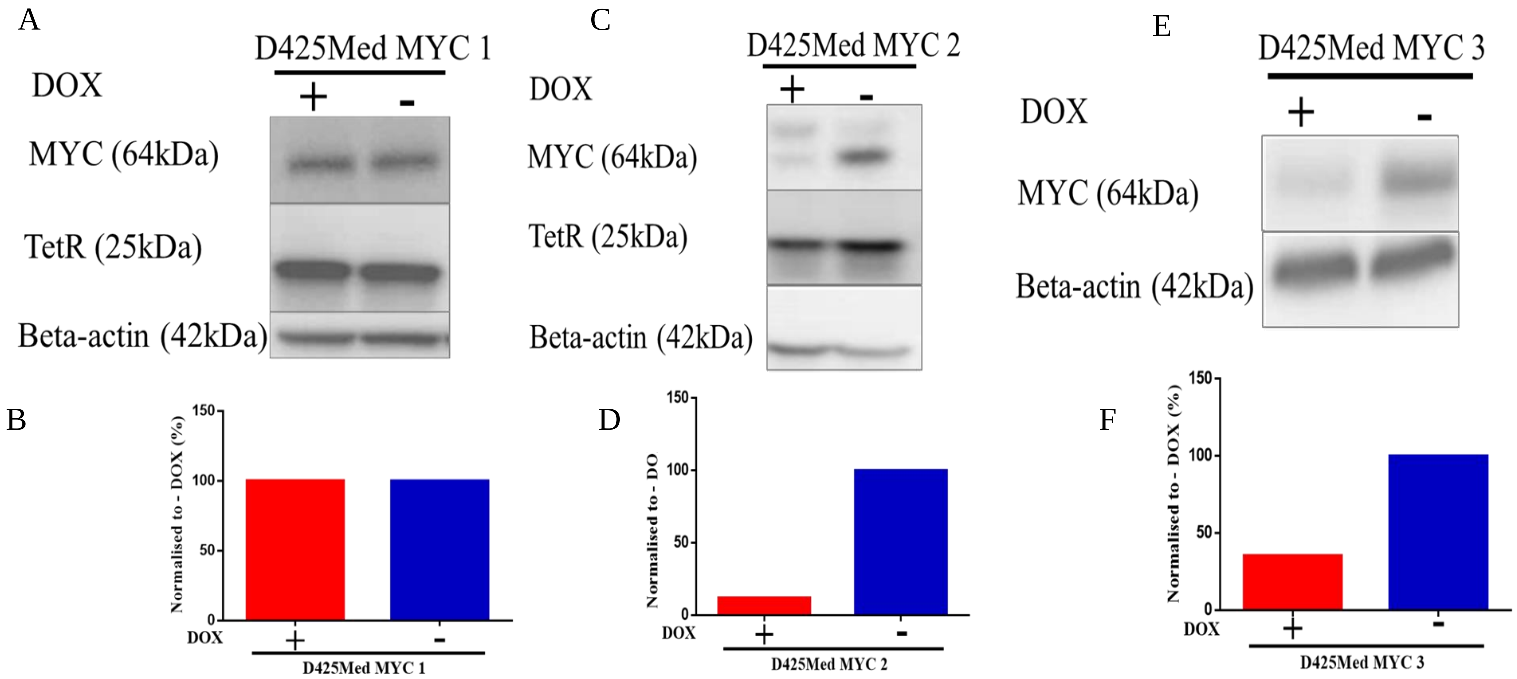

Figure 3.13 Western blot and densitometry analysis of D425Med transduced with MYC 1, MYC 2 and MYC 3 lentiviral supernatant in the absence or presence of DOX. Western blot analysis of D425Med transduced with MYC 1 lentiviral supernatant in the absence (- DOX) or presence (+ DOX) of DOX. B) Densitometry analysis of D425Med transduced with MYC 1 lentiviral supernatant in the absence (blue, - DOX) or presence (red, + DOX) of DOX. C) Western blot analysis of D425Med transduced with MYC 2 lentiviral supernatant in the absence (-DOX) or presence (+ DOX) of DOX. D) Densitometry analysis of D425Med transduced with MYC 2 lentiviral supernatant in the absence (- DOX) or presence (+ DOX) of DOX. E) Western blot analysis of D425Med transduced with MYC 3 lentiviral supernatant in the absence (-DOX) or presence (+ DOX) of DOX. F) Densitometry analysis of D425Med transduced with MYC 3 lentiviral supernatant in the absence (- DOX) or presence (+ DOX) of DOX. In all three western blots beta-actin served as a loading control and densitometry results were normalized to beta-actin and quantified with respect to appropriate without DOX (- DOX) samples.

3.4.4 Determining the multiplicity of infection for D425Med and HDMB03

To establish stably-infected cell lines, the amount of MYC 2, MYC 3 and NS lentiviral supernatant required for successful transduction for D425Med and HDMB03 was determined. D425Med and HDMB03 were infected at MOI 1 and MOI 3. After 24 hours incubation, the media was removed and replaced with selection media. Cells were grown until they reached confluence, at this point the cells were subcultured and $1x10^5$ cells were seeded in a 6 well plate and incubated for 8 hours before the addition of DOX to the appropriate wells. After 72 hours, cell pellets were harvested and the protein expression was confirmed by immunoblotting using an antibody against MYC. In D425Med, greater knockdown was achieved at a MOI 3 for both the MYC2 and MYC3 constructs (approximately 78% and 72% knockdown respectively vs 71% and 65% for MOI 1) (Figure 3.14 and 3.15). Therefore, D452Med cell lines infected with MOI 3 were selected for both shRNAs; these cell lines will be referred to as D425Med MYC 2 and D425Med MYC 3. In HDMB03, improved knockdown was also achieved with a MOI of 3 for both shRNAs (approximately 64% for both compared to 53% knockdown for the MOI 1) (Figure 3.15 and 3.16). Therefore, HDMB03 cell lines infected with MOI 3 were selected for both shRNAs; these cell lines will be referred to as HDMB03 MYC 2 and HDMB03 MYC 3.

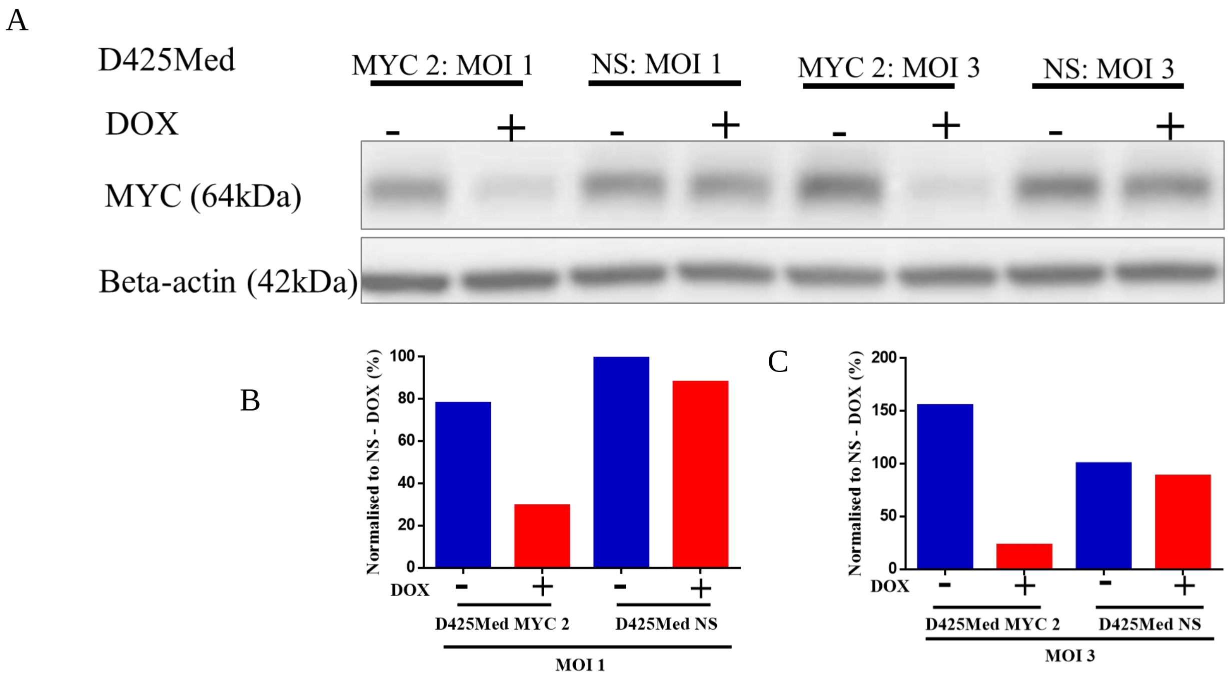

Figure 3.14 Analysis of D425Med transduced with MYC 2 and NS lentivirus at MOI 1 and MOI 3. A) Western blot analysis of MYC protein expression in D425Med MYC 2 and D425Med NS at MOI 1 and MOI 3, in the absence (- DOX) or presence (+ DOX) of DOX. Beta-actin served as a loading control. B) Densitometry result of the western blot analysis of D425Med NS and D425Med MYC 2 transduced with MOI 1, in the absence (blue, - DOX) or presence (red, + DOX) of DOX, the results were normalised to D425Med NS - DOX. C) Densitometry result of the western blot analysis of D425Med NS and D425Med MYC 2 transduced with MOI 3, in the absence (- DOX) or presence (+ DOX) of DOX, the results were normalised to D425Med NS - DOX. Densitometry results were normalized to beta-actin and quantified with respect to appropriate control (- DOX) samples.

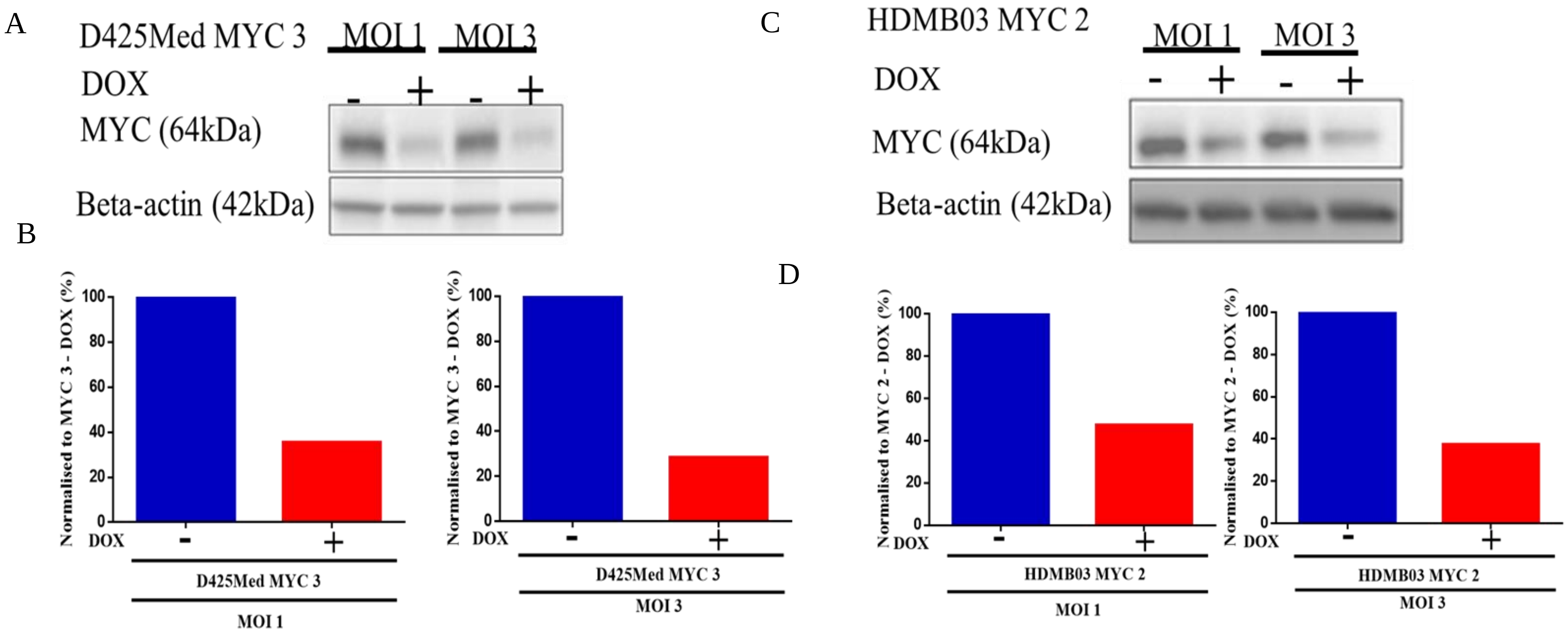

Figure 3.15 Analysis of D425Med transduced with MYC 3 lentivirus and HDMB03 transduced with MYC 2 lentivirus at MOI 1 and MOI 3. A) Western blot analysis of MYC protein expression in D425Med MYC 3 infected with MOI 1 and MOI 3, in the absence (- DOX) or presence (+ DOX) of DOX. Beta- actin served as a loading control. B) Densitometry result of the western blot analysis of D425Med MYC 3 transduced with MOI 1 and MOI 3 in the absence (blue, -DOX) or presence (red, + DOX) of DOX, densitometry results were normalized to beta-actin and quantified with respect to appropriate control (- DOX) sample .C) Western blot analysis of MYC protein expression in HDMB03 MYC 2 infected with MOI 1 or MOI 3in the absence (- DOX) or presence (+ DOX) of DOX. Beta-actin served as a loading control. D) Densitometry result of the western blot analysis of HDMB03 MYC 2 transduced with MOI 1 or MOI 3 in the absence (blue represents - DOX) or presence (red represents + DOX) of DOX, densitometry results were normalized to beta-actin and quantified with respect to appropriate control (- DOX) sample.

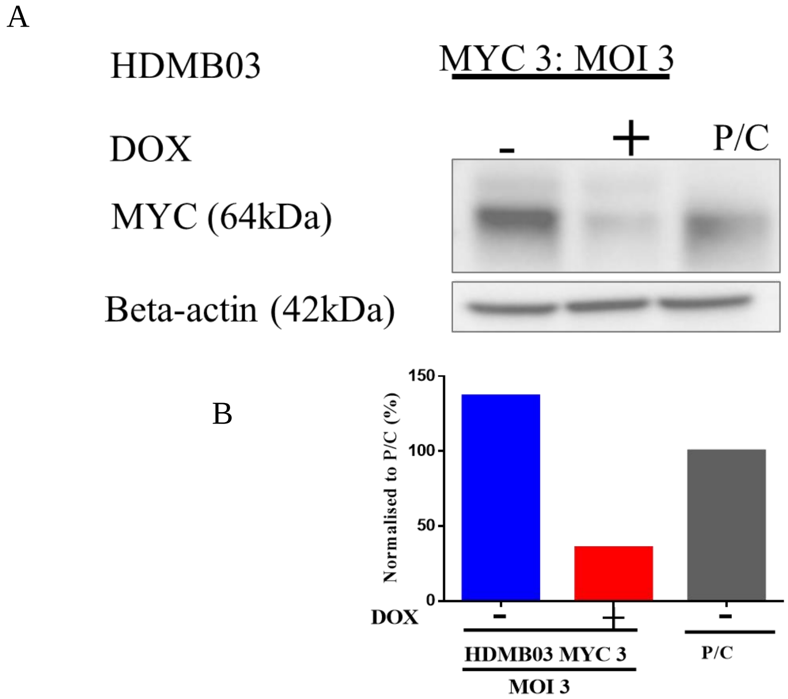

Figure 3.16 Analysis of HDMB03 transduced with MYC 3 lentivirus at MOI 3. . A) Western blot analysis of MYC protein expression in HDMB03 MYC 3 infected with MOI 3in the absence (blue, -DOX) or presence (red, +DOX) of DOX. Beta-actin served as a loading control. B) Densitometry result of the western blot analysis of HDMB03 MYC 3 transduced with MOI 3 in the absence (-DOX) or presence (+DOX) of DOX, the results were normalised to HDMB03 parent cell line, which served as a positive control (grey) (P/C).

3.4.5 Determining the minimum doxycycline concentration required to achieve maximum knockdown

To establish the minimum DOX concentration required to achieve maximum knockdown, 5 x 10^4 – 1 x 10^5 cells were seeded and incubated for 8 hours before the addition of selected DOX concentrations to the appropriate wells; a control well without DOX was also included. After 72 hours, cell pellets were harvested and MYC protein expression was examined by immunoblotting. In D425Med NS, a slight reduction of MYC expression was seen with the addition of 1µg/ml DOX (Figure 3.17 A and B) but this was minimal compared to D425Med MYC 2 which achieved 94% MYC knockdown (Figure 3.17 C and D). In HDMB03 NS, a decrease in MYC expression was observed with the addition of DOX (Figure 3.18 A and B), however in HDMB03 MYC 2, approximately 50% MYC knockdown was achieved in the presence of 1µg/ml DOX and higher DOX concentrations in HDMB03 MYC 2 showed minimal change in MYC protein expression (Figure 3.18 C and D). Therefore, 1µg/ml DOX was selected as the concentration to achieve maximum MYC knockdown in both cell lines.

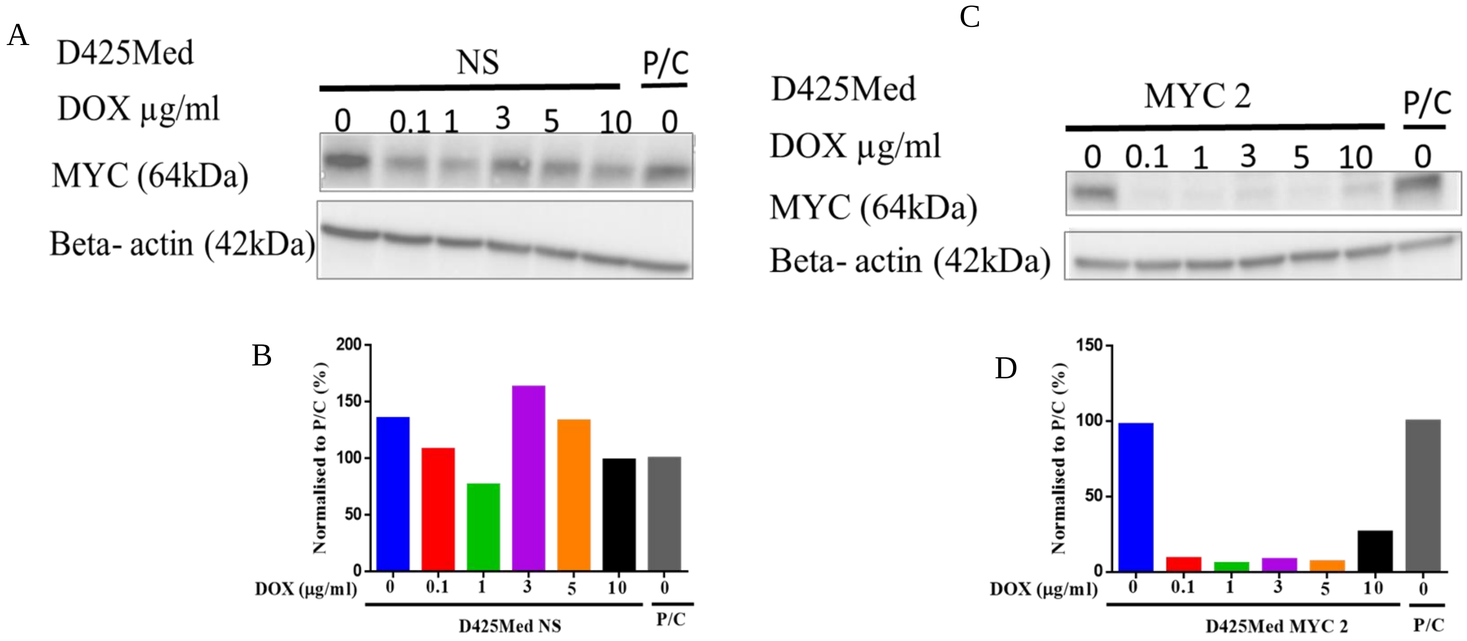

Figure 3.17 Western blot and densitometry analysis of D425Med MYC 2 and D425Med NS treated with a range of DOX concentrations. A) Western blot analysis of D425Med NS cells in the absence DOX (- DOX) or in the presence of 0.1µg/ml, 1µg/ml, 3µg/ml, 5µg/ml and 10µg/ml DOX, beta- actin served as a loading control. B) Densitometry results of D425Med NS western blot analysis. C) Western blot analysis of D425Med MYC 2 in the absence (- DOX) or in the presence of 0.1µg/ml, 1µg/ml, 3µg/ml, 5µg/ml and 10µg/ml DOX. D) Densitometry results of D425Med MYC 2 western blot analysis. Densitometry results were normalized to beta-actin and quantified with respect to control (D425Med (P/C)). The colours represent the following DOX concentrations: blue, 0µg/ml; red, 0.1µg/ml; green,1µg/ml; purple, 3µg/ml; orange,5µg/ml; black, 10µg/ml.

.

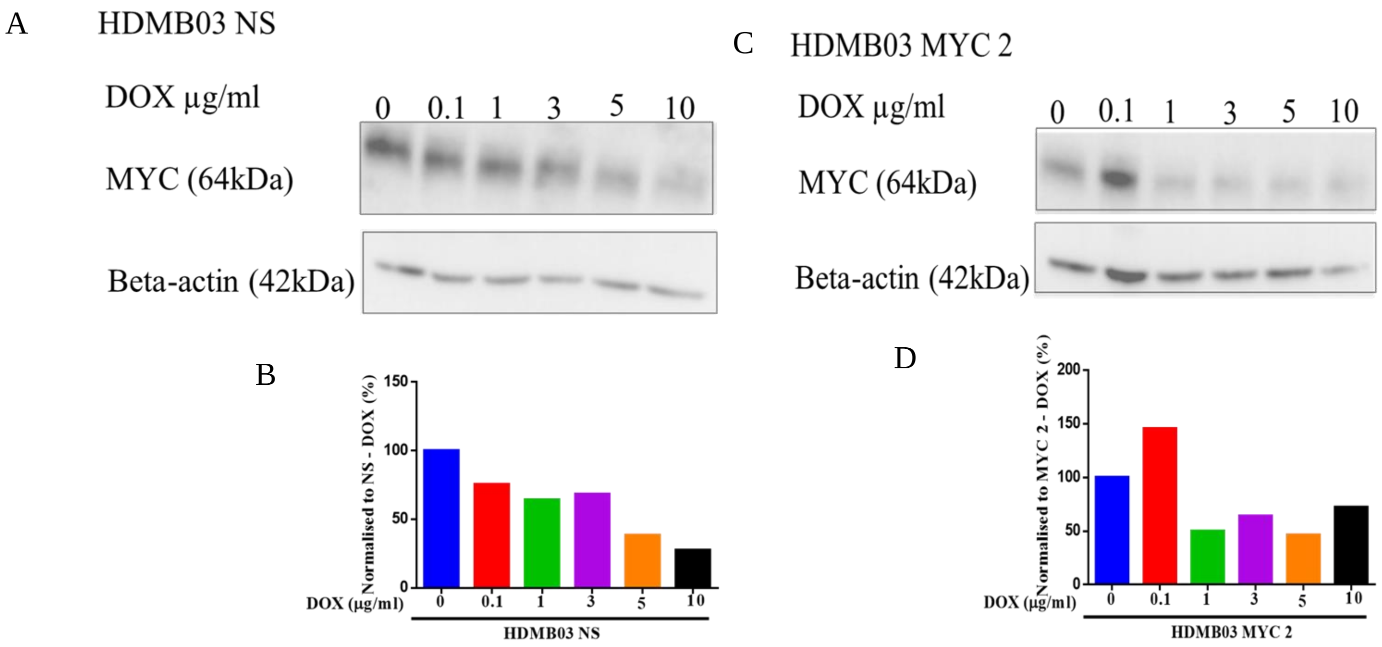

Figure 3.18 Western blot and densitometry analysis of HDMB03 NS and HDMB03 MYC 2 treated with a range of DOX concentrations. A) Western blot analysis of HDMB03 NS cells in the absence DOX (- DOX) or in the presence of 0.1µg/ml, 1µg/ml, 3µg/ml, 5µg/ml and 10µg/ml DOX, beta actin was used as a loading control. B) Densitometry results of HDMB03 NS western blot analysis, results were normalised to beta-actin and quantified with respect to HDMB03 NS - DOX. C) Western blot analysis of HDMB03 MYC 2 in the absence (- DOX) or in the presence of 0.1µg/ml, 1µg/ml, 3µg/ml, 5µg/ml and 10µg/ml DOX. D) Densitometry results of HDMB03 MYC 2 western blot analysis, results were normalized to beta-actin and quantified with respect to HDMB03 MYC 2 - DOX. The colours represent the following DOX concentrations: blue, 0µg/ml; red, 0.1µg/ml; green,1µg/ml; purple, 3µg/ml; orange,5µg/ml; black,10µg/ml.

3.4.6 Confirmation of reproducible MYC knockdown at the protein and mRNA level in D425Med and HDMB03.

After successful optimization of this system, stocks of D425Med NS, D425Med MYC 2, D425Med MYC 3, HDMB03 NS, HDMB03 MYC 2 and HDMB03 MYC 3 were made. MYC knockdown at both the protein and mRNA level were confirmed. Cells were seeded and incubated for 8 hours before the addition of DOX; after 72 hours, cell pellets were harvested and protein and RNA were extracted for analysis of MYC protein by immunoblotting against MYC antibody and measurement of the mRNA levels by quantitative RT-PCR (method described in 2.8.3). In D425Med NS in the presence of DOX, a minimal reduction in MYC protein expression was seen (Figure 3.19 A and B), however there was no change seen in *MYC* mRNA expression (Figure 3.19 C). In D425Med MYC 2 in the presence of DOX, about 90% MYC protein knockdown was achieved (Figure 3.19 A and B) and more than 2 fold reduction was seen in *MYC* mRNA expression (Figure 3.19 C). In D425Med MYC 3 in the presence of DOX, about 85% MYC protein knockdown was achieved (Figure 3.19 A and B) and more than 2-fold reduction was observed in *MYC* mRNA expression levels (Figure 3.19 C). A reduction in *MYC* mRNA expression levels was also seen in D425Med MYC 3 in the absence of DOX (relative to control) (Figure 3.19 C); this could mean that the MYC 3 construct shows some ‘leakage’. In HDMB03 NS in the absence of DOX a slight reduction in MYC protein expression was observed (relative to control), however in the presence of DOX no knockdown in MYC protein was seen (Figure 3.20 A and B). There was also no difference observed in *MYC* mRNA levels in absence or presence of DOX (Figure 3.20 E). In HDMB03 MYC 2 in the presence of DOX about 80% MYC protein knockdown was seen (Figure 3.20 A and C) and a decrease in MYC mRNA levels were also observed (Figure 3.20 E). In HDMB03 MYC 3 in the presence of DOX, approximately 80% reduction in MYC protein (Figure 3.20 A and D) and a decrease in *MYC* mRNA expression levels was seen (Figure 3.20 E). It was also observed that in the absence of DOX there was a reduction in *MYC* mRNA expression (Figure 3.20 E); again this could be evidence that the MYC 3 construct shows some leakage.

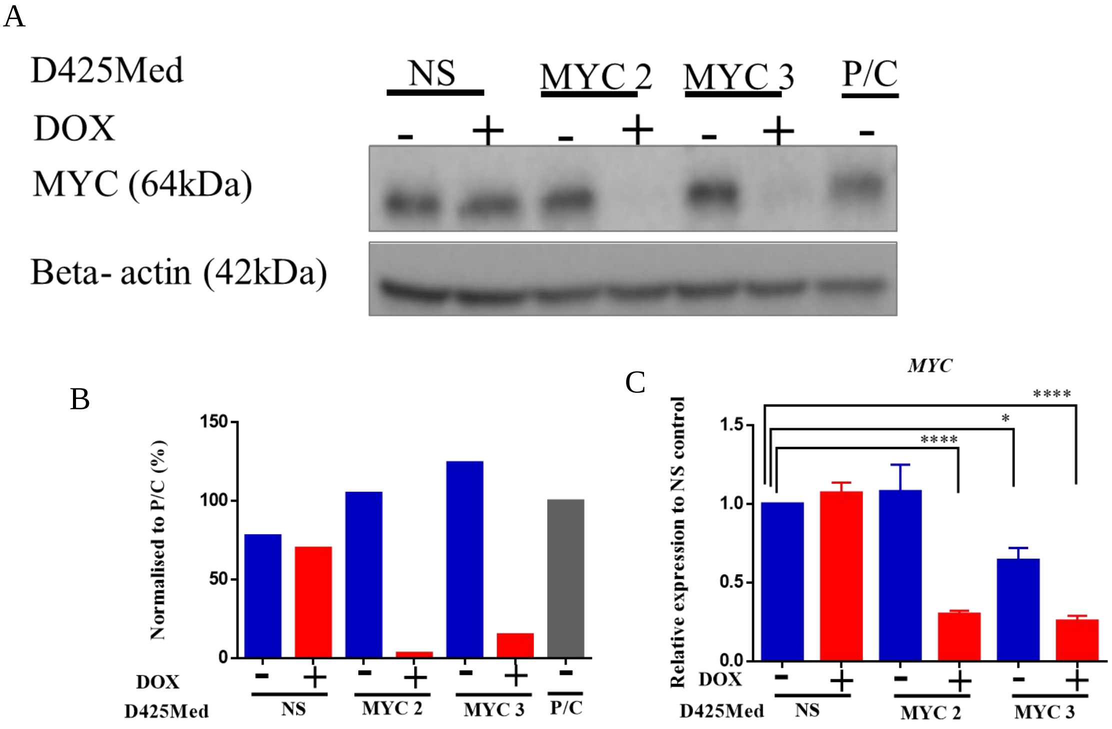

Figure 3.19 Analysis of MYC expression in D425Med NS, D425Med MYC 2 and D425Med MYC 3 in the presence or absence of DOX. A) Western blot analysis of MYC expression in D425Med NS, D425Med MYC 2 and D425Med MYC 3 in the absence (- DOX) or presence (+ DOX) of DOX. D425Med parent cell line was included as a positive control and beta- actin served as a loading control. B) Densitometry result of the western blot analysis of D425Med NS, D425Med MYC 2 and D425Med MYC 3 in the absence (blue, -DOX) or presence (red, + DOX) of DOX, (grey, P/C). Densitometry results were normalized to beta-actin and quantified with respect to control (P/C) C) *MYC* mRNA levels measured by real time qPCR and normalized for beta-2-microglobulin. The results are shown as mean ± SEM of three independent experiments and the significance was determined by unpaired Student’s t-test (*p< 0.05 and ****p< 0.0001 vs NS control).

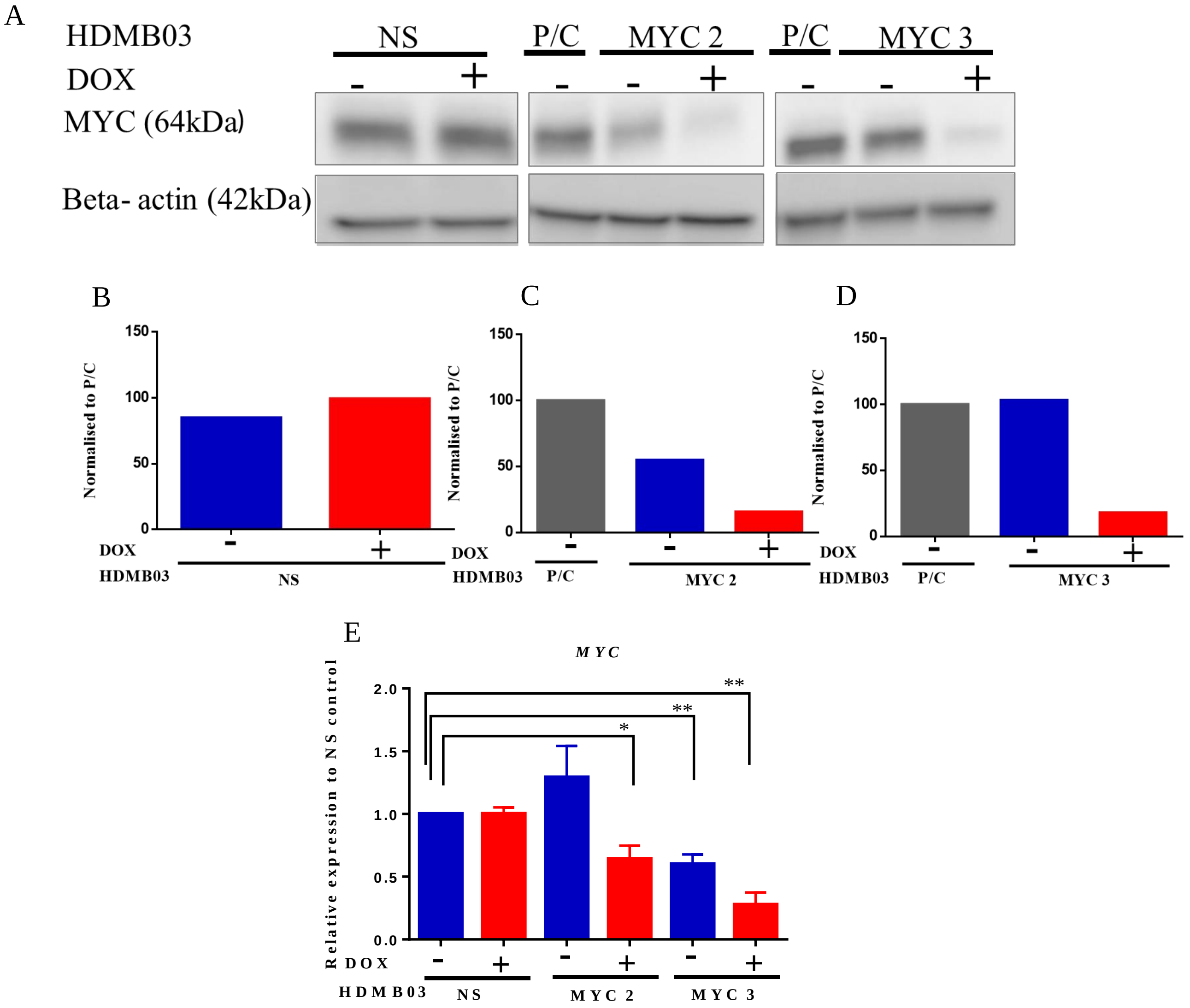

Figure 3.20 Analysis of MYC in HDMB03 NS, HDMB03 MYC 2 and HDMB03 MYC 3. Western blot analysis of MYC expression in HDMB03 NS, HDMB03 MYC 2 and HDMB03 MYC 3 in the absence (- DOX) or presence (+ DOX) of DOX. HDMB03 parent cell line was included as a positive control (P/C) and beta- actin served as a loading control. B) Densitometry result of the western blot analysis of HDMB03 NS in the absence (blue, - DOX) or presence (red, + DOX) of DOX. C) Densitometry result of the western blot analysis of HDMB03 MYC 2 in the absence (blue, - DOX) or presence (red, + DOX) of DOX. D) Densitometry result of the western blot analysis of HDMB03 MYC3 in the absence (blue, - DOX) or presence (red, + DOX) of DOX. Densitometry results were normalized to beta-actin and quantified with respect to control (P/C). E) *MYC* mRNA levels measured by real time qPCR and normalized for beta-2-microglobulin. The results are shown as mean ± SEM of three independent experiments and the significance was determined by unpaired Student's t-test (*p< 0.05 and p< 0.0001 vs NS control).

3.4.7 Immunohistochemical staining of MYC in D425Med NS and D425Med MYC 2.

Formalin fixed cell blocks were prepared for analyzing MYC expression in D425Med NS and D425Med MYC 2 in the presence or absence of DOX (method described in 2.9). Immunohistochemical staining of sections prepared from these cell blocks allows the visualization of MYC expression within single cells thereby facilitating an assessment of the heterogeneity of MYC expression within the cell population. The nuclear staining in D425Med MYC 2 in the presence of DOX was approximately the same and the majority of the cells show reduced or negative staining for MYC (Figure 3.21 D) compared to the positive staining seen in D425Med MYC 2 in the absence of DOX (Figure 3.21 C) and D425Med NS in the absence or presence of DOX (Figure 3.21 A and B).

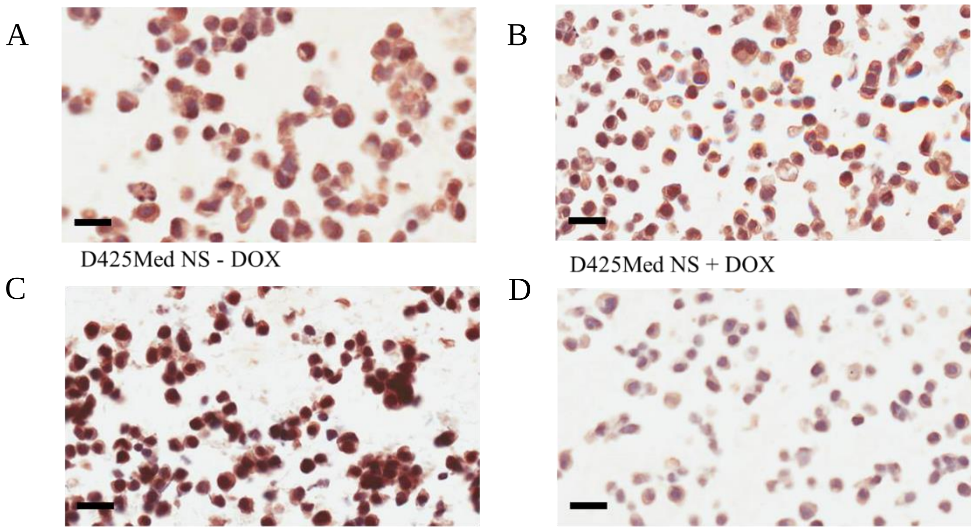

D425Med NS - DOX

D425Med NS + DOX

D425Med MYC 2 - DOX

D425Med MYC 2 + DOX

Figure 3.21 Immunohistochemical staining of MYC expression in D425Med NS and D425Med MYC 2 in the presence or absence of DOX. A) Immunohistochemical staining of MYC expression in D425Med NS in the absence of DOX (- DOX). B) Immunohistochemical staining of MYC expression in D425Med NS in the presence of DOX (+ DOX). C) Immunohistochemical staining of MYC expression in D425Med MYC 2 in the absence of DOX (- DOX). D) Immunohistochemical staining of MYC expression in D425Med MYC 2 in the presence of DOX (+ DOX). The scale bar is 20mm. (Work done by Stephen Crosier, Yuru Grabovska and Halimat Popoola).

3.5 Discussion

This study uses lentiviral vector systems to modulate the expression of MYC within MB cell lines. The protein coding sequence of *MYC* was successfully cloned into the SparQ all-in-one inducible lentiviral vector. This system was used to successfully generate DAOY MYC, a non MB_{GRP3} cell line in which MYC can be overexpressed with the addition of cumate. Optimal MYC overexpression was achieved using a multiplicity of infection of 3 viral particles per cell. This cumate-inducible overexpression of MYC vector was successfully optimized in the non MB_{GRP3} DAOY. The overexpression of MYC in the cell line DAOY has previously been reported (von Bueren *et al.*, 2009) and shown to sensitize this cell line to radio and chemotherapy. However, DAOY is thought to be derived from a MB_{SHH} (Ivanov *et al.*, 2016) and MYC amplification or overexpression is rare in this MB subtype so the model may not be relevant to MB_{GRP3} biology. Unfortunately, attempts made to generate an inducible version of the non MYC amplified MB_{GRP3} cell line CHLA-259 were unsuccessful, probably due to the growth characteristics of this cell line.

shRNAs to knockdown MYC, and a non-silencing shRNA control, were successfully cloned into the pLKO-Tet-on vector. The MYC-amplified MB_{GRP3} cell lines, D425Med and HDMB03 were successfully transduced with this system, generating D425Med NS, D425Med MYC 2, D425Med MYC 3, HDMB03 NS, HDMB03 MYC 2 and HDMB03 MYC 3. The optimal MYC knockdown was achieved using a multiplicity of infection of 3 viral particles per cell. The minimal DOX concentration for optimal knockdown was determined to be 1µg/ml. Cell blocks were successfully generated for D425Med NS and D425Med MYC 2 showing MYC knockdown in the majority of cells in the presence of DOX.

The successfully generated cell lines (D425Med NS, D425Med MYC 2, D425Med MYC 3, HDMB03 NS, HDMB03 MYC 2 and HDMB03 MYC 3) were taken forward for further analysis as described in Chapters 4 and 5.

Chapter 4 *In vitro* analysis of cellular phenotypes following MYC knockdown

4.1 Introduction

High *MYC* expression and amplification of *MYC* are predominately associated with $\mathrm{MB}_{\mathrm{GRP3}}$ and are associated with a poor outcome. MYC plays an important role in cell cycle, proliferation and apoptosis (Frenzel *et al.*, 2010). Studies have shown that MYC is required for cells to progress normally through the cell cycle; Rat 1 fibroblast cells lacking Myc can still divide but at a slower rate (Bretones *et al.*, 2015). MYC controls the transition of cells through the cell cycle by several mechanisms. For example, MYC can transcriptionally activate genes such as *cyclin D2*, *CDK4* and *CDC25A* (Nasi *et al.*, 2001). In quiescent cells, it has been shown that MYC overexpression stimulates the expression of E2F1, E2F2 and E2F3, proteins which play an important role in the G1-S transition. A deficiency in E2F2 or E2F3 impairs MYC ability to drive cells into the S- phase but this does not occur in the case of E2F1 deficiency (Bretones *et al.*, 2015). MYC can also induce or repress microRNAs (miRNA) that have either oncogenic (miR-17-92 cluster) (Frenzel *et al.*, 2010) or tumour suppressor properties such as miR-15a/16-1, miR-26a and miR-34a (Bretones *et al.*, 2015). These miRNAs regulate important genes involved in the cell cycle, for example *CDC25A*, *CDK6*, *Cyclin A*, *CCND1*, *CCND2* and *CCND3* are regulated by let-7 family members, whereas expression of *CDK4*, *CDK6*, *cyclin E2* and *E2F* is supressed by miRNA-34a (Bueno and Malumbres, 2011; Bretones *et al.*, 2015). Furthermore, CDK6, Cyclin D1 and D3 are inhibited by miR-15a/16-1 (Otsuka and Ochiya, 2014) and the expression of Cyclin D2 and E2 is supressed by miR-26a (Bretones *et al.*, 2015).

In addition, MYC can promote cell cycle progression by inhibiting the cyclin-dependent kinase inhibitor $\mathrm{p21}^{\mathrm{CiP1/Waf1}}$ through multiple mechanisms. MYC binds to MIZ1, which causes MIZ1 to function as a transcriptional repressor, supressing $\mathrm{p21}^{\mathrm{CiP1/Waf1}}$ (CDKN1A) induction by p53 (Hönnemann *et al.*, 2012; Bretones *et al.*, 2015). In addition, repression of $\mathrm{p21}^{\mathrm{CiP1/Waf1}}$(CDKN1A) can occur when MYC and MIZ1 recruit a corepressor protein (the DNA methyltransferase DMNT3A) or when MYC interacts with the transcription factor TFAP2C and a histone demethylase (KDM5B), highlighting the involvement of multiple epigenetic mechanisms (Bretones *et al.*, 2015). MYC can also transcriptionally activate *AP4* (TFAP4) which binds to a specific region in $\mathrm{p21}^{\mathrm{CiP1/Waf1}}$ (CDKN1A) promoter, repressing transcription (Jung and Hermeking, 2009; Bretones *et al.*, 2015). Finally, MYC can influence cell cycle progression through suppression of other cell cycle checkpoint genes such as *GAS1*, *CDKN2B* ($p15^{Ink4b}$) and *CDKN1B* ($p27^{KIP1}$) (Jung and Hermeking, 2009).

Another biological property of MYC is its ability to initiate or make cells sensitive to apoptosis. The specific apoptotic pathway stimulated depends on the cell type (Hoffman and Liebermann, 2008); there are various mechanisms by which MYC is involved in apoptosis. MYC can cause an imbalance between pro-apoptotic and anti-apoptotic proteins (Tansey, 2014). During the cell death process, MYC can allow the escape of cytochrome c from the mitochondria and into the cytoplasm, possibly through stimulation of the pro-apoptotic protein BAX. BAX is responsible for making the outer mitochondrial membrane permeable for the release of cytochrome c. Cytochrome c is able to bind to the apoptotic protease-activating factor-1 (Apaf-1) protein which enables the formations of the apoptosome. The apoptosome then initiates procaspase-9 activity which triggers activity of downstream caspases leading to apoptosis (Pelengaris and Khan, 2003). Another example of the imbalance between pro-apoptotic and anti-apoptotic stimuli caused by MYC, is MYC's ability to inhibit anti-apoptotic proteins such as BCL-2 and BCL-Xl and to stimulate BIM. BIM is another pro-apoptotic protein which promotes the escape of cytochrome c and other pro-apoptotic proteins which trigger cell death through the initiation of caspase activity (Tansey, 2014). MYC can also stimulate apoptosis through elevating ARF which prevents MDM2 from inhibiting tumour suppressor p53 activity, thereby increasing the levels of p53 to drive apoptosis (Nilsson and Cleveland, 2003).

Previous studies have generated versions of the MB cell lines, DAOY and UW228 (non MB_{GP3} cell lines) (Stearns *et al.*, 2006) which stably overexpress MYC. MYC overexpression caused an increase in both proliferation and apoptosis (Stearns *et al.*, 2006). Stearns *et al.* also showed that MYC overexpression can induce anaplasia within xenograft tumours formed from these cell lines. LCA histology is another poor prognostic factor in MB, frequently associated with MYC amplification; this histology consists of large cells exhibiting nuclear pleomorphism, an increased mitotic index and increased levels of apoptosis (Stearns *et al.*, 2006).

Research performed in a MB_{GRP3} orthotopic transplantation model that was developed by transplanting stem cells infected with *Myc* into the cerebellum, showed that the removal of *Myc* resulted in total regression of the tumour (Pei *et al.*, 2012; Roussel and Robinson, 2013). This occurrence is known as 'oncogenic addiction'; whereby tumour cells, although containing many genetic alterations enhancing their tumourgenic properties, remain dependent on a single oncogene for aspects of the malignant phenotype such as sustained proliferation (Weinstein and Joe, 2008).

Research carried out by von Bueren *et al.* down regulated MYC expression using an siRNA approach in several cell lines: a modified version of the non MB_{GRP3} cell line DAOY, stably transfected to overexpress MYC, and the MB_{GRP3} cell lines D425Med and D341Med. This study showed that MYC knockdown in these cell lines resulted in inhibition of cell proliferation, G_1 cell cycle arrest and a reduction in levels of apoptosis (von Bueren *et al.*, 2009) . Zang *et al.* also used an RNA interference approach to knockdown MYC in two MB_{SHH} cell lines (UW-228-2 and UW-228-3). In contrast to the study by von Bueren, they reported an S phase cell cycle arrest and an increase in apoptosis (Zhang *et al.*, 2006; von Bueren *et al.*, 2009).

Although these studies have given insight into MYC biology within MB, there has been limited work performed in MB_{GRP3} cell lines, which are the more disease relevant model as MYC is predominantly associated with this subgroup. The generation of stable isogenic cell lines with DOX inducible MYC silencing will allow for a more detailed and controlled investigation of the role of MYC in $MB_{GRP3.}$ To my knowledge these DOX inducible MYC knockdown isogenic models, described in chapter 3, are the first models which should allow study MYC-dependent biology within human MB_{GRP3} in a regulatable manner.

In this Chapter, the DOX-inducible, MYC-silencing isogenic models established in Chapter 3 were used to characterize phenotypic changes associated with MYC knockdown by measurement of parameters including: cellular proliferation, cell cycle distribution, expression of *CDKN1A* and induction of apoptosis.

4.2 Analysis of phenotypic effects of MYC knockdown in D425Med

4.2.1 MYC knockdown significantly decreases proliferation in independent clones of D425Med MYC 2 and D425Med MYC 3.

MYC plays a central role in cell proliferation. It was important to determine if the MB_{GRP3} cells remain addicted to MYC expression, as cultured cells could potentially have many genetic or epigenetic changes occurring within them that might compensate for MYC knockdown. The proliferation assays commonly used for MB cells are either metabolism-based cell proliferation or clonogenic survival assays. For this project, the CellTiter-Glo assay was selected to measure the ATP activity within the D425Med-derived cell lines. ATP viability assays are more sensitive than other viability assays because it requires less time to generate a luminescent signal (Riss *et al.*, 2016). To test reproducibility of MYC knockdown, two independent versions of each of the D425Med cell lines were made. These two independent D425Med cell lines showed similar levels of MYC knockdown (Western blot data not shown), the replicate cell lines of D425Med will be referenced as (2nd). Proliferation assessment of D425Med NS, D425Med NS (2nd) D425Med MYC 2, D425Med MYC 2 (2nd), D425Med MYC 3 and D425Med MYC 3 (2nd) cells were conducted from day 1 to day 5 after grown in the absence or presence of DOX.

In the first D425Med NS cell line (Figure 4.1 A), the proliferation rate for D425Med NS + DOX showed a slight but significant decrease when compared to D425Med NS – DOX, however for D425Med NS (2nd) cell line no significant difference was seen (Figure 4.1 B). When the two D425Med NS cell lines data were combined no difference in proliferation was observed (Figure 4.1 C). Combining the two D425Med NS cell lines gives increased statistical power to the data and shows that DOX itself doesn’t have a pronounced reproducible effect on proliferation. A decrease in the rate of proliferation was seen in both the treated and untreated cell line after three days (Figure 4.1 C).

MYC knockdown significantly decreased proliferation in D425Med MYC 2 (Figure 4.1 D), D425Med MYC 2 (2nd) (Figure 4.1 E) and when both D425Med MYC 2 clones are combined (Figure 4.1 F). MYC silencing significantly decreased proliferation in D425Med MYC 3 (Figure 4.1 G), D425Med MYC 3 (2nd) (Figure 4.1 H) and significant differences in cell number were observed from day 2 onwards when both D425Med MYC 3 clones are combined (Figure 4.1 I). This confirms that MYC knockdown has a pronounced and reproducible effect on cell proliferation and these cell lines remains addicted to MYC.

Morphological changes were not observed in D425Med NS after 3 days of MYC knockdown however changes were observed in D425Med MYC 2 and D425Med MYC 3; the cells became more adherent with the morphological change becoming more evident after 5 days of MYC silencing (Figure 4.2). Similar morphological changes were seen in D425Med MYC 2 (2nd) and D425Med MYC 3 (2nd) (data not shown).

A

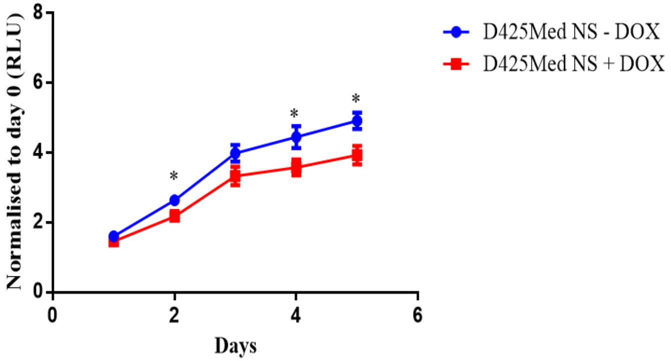
Normalised to day 0 (RLU)
8
6
4
2
0
0
2
4
6
Days
*
*
*
D425Med NS - DOX
D425Med NS + DOX

B

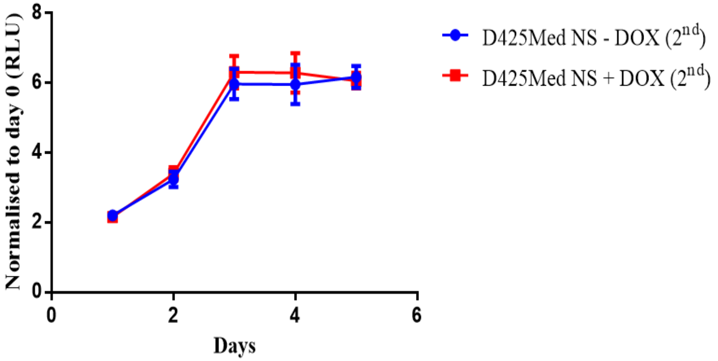
Normalised to day 0 (RLU)
8
6
4
2
0
0
2
4
6
Days
D425Med NS - DOX (2nd)
D425Med NS + DOX (2nd)

C

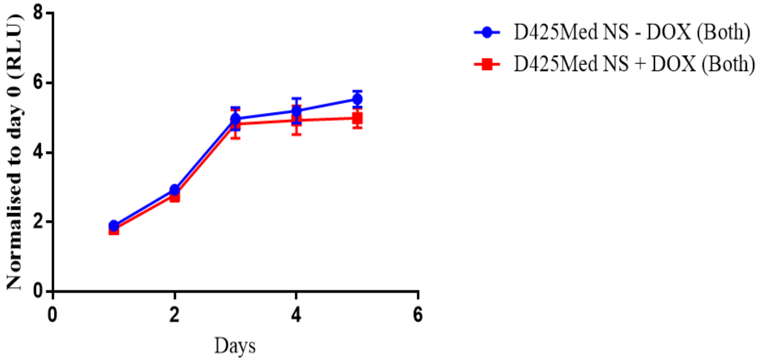
Normalised to day 0 (RLU)
8
6
4
2
0
0
2
4
6
Days
D425Med NS - DOX (Both)
D425Med NS + DOX (Both)

D

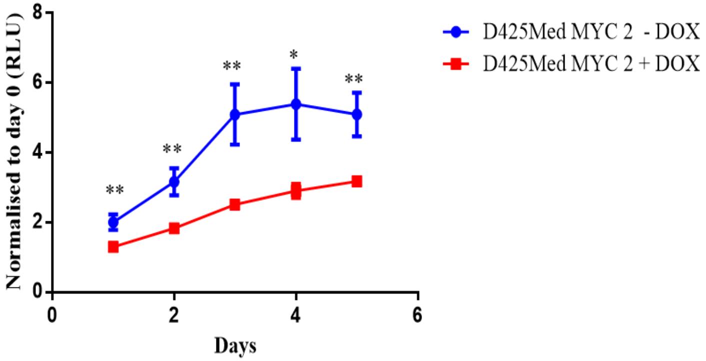
Normalised to day 0 (RLU)
8
6
4
2
0
0
2
4
6
Days
**
**
**
*
**
D425Med MYC 2 - DOX
D425Med MYC 2 + DOX

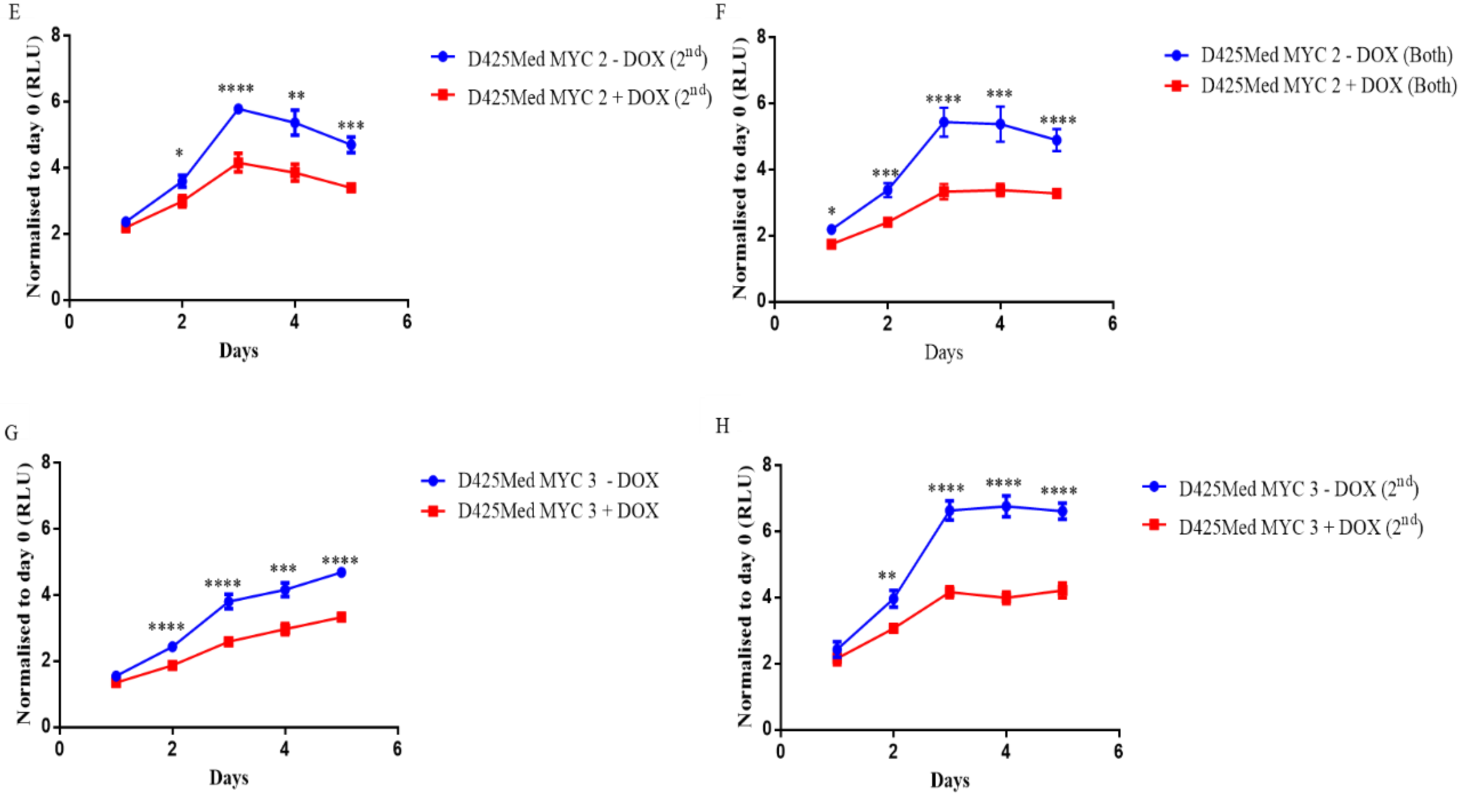
E
Normalised to day 0 (RLU)
Days
D425Med MYC 2 - DOX (2nd)
D425Med MYC 2 + DOX (2nd)
*
****
**
***
F
Normalised to day 0 (RLU)
Days
D425Med MYC 2 - DOX (Both)
D425Med MYC 2 + DOX (Both)
*
***
****
***
****
G
Normalised to day 0 (RLU)
Days
D425Med MYC 3 - DOX
D425Med MYC 3 + DOX
****
****
***
****
H
Normalised to day 0 (RLU)
Days
D425Med MYC 3 - DOX (2nd)
D425Med MYC 3 + DOX (2nd)
**
****
****
****
0
2
4
6
8

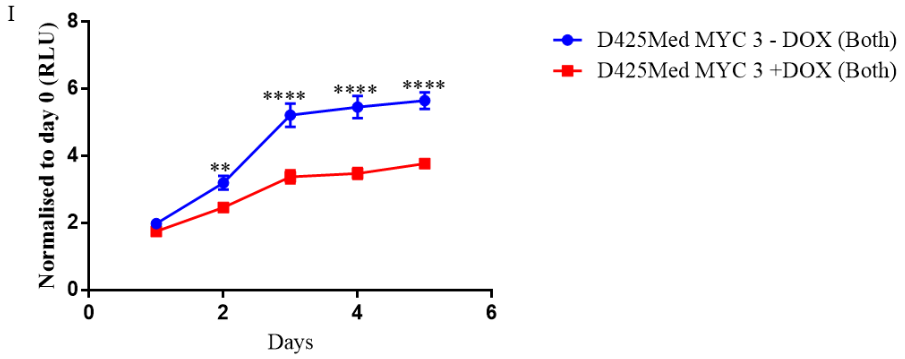

Figure 4.1 Effect of DOX inducible MYC silencing on proliferation in D425Med cells. A) A slight but significant difference in proliferation was observed in D425Med NS + DOX when compared to D425Med NS – DOX. (blue, – DOX; red, + DOX; y-axis, RLU, relative luminescence unit). B) No difference in proliferation was observed in D425Med NS + DOX (2nd) when compared to D425Med NS – DOX (2nd). C) No difference in proliferation was observed in D425Med NS + DOX (amalgamated data from both cell lines) when compared to D425Med NS – DOX. D) MYC knockdown in D425Med MYC 2 causes a significant reduction in proliferation when compared to the control (D425Med MYC 2 – DOX). E) MYC knockdown in D425Med MYC 2 (2nd) causes a significant reduction in proliferation when compared to the control (D425Med MYC 2 – DOX (2nd). F) MYC knockdown in D425Med MYC 2 (Both) resulted in significant inhibition of proliferation when compared to control (D425Med MYC 2 – DOX (Both). G) MYC knockdown in D425Med MYC 3 resulted in significant inhibition of proliferation when compared to control (D425Med MYC 3 – DOX). H) MYC knockdown in D425Med MYC 3 (2nd) resulted in significant inhibition of proliferation when compared to control (D425Med MYC 3 – DOX (2nd)). I) MYC knockdown in D425Med MYC 3 (both) causes a significant reduction in proliferation when compared to control (D425Med MYC 3 – DOX (Both). Proliferation was measured using the CellTiter-Glo luminescent assay as discussed in methods. The results are shown as means ± SEM of three to six individual experiments and the significance was determined by unpaired student's t-test (* $p < 0.05$, ** $p<0.01$, *** $p<0.001$, ****$p<0.0001$ vs control of the appropriate sample).

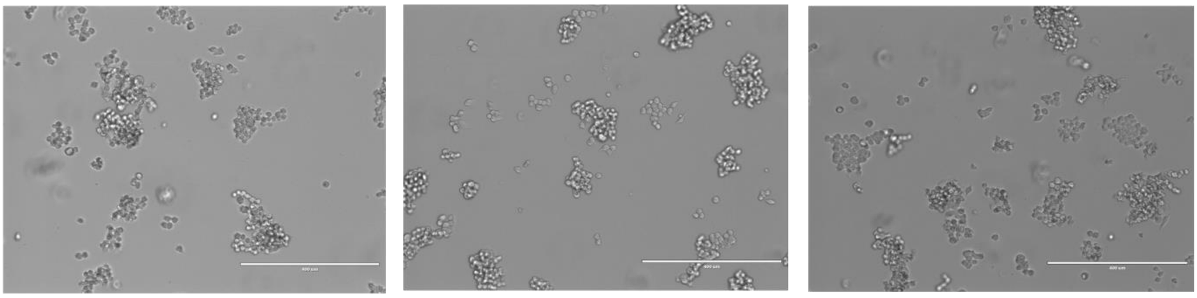

D425Med NS – DOX @ Day 3 D425Med MYC 2 - DOX @ Day 3 D425Med MYC 3 - DOX @ Day 3

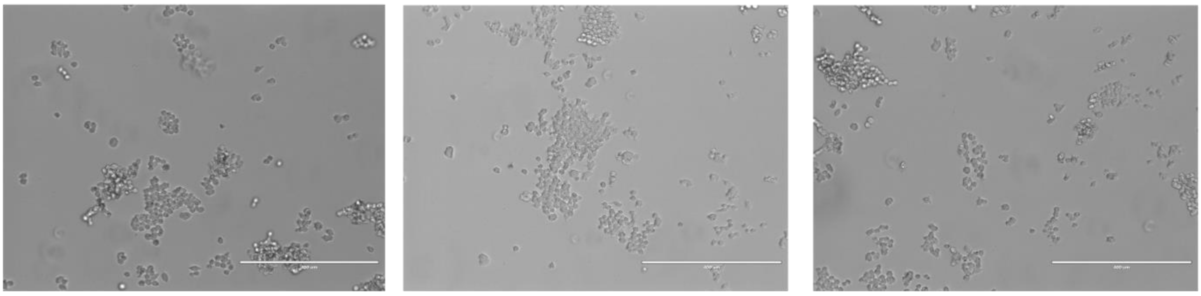

D425Med NS + DOX @ Day 3 D425Med MYC 2 + DOX @ Day 3 D425Med MYC 3 + DOX @ Day 3

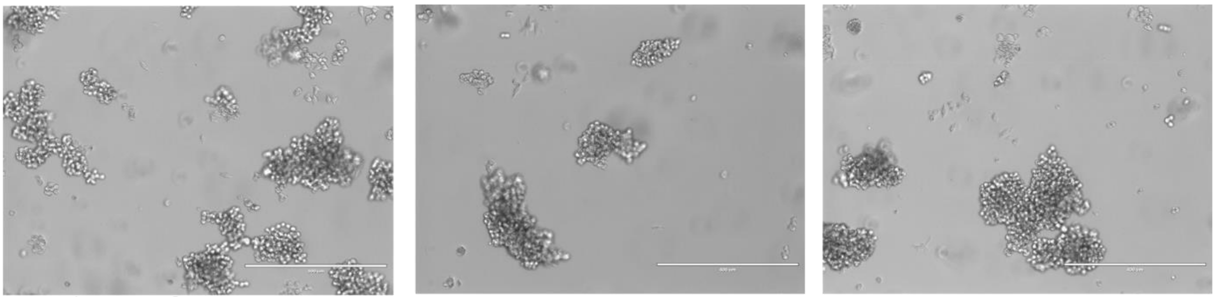

D425Med NS – DOX @ Day 5 D425Med MYC 2 - DOX @ Day 5 D425Med MYC 3 - DOX @ Day 5

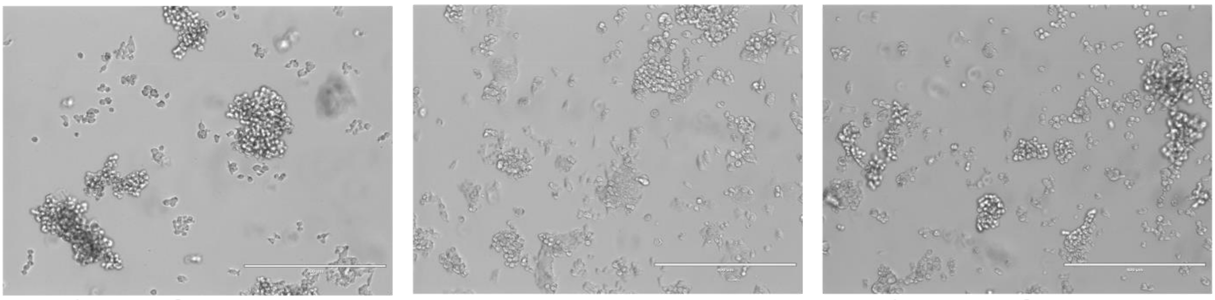

D425Med NS + DOX @ Day 5 D425Med MYC 2 + DOX @ Day 5 D425Med MYC 3 + DOX @ Day 5

Figure 4.2 Phase contrast images of D425Med NS, D425Med MYC 2 and D425Med MYC 3 grown in the absence or presence of DOX at day 3 and day 5. The cell morphology of D425Med MYC 2 + DOX and D425Med MYC 3 + DOX has visibly changed at day 3, the cells were more adherent when compared to D425Med MYC 2 – DOX, D425Med MYC 3 – DOX respectively and D425Med NS ± DOX. This change in D425Med MYC 2 + DOX and D425Med MYC 3 + DOX was more evident at day 5. The scale bar is 400um and similar morphological changes were observed between replicates (images not shown).

4.2.2 MYC Knockdown in D425Med causes a G_1 cell cycle arrest

To identify the possible mechanism by which silencing MYC slows down cell growth, flow cytometric analysis was performed. Analysis of cell cycle distribution was performed by flow cytometry for both D425Med cell lines grown in the absence or presence of DOX for 3 days. MYC silencing resulted in an increase in the number of cells in the G1 phase for the 1st clone of D425Med MYC 2 and D425Med MYC 3 cells (Figure 4.3 and Table 26), the increase was also seen in the D425Med MYC 2 (2nd) and D425Med MYC 3 (2nd) (Figure 4.4 and Table 26). The increase in the number of cells in the G1 phase were marginally different between the four independent D425Med MYC 2 and D42Med MYC 3 clones (Table 26). The increase in the number of cells in the G1 phase was more significant when the data was combined for both clones (Figure 4.5 and Table 27). MYC knockdown also resulted in a significant decrease in the number of cells in the S phase for the 1st clone of D425Med MYC 2, D425Med MYC 3 cells (Figure 4.3 and Table 26) and D425Med MYC 3 (2nd) (Figure 4.4 and Table 27). When data was combined for each clone, the decrease in the S phase of the cell cycle was more significant (Figure 4.5 and Table 27). There were no significant changes observed in the cell cycle distribution for D425Med NS cell lines (Figure 4.3; Figure 4.4; Figure 4.5; Table 26; Table 27).

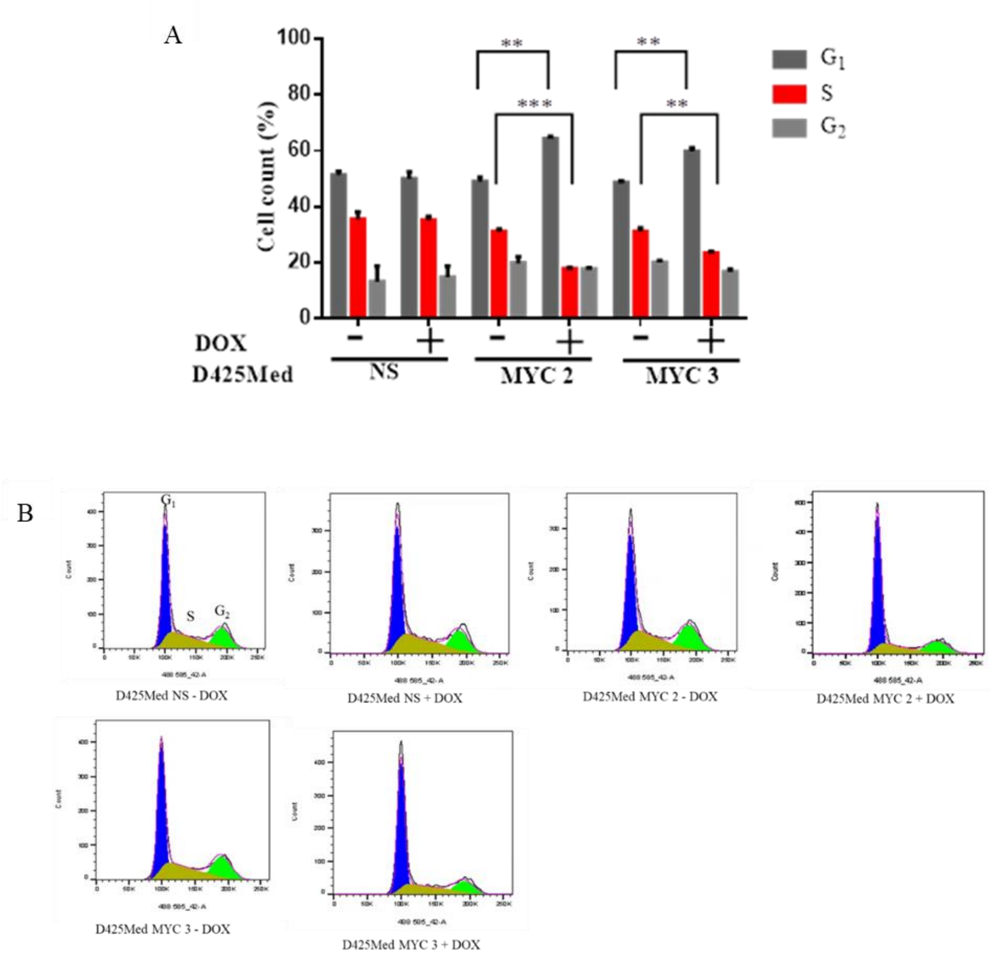

Figure 4.3 DOX inducible silencing of MYC in the first D425Med clone induces a G1 cell cycle arrest. A) Cell cycle analysis of D425Med NS, D425Med MYC 2, D425Med MYC 3 grown in the absence or presence of DOX, cells were harvested after 3 days and detached by trypsin, fixed in 70 % ethanol and stained with PI as described in methods (2.2.2). A total number of 10 000 events per sample were counted. MYC knockdown in both D425Med MYC 2 + DOX and D425Med MYC 3 + DOX resulted in a significant increase in the number of cells in the G1 phase of the cell cycle and a significant decrease in the number of cells in the S phase of the cell cycle when compared to controls (D425Med MYC 2 – DOX, D425Med MYC 3 – DOX). There was no significant change in the cell cycle distribution for D425Med NS + DOX when compared to D425Med NS – DOX. The results are shown as means ± SEM of three individual experiments and the significance was determined by unpaired student’s t-test (** $p<0.01$, ***$p<0.001$ vs control of the appropriate sample). Dark grey represents G1 phase, red represents S phase and light grey represents G2 phase. B) Representative cell cycle profiles derived by by FlowJo V10 software (x axis = 585/42).

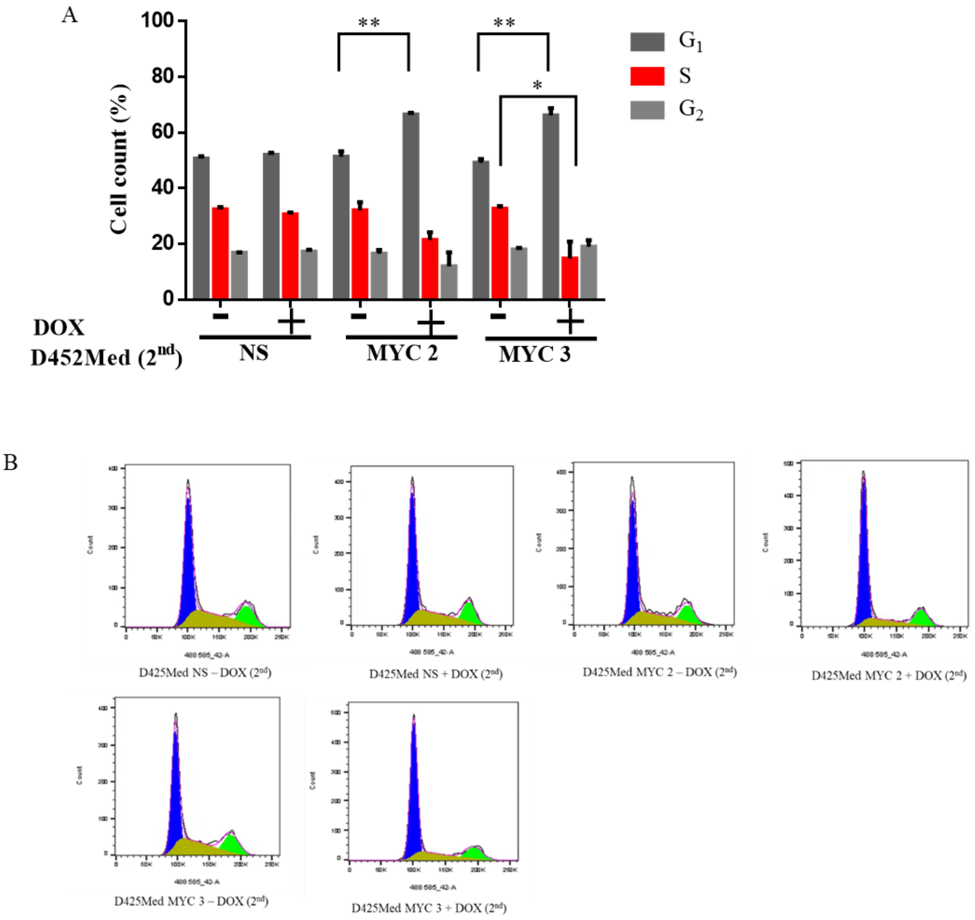

D425Med NS – DOX (2nd)

D425Med NS + DOX (2nd)

D425Med MYC 2 – DOX (2nd)

D425Med MYC 2 + DOX (2nd)

D425Med MYC 3 – DOX (2nd)

D425Med MYC 3 + DOX (2nd)

Figure 4.4 DOX inducible silencing of MYC in the first D425Med clone induces a G1 cell cycle arrest DOX inducible silencing of MYC in the second clone of D425Med induces a G1 cell cycle arrest. A) Cell cycle analysis of D425Med NS (2nd), D425Med MYC 2 (2nd), D425Med MYC 3(2nd) grown in the absence or presence of DOX, cells were harvested after 3 days and detached by trypsin, fixed in 70 % ethanol and stained with PI as described in methods. A total number of 10 000 events per sample were counted. MYC knockdown in both D425Med MYC 2 + DOX (2nd) and D425Med MYC 3 + DOX (2nd) resulted in a significant increase in the number of cells in the G1 phase of the cell cycle when compared to controls (D425Med MYC 2 – DOX (2nd), D425Med MYC 3 – DOX (2nd)). A significant decrease in the number of cells in the S phase of the cell cycle was seen in D425Med MYC 3 (2nd) when D425Med MYC 3 – DOX (2nd). There was no significant change in the cell cycle distribution for D425Med NS + DOX (2nd) when compared to D425Med NS – DOX (2nd). The results are shown as means ± SEM of three individual experiments and the significance was determined by unpaired student’s t-test (* $p<0.05$, **$p<0.01$ vs control of the appropriate sample). Dark grey represents G1 phase, red represents S phase and light grey represents G2 phase. B) Representative cell cycle profiles derived by by FlowJo V10 software (x axis = 585/42).

	FRACTION OF CELLS (%)		
	G_1	S	G_2
D425MED NS – DOX	51.27 ± 1.423	35.56 ± 2.577	13.17 ± 5.583
D425MED NS + DOX	50.03 ± 2.504	35.22 ± 1.343	14.75 ± 4.021
D425MED MYC 2- DOX	49.02 ± 1.601	31.12 ± 0.9295	19.87 ± 2.238
D425MED MYC 2 + DOX	64.33 ± 0.7826	17.90 ± 0.4048	17.77 ± 0.4718
D425MED MYC 3 -DOX	48.71 ± 0.4693	31.21 ± 1.262	20.08 ± 0.7732
D425MED MYC 3 +DOX	59.81 ± 1.223	23.41 ± 0.6381	16.78 ± 0.9281
D425MED NS - DOX (2^{ND})	50.67 ± 0.8774	32.49 ± 0.7961	16.84 ± 0.2357
D425MED NS + DOX (2^{ND})	52.01 ± 0.7969	30.69 ± 0.6668	17.30 ± 0.6359
D425MED MYC 2 - DOX (2^{ND})	51.36 ± 1.897	32.11 ± 2.962	16.54 ± 1.335
D425MED MYC 2 + DOX (2^{ND})	66.50 ± 0.6252	21.48 ± 2.732	12.02 ± 5.027
D425MED MYC 3 - DOX (2^{ND})	49.23 ± 1.283	32.71 ± 0.9594	18.07 ± 0.5828
D425MED MYC 3 +DOX (2^{ND})	66.20 ± 2.601	14.80 ± 6.099	19.00 ± 2.347

Table 26: The effect of MYC knockdown in both independent clones of D425Med cell cycle distribution, results are shown as mean ± SEM

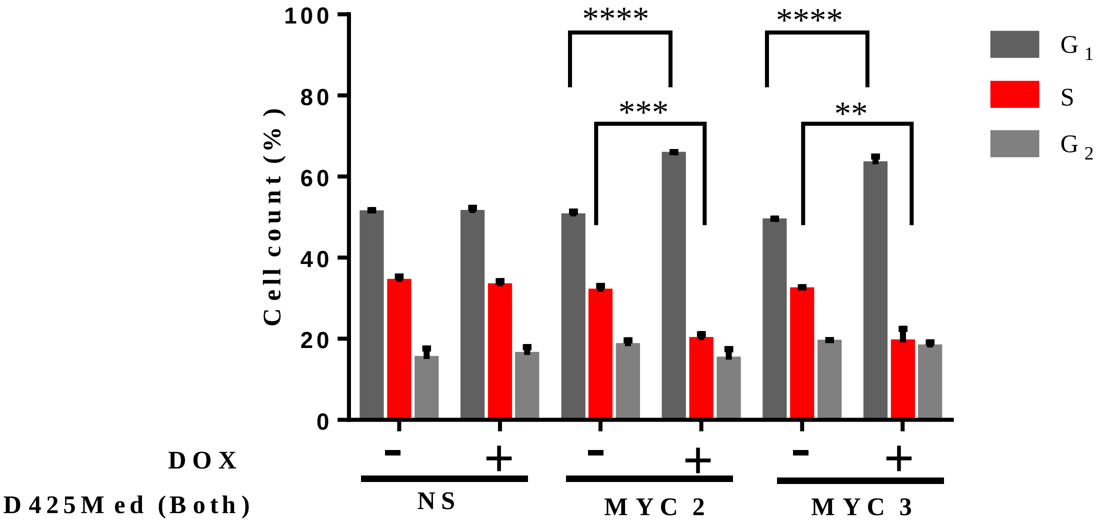

Figure 4.5 DOX inducible silencing of MYC in D425Med (both) induces a G1 cell cycle arrest. Cell cycle analysis of both D425Med NS, D425Med MYC 2, D425Med MYC 3 constructs. MYC knockdown in D425Med MYC 2 + DOX (Both) and D425Med MYC 3 + DOX (Both) resulted in a significant increase in the number of cells in the G1 phase of the cell cycle and a significant decrease in the number of cells in the S phase of the cell cycle when compared to controls (D425Med MYC 2 – DOX (Both), D425Med MYC 3 – DOX (Both). There was no significant change in the cell cycle distribution for D425Med NS + DOX (Both) when compared to D425Med NS – DOX (Both). The results are shown as means ± SEM of six individual experiments and the significance was determined by unpaired student's t-test (** $p<0.01$, ***$p<0.001$, ***$p<0.0001$ vs control of the appropriate sample). Dark grey represents G1 phase, red represents S phase and light grey represents G2 phase.

PHASE OF THE CELL CYCLE (%)	**D425MED NS - DOX (BOTH)**	**D425MED NS + DOX (BOTH)**	**D425MED MYC 2 - DOX (BOTH)**	**D425MED MYC 2 + DOX (BOTH)**	**D425MED MYC 3 - DOX (BOTH)**	**D425MED MYC 3 + DOX (BOTH)**
G_1	50.97 ± 0.7594	51.02 ± 1.256	50.19 ± 1.227	65.41 ± 0.6614	48.97 ± 0.6216	63.01 ± 1.921
S	34.03 ± 1.387	32.95 ± 1.215	31.61 ± 1.406	19.69 ± 1.472	31.96 ± 0.7838	19.10 ± 3.351
G_2	15.00 ± 2.630	16.03 ± 1.908	18.20 ± 1.383	14.89 ± 2.599	19.07 ± 0.6244	17.89 ± 1.233

Table 27:The effect of MYC knockdown on D425Med cell cycle distribution, results are shown as mean ± SEM

4.2.3 MYC knockdown increases expression of CDKN1A in D425Med MYC 2 and D425Med MYC 3

The expression of *CDKN1A* was evaluated in both D425Med NS, D425Med MYC 2 and D425Med MYC 3 cells grown in the absence or presence of DOX for 3 days, and the expression was measured by quantitative RT-PCR. *CDKN1A* expression was evaluated because it is a known cyclin dependent kinase inhibitor that plays a key role in regulating the transition of cells through the G_1/S phase of the cell cycle (Fiorentino *et al*., 2016) and a gene which is frequently repressed in *MYC* amplified tumours (Westermann *et al*.,2008). The data from all D425Med NS, D425Med MYC 2 and D425Med MYC 3 constructs were combined and showed that MYC knockdown increases *CDKN1A* expression in D425Med MYC 2 (both) and D425Med MYC 3 (both) (Figure 4.6). This data indicates that *CDKN1A* plays a role in the observed G_1 arrest and confirms a MYC-dependent effect.

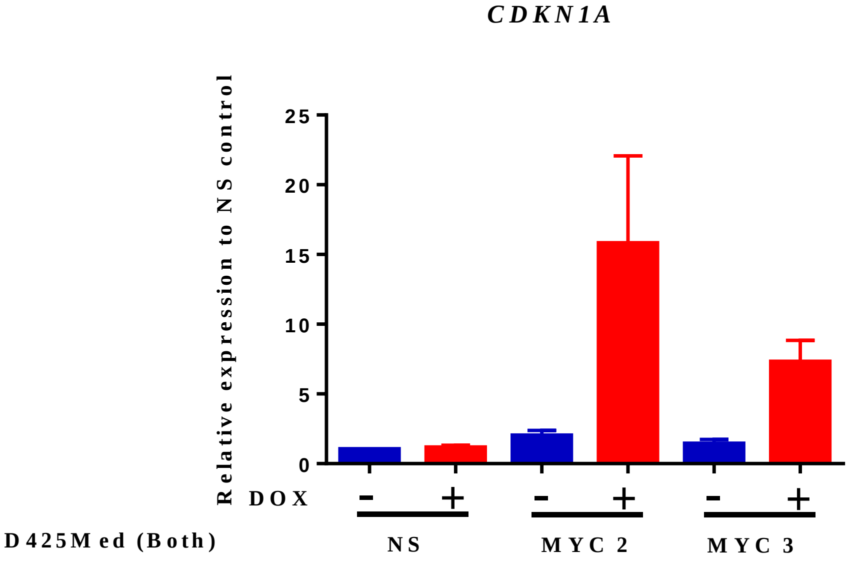

Figure 4.6 Expression of *CDKN1A* in D425Med (both) grown in the absence or presence of DOX for 3 days (blue represents – DOX and red represents + DOX). MYC knockdown in both D425Med MYC 2 and D425Med MYC 3 caused an upregulation of *CDKN1A* expression when compared to D425Med NS - DOX (control). The expression of mRNA was normalised to GAPDH and D425Med NS – DOX was used as the calibrator. Data are presented as mean ± SEM of six individual experiments. Significance was determined by unpaired student's t-test and no significance was observed.

4.2.4 MYC knockdown decreases apoptosis in D425Med

To further determine if the inhibition in proliferation due to MYC knockdown was also a result of increased apoptosis, the effect of MYC silencing on apoptosis was investigated using a caspase 3/7 assay. This assay quantifies the caspase 3 and 7 activity within the cells (described in methods 2.23). MYC silencing decreased apoptosis significantly at day 5 in D425Med MYC 2 (Figure 4.7 B) and at day 4 for D425Med MYC 3 (Figure 4.7 C). A decrease was also observed in D425Med MYC 2 (2^{nd}) (Figure 4.7 E) and D425Med MYC 3 (2^{nd}) at day 5 (Figure 4.7 F), however this did not reach statistical significance. The effect of MYC knockdown on apoptosis is consistent between replicates, but is a later and less pronounced effect than that on proliferation, therefore more technical replicates are needed to demonstrate significance in the case of the second replicate clones. Combining the two datasets showed a significant reduction in apoptosis was observed at both day 4 and 5 for D425Med MYC 2 (both) (Figure 4.7 H) and at day 5 for D425Med MYC 3 (both) (Figure 4.7 I).

A

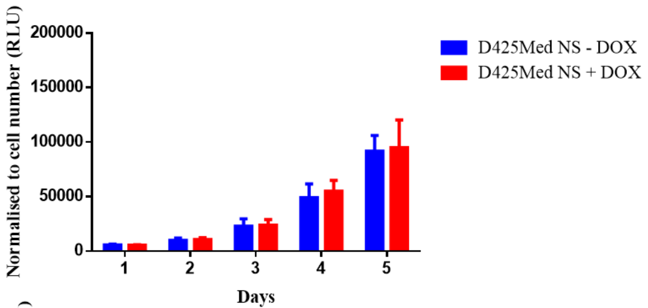
Normalised to cell number (RLU)
200000
150000
100000
50000
0
1
2
3
4
5
Days
D425Med NS - DOX
D425Med NS + DOX

B

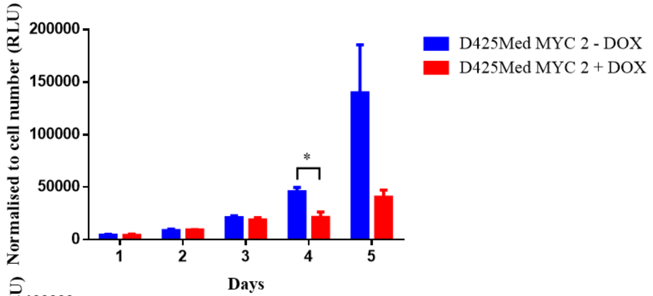
Normalised to cell number (RLU)
200000
150000
100000
50000
0
*
1
2
3
4
5
Days
D425Med MYC 2 - DOX
D425Med MYC 2 + DOX

C

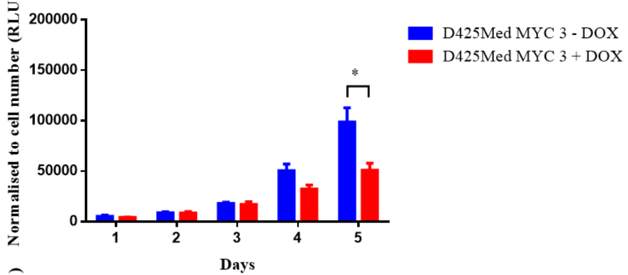
Normalised to cell number (RLU)
200000
150000
100000
50000
0
*
1
2
3
4
5
Days
D425Med MYC 3 - DOX
D425Med MYC 3 + DOX

D

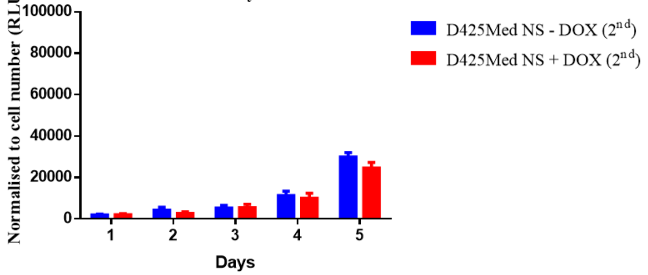
Normalised to cell number (RLU)
100000
80000
60000
40000
20000
0
1
2
3
4
5
Days
D425Med NS - DOX (2nd)
D425Med NS + DOX (2nd)

E

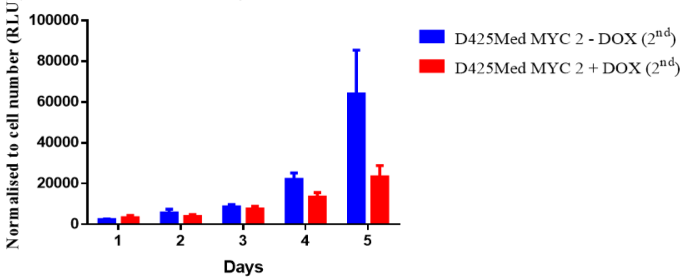
Normalised to cell number (RLU)
100000
80000
60000
40000
20000
0
1
2
3
4
5
Days
D425Med MYC 2 - DOX (2nd)
D425Med MYC 2 + DOX (2nd)

F

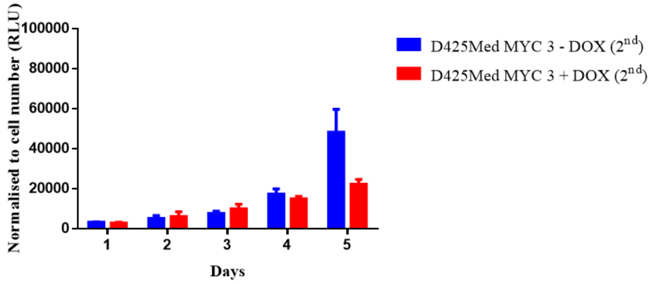
Normalised to cell number (RLU)
100000
80000
60000
40000
20000
0
1
2
3
4
5
Days
D425Med MYC 3 - DOX (2nd)
D425Med MYC 3 + DOX (2nd)

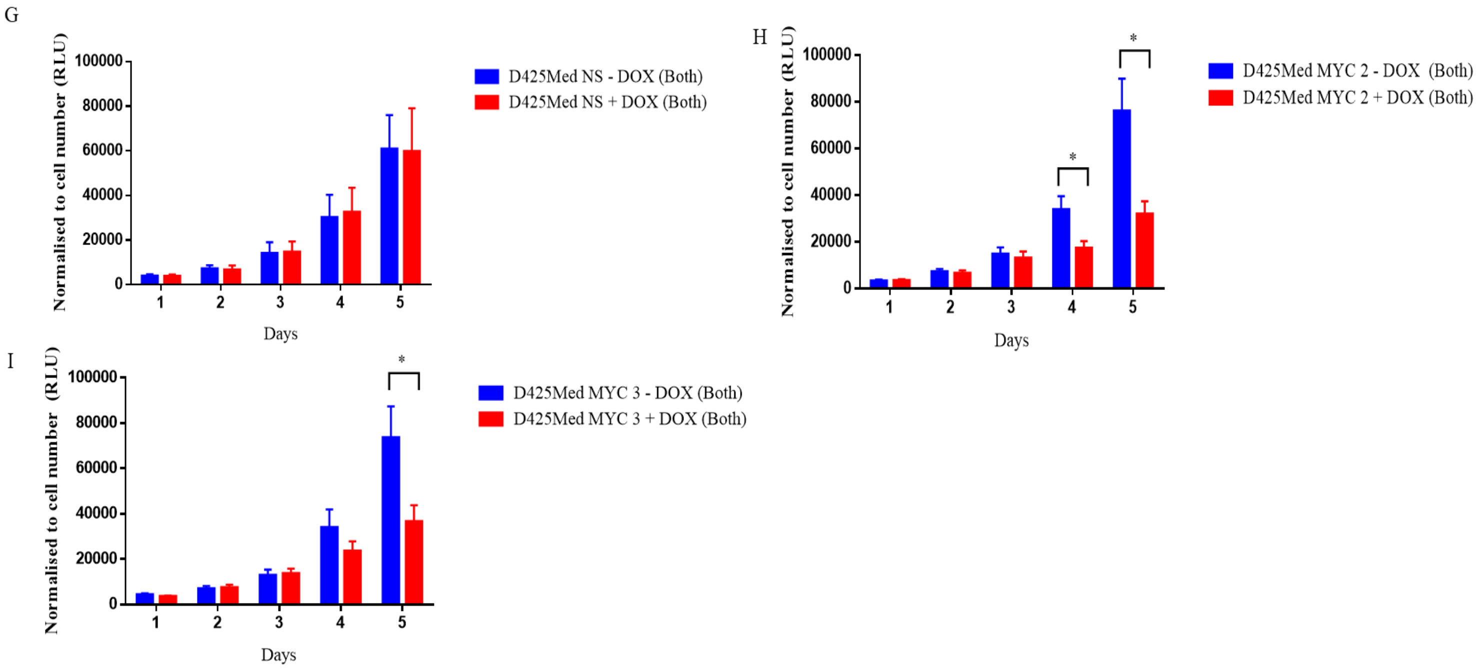

Figure 4.7 Effect of DOX inducible MYC silencing on apoptosis in D425Med cells. A) No significant difference was observed in D425Med NS + DOX when compared to control (D425Med NS – DOX) (blue, – DOX; red, + DOX; y-axis, RLU (relative luminescence unit)). B) MYC knockdown in D425Med MYC 2 causes a significant reduction in apoptosis at day 4 when compared to control (D425Med MYC 2 – DOX). C) MYC knockdown in D425Med MYC 3 resulted in a significant decrease in apoptosis at day 5 when compared to control (D425Med MYC 3 – DOX). D) No significant difference was observed in D425Med NS + DOX (2nd) when compared to control (D425Med NS – DOX (2nd). E) No significant difference was observed in D425Med MYC 2 + DOX (2nd) when compared to control (D425Med MYC 2 – DOX (2nd). F) No significant difference was observed in D425Med MYC 3 + DOX (2nd) when compared to control (D425Med MYC 3 – DOX (2nd). G) No significant difference was observed in D425Med NS + DOX (both) when compared to control (D425Med NS – DOX (both). H) MYC knockdown in D425Med MYC 2 (both) causes a significant reduction in apoptosis at day 4 and day 5 when compared to control (D425Med MYC 2 – DOX (both). I) MYC knockdown in D425Med MYC 3 (Both) resulted in a significant decrease in apoptosis at day 5 when compared to control (D425Med MYC 3 – DOX (Both). The results are shown as means ± SEM of three and six individual experiments and the significance was determined by unpaired student's t-test (* $p< 0.05$ vs control of the appropriate sample).

4.3 Analysis of the phenotypic effects of MYC knockdown in HDMB03

4.3.1 Knockdown of MYC has adverse effects on HDMB03 proliferation

Assessment of proliferation in HDMB03 was difficult compared to the D425Med cell lines. Sustained proliferation was observed for HDMB03 NS cells (Figure 4.8 A), however for HDMB03 MYC 2 (Figure 4.8 B) and HDMB03 MYC 3 (Figure 4.8 C), cell lines stopped growing after 2 days (n=12) in both the absence and presence of DOX. This happened each time the experiment was repeated (n=3). There were no morphological changes observed when viewed microscopically (Figure 4.9). The problematic assessment of HDMB03 constructs could be due to the leakiness caused by the promoter being too active in the absence of DOX, leading to a cell cycle arrest. Initial testing of MYC knockdown on a protein level showed no evidence of leakiness (Figure 3.15 C and D and Figure 3.16). However, when MYC knockdown in HDMB03 MYC 2 was tested again, some leakiness was observed for HDMB03 MYC 2 in the absence of DOX (Figure 3.20). The knockdown of MYC in HDMB03 MYC 2 in the absence and presence of DOX could have affected the viability, however similar results were seen with HDMB03 MYC 3. After 2 days, the growth rate in HDMB03 MYC 3 decreased in the absence and presence of DOX, MYC knockdown significantly decreased cell numbers from day 3 onwards relative to the control (Figure 4.8 C).

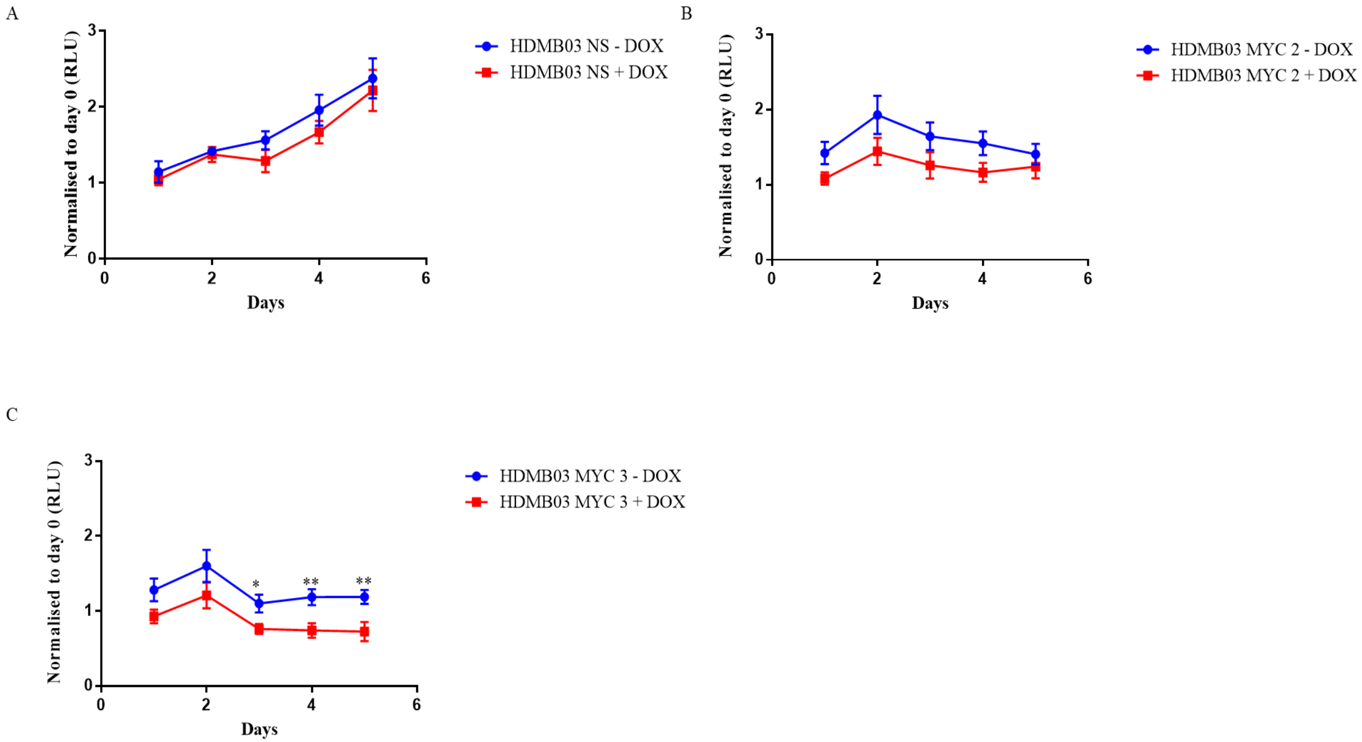

Figure 4.8 Effect of DOX inducible MYC silencing on proliferation in HDMB03 cells. A) No difference was observed in HDMB03 NS + DOX when compared to control (HDMB03 NS – DOX) (blue, – DOX; red, + DOX; RLU, relative luminescence unit). B) There was no difference in proliferation for HDMB03 MYC 2 + DOX when compared to control (D425Med MYC 2 – DOX). C) MYC knockdown in HDMB03 MYC 3 + DOX resulted in a significant reduction in cell number when compared to control (HDMB03 MYC 3 – DOX). Proliferation was measured using the CellTiter-Glo luminescent assay as discussed in methods (2.2.1). The results are shown as means ± SEM of three individual experiments and the significance was determined by the student's t-test (* $p < 0.05$, ** $p < 0.01$, vs control of the appropriate sample).

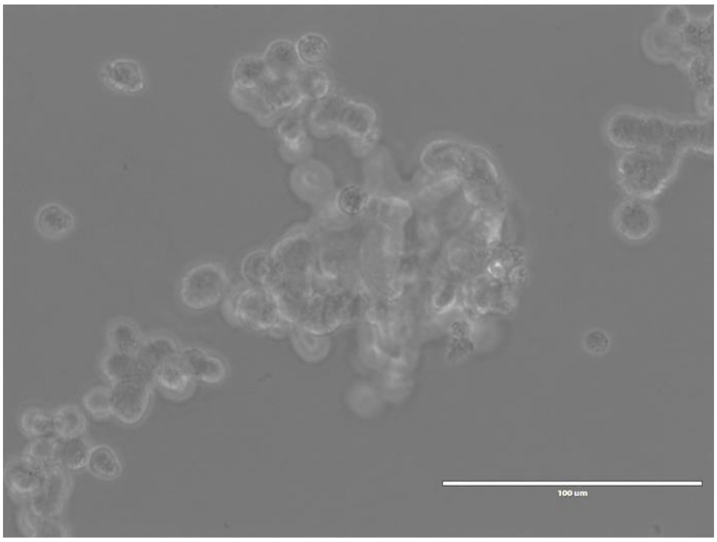

HDMB03 MYC 3

Figure 4.9 Phase contrast image of HDMB03 MYC 3. HDMB03 MYC 3 cells cluster in neurophere like clumps, the scale bar is 100um.

4.3.2 Effect of MYC knockdown on HDMB03 cell cycle

Assessment of the cell cycle progression for HDMB03 NS, HDMB03 MYC 2 and HDMB03 MYC 3 in the absence or presence of DOX were conducted after 3 days by flow cytometry. The inconsistency observed in the proliferation results is also observed in the cell cycle results. Analysing the cell cycle distribution for this cell line had its challenges. HDMB03 samples didn't always produce the correct cell cycle distribution histogram as indicated by the red arrow (Figure 4.10 B). The software was unable determine the S phase for HDMB03 MYC 3 – DOX sample. There were no changes detected in the cell cycle distribution for HDMB03 NS + DOX when compared to HDMB03 NS – DOX (Figure 4.10 A) There was also no significant change detected in the cell cycle distribution for HDMB03 MYC 2 + DOX when compared to HDMB03 MYC 2 – DOX (Figure 4.10 B). A significant decrease in cell numbers in the S phase of the cell cycle for HDMB03 MYC 3 + DOX was observed when compared to HDMB03 MYC 3 – DOX (Figure 4.10A and Table 28).

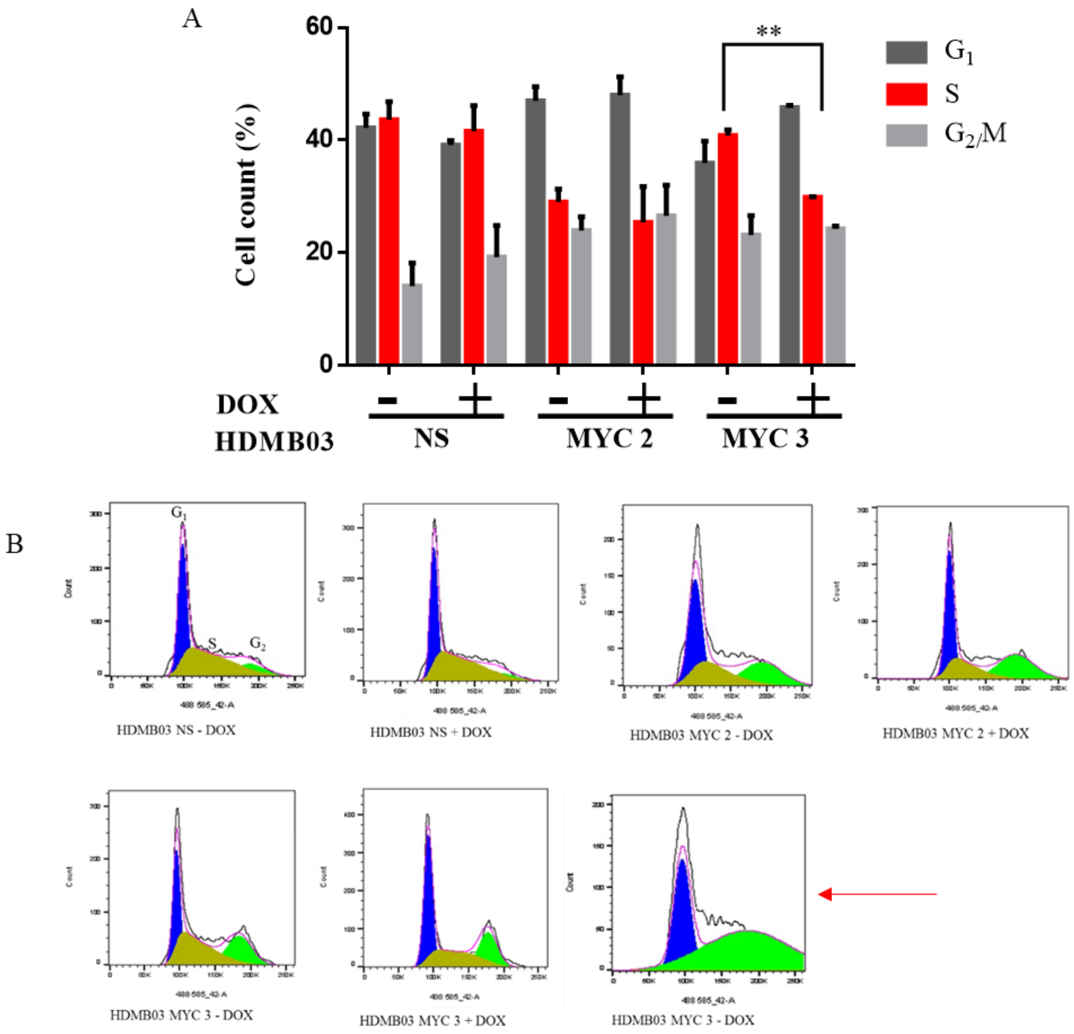

HDMB03 NS - DOX

HDMB03 NS + DOX

HDMB03 MYC 2 - DOX

HDMB03 MYC 2 + DOX

HDMB03 MYC 3 - DOX

HDMB03 MYC 3 + DOX

HDMB03 MYC 3 - DOX

Figure 4.10 DOX inducible silencing of MYC in HDMB03. A) Cell cycle analysis of HDMB03 NS, HDMB03 MYC 2 and HDMB03 MYC 3 in the presence or absence of DOX, cells were harvested after 3 days were detached by trypsin, fixed in 70 % ethanol and stained with PI as described in methods (2.2.2). A total number of 10 000 events per sample were counted. MYC knockdown in HDMB03 MYC 3 + DOX resulted in a significant decrease in the number of cells in the S phase of the cell cycle when compared to HDMB03 MYC 3 – DOX). There was no significant change in the cell cycle distribution for both HDMB03 NS + DOX and HDMB03 MYC 2 when compared to control (HDMB03 NS – DOX AND HDMB03 MYC 2 – DOX). The results are shown as means ± SEM of four individual experiments for HDMB03 NS ± DOX, three individual experiments for HDMB03 MYC 2 and two individual experiments for HDMB03 MYC 3 and the significance was determined by the student’s t-test (** $p<0.01$ vs control of the appropriate sample). Dark grey represents G1 phase, red represents S phase and light grey represents G2 phase. B) Representative cell cycle profiles derived by by FlowJo V10 software (x axis = 585/42).

PHASE OF THE CELL CYCLE (%)	**HDMB03 NS - DOX**	**HDMB03 NS + DOX**	**HDMB03 MYC 2 - DOX**	**HDMB03 MYC 2 + DOX**	**HDMB03 MYC 3 - DOX**	**HDMB03 MYC 3 + DOX**
G_1	42.21 ± 2.447	39.10 ± 0.8151	47.02 ± 2.504	48.00 ± 3.276	35.91 ± 3.890	45.84 ± 0.38
S	43.68 ± 3.219	41.61 ± 4.543	29.03 ± 2.318	25.43 ± 6.324	40.90 ± 0.9975	29.88 ± 0.09
G_2/M	14.11 ± 4.099	19.29 ± 5.568	23.95 ± 2.448	26.57 ± 5.440	23.19 ± 3.441	24.27 ± 0.48

Table: 28 The effect of MYC knockdown on HDMB03 cell cycle distribution, results are shown as mean ± SEM

4.3.3 MYC knockdown increases expression of CDKN1A in HDMB03 MYC 3

The expression of *CDKN1A* was evaluated in HDMB03 NS, HDMB03 MYC 2 and HDMB03 MYC 3 cells grown in the absence or presence of DOX for 3 days and the expression was measured by quantitative RT-PCR. An increase in *CDKN1A* expression was observed in HDMB03 MYC 3 (Figure 4.11) but no clear increase was observed for HDMB03 MYC 2 (Figure 4.11) even though MYC knockdown was observed for HDMB03 MYC 2 on a protein level (Figure 3.20).

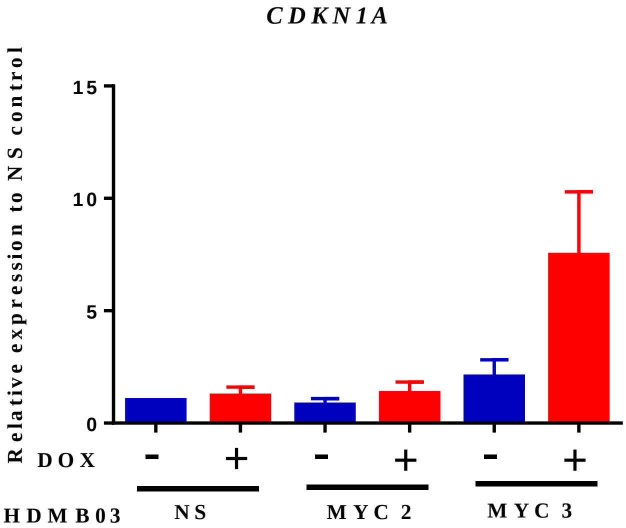

Figure 4.11 Expression of *CDKN1A* in HDMB03 NS, HDMB03 MYC 2 and HDMB03 MYC 3 cells grown in the absence or presence of DOX for 72 hours (blue represents – DOX and red represents + DOX). MYC knockdown in HDMB03 MYC 3 caused an upregulation of *CDKN1A* expression when compared to HDMB03 NS - DOX (control). The expression of mRNA was normalised to *GAPDH* and HDMB03 NS – DOX were used as the calibrator. Data are presented as mean ± SEM of three individual experiments and no significant changes was observed. Significance was determined by unpaired student’s t-test.

4.3.4 Effect of MYC knockdown on HDMB03 NS, HDMB03 MYC 2 and HDMB03 MYC 3 apoptosis

We continued with investigating the effect MYC silencing has HDMB03 MYC 2 and HDMB03 MYC 3 by conducting caspase 3/7 apoptotic analysis in a time dependent manner. The inconsistency was also observed in the apoptotic results. There was no change detected for HDMB03 NS + DOX when HDMB03 NS – DOX (Figure 4.12 A). There was a significant decrease in apoptosis observed at day 5 for HDMB03 MYC 2 +

DOX when compared to HDMB03 MYC 2 – DOX (Figure 4.12 B). A significant decrease in apoptosis was detected at day 2 for HDMB03 MYC 3 + DOX when compared to HDMB03 – DOX (Figure 4.12 C).

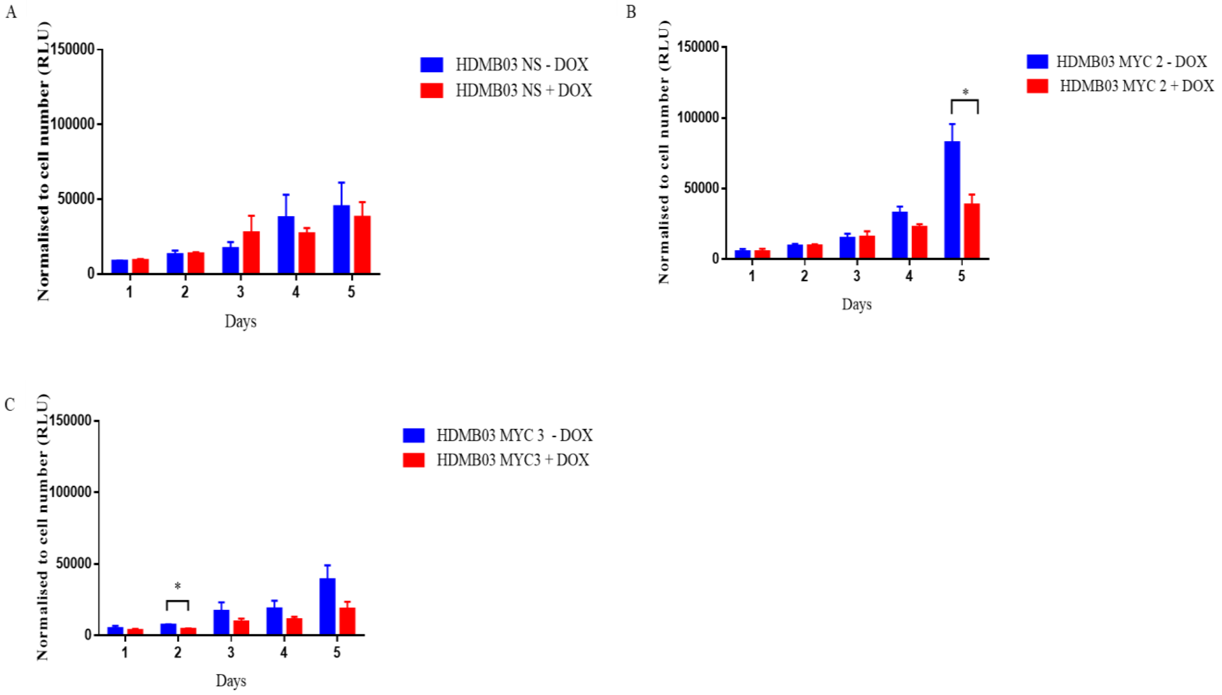

Figure 4.12 Effect of DOX inducible MYC silencing on apoptosis in HDMB03 cells. A) No difference was observed in HDMB03 NS + DOX when compared to control (HDMB03 NS – DOX). B) MYC knockdown in HDMB03 MYC 2 causes a significant reduction in apoptosis at day 5 when compared to control (HDMB03 MYC 2 – DOX). C) MYC knockdown in HDMB03 MYC 3 resulted in a significant decrease in apoptosis at day 2 when compared to control (HDMB03 MYC 3 – DOX). Apoptosis was measured using Caspase-Glo 3/7 luminescent assay as discussed in methods (2.2.3). The results are shown as means ± SEM of three individual experiments and the significance was determined by the student's t-test (* $p < 0.05$ vs control of the appropriate sample).

4.4 Discussion

In this chapter, DOX inducible MYC knockdown was performed in two MB_{GRP3} cell lines (D425Med and HDMB03) with *MYC* amplification and high *MYC* expression. A decrease in the rate of proliferation was seen in both the DOX treated and untreated D425Med NS cell line after three days. This could be due to the growth characteristics of the cell line as they grow the cell aggregates increase in size which affects the nutrient supply and a slow increase in metabolic waste within the cells occurs, which could possibly affect proliferation (Hossain *et al.*, 2007). MYC knockdown in D425Med showed a strong reproducible significant slower rate on cell proliferation. Knockdown of MYC within

D425Med resulted in a G_1 cell cycle arrest and an increase in the expression of the cell cycle inhibitor *CDKN1A*. In addition, MYC knockdown resulted in a decrease in apoptotic levels which indicates that inhibition of proliferation is not due to apoptosis but due to a different mechanism. Research carried out by von Beuren *et al* following MYC knockdown observed a decrease in proliferation at day 6 and a reduction in apoptosis was observed 3 days post transfection and an increase in *CDKN1A* was observed 3 days post transfection (von Bueren *et al.*, 2009). Whereas in this study the reduction in proliferation was seen at day 2, decreases in apoptosis at day 4 and an increase in *CDKN1A* at day 3. However, the difference in timing could reflect a difference in the two methods used to achieve knockdown. These results concords with previous observations made by von Bueren *et al* following MYC knockdown by siRNA (transient transfection) in the MB_{GP3} cell lines D425Med and D341Med. These results demonstrate that D425Med exhibits 'oncogene addition' and maintains a reliance on MYC for rapid proliferation and therefore validates as a model to investigate MYC-dependent biology and therapeutics.

Furthermore, silencing of MYC in D425Med caused morphological changes, the cells became more adherent, consistent with MYC's role in downregulating genes involved in cell adhesion such as lymphocyte function associated antigen-1 adhesion molecules (Inghirami *et al.*, 1990) and beta 1 integrin (Waikel *et al.*, 2001).

Cell lines generated for HDMB03 behaved in a less reproducible and robust manner than those made for D425Med. Sustained cell proliferation was difficult to achieve. Knocking down MYC resulted in different outcomes for HDMB03 MYC 2 and HDMB03 MYC 3. Although there were some problems with the reproducibility of experiments performed using HDMB03 MYC 3; MYC knockdown significantly and consistently reduced cell numbers in a proliferation assay compared to the control, significantly decreased the proportion of the cells in the S phase and resulted in upregulation of *CDKN1A* expression. These results are consistent with those observed for MYC knockdown in D425Med. HDMB03 MYC 2 did not give the same results, although it appeared to give a similar knockdown of MYC at the protein level (Figure 3.20). The discrepancies of the results could be due to leakiness of constructs; subsequent RNA-seq results showed that HDMB03 MYC 2 and HDMB03 MYC 3 grown in the absence of DOX separated slightly along the PC3 axis away from the NS control (discussed in 5.4), this could indicate leakiness of constructs. Another possibility could be that as HDMB03 MYC 2 and HDMB03 MYC 3 (Figure 4.9) aggregates grew, the nutrient supply decreased within the cell and metabolic waste increased which could have affected the viability, however this did not occur in the case of the NS line. The problem of aggregation could possibly be solved by gently pipetting the aggregates to disrupt them. However other studies have shown that aggregation can promote proliferation (Mori *et al.*, 2006) and it is difficult to disaggregate cells in a reproducible manner and maintain inter-replicate consistency. These experiments would have to be repeated due to the inconsistency between HDMB03 MYC 2 and HDMB03 MYC 3 and HDMB03 NS observed. These discrepancies are discussed further in Chapter 5. MYC knockdown resulted in a decrease in apoptosis in both HDMB03 MYC 2 and HDMB03 MYC 3, consistent with the results seen for D425Med. The potential transcriptional changes associated with the phenotypic changes caused by MYC knockdown will be further discussed in Chapter 5.

Chapter 5 Gene expression profiling of inducible isogenic models of MYC-driven Group 3 medulloblastoma

5.1 Introduction

MYC is a basic-helix-loop-helix leucine zipper transcription factor. *In vivo* studies estimate that MYC binds to 25000 sites in the genome, thereby controlling the expression of about 10 to 15 % of genes (Ben-Israel *et al.*, 2008). MYC binds to the canonical E-box sequence CACGTG, but also to non-canonical promoters. For MYC to regulate transcription of genes it first must form a heterodimeric complex with MAX, which then binds to E-box sites (Adhikary and Eilers, 2005b). Transcription by MYC can be activated via all three RNA polymerases (I, II and III) (Hann, 2014). MYC cannot initiate transcription *de novo,* but requires pre-existing open chromatin; CpG islands and E boxes lying within closed chromatin are not bound by MYC (Kress *et al.*, 2015). However, MYC is known to be able to activate or inactivate the transcription of many target genes (Adhikary and Eilers, 2005b) (discussed in chapter 1.5.3) through recruitment of multiple chromatin remodelling cofactors (Poole and van Riggelen, 2017).

MYC activates transcription through recruiting cofactors such as TRAPP, an adaptor protein that is a member of multiple histone acetyltransferase (HAT) containing complexes. TRAPP also helps to bind other cofactors indirectly to MYC, including the General Control of Amino Acid Synthesis Protein 5-Like 2 (GCN5), 60kDa Tat Interacting Protein (TIP60), Switch/Sucrose Non-Fermentable (SWI/SNF) related histone-exchange protein and E1A-Binding protein p400 (p400). When HATs, GCN5 and TIP60 interact indirectly with MYC, GCN5 acetylates lysine residues on histone 3 at positions 9, 14 and 18 and TIP60 acetylates histones H4 and H2A at positions 5,8,12 and 5 respectively. The histone acetylation process weakens the nucleosome's grip and makes the DNA accessible for gene transcription (Poole and van Riggelen, 2017). Gene transcription can also be stimulated through MYC recruiting cofactors like CREB-binding protein (CBP) and p300, or through the recruitment of members of the APIS complex to the E-box regions via MYC binding with E3 ubiquitin ligase SCF^{SKP2}. MYC transcriptional activity can be repressed by complexes such as MAD-MAX and MNT-MAX, which recruit histone deacetylase cofactors(Adhikary and Eilers, 2005b). MYC can cause gene silencing through binding to other transfactors including MIZ-1, SP1, nuclear factor Y, ying yang 1 and transcription factor III. MYC-MAX/MIZ1, which is the most studied complex, represses genes through recruiting DNA methyltransferases which silence genes such as *CDKN1A* and *CDKN2B* by hypermethylating CpGs within the surrounding area (Poole and van Riggelen, 2017). The MYC-MAX/MIZ1 complex also represses target genes through recruiting HDAC1 and HDAC3 corepressors which are involved in histone deacetylation. In addition, MYC can silence important developmental genes through binding to the PRC2 complex (Poole and van Riggelen, 2017).

Transcriptional regulation by MYC is complex, due to its large number of interactions and its ability to regulate the expression of several other transcription factors as detailed above. The ability to amplify expression at active promoters leads to cell context dependent signatures and an increased RNA content within cells (Kress *et al.*, 2015). Research has highlighted a core set of genes common to multiple cells types, these genes are involved in ribosomal biogenesis and RNA processing (Ji *et al.*, 2011). However, in general there is little overlap of MYC target genes between different cell lines (Poole and van Riggelen, 2017).

Therefore, due to the context dependent role of MYC, it is important to understand the effect of MYC modulation on the transcriptional profile of MB_{GRP3} and to identify MYC target genes within this tumour using RNAseq technology. This identification of key downstream pathways may highlight suitable therapeutic strategies and will generate an important data set for comparison with primary tumour data, highlighting the MYC directed expression changes in $MB_{GRP3.}$ In addition, it will allow future comparison with the effect on transcription of MYC targeting therapeutics, allowing an assessment of their specificity.

This aim of this Chapter was to profile the DOX -inducible MYC silencing models before and after modulation of MYC by RNA-seq in order to identify important gene networks/pathways (Gene set enrichment analysis and Ingenuity pathway analysis). Furthermore, to cross-reference the gene expression profiles of the DOX-inducible MYC silencing models with MB_{GRP3} primary tumour profiles to identify which features seen in the primary tumours are MYC dependent and may represent a clinically relevant druggable target.

The cell lines used for sequencing were D425Med NS, D425 Med MYC 2, D425Med MYC 3, D425Med NS (2nd), D425Med MYC 2 (2nd), D425Med MYC 3 (2nd), HDMB03 NS, HDMB03 MY2 and HDMB03 MYC 3. Cell lines were harvested after 72 hours grown either in the absence or presence of DOX. Each sample had two biological replicates with about 50 million paired end reads per sample.

5.2 RNA-seq analysis

5.2.1 Sample preparation

RNA was extracted from cells as described in 2.7.1 and analysed using the Agilent 2100 bioanalyzer. The bioanalyzer uses microfluidics, electrophoresis and fluorescence to determine the integrity and concentration of RNA (Schipor *et al.*, 2016). All RNA samples had an RNA integrity number (RIN score) greater than 7 (Figure 5.1) and a ribosomal RNA (rRNA) (28S:18S) band ratio of 2 or greater indicating the absence of RNA degradation (Figure 5.1). This quality control experiment validated all RNA samples as being of suitable quality for downstream applications, such as mRNAseq.

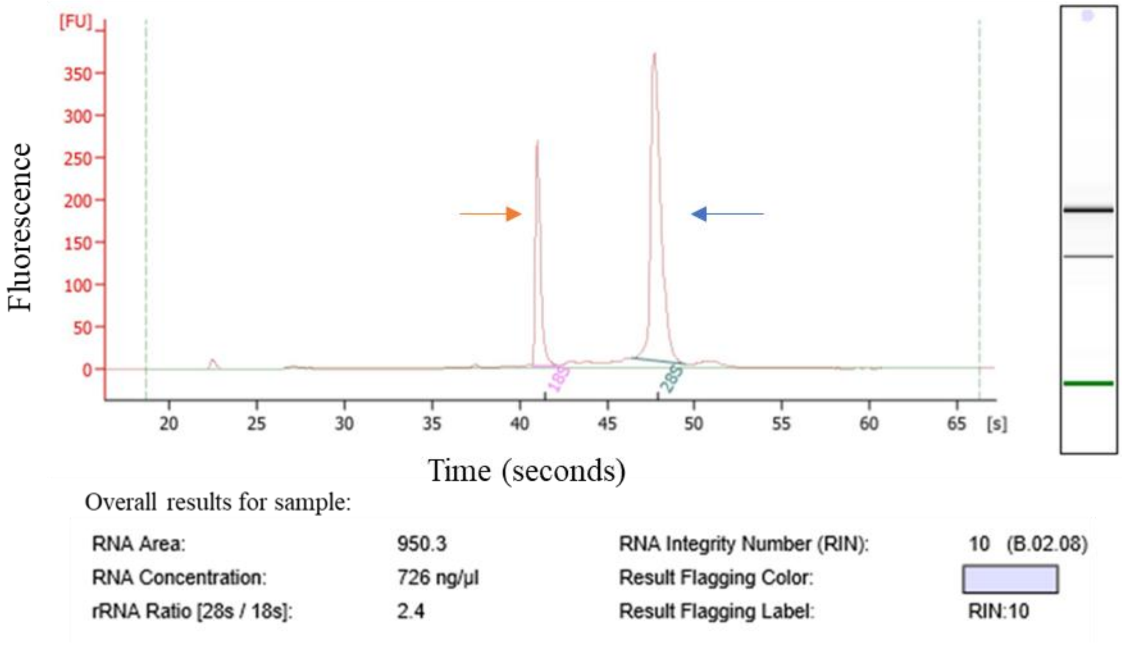

Overall results for sample:

RNA Area:	950.3	RNA Integrity Number (RIN):	10 (B.02.08)
RNA Concentration:	726 ng/µl	Result Flagging Color:	🟪
rRNA Ratio [28s / 18s]:	2.4	Result Flagging Label:	RIN:10

Figure 5.1 Electropherogram of a typical sample showing the integrity and concentration of the RNA alongside the rRNA ratio. The red arrow represents the 18S fragment and the blue arrow represents the 28S fragment.

5.2.2 Validating the transcriptional effect of MYC knockdown

To identify genes which are consistent *MYC* transcriptional targets, genes which change in expression following MYC modulation in cell lines from multiple other cancer types were identified from the published literature (Schuhmacher *et al.*, 2001; Menssen and Hermeking, 2002; Ellwood-Yen *et al.*, 2003; Yu *et al.*, 2005; Bild *et al.*, 2006; Kim *et al.*, 2006; O'Donnell *et al.*, 2006) and these were cross referenced with low and high *MYC* expression MB$_{GRP3}$ primary tumour data. Genes that showed a strong relationship with *MYC* expression in MB$_{GRP3}$ were analyzed using previous RNAseq data generated from the parental cell lines D425Med and HDMB03 for evidence of expression. *TRAP1 and RCC1* were positively correlated with *MYC* expression (data not shown). These genes were therefore selected as candidate genes to validate the DOX inducible MYC knockdown models for further analysis. The expression of *TRAP1* and *RCC1* was evaluated in both D425Med NS, D425Med MYC 2 and D425Med MYC 3 cell lines. The expression of *TRAP1* and *RCC1* was also evaluated in HDMB03 NS, HDMB03 MYC 2 and HDMB03 MYC 3 cell lines. Cells were grown in the absence or presence of DOX for 3 days, and expression was measured by quantitative RT-PCR. The data from both D425Med NS, D425Med MYC 2 and D425Med MYC 3 cell lines were combined and this showed that MYC knockdown decreased *TRAP1* and *RCC1* expression in D425MED MYC 2 and MYC3, although the decrease did not achieve significance in the MYC3 cell lines (Figure 5.2 A and B). MYC knockdown caused a decrease (not significant) in *TRAP1* expression in HDMB03 MYC 2 and HDMB03 MYC 3. A minimal but not significant decrease was observed in *RCC1* expression in HDMB03 MYC 2, but a significant decrease was observed in *RCC1* expression in HDMB03 MYC 3 (5.2 C and D). Despite the fact that some decreases did not reach statistical significance, the consistency of the observed trends, together with the observed knockdown of *MYC* at the transcriptional level and the consistent induction of *CDKN1A* expression (Chapter 4.2.3) was taken as sufficient evidence that the expected transcriptional effects were being seen following MYC knockdown.

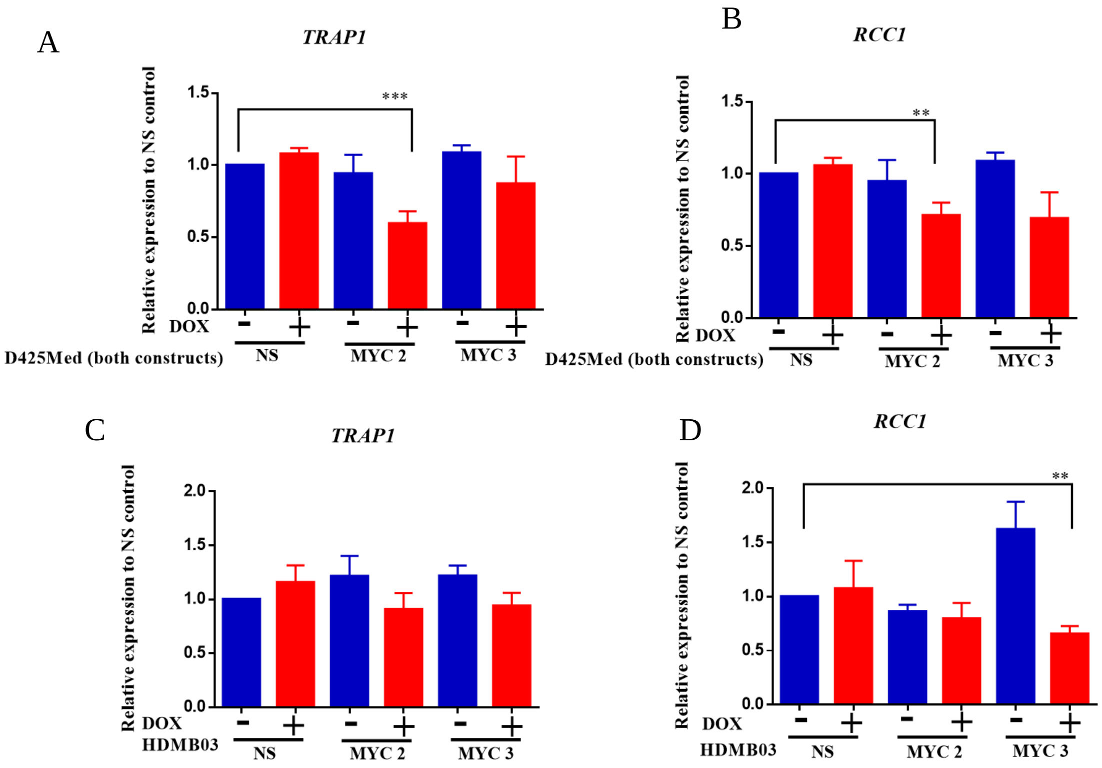

Figure 5.2 Expression of *TRAP1* and *RCC1* in D425Med and HDMB03 following growth in the absence or presence of DOX for 3 days (blue indicates - DOX and red indicates + DOX). A) MYC knockdown in both D425Med MYC 2 and D425Med MYC 3 caused a downregulation of TRAP1 expression when compared to D425Med NS - DOX (control). B) MYC knockdown in both D425Med MYC 2 and D425Med MYC 3 caused a downregulation of RCC1 expression when compared to D425Med NS - DOX (control). C) MYC knockdown in HDMB03 caused a downregulation of TRAP1 expression when compared to HDMB03 NS - DOX (control). D) MYC knockdown in HDMB03 caused a downregulation of RCC1 expression when compared to HDMB03 NS - DOX (control). The expression of mRNA was normalised to GAPDH and D425Med NS – DOX or HDMB03 NS - DOX were used as the calibrator. Data are presented as mean ± SEM of three or six individual experiments.

5.2 mRNA-seq quality control analysis

All raw sequencing data (method described in 2.11.1) obtained were subjected to quality control checks using FastQC software created by the Babraham Institute bioinformatics group. All samples passed quality control checks determined by FastQC analysis. For example, the phred quality score for a typical sample (Figure 5.3) was above 30, this indicates that only 1% of base calling was inaccurately called. The sequence content showed that the first 13 base pairs had a bias distribution, however this is normal due to the use of random hexamer primers (Figure 5.4) (Kumar *et al.*,2012). After this biased nucleotide distribution, a stable distribution of nucleotides were observed (Figure5.4). The GC content fits with the expected theoretical distribution bell shape curve (Figure

5.5). The number of mapped read counts achieved was around 38,640,000 for every sample.

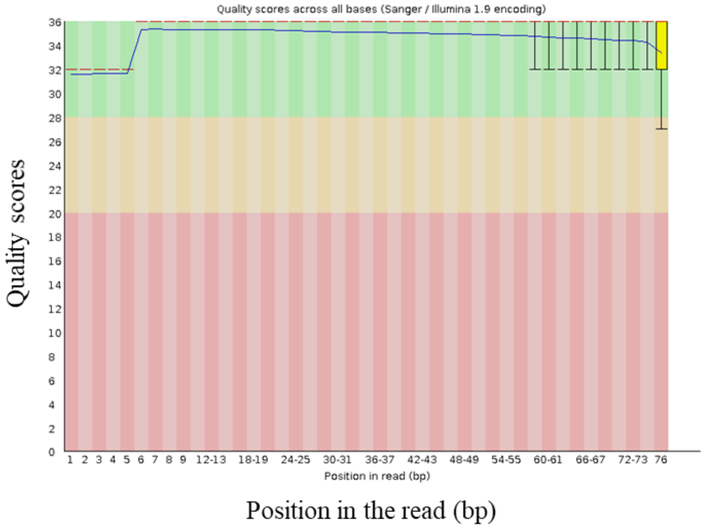

Figure 5.3 Overview of per base sequence quality for a typical sample. The y-axis shows the quality scores and the x-axis shows the position in the read (bp). The background of the plot shows three different colours: Green indicates good quality score, orange indicates a reasonable quality score and red indicates a poor quality score.

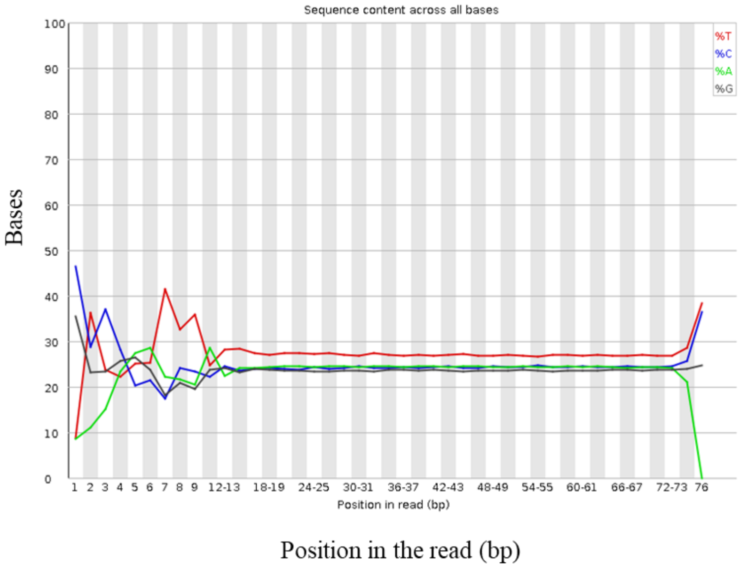

Figure 5.4 FastQC plot of the sample showing the sequence content of all bases for a typical sample. The y-axis shows the bases and the x-axis shows the position in the read (bp). Each nucleobase is represented by a different colour, thymine (T) is represented by red, cytosine (C) is represented by blue, adenine (A) is represented by green and guanine (G) is represented by black. A stable distribution of nucleotides occurs after the first 13 base pairs.

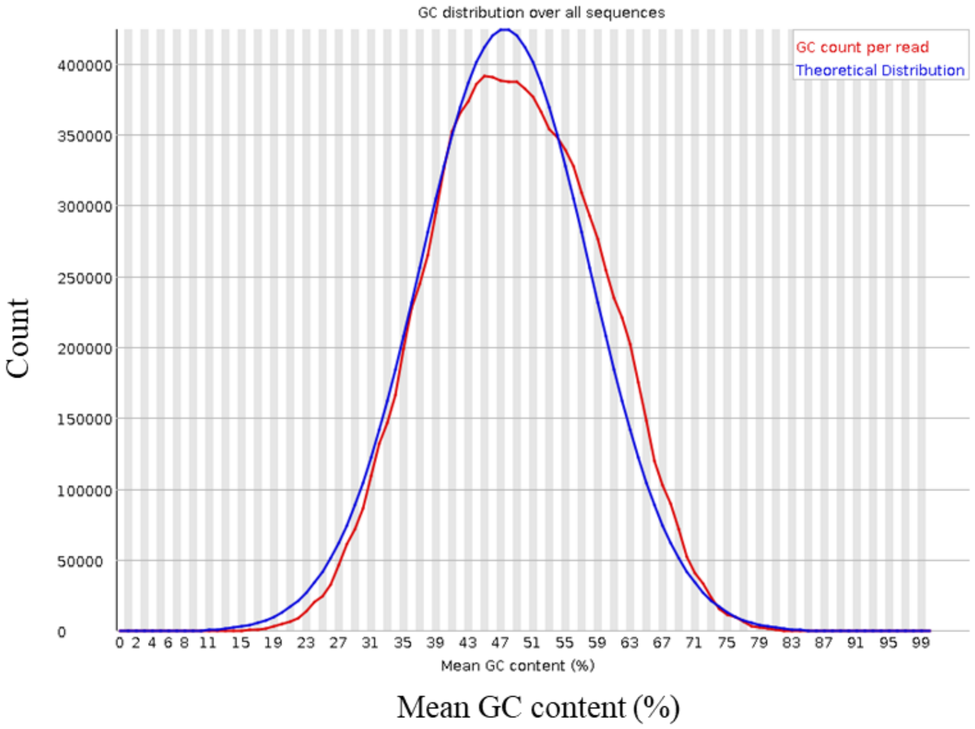

Figure 5.5 FastQC plot of a typical sample showing the per sequence GC content. The red line represents the GC count per read of sequencing data and the blue line represents the theoretical distribution curve. The GC count per read bell shape curve fits closely to the theoretical data which is an indication of good data.

5.3 Differential expression between DOX inducible MYC knockdown models in the absence and presence of DOX

The mRNA seq data analysis was processed by Dr Daniel Williamson, briefly the DEseq2 bioconductor package was used to identify differential expressed genes between the DOX-inducible MYC silencing models (D425Med and HDMB03) grown the absence or presence of DOX. DEseq is based on the negative binomal distribution model that is classified by two parameters; namely mean and dispersion of data (Anders and Huber, 2010; Soneson and Delorenzi, 2013). This software provides a quantitative analysis by applying a shrinkage approach to estimate the dispersion of transcriptional counts and fold change (Love *et al.*, 2014). The raw count data were analysed in a pair wise manner using this software. The scatter plot shows the fold changes of differentially expressed genes at a 10% false discovery rate when the Benjamini and Hochberg procedure was performed. The significant differentially expressed genes are coloured in red (Figure 5.6).

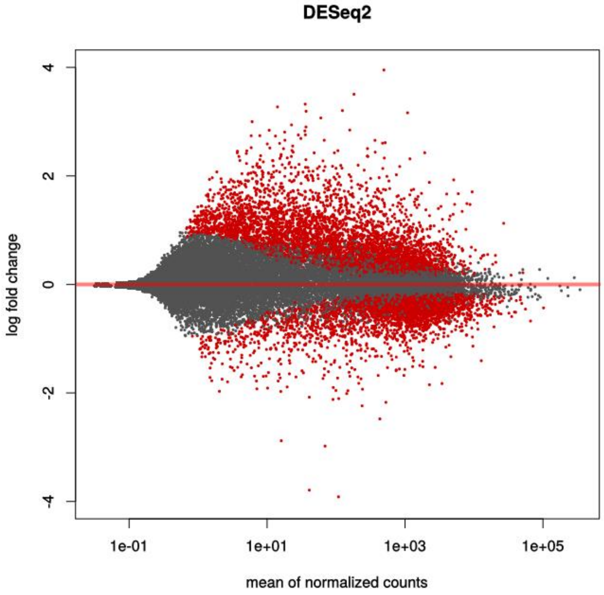

Figure 5.6 Testing for differential expression between DOX inducible MYC knockdown models (D425Med and HDMB03) grown in the absence or presence of DOX. Scatter plot of log fold change versus mean of normalized counts. The red dots represent genes that are differentially expressed at a 10% FDR when a Benjamini and Hochberg correction is applied. The red dots at the upper or lower end of the scatter plot represents genes with either very low or high log fold change.

5.4 Principal component analysis (PCA) of gene expression signatures from DOX inducible MYC knockdown models indicates consistent gene expression changes following MYC knockdown.

PCA was performed on significant genes (adjusted p-value <0.01, moderate log fold change ≤ -2 and ≥ +2). PCA allows the visualization of data by limiting the dimensionality of data with a reduced loss of statistical information (Jolliffe and Cadima, 2016). The PCA revealed that the gene expression signatures from all MYC expressing D425Med cells clustered together i.e. replicates of the D425Med NS grown in both the absence and presence of DOX, along with the D425Med MYC 2 and D425 Med MYC 3 replicates grown in the absence of DOX. The D425Med MYC 2 and D425 Med MYC 3 replicates grown in the presence of DOX formed a separate cluster (Figure 5.7). This indicates that MYC knockdown causes a reproducible change in gene expression. The PCA showed that HDMB03 NS samples grown in the absence and presence of DOX clustered together. In contrast to D425Med, HDMB03 MYC 2 and MYC3 grown in the absence of DOX had a slight separation along the PC3 axis away from the NS controls, perhaps indicating some leakiness of the constructs in this cell line (see Chapter 4.3). HDMB03 MYC 2 grown in the presence of DOX didn't separate along the PC3 axis to the same extent as HDMB03 MYC 3 (Figure 5.7). This could be an indication that the degree of MYC knockdown is greater in HDMB03 MYC 3.

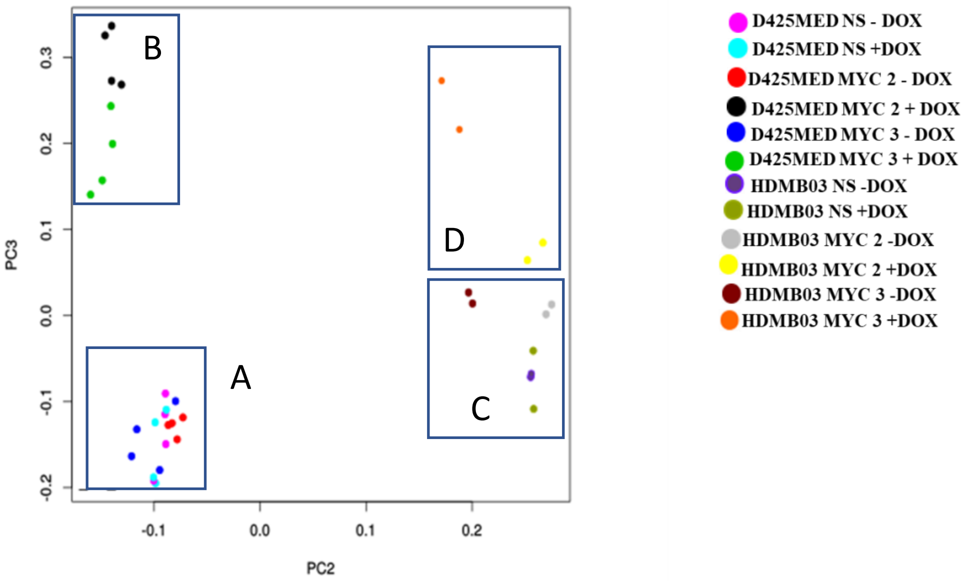

Figure 5.7 Supervised principal component analysis of gene expression signatures in DOX inducible MYC knockdown models. This PCA plot shows different biological samples. Replicates of the same condition are coloured the same and each dot is an individual replicate. A) D425Med cells expressing MYC (NS or –DOX) B) D425 cells following MYC knockdown (+DOX). C) HDMB03 cells expressing MYC (NS or –DOX) D) HDMB03 cells following MYC knockdown (+DOX). The x-axis is the second component (PC2 related to cell line identity) and the y axis the third component (PC3 related to MYC expression).

5.5 MYC knockdown leads to consistent expression changes in medulloblastoma cell lines.

Filtered data with an adjusted p-value < 0.01 and moderate log fold change ≤ -2 and ≥ 2 for D425Med NS, D425Med MYC 2, D425Med MYC 3 (Figure 5.8), HDMB03 NS, HDMB03 MYC 2 and HDMB03 MYC 3 (Figure 5.9) grown in the absence or presence of DOX were used to create a heatmap representing the top 100 significantly deregulated genes, when both cell lines were analysed together. These heatmaps show that MYC knockdown causes both downregulation and upregulation of genes, consistent with its dual role as a transcriptional activator and repressor. It also shows that these genes behave consistently between the two cell lines. The relative difference based on statistical significance in expression of selected genes for D425Med and HDMB03 isogenic models are represented as boxplots (Figure 5.10). Amongst the genes showing the largest decrease in expression following MYC knockdown are those genes involved in metabolism and ribosomal biogenesis (eg *SLC19A3*, *RRP1B* and *GLDC* (Figure 5.10 A)(Kim *et al.*, 2014; Su *et al.*, 2015; Flønes *et al.*, 2016). MYC is known to have a direct role in ribosomal biogenesis and can regulate genes involved in the cellular metabolism, thereby assisting with the essential building blocks required by cancer cells to proliferate (Le and Dang, 2013). Genes showing the greatest increase in expression following MYC knockdown include *TGFB1* and *NRL* (Figure 5.10 B). In many different cells TGFB1 can negatively regulate proliferation (Buckwalter *et al.*, 2006) and can inhibit the synthesis of MYC (Munger *et al.*, 1992). MYC can also inhibit genes stimulated by TGFB1 (Smith *et al.*, 2009). NRL is involved in rod photoreceptor differentiation (Kautzmann *et al.*, 2011), MYC is known to have a role in differentiation (Lin *et al.*, 2000) and can cause dedifferentiation of cells to a more stem cell like state (Ramesh *et al.*, 2009).

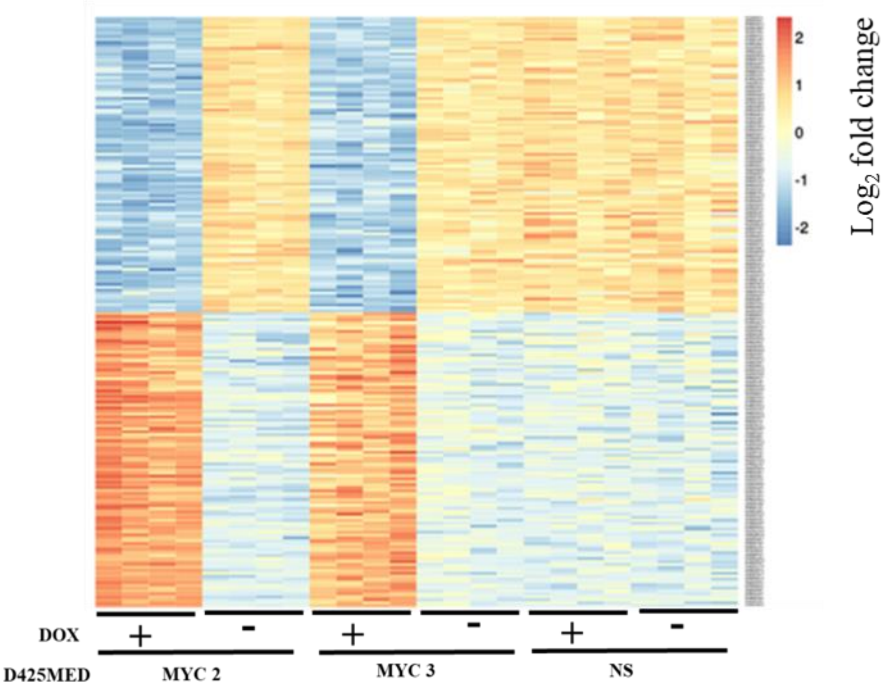

Figure 5.8 Heatmap of the top 100 significantly differentially expressed genes in D425Med NS, D425Med MYC 2 and D425Med MYC 3 grown in the absence and presence of DOX showing high reproducibility between replicates. Each row represents a gene and each column a sample. The light to dark blue colour represents genes that are downregulated and the light to dark orange colour represents genes that are upregulated.

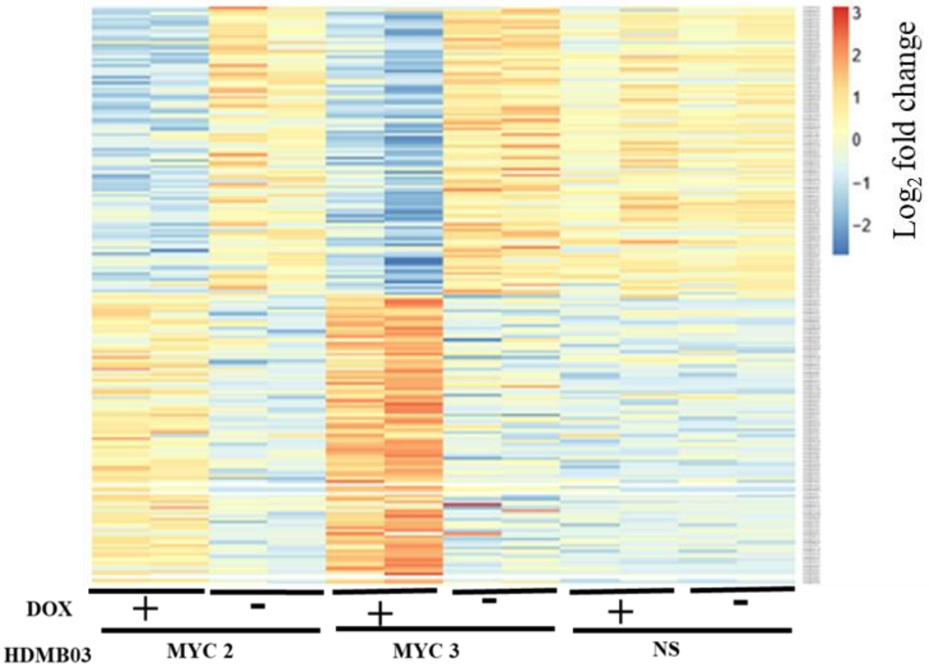

Figure 5.9 Heatmap of the top 100 significantly differentially expressed genes in HDMB03 NS, HDMB03 MYC 2 and HDMB03 MYC 3 grown in the absence and presence of DOX. Each lane represents a gene (same gene set as shown in Figure 5.8) and each column a sample. The light to dark blue colour represents genes that are downregulated and the light to dark orange colour represents genes that are upregulated.

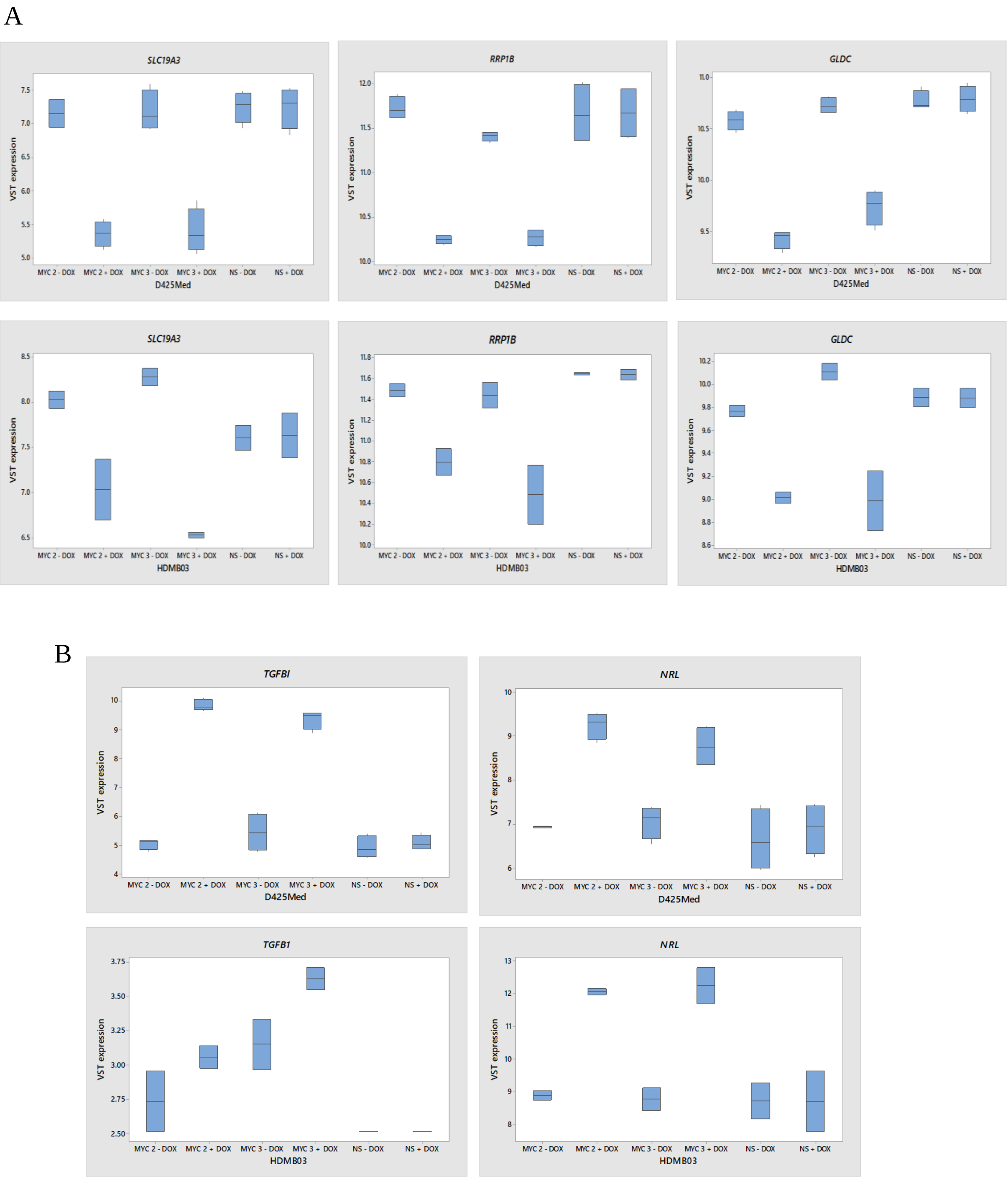

Figure 5.10 Relative expression of selected differentially expressed genes in D425Med NS, D425Med MYC 2, D425Med MYC 3, HDMB03 NS, HDMB03 MYC 2 and HDMB03 MYC 3. A) Relative expression of genes that are downregulated in D425Med MYC 2, D425Med MYC 3 HDMB03 MYC 2 and HDMB03 MYC 3 grown in the presence of DOX. B) Relative expression of genes that are upregulated in D425Med MYC 2, D425Med MYC 3, HDMB03 MYC 2 and HDMB03 MYC 3 grown in the presence of DOX. The x-axis represents the sample names and the y-axis represents the variant stabilised transformed (VST) expression. Box plots shows median and quartile ranges.

5.6 Gene set enrichment analysis (GSEA)

GSEA is a computational method that distinguishes if a predetermined gene set shows any statistically significant difference between two experimental conditions, for example MYC knockdown vs control or MB_{GRP3} primary tumours vs MB belonging to other subgroups. GSEA analysis was performed to identify biological or cancer signalling pathways enriched within MB_{GRP3} primary tumours and affected by MYC knockdown in the DOX inducible knockdown MYC models. A pre-ranked gene list was used to perform the analysis against the Hallmark molecular signature databases (MSigDB). The MSigDB are gene sets selected from published datasets or trusted gene ontologies. The Hallmark MSigDB gene sets were created through computational modelling to obtain gene sets that overlap in other MSigDB. (http://software.broadinstitute.org/gsea/index.jsp). The analysis performed by Dr Janet Lindsey and Samuel Steele.

GSEA analysis was performed using RNA seq data collected on a cohort of 250 patient MBs. The patient cohort consisted of 164 males and 83 females, 40 of which had tumours which were MB_{GRP3}, 29 MB_{WNT}, 54 MB_{SHH} and 105 MB_{GRP4}. MB_{GRP3} tumours from seven male and two female patients showed evidence of *MYC* amplification. GSEA analysis against the Hallmark gene set database identified 8 gene sets that were positively enriched (FDR of <25%, 5 of which had a NOM (nominal) p value of < 1%) in MB_{GRP3} vs other MB (cohort of 250 primary MBs) and 24 gene sets that were negatively enriched (FDR of < 25%; 10 p<1%). Comparing MYC knockdown in the cell lines to MYC expressing controls this analysis identified 16 gene sets that were positively enriched (11 p < 1%) and 15 gene sets that were negatively enriched (8 p <1%).

5.6.1 GSEA confirms knockdown of MYC target genes and changes in the expression of genes involved in the cell cycle

GSEA results showed that MYC knockdown caused the expected downregulation of 'Hallmark MYC targets', a subgroup of genes that have been categorised as MYC regulated using several published datasets where MYC expression is regulated or altered (http://software.broadinstitute.org/gsea/msigdb/genesets.jsp?collection=H#). In contrast the majority of MYC target genes were upregulated in $MB_{GRP\ 3}$ primary samples (Figure 5.11). For example genes such as *HDAC2*, *CUL1*, *CCNA2* and *PA2G4* were upregulated in MB_{GRP3} and downregulated following MYC knockdown. HDAC2 is involved in multiple processes such as cell cycle, senescence, proliferation, differentiation and apoptosis (Yao and Rahman, 2012). HDAC inhibitors have been tested in MB and have shown an inhibitory effect on metabolic activity and proliferation (Ecker *et al.*, 2015) . Cullin 1 (CUL1) forms part of the SKP-CUL1-F-BOX-Protein (SCF) E3 ligases, which has an essential role in cell cycle, DNA replication, signal transduction and development (Xie *et al.*, 2013). The cyclin CCNA2 (Cyclin A2) has an important function in controlling the transition of cells in the G1/S and the G2/M phase of the cell cycle. CCNA2 also has an important role in hematopoietic cell lineage and embryonic cells (Gao *et al.*, 2014). PA2G4 has a role in mediating proliferation (Ko *et al.*, 2017).

Silencing of MYC caused a downregulation of genes involved in G2/M checkpoints and E2F targets, whereas these gene sets were positively enriched in MB_{GRP3} (Figure 5.11). G2/M checkpoint genes such *CUL1, CCNA2, E2F2* and *E2F3* genes have a negative rank metric score following MYC knockdown and a positive rank metric score in MB_{GRP3}. E2F2 is involved in the G1/S transition phase of the cell cycle (Rady *et al.*, 2013). MYC is required to mediate E2F protein interaction with E2F gene promoters (Dong *et al.*, 2014). In the E2F target gene set *CCNE1* (Cyclin E) has a positive rank metric score in MB_{GRP3} and a negative rank metric score in following MYC knockdown. *CCNE1* is involved in G1/S transition of the cell cycle and is an E2F target gene (Hwang and Clurman, 2005). These results indicate the potential mechanisms by which MYC knockdown decreases proliferation and triggers G1 cell cycle arrest as discussed in Chapter 4.

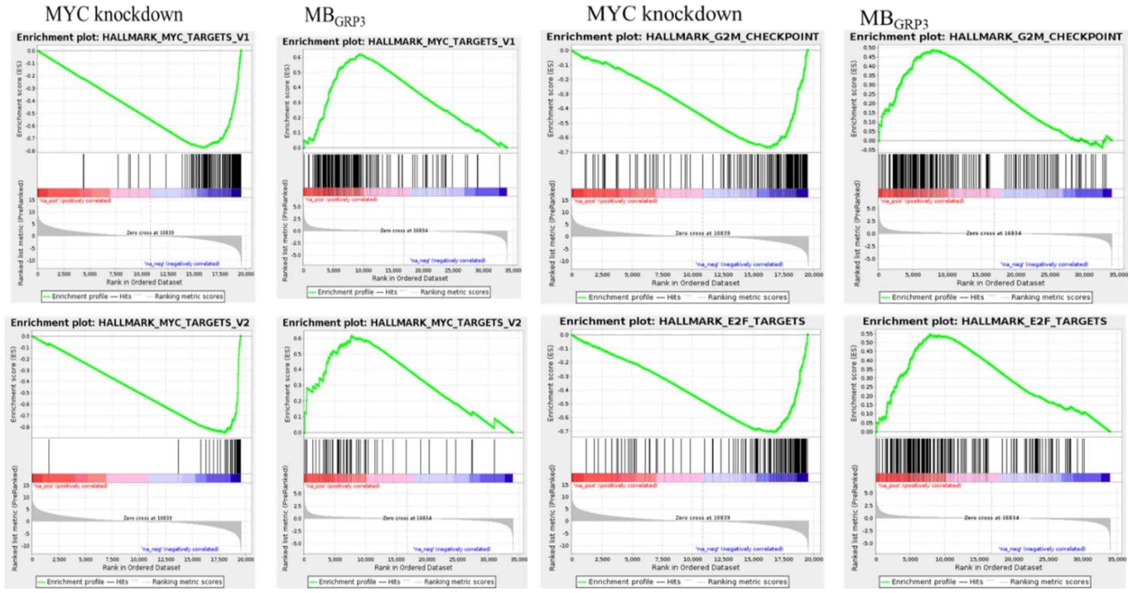

Figure 5.11 Selected hallmark GSEA enrichment plots of pathways positively or negatively enriched in either MYC knockdown or in MB_{GRP3} gene sets. The enrichment scores are the peaks occurring at the top or bottom of the plot, these peaks display the extent of which a gene is represented within the ranked list. The leading edge subset is represented by the vertical lines as these indicate the genes that contribute most to

the enrichment scores. The ranking matrix is at the bottom of the enrichment plot. As you move down the rank list, the ranking matric values move from positive to negative.

5.6.2 MYC knockdown downregulates MTORC1 signalling pathway

GSEA results show that silencing of MYC caused a downregulation in MTORC1 signalling which is upregulated in MB_{GRP3} primary tumour data (Figure 5.12). The mammalian target of rapamycin complex 1 (MTORC1) is involved in multiple processes such as lipid synthesis, mitochondrial metabolism, biogenesis and autophagy which promotes cell growth and survival (Laplante and Sabatini, 2009). For example MTORC1 mediates protein synthesis by phosphorylating Eif-4E-binding protein 1 (4E-BP1) and S6 Kinase 1 (s6k1). Protein synthesis is needed for cell growth to occur (Laplante and Sabatini, 2009). In the MTORC1 signalling pathway genes such as *PGK1*, *HMGCR* and *CCNF* are negatively enriched following MYC knockdown and positively enriched in MB_{GRP3} primary tumour data. The phosphoglycerate kinase 1 (PGK1) controls energy production through its involvement in the serine synthesis and cellular redox pathway (Wang *et al.*, 2015). The rate limiting enzyme known as 3-Hydroxy-3-Methyglutaryl-CoA Reductase is involved in the synthesis of cholesterol (Sharpe and Brown, 2013). Cyclin F (CCNF) is involved during the G2 phase of the cell cycle by having a role in mitosis and the integrity of the genome (Noh *et al.*, 2015). MTORC1 is also needed for the translation of MYC (Babcock *et al.*, 2013).

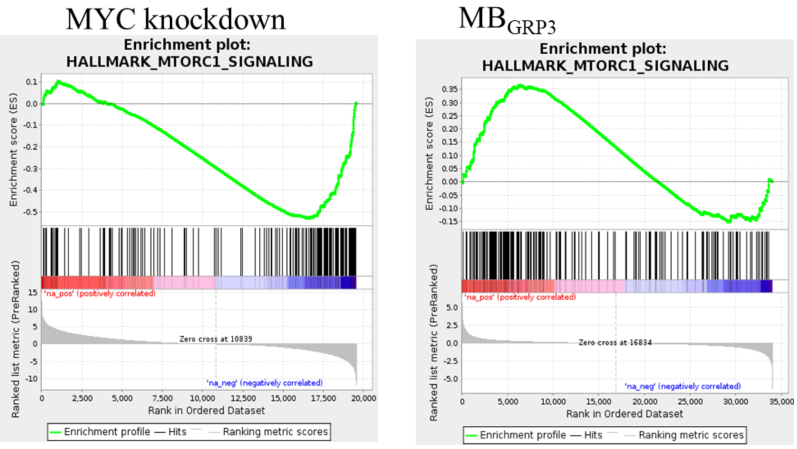

Figure 5.12 Enrichment plots of MTORC1 signalling pathway which is negatively enriched in MYC knockdown and positively enriched in MB_{GRP3} primary tumours. The enrichment scores are the peaks occurring at the top or bottom of the plot, these peaks display the extent of which a gene is represented within the ranked list. The leading edge subset is represented by the vertical lines as these indicates the genes that contributes most to the enrichment scores. The ranking matrix is at the bottom of the

enrichment plot. As you move down the rank list, the ranking matric values move from positive to negative.

5.6.3 MYC knockdown upregulates hypoxia and epithelial mesenchymal transition

GSEA analysis shows that knockdown of MYC caused an upregulation in genes with a role in the epithelial to mesenchymal transition and hypoxia, these gene sets are downregulated in MB_{GRP3} primary tumour data (Figure 5.13). Hypoxia is defined as an inadequate supply of oxygen to the cells (Muz *et al.*, 2015; Eales *et al.*, 2016), if the low levels of oxygen continue for a long period it can cause apoptosis (Muz *et al.*, 2015). Cancer cells can however adapt to grow and survive in a hypoxic environment (Ruan *et al.*, 2009), by changing to anaerobic metabolism and by adapting blood vessel formation (Muz *et al.*, 2015). Hypoxia can also induce epithelial mesenchymal transition which promotes cancer cells metastasis (Muz *et al.*, 2015). Research has shown that overexpression of MYC can change cells from an epithelial to a mesenchymal phenotype (Cowling and Cole, 2007). It is therefore possible that an upregulation in EMT is due to hypoxia. The hypoxia inducible factor 1 (HIF-1 alpha and beta) transcription factors is the key regulator of the adaptive hypoxic responses (Zhang *et al.*, 2013). Studies have reported that HIF antagonises MYC activity under physiological conditions, but when MYC is deregulated then the two transcription factors have a synergistic relationship (Podar and Anderson, 2010). Genes that contribute to the leading edge subset in the hypoxia data set are *TGFB1* and *SLC2A3* (*SLC2A3* is involved in glucose metabolism (Masin *et al.*, 2014). In the EMT gene set *TIMP* (Tissue inhibitor of metalloproteinases) (Brew and Nagase, 2010) and *PDGFRB* (Platelet Derived Growth Factor Receptor Beta) (Steller *et al.*, 2013). These genes are positively enriched following MYC knockdown and negatively enriched in primary MB_{GRP3} data.

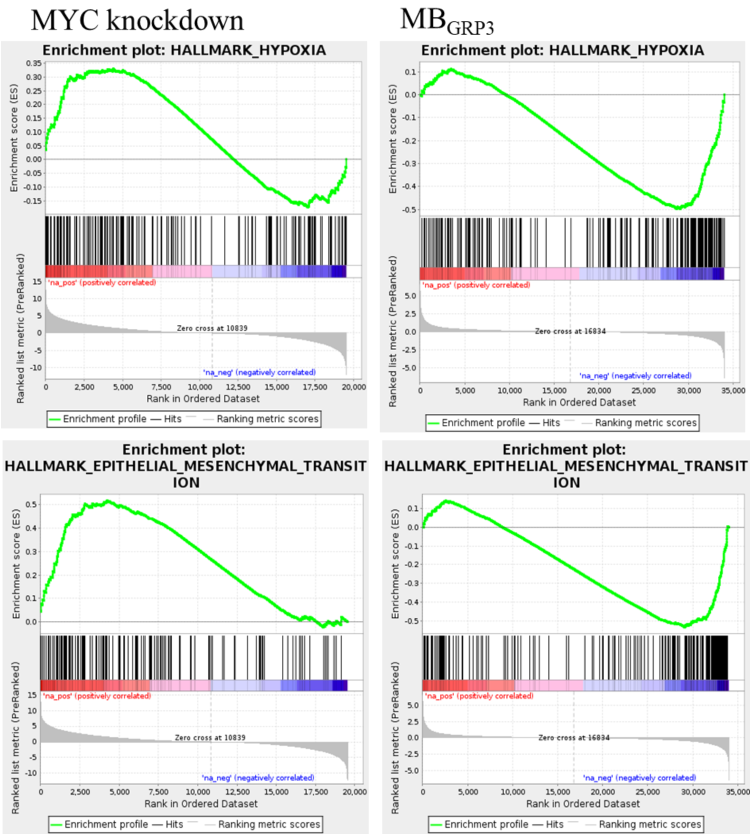

Figure 5.13 Enrichment plots of hypoxia and epithelial mesenchymal transition phenomenon, which is positively enriched following MYC knockdown and negatively enriched in MB_{GRP3} primary tumours. The enrichment scores are the peaks occurring at the top or bottom of the plot, these peaks display the extent of which a gene is represented within the ranked list. The leading edge subset is represented by the vertical lines as these indicates the genes that contributes most to the enrichment scores. The ranking matrix is at the bottom of the enrichment plot. As you move down the rank list, the ranking matric values move from positive to negative.

5.6.4 MYC knockdown upregulates IL6-JAK-STAT 3 signalling pathway

GSEA showed that silencing of MYC caused an upregulation of genes involved in IL-JAK-STAT 3 signalling pathway, whereas this signalling pathway is downregulated in primary MB_{GRP3} (Figure 5.14). The interleukin 6-Janus kinase/signal transducer and activator of transcription 3 (IL-JAK-STAT 3) is a cytokine signalling pathway that promotes tumourgenesis . JAK needs to be activated by IL6 in order to activate STAT3, activated STAT3 undergoes phosphorylation and is able to bind to other STAT3 members, which form a STAT 3 complex. The STAT3 complex moves from the cytoplasm to the nucleus to stimulates transcription of its target genes such as MYC (Wang and Sun, 2014). The upregulation of this pathway upon MYC knockdown indicates a potential feedback loop and could suggest a combined therapeutic option targeting MYC and the IL6-JAK-STAT 3 pathway.

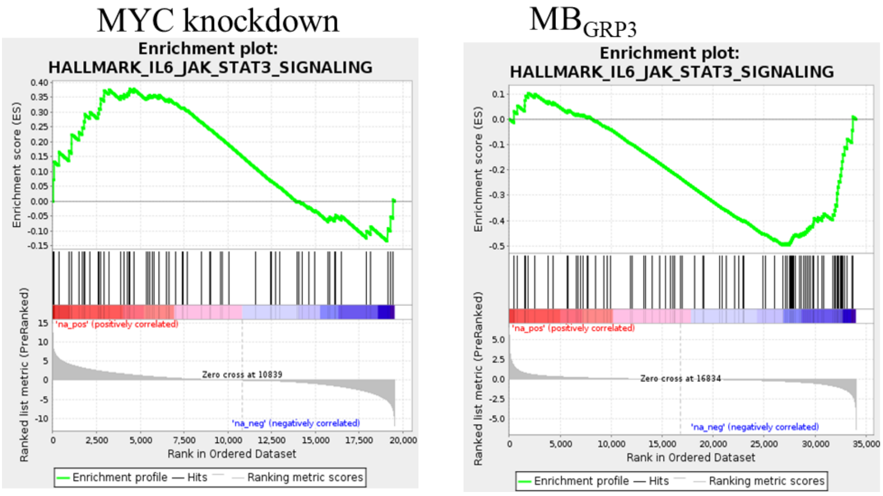

Figure 5.14 Enrichment plots of IL6-JAK-STAT 3 signalling which is positively enriched in MYC knockdown data and negatively enriched in MB_{GRP3} data. The enrichment scores are the peaks occurring at the top or bottom of the plot, these peaks display the extent of which a gene is represented within the ranked list. The leading edge subset is represented by the vertical lines as these indicates the genes that contributes most to the enrichment scores. The ranking matrix is at the bottom of the enrichment plot. As you move down the rank list, the ranking matric values move from positive to negative.

5.7 Ingenuity pathway analysis (IPA)

IPA (www.qiagenbioinformatics.com/products/ingenuity-pathway-analysis) is a web-based computational software that analyses high throughput sequencing data to identify canonical pathways relevant to the gene set. IPA uses the Ingenuity Knowledge Base which is a manually curated data repository that contains comprehensive biological and chemical information. This information is extracted from a variety of trusted sources such as textbooks and published biomedical literature and databases. IPA analysis (performed by Dr Janet Lindsey and Samuel Steele) of the MB_{GRP3} gene set revealed several important canonical pathways, the top 5 are listed in Table 29. The top two canonical pathways identified were the phototransduction pathway and axonal guidance signalling. IPA analysis of DOX inducible MYC knockdown models also revealed the same top two canonical pathways as important (Table 30). The Phototransduction pathway was also one of the major pathways identified through KEGG (Kyoto Encyclopedia of Genes and Genome) analysis (Figure 5.15). The following phototransduction pathway genes:

CNGA1;PDE6H; PDE6A;GNB3;CNGB1;GNAT1;PDC;SAG;GNGT2 are upregulated in MB$_{GRP3}$ primary tumour data and downregulated following MYC knockdown and *GNB3;GNAT1* are also involved in the axonal guidance signalling pathway.

The cell of origin of MB$_{GRP3}$ is controversial but recent research by Hooper *et al* compared the expression profiles of normal fetal germinal matrix, normal fetal brain and neural stem cells (classified as the neuro-development continuum) to two primary MB cohorts and concluded that MB$_{GRP3}$ were derived from rod precursor type cells (Hooper *et al.*, 2014). This could explain why many phototransduction related genes show enriched expression in MB$_{GRP3}$ (Northcott *et al.*, 2012a) (Sengupta *et al.*, 2017) MYC causes dedifferentiation and reprogramming towards a more stem cell like state (Ramesh *et al.*, 2009), which could repress lineage specific genes. MYC knockdown could lead to re expression of these genes for example GRK1 the gene for rhodopsin kinase (Figure 5.16) and NRL (discussed in 5.5). This IPA analysis could support the evidence that MB$_{GRP3}$ cells of origin are related to rod precursor cells. Also in *MYC* amplified MB$_{GRP3}$ a few photoreceptor genes that are down regulated are upregulated when MYC is knocked down. One of the top upstream regulators identified by IPA analysis is *CRX* (Table 31) which is a transcriptional regulator which plays a role in differentiation of photoreceptor cells. IPA analysis showed that genes regulated by CRX are upregulated when MYC is knocked down. It is possible that dedifferentiation is caused by MYC leading to the inhibition of the expression of lineage specific genes, which are re-expressed following MYC knock down. Research by Garancher *et al* showed that MB$_{GRP3}$ a cerebellum tumour is transcriptionally characterised by photoreceptor differentiation program and identified *NRL* and *CRX* as two main transcriptional factors responsible for initiating and maintaining MB$_{GRP3}$ phenotype (Garancher *et al.*, 2018). This study shows that cancer cells can express differentiation programs that is not related to their tissue of origin (Garancher *et al.*, 2018). The second common pathway is the axon guidance signalling; during neural development is it essential that axons reach the correct target. This process is mediated through various axon guidance molecules that can either direct the axon towards the correct target or steer it away from in wrong target. The classes of axon guidance molecules are known as netrins, slits, semaphorins and ephrins (Yaron and Zheng, 2007). Studies showed that members of netrins and semaphorins can stimulate the expression of *myc (*Flannery *et al., 2010).*

INGENUITY CANONICAL PATHWAYS	**-LOG P VALUE**	**RATIO**	**GENES**
PHOTOTRANSDUCTION PATHWAY	1.18E+01	3.77E-01	*RGS9,PDE6G,GUCA1A,GUCY2D,GNGT1,GUCA1C,GRK1,CNGA1,PDE6H,PDE6A,GNB3,CNGB1,GNAT1,RHO,PDC,RGS9BP,SAG,CNGB3,GNGT2,RCVRN*
AXONAL GUIDANCE SIGNALING	6.69E+00	1.16E-01	*PAPPA2,BMP4,GLI2,ECEL1,NTN1,GNB3,GNAT1,WNT7B,ABLIM3,MYL4,FES,FGFR1,FGFR2,MMP2,HHIP,GNG3,MYL7,DOCK1,EPHA6,ADAM12,GAB1,FZD5,EPHA2,FZD10,ADAMTS7,PDGFA,SEMA6A,NOTUM,FZD1,ABLIM1,PDGFC,EPHA8,IGF1,GLI3,NGFR,ADAM19,SMO,DCC,ROBO2,EPHB4,PLXNC1,CXCR4,NFATC4,EFNA4,MYL1,SEMA3A,WNT10A,NTRK3,SEMA3C,WNT11,NTN3,WNT5A*
WNT/B-CATENIN SIGNALING	6.39E+00	1.60E-01	*FZD10,SOX1,TGFBR3,TLE1,FZD1,SOX2,MYC,WIF1,NLK,TGFB1,WNT7B,SMO,TGFB2,DKK2,PPP2R2C,DKKL1,CDH12,WNT10A,APC2,PPP2R2B,DKK4,FZD5,LEF1,SOX9,SFRP1,WNT11,WNT5A*
HEPATIC FIBROSIS / HEPATIC STELLATE CELL ACTIVATION	5.70E+00	1.48E-01	*COL8A2,PDGFA,FGF2,PDGFC,IGF1,TGFB1,NGFR,PDGFRA,TGFB2,MYL4,COL27A1,EGFR,TNFRSF11B,COL19A1,IL1RAPL2,COL6A2,FGFR1,COL2A1,FGFR2,MYH7,MMP2,MYL1,MYL7,COL13A1,COL6A3,TGFA,COL25A1*
HUMAN EMBRYONIC STEM CELL PLURIPOTENCY	5.60E+00	1.61E-01	*FZD10,BMP4,PDGFA,FGF2,FGFR1,FGFR2,FZD1,LEFTY2,PDGFC,SOX2,WNT10A,GAB1,NTRK3,TGFB1,WNT7B,PDGFRA,SMO,TGFB2,FZD5,LEF1,FGFRL1,WNT11,WNT5A*

Table 29:Top 5 ingenuity canonical pathways in primary MB_{GRP3}

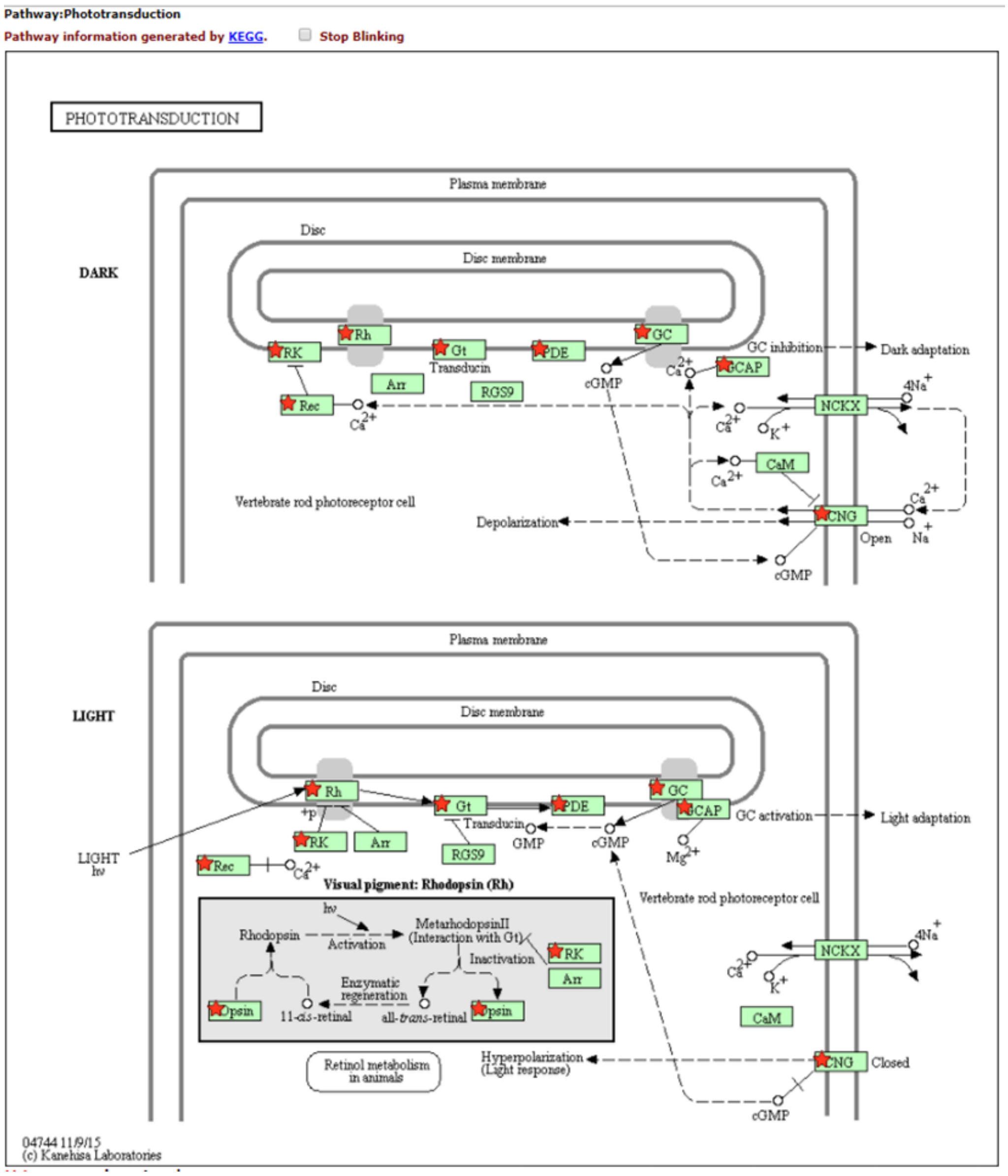

Pathway:Phototransduction

Pathway information generated by KEGG. ☐ **Stop Blinking**

PHOTOTRANSDUCTION
DARK
Plasma membrane
Disc
Disc membrane
Rh
GC
RK
Gt
Transducin
PDE
cGMP
Ca^{2+}
GCAP
GC inhibition
Dark adaptation
Arr
RGS9
Rec
Ca^{2+}
$4Na^{+}$
NCKX
Ca^{2+}
K^{+}
CaM
Ca^{2+}
Vertebrate rod photoreceptor cell
Depolarization
CNG
Open
Ca^{2+}
Na^{+}
cGMP
LIGHT
Plasma membrane
Disc
Disc membrane
Rh
+p
RK
Arr
Gt
Transducin
PDE
GMP
cGMP
GC
GCAP
Mg^{2+}
GC activation
Light adaptation
RGS9
LIGHT
hν
Rec
Ca^{2+}
Visual pigment: Rhodopsin (Rh)
hν
Rhodopsin
Activation
MetarhodopsinII
(Interaction with Gt)
Inactivation
RK
Arr
Enzymatic regeneration
Opsin
11-cis-retinal
all-trans-retinal
Opsin
Vertebrate rod photoreceptor cell
$4Na^{+}$
NCKX
Ca^{2+}
K^{+}
CaM
Retinol metabolism in animals
Hyperpolarization
(Light response)
CNG
Closed
cGMP
04744 11/9/15
(c) Kanehisa Laboratories

Figure 5.15 KEGG pathway analysis of phototransduction pathway. Genes that are differentially regulated in both MB$_{GRP3}$ primary tumours vs medulloblastomas belonging to other subgroups and MYC knockdown vs control are highlighted in red.

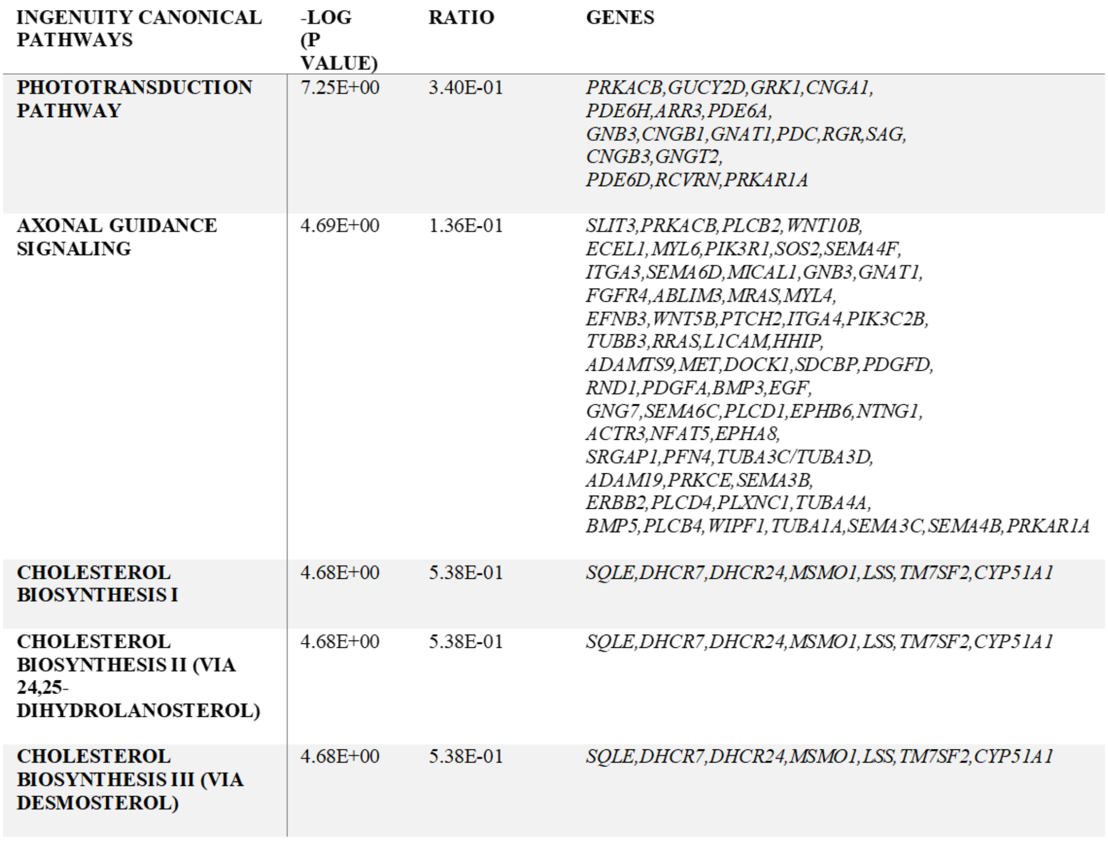

INGENUITY CANONICAL PATHWAYS	-LOG (P VALUE)	RATIO	GENES
PHOTOTRANSDUCTION PATHWAY	7.25E+00	3.40E-01	*PRKACB,GUCY2D,GRK1,CNGA1,PDE6H,ARR3,PDE6A,GNB3,CNGB1,GNAT1,PDC,RGR,SAG,CNGB3,GNGT2,PDE6D,RCVRN,PRKAR1A*
AXONAL GUIDANCE SIGNALING	4.69E+00	1.36E-01	*SLIT3,PRKACB,PLCB2,WNT10B,ECEL1,MYL6,PIK3R1,SOS2,SEMA4F,ITGA3,SEMA6D,MICAL1,GNB3,GNAT1,FGFR4,ABLIM3,MRAS,MYL4,EFNB3,WNT5B,PTCH2,ITGA4,PIK3C2B,TUBB3,RRAS,L1CAM,HHIP,ADAMTS9,MET,DOCK1,SDCBP,PDGFD,RND1,PDGFA,BMP3,EGF,GNG7,SEMA6C,PLCD1,EPHB6,NTNG1,ACTR3,NFAT5,EPHA8,SRGAP1,PFN4,TUBA3C/TUBA3D,ADAM19,PRKCE,SEMA3B,ERBB2,PLCD4,PLXNC1,TUBA4A,BMP5,PLCB4,WIPF1,TUBA1A,SEMA3C,SEMA4B,PRKAR1A*
CHOLESTEROL BIOSYNTHESIS I	4.68E+00	5.38E-01	*SQLE,DHCR7,DHCR24,MSMO1,LSS,TM7SF2,CYP51A1*
CHOLESTEROL BIOSYNTHESIS II (VIA 24,25-DIHYDROLANOSTEROL)	4.68E+00	5.38E-01	*SQLE,DHCR7,DHCR24,MSMO1,LSS,TM7SF2,CYP51A1*
CHOLESTEROL BIOSYNTHESIS III (VIA DESMOSTEROL)	4.68E+00	5.38E-01	*SQLE,DHCR7,DHCR24,MSMO1,LSS,TM7SF2,CYP51A1*

Table 30: Top 5 Ingenuity canonical pathways for DOX inducible MYC knockdown models

UPSTREAM REGULATOR	MOLECULE TYPE	ACTIVATION Z-SCORE	P-VALUE OF OVERLAP
CRX	transcription regulator	1.842	1.25E-08
CREB1	transcription regulator	0.688	3.86E-08
L-DOPA	chemical - endogenous mammalian	-1.027	5.56E-08
F2	peptidase	3.392	2.89E-07
NRL	transcription regulator	-0.549	1.08E-06
PROGESTERONE	chemical - endogenous mammalian	-0.891	1.29E-06
MYC	transcription regulator	-4.469	2.37E-06
2-AMINO-5-PHOSPHONOVALERIC ACID	chemical - other	-0.846	8.44E-06
TGFB1	growth factor	6.042	9.99E-06
EPAS1	transcription regulator	0.999	1.39E-05

Table 31:Selected upstream regulators for DOX inducible MYC knockdown models

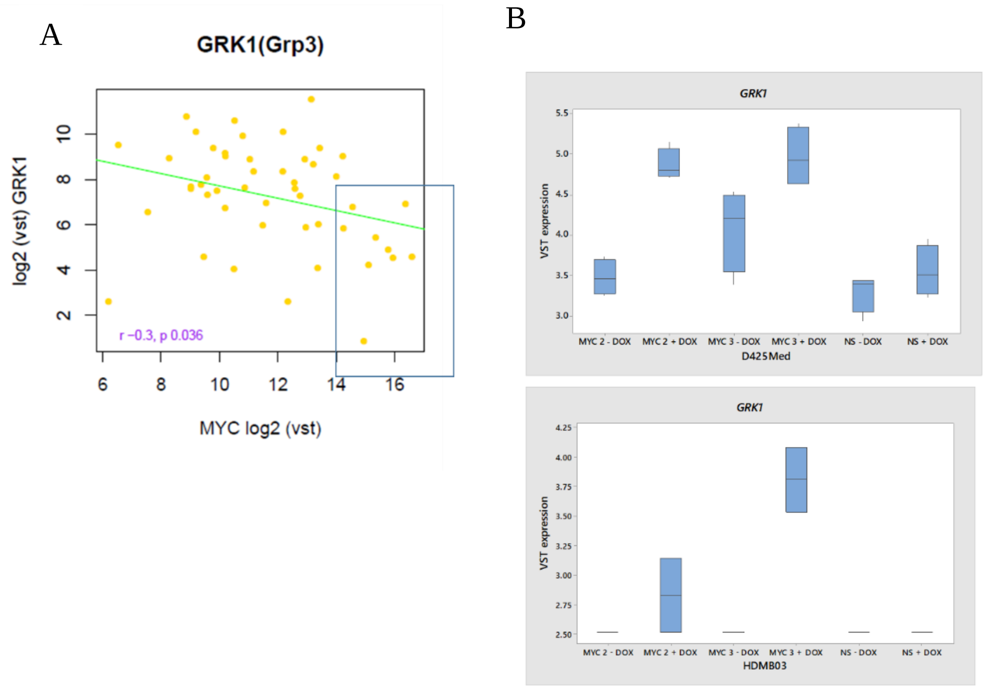

Figure 5.16 GRK1 expression in MB$_{GRP3}$ and in isogenic MB cell lines. A) Graph of GRK1 expression in MB$_{GRP3}$ showing a negative correlation with MYC expression. The MYC amplified primary tumour samples (n=9) are within the rectangle. B) Relative expression GRK1 in D425Med and HDMB03 isogenic cell lines. MYC silencing causes upregulation of GRK1. The x-axis represents the sample names and the y-axis represents the variant stabilised transformed (VST) expression. Box plots shows median and quartile ranges.

5.8 Discussion

RNASeq data showed extensive and consistent gene expression changes when MYC was knocked down in D425Med MYC 2, D425Med MYC 3, HDMB03 MYC 2 and HDMB03 MYC 3. Changes included genes involved in metabolism and ribosomal biogenesis, which are consistent with changes seen in other cancers following MYC regulation (Dai and Lu, 2008; van Riggelen *et al.*, 2010; Miller *et al.*, 2012).

GSEA and IPA analysis highlighted specific pathways and genes regulated by MYC and dysregulated in primary MB$_{GRP3}$ highlighting that many of the expression differences in MB$_{GRP3}$ relative to other medulloblastomas are as a consequence of MYC amplification and/ or over-expression within this subgroup. These pathways included those involved in cell cycle control, metabolism, and differentiation and signalling pathways which could be therapeutically targeted.

The RNAseq results and subsequent analysis indicate specific transcriptional changes effected by MYC (G2/M checkpoint and E2F targets) consistent with the phenotypic observations of cell cycle disruption made in Chapter 4.

This Chapter highlighted that MYC knockdown caused adaptive responses to be triggered. These adaptive responses triggered by the cells were upregulation of tumour hypoxia and IL6-JAK-STAT 3 signalling pathway. Tumour hypoxia is associated with poor prognostic variables such as chemoresistance, radioresistance, angiogenesis, vasculogenesis, invasiveness and metastasis (Wilson and Hay, 2011). However, in primary MB tumour hypoxia might not be upregulated in response to MYC knockdown. For example, von Bueren *et al* showed that MYC sensitizes MB cell lines to chemotherapy and radiation therapy but this sensitivity was not observed in primary MB patients (von Bueren *et al.*, 2011), therefore further studies are needed to determine if tumour hypoxia is upregulated in primary MB patients in response to MYC knockdown. The upregulation of IL6-JAK-STAT 3 signalling pathway could be due to a possible feedback loop that is triggered in response to MYC knockdown as JAK-STAT 3 signalling can result in upregulation of MYC (Chen *et al.*, 2003). These results aren't a negative result but shows that targeting MYC is complex. These results indicate that a therapeutic option directed towards MYC would be needed as well as a therapeutic option would be needed to overcome the adaptive responses triggered following MYC knockdown.

This Chapter highlighted possible signalling pathways that could be targeted therapeutically. However, further validation is needed but possible inhibitors or strategies will be further discussed in Chapter 6.

Chapter 6 Conclusion

MB is the most common malignant brain tumour of childhood (Northcott *et al.*, 2012a) and accounts for 10% of cancer related deaths in children (Pizer and Clifford, 2009). MB has been classified into four distinct subgroups each with their own demographics, DNA copy number aberrations, histopathology and clinical outcome (Northcott *et al.*, 2011; Taylor *et al.*, 2012) and different cell of origin (Hooper *et al.*, 2014). These subgroups are known as MB$_{WNT}$, MB$_{SHH}$, MB$_{GRP3}$, MB$_{GRP4}$ (Taylor *et al.*, 2012). Patients with MB$_{GRP3}$ have the worst outcome with an OS of ~ 50% (Schroeder and Gururangan, 2014). MB$_{GRP3}$ patients are enriched at presentation for metastatic disease, LCA histology and high *MYC* expression and amplification (Pei *et al.*, 2012). MYC amplification is the most frequent focal genetic defect (approximately 15% of MB$_{GRP3}$) in these tumours and is associated with an extremely poor prognosis (<20% 5year overall survival) using conventional therapeutics; therefore, new therapeutic approaches are urgently needed to improve the survival of these patients (Henssen *et al.*, 2013; Li *et al.*, 2013; Schroeder and Gururangan, 2014; Venkataraman *et al.*, 2014).

MYC is difficult to target directly, due to its nuclear location which precludes targeting by an antibody based therapy and its lack of enzymatic function or small molecule interactions (Koh *et al.*, 2016). Several alternative potential therapeutic strategies have been suggested to indirectly target MYC including inhibiting MYC transcription, destabilising the protein or inhibiting the function of downstream targets (Figure 6.1), (discussed in Chapter 1.6). These strategies have shown promise in other cancer types; for example in multiple myeloma models the use of JQ1, which is a bromodomain inhibitor, caused anti-proliferative effects and suppression of MYC transcription (Delmore *et al.*, 2011). The downregulation of MYC following BET inhibitor treatment was also seen in other experimental models of blood cancers (Sun and Gao, 2017), burkitt lymphoma (Mertz *et al.*, 2011; Dawson and Kouzarides, 2012), glioblastoma (Cheng *et al.*, 2013; Wadhwa and Nicolaides, 2016) and MB (Henssen *et al.*, 2013; Bandopadhayay *et al.*, 2014; Venkataraman *et al.*, 2014; Wadhwa and Nicolaides, 2016). Inhibition of Aurora kinases to target MYC has been successful in lymphoma experimental models (den Hollander *et al.*, 2010; Yang *et al.*, 2010; Diaz *et al.*, 2015), liver cancer (Dauch *et al.*, 2016), small cell lung cancer (Mollaoglu *et al.*, 2017) and MB (Diaz *et al.*, 2015). Other indirect strategies that have been successful in MYC driven cancers include cell cycle inhibitors which have shown success in lymphoma experimental models (Höglund *et al.*, 2011; Ferrao *et al.*, 2012) and pancreatic tumours (Murga *et al.*, 2011a; Horiuchi *et al.*, 2014b). Lastly, the use of the metabolic inhibitors such has the glutaminase inhibitor, BPTES, caused antiproliferative effects in MYC driven B- cell lymphoma cell line (Xiang *et al.*, 2015a; Cramer and Schmitt, 2016) and renal cell carcinoma experimental models (Shroff *et al.*, 2015). There is progress being made in this area of research of possible therapeutic options for treatment of MYC driven cancers.

MYC is known to be involved in many biological processes such as cell cycle regulation, proliferation and apoptosis (Frenzel *et al.*, 2010) (discussed in Chapters 1 and 4) and MYC's control over growth differs between various cellular contexts (Schlosser *et al.*, 2003). Therefore, modelling MYC in the appropriate context is important. Previous research on MYC in the context of MB has been reported (Stearns *et al.*, 2006; von Bueren *et al.*, 2009; Pei *et al.*, 2012; Roussel and Robinson, 2013). These studies have given insight into MYC biology within MB, however limited work has been conducted in $\mathrm{MB}_{\mathrm{GRP3}}$. This study was conducted to provide understanding of MYC biology within $\mathrm{MB}_{\mathrm{GRP3}}$, through generation of $\mathrm{MB}_{\mathrm{GRP3}}$ isogenic cell lines in which MYC expression could be modulated to facilitate an investigation of the direct role played by MYC, its associated biology, and the investigation of disease relevant therapeutic approaches.

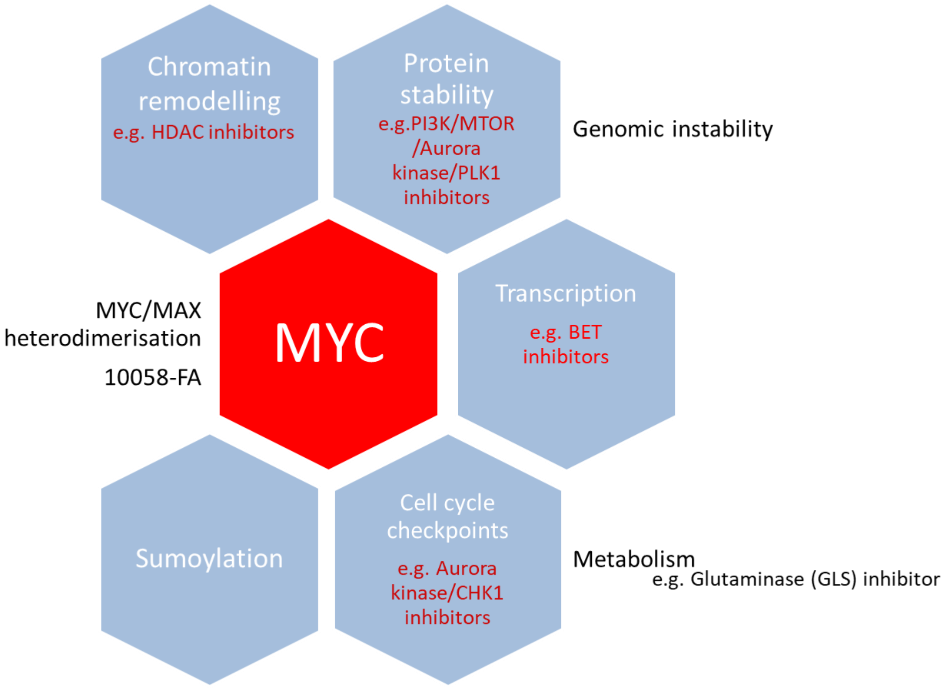
Chromatin remodelling
e.g. HDAC inhibitors
Protein stability
e.g.PI3K/MTOR /Aurora kinase/PLK1 inhibitors
Genomic instability
MYC/MAX heterodimerisation
10058-FA
MYC
Transcription
e.g. BET inhibitors
Sumoylation
Cell cycle checkpoints
e.g. Aurora kinase/CHK1 inhibitors
Metabolism
e.g. Glutaminase (GLS) inhibitor

Figure 6.1 Schematic diagram showing potential therapeutic strategies directed at targeting MYC or its associated downstream effects.

Isogenic $\mathrm{MB}_{\mathrm{GRP3}}$ cell lines (D425Med and HDMB03) were successfully generated and showed robust and reproducible MYC knockdown. Importantly, although cell lines are derived from aggressive tumours, they do harbour additional defects such as TP53 mutation (in the D425Med line) which may have been acquired in culture. However, this study has shown that knockdown of MYC has an impact on proliferation. Therefore, these cells remain ‘addicted’ to MYC expression, which highlights the promise of therapies targeting MYC, and the utility of these cell line models to investigate them.

Ontology analysis (discussed in Chapter 5) highlighted many possible strategies to indirectly target MYC, for example one of the strategies could be to target the cell cycle by using CDK inhibitors which could possibly cause an anti-proliferative effect or cell death (Dickson and Schwartz, 2009). There are many CDK inhibitors that have entered clinical trials for example CDK 4/6 inhibitors such as palbociclib (PD-0332991), ribociclib (LEE011) and abemaciclib (LY2835219) (Asghar *et al.*, 2015; Finn *et al.*, 2016). The palbociclib inhibitor has shown the most promising success (Tarrado-Castellarnau *et al.*, 2017) and has been approved to treat patients with estrogen receptor positive and HER negative breast cancer (Schröder and McDonald, 2015). Palbociclib has also been shown to cause a G_1 cell cycle arrest in Rb-positive carcinoma cells and caused tumour regression in colon cancer (Fry *et al.*, 2004; Asghar *et al.*, 2015), and *in vitro* experimental models of glioblastoma showed sensitivity to palbociclib (Schröder and McDonald, 2015). In addition, a study performed by Hanaford *et al* in a MB_{GRP3} experimental model showed that treatment with palbociclib caused an anti-proliferative effect, increased cell death and prolonged the survival of xenograph models (Hanaford *et al.*, 2016). Even though it has shown effectiveness, acquired resistance to CDK 4/6 inhibition has become evident and the underlying mechanism is due to *RB1* loss or *CCNE1* amplification (Herrera-Abreu *et al.*, 2016; Tarrado-Castellarnau *et al.*, 2017). However, work by Herrera-Abreu *et al* showed that resistance can be overcome by combinational (CDK 4/ 6 and PI3K inhibition) or triple combinational therapy (endocrine therapy, CDK 4/ 6 and PI3K inhibition) (Herrera-Abreu *et al.*, 2016). In addition, work by Castellarnau *et al* showed that depletion of CDK 4/6 caused upregulation of MYC along with MYC downstream targets which includes glutaminolysis, mTOR signalling pathway and downregulation of HIF-α. This study shows that combinational therapy (CDK 4/6 and glutaminase 1 inhibition) caused an anti-proliferative effect and could be a way to overcome acquired resistance (Tarrado-Castellarnau *et al.*, 2017). These finding suggest that inhibition of CDK 4/6 along with targeting downstream targets of MYC could be an effective therapeutic option for MYC-driven cancers (Tarrado-Castellarnau *et al.*, 2017).

A therapeutic approach that would cause a growth inhibitory effect and reduce MYC expression would probably be more effective in MB_{GRP3}.The transcriptional analysis in this study highlighted MYC-dependent downstream changes in the expression of genes involved in the cell cycle (targeting the cell cycle was mentioned above), metabolism, ribosomal biogenesis, MTORC1 signalling pathway (downregulated), hypoxia (upregulated), epithelial mesenchymal transition (upregulated) and IL6-JAK-STAT3 (upregulated) signalling pathways.

Targeting genes involved in metabolism could possibly reverse tumourgenesis, such as inhibiting GLDC, which is involved in glycine metabolism (Zhang *et al.*, 2012). Research has shown that knockdown of GLDC in lung cancer cells resulted in a reduction in tumourgenic properties (Dominy *et al.*, 2012; Zhang *et al.*, 2012) or antimetabolic compounds could be used to target the serine/glycine metabolic pathway (Amelio *et al.*, 2014). Another strategy to explore is ribosomal biogenesis as this pathway is a consistent change observed in cancer where MYC is upregulated (van Riggelen *et al.*, 2010). Research has shown that cancer cells with wild type P53 and with a higher level of ribosomal biogenesis were responsive to ribosomal inhibitors such as actinomycin D, doxorubicin, 5-fluorouracil and CX-5461 (Brighenti *et al.*, 2015; Scala *et al.*, 2016). These inhibitors could potentially have similar effects in $MB_{GRP3,}$ as MB_{GRP3} has a high rate of ribosomal biogenesis (Roussel and Robinson, 2013; Staal *et al.*, 2015).

Another therapeutic pathway to target could be mTOR, targeting mTOR will not only reduce ATP production but also affect the ability of cancer cells to absorb nutrients (Sabnis *et al.*, 2017) and interfere with the translation of MYC protein (Wiegering *et al.*, 2015). There are already mTOR inhibitors that are in clinical trials that prove to be effective in treating certain cancers (Zarogoulidis *et al.*, 2014). There are the first generation of mTORC1 Inhibitors known as rapamycin (Xie *et al.*, 2016) and its rapamycin analogues known as CC1-799, RAD001 and AP23573 (Liu *et al.*, 2009; Zaytseva *et al.*, 2012; Sabnis *et al.*, 2017). The rapalogs has better solubility within mammals. The mechanism of rapamycin is to destabilize the interaction of mTOR and raptor thereby having an inhibitory effect on the mTORC1 (Sabnis *et al.*, 2017). The first generation of mTOR inhibitors only partially blocks mTORC1; it cannot inhibit the phosphorylation of 4E-BP1 at the Thr-37 and Thr-46 sites (Xie *et al.*, 2016; Faes *et al.*, 2017). These inhibitors have however shown promising results, for example ridaforolimus (AP23573) has demonstrated to have anticancer effects either alone or in combination with other drugs in sarcoma and endometrial experimental models (Squillace *et al.*, 2011). In addition, a phase 2 trial showed that ridaforolimus was well tolerated in patients with advanced bone and soft tissue sarcomas (Chawla *et al.*, 2012). The CC1-779 (temsirolimus) inhibitor has demonstrated to have anticancer effects either alone or in combination with chemotherapeutic agents in a non-MB_{GRP3} experimental model (Geoerger *et al.*, 2012). Out of these first generation inhibitors CC1-779 (temsirolimus) in 2007 was approved to treat patients with advanced renal carcinoma, followed by RAD001 to treat neuroendocrine tumours and HER2-positive breast cancer. There has also been the generation of dual PI3K/mTOR inhibitor which targets both PI3K and mTOR pathway these derivatives developed are NVP-BEZ235, GSK2126458 and XL765 (Xie *et al.*, 2016). The NVP-BEZ235 inhibitor shows the most potential out of the three inhibitors because it is effective *in vivo* (Xie et al., 2016) for example NVP-BEZ235 inhibitor has shown to cause anti-tumourgenic effects in MYCN-driven neuroblastoma experimental models (Vaughan *et al.*, 2010) . In addition, this NVP-BEZ235 has a good synergistic effect with mitogenic pathway inhibitors (Engelman *et al.*, 2008; Aziz *et al.*, 2010; Xie *et al.*, 2016). There are also the second generation of mTOR inhibitors, whose mechanism is to prevent the catalytic function of mTOR; therefore, these inhibitors can have an inhibitory effect on both mTOR complexes (Xie *et al.*, 2016; Faes *et al.*, 2017). These inhibitors are known as AZD8055, INK128 (MLN0128) and OS1027 (Xie *et al.*, 2016). The MLN0128 inhibitor, which prevents the phosphorylation of the rapamycin resistant sites in 4E-BP1 (Pourdehnad *et al.*, 2013; Xie *et al.*, 2016), was shown to cause an antitumorgenic effects in MYC driven haematological experimental models (Pourdehnad *et al.*, 2013) and showed promising results in bone and soft tissue sarcoma cancer models (Slotkin *et al.*, 2015). Lastly, rapalink, a third generation inhibitor which contains rapamycin and mTOR kinase inhibitory activity in the same molecule was developed to overcome mTOR resistance mutations that are associated with the first and second generation of mTOR inhibitors (Rodrik-Outmezguine *et al.*, 2016; Xie *et al.*, 2016; Faes *et al.*, 2017).

This study also highlighted upregulation of tumour hypoxia following MYC knockdown. Tumour hypoxia is associated with many adaptive responses such as chemoresistance, radioresistance, angiogenesis, vasculogenesis, invasiveness, metastatsis, changes in metabolism, genetic instability and apoptotic resistance (Wilson and Hay, 2011), that favour the survival of cancer cells (Semenza, 2003). Therefore, targeting MYC alongside targeting the adaptive response signalling pathway such as the HIF pathway could be a possible therapeutic option. There are many inhibitors available and a few of them have entered clinical trials; these inhibitors can either directly or indirectly interfere with HIF (Yu *et al.*, 2017). Inhibitors that have entered clinical trials and interfere with HIF-1 activity are topotecan. which affects mRNA synthesis, CAY10585, which interferes with transcriptional activity and protein synthesis, echinomycin which interferes with DNA binding and FM19G11 which interferes with transcriptional activity (Yu *et al.*, 2017). As hypoxia can stimulate the epithelial mesenchymal transition (Zhang *et al.*, 2013; Muz *et al.*, 2015), targeting hypoxia might be hypothesised to inhibit the mesenchymal phenotype. However, another combinational therapeutic option could be to target MYC alongside targeting the epithelial mesenchymal transition. There are compounds such as rapamycin, 17AAG and LY294002 that can inhibit epithelial mesenchymal transition (Reka *et al.*, 2011). The use of mTOR inhibitors could be an effective drug as it targets both the MTOR and can block the mesenchymal phenotype.

Downregulation of MYC caused an upregulation of IL6-JAK-STAT3 pathway. Work from Hatz *et al* showed that MYCN overexpression downregulates IL6 (Hatzi *et al.*, 2002). Therefore, it is possible that knockdown of MYC may upregulate IL6. The IL6 cytokine is required to activate the IL6-JAK-STAT3 pathway (Banerjee and Resat, 2016). In addition, knockdown of MYC could have initiated a stress response where IL6 compensates for MYC downregulation; work from Brady *et al* showed that IL6 can replace viral MYC and could induce pluripotency along with the other three reprogramming factors (Oct 4, Sox 2 and Klf 4) (Brady *et al.*, 2013). Lastly, another possible combinational therapeutic option directed towards MYC and IL6-JAK-STAT3 could be effective in MB_{GRP3}, by targeting MYC via the approaches discussed above and by using JAK inhibitors such as A2D1480 which was shown to have a growth inhibitory effect in solid tumours (Hedvat *et al.*, 2009). Other inhibitors that could be tested in MB are known as CNT0328 which inhibits IL6, tocilizumab which blocks the IL6 receptor (Bournazou and Bromberg, 2013; Wang and Sun, 2014), and SB1518 and SB1578 which blocks JAK 1/ 2 (Bournazou and Bromberg, 2013). In addition, inhibition of STAT3 phosphorylation was tested in MB by treating non MB_{GRP3} cells UW228-2 and UW228-3 with resveratrol, and UW228- 3 with AG49 inhibitors. Cells treated with resveratrol caused inhibition of STAT3 downstream genes (*Survivin*, *CCND1*, *COX-2*, *MYC*) however an increase in leukemia inhibitory factor and BCL-2 expression was observed. The AG49 inhibitor performed better in UW228-3 cells which caused an anti-proliferative effect and suppressed STAT3 downstream genes (Yu *et al.*, 2008). These approaches and inhibitors could first be tested *in vitro* in $\mathrm{MB}_{\mathrm{GRP3}}$ to determine if they have the same anticancer effects.

Targeting MYC is complicated because many processes and genes are controlled by MYC (Horiuchi *et al.*, 2014a) as well as MYC has no enzymatic activity for inhibitors to bind too (Koh *et al.*, 2016) and MYC is cell context specific (Dang, 2013) which will add further difficulties to successfully drugging MYC. Currently there are no clinically approved inhibitors to target MYC. However, many strategies are being attempted to therapeutically target MYC (Whitfield *et al.*, 2017) a few of them include targeting the cell cycle and mTOR signalling pathway (as discussed above). Targeting the cell cycle by using CDK inhibitors could possibly inhibit proliferation or induce apoptosis (Dickson and Schwartz, 2009). However, one of the challenges associated with CDK inhibitors is their non-specificity inhibitory activity. For example, the most studied CDK inhibitor known as flavopiridol inhibits multiple CDKs (CDK 1, CDK 2, CDK 4, CDK 6, CDK 7 and CDK 9) (Sedlacek *et al.*, 1996; Asghar *et al.*, 2015). This inhibitory effect causes a G1 and G2 cell cycle arrest but also causes a cytotoxic response in certain cellular context (Asghar *et al.*, 2015). This might be due to inhibition of CDK 7 and CDK 9 which downregulates transcription of multiple proteins (Bose *et al.*, 2013; Asghar *et al.*, 2015). Also healthy cells are at risk because CDK inhibitors targets proteins that are important for normal cell proliferation (example CDK 1) and survival (example CDK 9). However, developing CDK inhibitors that have specific inhibitory activity and understanding the exact mechanism responsible for the therapeutic result might be a more effective cancer drug (Asghar *et al.*, 2015). For example, a single inhibitor targeting CDK 9 has shown to cause antitumourgenic effects in MYC driven cancer, showing a synthetic relationship with MYC (Huang *et al.*, 2014; Asghar *et al.*, 2015). However, more studies are needed to determine the effect of inhibition of CDK 9 in different cellular context. As mentioned before targeting the MTOR signalling pathway can inhibit the translation of MYC (Wiegering *et al.*, 2015) and there are many clinically approved inhibitors targeting mTOR complex (Roohi and Hojjat-Farsangi, 2017; Whitfield *et al.*, 2017). However, the effect seen might not only be due to inhibiting MYC (Whitfield *et al.*, 2017). One of the challenges associated with inhibiting the mTORC 1 kinase complex is the possibility of a feedback loop that activates a different proliferative signalling pathway that could hinder the effect of mTORC 1 inhibitors. For example, in response to mTORC inhibitors causes excessive activation of phosphoinositide- dependent kinase 1 which could induce AKT Thr308 phosphorylation which could be enough to promote proliferation (Laplante and Sabatini, 2009). Another factor to consider is tumour hypoxia which adds another level of complexity because hypoxia may or may not inhibit mTORC 1 activity. If it does inhibit mTORC 1 activity it can result in resistance to mTORC 1 inhibitors. This however dependence on the cellular context of the cancer cells (Faes *et al.*, 2017). In conclusion each strategy to inhibit MYC have both positive and negative outcomes therefore a combinational approach would be best.

6.1 Limitations

This study investigated the role of MYC within $\mathrm{MB_{GRP3}}$ through the generation of DOX-inducible MYC silencing isogenic models (D425Med and HDMB03). One of the limitations of this study is that only two cell lines were used, however a third DOX inducible MYC silencing isogenic model was generated. MYC knockdown in the third model caused similar proliferative effects (J. Lindsey personal communication). In addition, cell line models have limitations as they may not accurately reflect primary tumours. The second limitation of this study was Chla259 inability to be successfully transduced with MYC construct to generate an inducible overexpression MYC $\mathrm{MB_{GRP3}}$ cell line. Numerous optimization methods were attempted such as concentrating MYC lentivirus, higher MOIs and conditioning the media. To generate an inducible overexpression MYC $\mathrm{MB_{GRP3}}$ cell line perhaps a constitutive expression vector could be used instead of the inducible system. However, constantly expressing MYC might be detrimental to the cells as MYC has the ability to cause apoptosis as well. If this is the case the cells might not be viable for long timescales experiments, this approach would have to be tested to determine if constitutive expression would be successful. Thirdly this study highlighted possible therapeutic strategies but also highlighted that MYC knockdown triggers adaptive responses, which shows that not only does therapeutic strategies need to be directed towards inhibiting MYC function but also directed towards overcoming the adaptive responses triggered. Lastly while this study’s transcriptional analysis highlighted possible therapeutic strategies, further validation is needed because gene expression levels and bioinformatics predictions might not always relate to protein levels or pathway activation (Runge and Patterson, 2007; Maier *et al.*, 2009; Vogel and Marcotte, 2012).

6.2 Future works

The generation of these DOX-inducible MYC silencing isogenic models provides an essential tool to advance our understanding of MYC in MB. To gain further insight into MYC biology these models could be used for:

6.2.1 Optimization of HDMB03 DOX- inducible MYC silencing isogenic models

As mentioned before, HDMB03 DOX-inducible MYC silencing isogenic models indicated leakiness which means MYC was knockdown in the absence of DOX. To overcome this leakiness cells could be transduced with a lower MOI or instead of a polyclonal cell population a single clone that does not indicate leakiness can be selected and then a cell population could be grown from this single clone.

6.2.2 Proteomic profiling of DOX- inducible MYC silencing isogenic models

As mentioned before, gene expression levels might not correspond to protein levels or pathway activation status (Runge and Patterson, 2007; Vogel and Marcotte, 2012). Therefore, it is important to investigate the changes in protein levels associated with MYC knockdown. Protein quantification can be analysed through mass spectrometry quantitative proteomics (Zhang *et al.,* 2010). These results will validate findings at the mRNA level and highlight pathways for further investigation towards potential therapeutic targeting.

6.2.3 High- throughput functional screening of DOX-inducible MYC silencing isogenic models

In a forthcoming drug screen, these DOX inducible MYC silencing isogenic models will be used to investigate the MYC dependency to the response to a large panel of cancer therapeutics, to identify drugs which target both MYC and which synergise with MYC knockdown. Drugs which have a greater effect on the proliferation of MYC expressing cells potentially target MYC, whereas greater sensitivity following MYC knockdown may indicate an additive or synergistic effect.

6.2.4 *Metabolic profiling of DOX-inducible MYC silencing isogenic models*

MYC controls many aspects of cellular metabolism; MYC overexpression is the driver of many metabolic changes occurring within cancer cells (Miller *et al.*, 2012). Therefore, metabolic profiling will not only complement the genomic and proteomic data generated from these DOX inducible MYC silencing models but will also give insight into the metabolic changes associated with MYC deregulation. There are two techniques that could be used to analyse the metabolomics, namely mass spectrometry or nuclear magnetic resonance spectroscopy. However, the technique mostly used is mass spectrometry. Mass spectrometry is more sensitive than nuclear magnetic resonance (Markley *et al.*, 2017). Mass spectrometry together with bioinformatics technology could identify possible metabolic enzymatic inhibitors. The aim would be to identify upregulated metabolites that are associated with MYC ability to drive tumourgenesis, the enzymes producing these metabolites could possibly be a therapeutic option (Rabinowitz *et al.*, 2011). In addition, integrative analysis of omics data could provide a better understanding of MYC biology within MB.

6.2.5 Assessment of candidate therapeutic agents within mouse models

Once candidate therapeutic agents have been identified the next step would be to test these agents within a human tumour xenograft and/or GEMM models to determine whether these therapeutic agents are effective in treating MB_{GRP3} models in vivo before proceeding to clinical trials.

6.2.6 Knockout of MYC or genome wide screen by CRISPR/Cas 9

Another approach to gain understanding of MYC biology within MB_{GRP3} is to use Clustered Regularly Interspaced Short Palindromic Repeats (CRISPR)/Cas 9 to knockout MYC in MB_{GRP3} cell lines as knockout phenotype and downstream analysis might differ from knockdown phenotype. The difference between RNAi technologies and CRISPR/Cas 9 is that it results in a permanent inactivation of gene expression (Gurumurthy *et al.*, 2016). A whole genome screen using CRISPR on the inducible MYC silencing models can be done to individually knockout over 19000 genes/miRNA targets but a neomycin inducible MYC silencing models would need to be generated to make it compatible with the puromycin Genome- scale CRISPR knockout library.

6.3 Final Conclusion

This study was performed to provide understanding of MYC biology within MB_{GRP3}, through generation of DOX inducible MYC silencing MB_{GRP3} isogenic models. The DOX inducible MYC silencing MB_{GRP3} isogenic models were successfully generated and showed that MYC knockdown caused an effect on proliferation even though these cell lines have many defects (Table 24) indicating that these cell lines are addicted to MYC. The generation of these important models will enable us to gain a better understanding of MYC biology within MB to develop targeted therapeutics.

Chapter 7 References

Adhikary, S. and Eilers, M. (2005a) 'Transcriptional regulation and transformation by Myc proteins', Nature reviews Molecular cell biology, 6(8), pp. 635-645.

Adhikary, S. and Eilers, M. (2005b) 'Transcriptional regulation and transformation by Myc proteins', Nat Rev Mol Cell Biol, 6(8), pp. 635-45.

Albertson, D.G. (2006) 'Gene amplification in cancer', Trends Genet, 22(8), pp. 447-55.
Amati, B., Frank, S.R., Donjerkovic, D. and Taubert, S. (2001) 'Function of the c-Myc oncoprotein in chromatin remodeling and transcription', Biochimica et Biophysica Acta (BBA)-Reviews on Cancer, 1471(3), pp. M135-M145.

Amelio, I., Cutruzzolá, F., Antonov, A., Agostini, M. and Melino, G. (2014) 'Serine and glycine metabolism in cancer', Trends in biochemical sciences, 39(4), pp. 191-198.

An, K., Liu, H.-p., Zhong, X.-l., Deng, D.Y.B., Zhang, J.-j. and Liu, Z.-h. (2017) 'hTERT-Immortalized Bone Mesenchymal Stromal Cells Expressing Rat Galanin via a Single Tetracycline-Inducible Lentivirus System', Stem Cells International, 2017.

Anchineyan, P., Mani, G.K., Amalraj, J., Karthik, B. and Anbumani, S. (2014) 'Use of Flattening Filter-Free Photon Beams in Treating Medulloblastoma: A Dosimetric Evaluation', ISRN Oncology, 2014, p. 5.

Anders, S. and Huber, W. (2010) 'Differential expression analysis for sequence count data', Genome biology, 11(10), p. R106.

Anders, S., Pyl, P.T. and Huber, W. (2015) 'HTSeq--a Python framework to work with high-throughput sequencing data', Bioinformatics, 31(2), pp. 166-9.

Andresen, C., Helander, S., Lemak, A., Farès, C., Csizmok, V., Carlsson, J., Penn, L.Z., Forman-Kay, J.D., Arrowsmith, C.H., Lundström, P. and Sunnerhagen, M. (2012) 'Transient structure and dynamics in the disordered c-Myc transactivation domain affect Bin1 binding', Nucleic Acids Research, 40(13), pp. 6353-6366.

Aquino, G., Marra, L., Cantile, M., De Chiara, A., Liguori, G., Curcio, M.P., Sabatino, R., Pannone, G., Pinto, A., Botti, G. and Franco, R. (2013) 'MYC chromosomal aberration in differential diagnosis between Burkitt and other aggressive lymphomas', Infect Agent Cancer, 8(1), p. 37.

Archer, T.C., Weeraratne, S.D. and Pomeroy, S.L. (2012) 'Hedgehog-GLI pathway in medulloblastoma', J Clin Oncol, 30(17), pp. 2154-6.

Asghar, U., Witkiewicz, A.K., Turner, N.C. and Knudsen, E.S. (2015) 'The history and future of targeting cyclin-dependent kinases in cancer therapy', Nature reviews Drug discovery, 14(2), pp. 130-146.

Aziz, S.A., Jilaveanu, L.B., Zito, C., Camp, R.L., Rimm, D.L., Conrad, P. and Kluger, H.M. (2010) 'Vertical targeting of the phosphatidylinositol-3 kinase pathway as a strategy for treating melanoma', Clinical Cancer Research, 16(24), pp. 6029-6039.

Babcock, J.T., Nguyen, H.B., He, Y., Hendricks, J.W., Wek, R.C. and Quilliam, L.A. (2013) 'Mammalian target of rapamycin complex 1 (mTORC1) enhances bortezomib-induced death in tuberous sclerosis complex (TSC)-null cells by a c-MYC-dependent induction of the unfolded protein response', J Biol Chem, 288(22), pp. 15687-98.

Bandopadhayay, P., Bergthold, G., Nguyen, B., Schubert, S., Gholamin, S., Tang, Y., Bolin, S., Schumacher, S.E., Zeid, R., Masoud, S., Yu, F., Vue, N., Gibson, W.J., Paolella, B.R., Mitra, S.S., Cheshier, S.H., Qi, J., Liu, K.W., Wechsler-Reya, R., Weiss, W.A., Swartling, F.J., Kieran, M.W., Bradner, J.E., Beroukhim, R. and Cho, Y.J. (2014) 'BET bromodomain inhibition of MYC-amplified medulloblastoma', Clin Cancer Res, 20(4), pp. 912-25.

Banerjee, K. and Resat, H. (2016) 'Constitutive activation of STAT3 in breast cancer cells: A review', Int J Cancer, 138(11), pp. 2570-8.

Barde, I., Zanta-Boussif, M.A., Paisant, S., Leboeuf, M., Rameau, P., Delenda, C. and Danos, O. (2006) 'Efficient control of gene expression in the hematopoietic system using a single Tet-on inducible lentiviral vector', Molecular Therapy, 13(2), pp. 382-390.

Bartlett, F., Kortmann, R. and Saran, F. (2013) 'Medulloblastoma', Clin Oncol (R Coll Radiol), 25(1), pp. 36-45.

Bavetsias, V. and Linardopoulos, S. (2015) 'Aurora kinase inhibitors: current status and outlook', Frontiers in oncology, 5.

Ben-Israel, H., Sharf, R., Rechavi, G. and Kleinberger, T. (2008) 'Adenovirus E4orf4 protein downregulates MYC expression through interaction with the PP2A-B55 subunit', Journal of virology, 82(19), pp. 9381-9388.

Benabdellah, K., Cobo, M., Muñoz, P., Toscano, M.G. and Martin, F. (2011) 'Development of an all-in-one lentiviral vector system based on the original TetR for the easy generation of Tet-ON cell lines', PloS one, 6(8), p. e23734.

Berg, T., Cohen, S.B., Desharnais, J., Sonderegger, C., Maslyar, D.J., Goldberg, J., Boger, D.L. and Vogt, P.K. (2002) 'Small-molecule antagonists of Myc/Max dimerization inhibit Myc-induced transformation of chicken embryo fibroblasts', Proc Natl Acad Sci U S A, 99(6), pp. 3830-5.

Bild, A.H., Yao, G., Chang, J.T., Wang, Q., Potti, A., Chasse, D., Joshi, M.-B., Harpole, D., Lancaster, J.M. and Berchuck, A. (2006) 'Oncogenic pathway signatures in human cancers as a guide to targeted therapies', Nature, 439(7074), pp. 353-357.

Bose, P., Simmons, G.L. and Grant, S. (2013) 'Cyclin-dependent kinase inhibitor therapy for hematologic malignancies', Expert opinion on investigational drugs, 22(6), pp. 723-738.
Bouard, D., Alazard-Dany, N. and Cosset, F.L. (2009) 'Viral vectors: from virology to transgene expression', British journal of pharmacology, 157(2), pp. 153-165.

Bournazou, E. and Bromberg, J. (2013) 'Targeting the tumor microenvironment: JAK-STAT3 signaling', Jakstat, 2(2), p. e23828.

Boxer, L.M. and Dang, C.V. (2001) 'Translocations involving c-myc and c-myc function', Oncogene, 20(40), pp. 5595-610.

Brady, J.J., Li, M., Suthram, S., Jiang, H., Wong, W.H. and Blau, H.M. (2013) 'Early role for IL-6 signalling during generation of induced pluripotent stem cells revealed by heterokaryon RNA-Seq', Nat Cell Biol, 15(10), pp. 1244-52.

Bretones, G., Delgado, M.D. and Leon, J. (2015) 'Myc and cell cycle control', Biochim Biophys Acta, 1849(5), pp. 506-516.

Brew, K. and Nagase, H. (2010) 'The tissue inhibitors of metalloproteinases (TIMPs): an ancient family with structural and functional diversity', Biochim Biophys Acta, 1803(1), pp. 55-71.

Brighenti, E., Treré, D. and Derenzini, M. (2015) 'Targeted cancer therapy with ribosome biogenesis inhibitors: a real possibility?', Oncotarget, 6(36), pp. 38617-38627.

Brockmann, M., Poon, E., Berry, T., Carstensen, A., Deubzer, Hedwig E., Rycak, L., Jamin, Y., Thway, K., Robinson, Simon P., Roels, F., Witt, O., Fischer, M., Chesler, L. and Eilers, M. (2013) 'Small Molecule Inhibitors of Aurora-A Induce Proteasomal Degradation of N-Myc in Childhood Neuroblastoma', Cancer Cell, 24(1), pp. 75-89.

Brugieres, L., Remenieras, A., Pierron, G., Varlet, P., Forget, S., Byrde, V., Bombled, J., Puget, S., Caron, O., Dufour, C., Delattre, O., Bressac-de Paillerets, B. and Grill, J. (2012) 'High frequency of germline SUFU mutations in children with desmoplastic/nodular medulloblastoma younger than 3 years of age', J Clin Oncol, 30(17), pp. 2087-93.

Buckwalter, M.S., Yamane, M., Coleman, B.S., Ormerod, B.K., Chin, J.T., Palmer, T. and Wyss-Coray, T. (2006) 'Chronically Increased Transforming Growth Factor-β1 Strongly Inhibits Hippocampal Neurogenesis in Aged Mice', The American Journal of Pathology, 169(1), pp. 154-164.

Buechner, J. and Einvik, C. (2012) 'N-myc and noncoding RNAs in neuroblastoma', Mol Cancer Res, 10(10), pp. 1243-53.

Bueno, M.J. and Malumbres, M. (2011) 'MicroRNAs and the cell cycle', Biochimica et Biophysica Acta (BBA) - Molecular Basis of Disease, 1812(5), pp. 592-601.

Cai, B. and Jiang, X. (2014) 'Revealing Biological Pathways Implicated in Lung Cancer from TCGA Gene Expression Data Using Gene Set Enrichment Analysis', Cancer Inform, 13(Suppl 1), pp. 113-21.

Cancer Incidence Statistics, Cancer Research UK. Available at: http://www.cancerresearchuk.org/health-professional/cancer-statistics/incidence#heading-One (Accessed: 15 November).

Cancer Mortality Statistics, Cancer Research UK. Available at: http://www.cancerresearchuk.org/health-professional/cancer-statistics/mortality#heading-Zero (Accessed: 15 November).

Caracciolo, V. and Giordano, A. (2012) 'Medulloblastoma: Classification (A Review)', in Hayat, M.A. (ed.) Tumors of the Central Nervous System, Volume 8. Springer Netherlands, pp. 23-33.

Carrie, C., Grill, J., Figarella-Branger, D., Bernier, V., Padovani, L., Habrand, J.L., Benhassel, M., Mege, M., Mahe, M., Quetin, P., Maire, J.P., Baron, M.H., Clavere, P., Chapet, S., Maingon, P., Alapetite, C., Claude, L., Laprie, A. and Dussart, S. (2009) 'Online quality control, hyperfractionated radiotherapy alone and reduced boost volume for standard risk medulloblastoma: long-term results of MSFOP 98', J Clin Oncol, 27(11), pp. 1879-83.

Cassidy, L., Stirling, R., May, K., Picton, S. and Doran, R. (2000) 'Ophthalmic complications of childhood medulloblastoma', Med Pediatr Oncol, 34(1), pp. 43-7.

Cavallaro, U. and Christofori, G. (2001) 'Cell adhesion in tumor invasion and metastasis: loss of the glue is not enough', Biochim Biophys Acta, 1552(1), pp. 39-45.

Cesare, A.J. and Reddel, R.R. (2013) 'Alternative lengthening of telomeres in mammalian cells'.

Chawla, S.P., Staddon, A.P., Baker, L.H., Schuetze, S.M., Tolcher, A.W., D'Amato, G.Z., Blay, J.Y., Mita, M.M., Sankhala, K.K., Berk, L., Rivera, V.M., Clackson, T., Loewy, J.W., Haluska, F.G. and Demetri, G.D. (2012) 'Phase II study of the mammalian target of rapamycin inhibitor ridaforolimus in patients with advanced bone and soft tissue sarcomas', J Clin Oncol, 30(1), pp. 78-84.

Chen, H., Hutt-Fletcher, L., Cao, L. and Hayward, S.D. (2003) 'A positive autoregulatory loop of LMP1 expression and STAT activation in epithelial cells latently infected with Epstein-Barr virus', Journal of virology, 77(7), pp. 4139-4148.

Cheng, Z., Gong, Y., Ma, Y., Lu, K., Lu, X., Pierce, L.A., Thompson, R.C., Muller, S., Knapp, S. and Wang, J. (2013) 'Inhibition of BET bromodomain targets genetically diverse glioblastoma', Clinical cancer research, 19(7), pp. 1748-1759.

Children Cancer Statistics, Cancer Research UK. Available at: http://www.cancerresearchuk.org/health-professional/cancer-statistics/childrens-cancers (Accessed: 16 November).

Children with Cancer UK, S.R. (2017). Available at: www.childrenwithcancer.org.uk.

Ciuffi, A. (2008) 'Mechanisms governing lentivirus integration site selection', Current gene therapy, 8(6), pp. 419-429.

Clifford, S.C., Lusher, M.E., Lindsey, J.C., Langdon, J.A., Gilbertson, R.J., Straughton, D. and Ellison, D.W. (2006) 'Wnt/Wingless pathway activation and chromosome 6 loss characterize a distinct molecular sub-group of medulloblastomas associated with a favorable prognosis', Cell Cycle, 5(22), pp. 2666-70.

CNS Incidence Statistics, C.R.U. (2017).

Collange, N.Z., Brito, S.d.A., Campos, R.R., Santos, E.A.S. and Botelho, R.V. (2016) 'Treatment of medulloblastoma in children and adolescents', Revista da Associação Médica Brasileira, 62(4), pp. 298-302.

Collins, K., Jacks, T. and Pavletich, N.P. (1997) 'The cell cycle and cancer', Proceedings of the National Academy of Sciences, 94(7), pp. 2776-2778.

Conesa, A., Madrigal, P., Tarazona, S., Gomez-Cabrero, D., Cervera, A., McPherson, A., Szcześniak, M.W., Gaffney, D.J., Elo, L.L. and Zhang, X. (2016) 'A survey of best practices for RNA-seq data analysis', Genome biology, 17(1), p. 13.

Cowling, V.H. and Cole, M.D. (2007) 'E-cadherin repression contributes to c-Myc-induced epithelial cell transformation', Oncogene, 26(24), pp. 3582-3586.

Cramer, T. and Schmitt, C.A. (2016) Metabolism in cancer. Springer.

Crawford, J.R., MacDonald, T.J. and Packer, R.J. (2007) 'Medulloblastoma in childhood: new biological advances', Lancet Neurol, 6(12), pp. 1073-85.

Dai, M.S. and Lu, H. (2008) 'Crosstalk between c-Myc and ribosome in ribosomal biogenesis and cancer', J Cell Biochem, 105(3), pp. 670-7.

Dang, C.V. (1999) 'c-Myc target genes involved in cell growth, apoptosis, and metabolism', Molecular and cellular biology, 19(1), pp. 1-11.

Dang, C.V. (2012) 'MYC on the path to cancer', Cell, 149(1), pp. 22-35.

Dang, C.V. (2013) 'MYC, metabolism, cell growth, and tumorigenesis', Cold Spring Harb Perspect Med, 3(8).

Dauch, D., Rudalska, R., Cossa, G., Nault, J.-C., Kang, T.-W., Wuestefeld, T., Hohmeyer, A., Imbeaud, S., Yevsa, T. and Hoenicke, L. (2016) 'A MYC-aurora kinase A protein complex represents an actionable drug target in p53-altered liver cancer', Nature medicine.

Dawson, M.A. and Kouzarides, T. (2012) 'Cancer epigenetics: from mechanism to therapy', Cell, 150(1), pp. 12-27.

de Alboran, I.M., O'Hagan, R.C., Gärtner, F., Malynn, B., Davidson, L., Rickert, R., Rajewsky, K., DePinho, R.A. and Alt, F.W. (2001) 'Analysis of C-MYC function in normal cells via conditional gene-targeted mutation', Immunity, 14(1), pp. 45-55.

De Braganca, K.C. and Packer, R.J. (2013) 'Treatment Options for Medulloblastoma and CNS Primitive Neuroectodermal Tumor (PNET)', Curr Treat Options Neurol, 15(5), pp. 593-606.

De Luca, A., Cerrato, V., Fucà, E., Parmigiani, E., Buffo, A. and Leto, K. (2016) 'Sonic hedgehog patterning during cerebellar development', Cellular and molecular life sciences, 73(2), pp. 291-303.

Delmore, J.E., Issa, G.C., Lemieux, M.E., Rahl, P.B., Shi, J., Jacobs, H.M., Kastritis, E., Gilpatrick, T., Paranal, R.M., Qi, J., Chesi, M., Schinzel, A.C., McKeown, M.R., Heffernan, T.P., Vakoc, C.R., Bergsagel, P.L., Ghobrial, I.M., Richardson, P.G., Young, R.A., Hahn, W.C., Anderson, K.C., Kung, A.L., Bradner, J.E. and Mitsiades, C.S. (2011) 'BET bromodomain inhibition as a therapeutic strategy to target c-Myc', Cell, 146(6), pp. 904-17.

den Hollander, J., Rimpi, S., Doherty, J.R., Rudelius, M., Buck, A., Hoellein, A., Kremer, M., Graf, N., Scheerer, M. and Hall, M.A. (2010) 'Aurora kinases A and B are up-regulated by Myc and are essential for maintenance of the malignant state', Blood, 116(9), pp. 1498-1505.

DeSouza, R.M., Jones, B.R., Lowis, S.P. and Kurian, K.M. (2014) 'Pediatric medulloblastoma - update on molecular classification driving targeted therapies', Front Oncol, 4, p. 176.

Dhall, G. (2009) 'Medulloblastoma', J Child Neurol, 24(11), pp. 1418-30.

Diaz, R.J., Golbourn, B., Faria, C., Picard, D., Shih, D., Raynaud, D., Leadly, M., MacKenzie, D., Bryant, M. and Bebenek, M. (2015) 'Mechanism of action and therapeutic efficacy of Aurora kinase B inhibition in MYC overexpressing medulloblastoma', Oncotarget, 6(5), p. 3359.

Dickson, M.A. and Schwartz, G.K. (2009) 'Development of cell-cycle inhibitors for cancer therapy', Current Oncology, 16(2), p. 36.

Dobin, A., Davis, C.A., Schlesinger, F., Drenkow, J., Zaleski, C., Jha, S., Batut, P., Chaisson, M. and Gingeras, T.R. (2013) 'STAR: ultrafast universal RNA-seq aligner', Bioinformatics, 29(1), pp. 15-21.

Dominguez-Sola, D. and Gautier, J. (2014) 'MYC and the Control of DNA Replication', Cold Spring Harbor perspectives in medicine, 4(6), p. a014423.

Dominy, J.E., Vazquez, F. and Puigserver, P. (2012) 'Glycine decarboxylase cleaves a “malignant” metabolic path to promote tumor initiation', Cancer cell, 21(2), pp. 143-145.

Dong, P., Maddali, M.V., Srimani, J.K., Thelot, F., Nevins, J.R., Mathey-Prevot, B. and You, L. (2014) 'Division of labour between Myc and G1 cyclins in cell cycle commitment and pace control', Nat Commun, 5, p. 4750.

Dunkel, I.J., Gardner, S.L., Garvin, J.H., Goldman, S., Shi, W. and Finlay, J.L. (2010) 'High-dose carboplatin, thiotepa, and etoposide with autologous stem cell rescue for patients with previously irradiated recurrent medulloblastoma', Neuro-oncology, 12(3), pp. 297-303.

Eales, K.L., Hollinshead, K.E. and Tennant, D.A. (2016) 'Hypoxia and metabolic adaptation of cancer cells', Oncogenesis, 5, p. e190.

Ecker, J., Oehme, I., Mazitschek, R., Korshunov, A., Kool, M., Hielscher, T., Kiss, J., Selt, F., Konrad, C., Lodrini, M., Deubzer, H.E., von Deimling, A., Kulozik, A.E., Pfister, S.M., Witt, O. and Milde, T. (2015) 'Targeting class I histone deacetylase 2 in MYC amplified group 3 medulloblastoma', Acta Neuropathologica Communications, 3, p. 22.

Eilers, M. and Eisenman, R.N. (2008) 'Myc's broad reach', Genes Dev, 22(20), pp. 2755-66.

Eischen, C.M., Woo, D., Roussel, M.F. and Cleveland, J.L. (2001) 'Apoptosis Triggered by Myc-Induced Suppression of Bcl-X(L) or Bcl-2 Is Bypassed during Lymphomagenesis', Molecular and Cellular Biology, 21(15), pp. 5063-5070.

Ellison, D. (2002) 'Classifying the medulloblastoma: insights from morphology and molecular genetics', Neuropathology and applied neurobiology, 28(4), pp. 257-282.

Ellison, D.W. (2010) 'Childhood medulloblastoma: novel approaches to the classification of a heterogeneous disease', Acta neuropathologica, 120(3), pp. 305-316.

Ellison, D.W., Dalton, J., Kocak, M., Nicholson, S.L., Fraga, C., Neale, G., Kenney, A.M., Brat, D.J., Perry, A., Yong, W.H., Taylor, R.E., Bailey, S., Clifford, S.C. and Gilbertson, R.J. (2011) 'Medulloblastoma: clinicopathological correlates of SHH, WNT, and non-SHH/WNT molecular subgroups', Acta Neuropathol, 121(3), pp. 381-96.

Ellwood-Yen, K., Graeber, T.G., Wongvipat, J., Iruela-Arispe, M.L., Zhang, J., Matusik, R., Thomas, G.V. and Sawyers, C.L. (2003) 'Myc-driven murine prostate cancer shares molecular features with human prostate tumors', Cancer cell, 4(3), pp. 223-238.

Engelman, J.A., Chen, L., Tan, X., Crosby, K., Guimaraes, A.R., Upadhyay, R., Maira, M., McNamara, K., Perera, S.A. and Song, Y. (2008) 'Effective use of PI3K and MEK inhibitors to treat mutant Kras G12D and PIK3CA H1047R murine lung cancers', Nature medicine, 14(12), pp. 1351-1356.

Facchini, L.M. and Penn, L.Z. (1998) 'The molecular role of Myc in growth and transformation: recent discoveries lead to new insights', FASEB J, 12(9), pp. 633-51.

Faes, S., Demartines, N. and Dormond, O. (2017) 'Resistance to mTORC1 Inhibitors in Cancer Therapy: From Kinase Mutations to Intratumoral Heterogeneity of Kinase Activity', Oxidative medicine and cellular longevity, 2017.

Farrell, A.S. and Sears, R.C. (2014) 'MYC degradation', Cold Spring Harbor perspectives in medicine, 4(3), p. a014365.

Fellmann, C. and Lowe, S.W. (2014) 'Stable RNA interference rules for silencing', Nature cell biology, 16(1), pp. 10-18.

Ferrao, P.T., Bukczynska, E.P., Johnstone, R.W. and McArthur, G.A. (2012) 'Efficacy of CHK inhibitors as single agents in MYC-driven lymphoma cells', Oncogene, 31(13), pp. 1661-1672.

Finn, R.S., Aleshin, A. and Slamon, D.J. (2016) 'Targeting the cyclin-dependent kinases (CDK) 4/6 in estrogen receptor-positive breast cancers', Breast Cancer Research, 18(1), p. 17.

Flannery, E., VanZomeren-Dohm, A., Beach, P., Holland, W.S. and Duman-Scheel, M. (2010) 'Induction of cellular growth by the axon guidance regulators netrin A and semaphorin-1a', Dev Neurobiol, 70(7), pp. 473-84.

Fletcher, S. and Prochownik, E.V. (2015) 'Small-molecule inhibitors of the Myc oncoprotein', Biochimica Et Biophysica Acta (BBA)-Gene Regulatory Mechanisms, 1849(5), pp. 525-543.

Flønes, I., Sztromwasser, P., Haugarvoll, K., Dölle, C., Lykouri, M., Schwarzlmüller, T., Jonassen, I., Miletic, H., Johansson, S. and Knappskog, P.M. (2016) 'Novel SLC19A3 promoter deletion and allelic silencing in biotin-thiamine-responsive basal ganglia encephalopathy', PloS one, 11(2), p. e0149055.

Forment, J.V., Kaidi, A. and Jackson, S.P. (2012) 'Chromothripsis and cancer: causes and consequences of chromosome shattering', Nat Rev Cancer, 12(10), pp. 663-70.

Fossati, P., Ricardi, U. and Orecchia, R. (2009) 'Pediatric medulloblastoma: toxicity of current treatment and potential role of protontherapy', Cancer Treat Rev, 35(1), pp. 79-96.

Frenzel, A., Loven, J. and Henriksson, M.A. (2010) 'Targeting MYC-Regulated miRNAs to Combat Cancer', Genes Cancer, 1(6), pp. 660-7.

Friedl, P. and Wolf, K. (2003) 'Tumour-cell invasion and migration: diversity and escape mechanisms', Nature Reviews Cancer, 3(5), pp. 362-374.

Fry, D.W., Harvey, P.J., Keller, P.R., Elliott, W.L., Meade, M., Trachet, E., Albassam, M., Zheng, X., Leopold, W.R. and Pryer, N.K. (2004) 'Specific inhibition of cyclin-dependent kinase 4/6 by PD 0332991 and associated antitumor activity in human tumor xenografts', Molecular cancer therapeutics, 3(11), pp. 1427-1438.

Gajjar, A. and Pizer, B. (2010) 'Role of high-dose chemotherapy for recurrent medulloblastoma and other CNS primitive neuroectodermal tumors', Pediatr Blood Cancer, 54(4), pp. 649-51.

Gajjar, A.J. and Robinson, G.W. (2014) 'Medulloblastoma [mdash] translating discoveries from the bench to the bedside', Nature reviews Clinical oncology, 11(12), pp. 714-722.

Gandarillas, A. and Watt, F.M. (1997) 'c-Myc promotes differentiation of human epidermal stem cells', Genes Dev, 11(21), pp. 2869-82.

Gao, T., Han, Y., Yu, L., Ao, S., Li, Z. and Ji, J. (2014) 'CCNA2 is a prognostic biomarker for ER+ breast cancer and tamoxifen resistance', PLoS One, 9(3), p. e91771.

Garancher, A., Lin, C.Y., Morabito, M., Richer, W., Rocques, N., Larcher, M., Bihannic, L., Smith, K., Miquel, C. and Leboucher, S. (2018) 'NRL and CRX Define Photoreceptor Identity and Reveal Subgroup-Specific Dependencies in Medulloblastoma', Cancer cell, 33(3), pp. 435-449. e6.

Geoerger, B., Kieran, M.W., Grupp, S., Perek, D., Clancy, J., Krygowski, M., Ananthakrishnan, R., Boni, J.P., Berkenblit, A. and Spunt, S.L. (2012) 'Phase II trial of temsirolimus in children with high-grade glioma, neuroblastoma and rhabdomyosarcoma()', European journal of cancer (Oxford, England : 1990), 48(2), pp. 253-262.

Gerber, N.U., Mynarek, M., von Hoff, K., Friedrich, C., Resch, A. and Rutkowski, S. (2014) 'Recent developments and current concepts in medulloblastoma', Cancer Treat Rev, 40(3), pp. 356-65.

Giacinti, C. and Giordano, A. (2006) 'RB and cell cycle progression', Oncogene, 25(38), pp. 5220-7.

Gibson, P., Tong, Y., Robinson, G., Thompson, M.C., Currle, D.S., Eden, C., Kranenburg, T.A., Hogg, T., Poppleton, H., Martin, J., Finkelstein, D., Pounds, S., Weiss, A., Patay, Z., Scoggins, M., Ogg, R., Pei, Y., Yang, Z.J., Brun, S., Lee, Y., Zindy, F., Lindsey, J.C., Taketo, M.M., Boop, F.A., Sanford, R.A., Gajjar, A., Clifford, S.C., Roussel, M.F., McKinnon, P.J., Gutmann, D.H., Ellison, D.W., Wechsler-Reya, R. and Gilbertson, R.J. (2010) 'Subtypes of medulloblastoma have distinct developmental origins', Nature, 468(7327), pp. 1095-9.

Gilbertson, R.J. and Ellison, D.W. (2008) 'The origins of medulloblastoma subtypes', Annu Rev Pathol, 3, pp. 341-65.

Gopalakrishnan, V., Tao, R.-H., Dobson, T., Brugmann, W. and Khatua, S. (2015) 'Medulloblastoma development: tumor biology informs treatment decisions'.
Gossen, M., Bonin, A.L., Freundlieb, S. and Bujard, H. (1994) 'Inducible gene expression systems for higher eukaryotic cells', Current Opinion in Biotechnology, 5(5), pp. 516-520.

Guo, J., Parise, R.A., Joseph, E., Egorin, M.J., Lazo, J.S., Prochownik, E.V. and Eiseman, J.L. (2009) 'Efficacy, pharmacokinetics, tisssue distribution, and metabolism of the Myc–Max disruptor, 10058-F4 [Z, E]-5-[4-ethylbenzylidine]-2-thioxothiazolidin-4-one, in mice', Cancer chemotherapy and pharmacology, 63(4), pp. 615-625.

Gurumurthy, C.B., Grati, M.h., Ohtsuka, M., Schilit, S.L., Quadros, R.M. and Liu, X.Z. (2016) 'CRISPR: a versatile tool for both forward and reverse genetics research', Human genetics, 135(9), pp. 971-976.

Hahn, H., Wicking, C., Zaphiropoulous, P.G., Gailani, M.R., Shanley, S., Chidambaram, A., Vorechovsky, I., Holmberg, E., Unden, A.B., Gillies, S., Negus, K., Smyth, I., Pressman, C., Leffell, D.J., Gerrard, B., Goldstein, A.M., Dean, M., Toftgard, R., Chenevix-Trench, G., Wainwright, B. and Bale, A.E. (1996) 'Mutations of the human homolog of Drosophila patched in the nevoid basal cell carcinoma syndrome', Cell, 85(6), pp. 841-51.

Hanaford, A.R., Archer, T.C., Price, A., Kahlert, U.D., Maciaczyk, J., Nikkhah, G., Kim, J.W., Ehrenberger, T., Clemons, P.A. and Dančík, V. (2016) 'DiSCoVERing innovative therapies for rare tumors: combining genetically accurate disease models with in silico analysis to identify novel therapeutic targets', Clinical Cancer Research, 22(15), pp. 3903-3914.

Hanahan, D. and Weinberg, R.A. (2000) 'The hallmarks of cancer', Cell, 100(1), pp. 57-70.

Hanahan, D. and Weinberg, R.A. (2011) 'Hallmarks of cancer: the next generation', Cell, 144(5), pp. 646-74.

Hann, S.R. (2014) 'MYC cofactors: molecular switches controlling diverse biological outcomes', Cold Spring Harbor perspectives in medicine, 4(9), p. a014399.

Hatzi, E., Murphy, C., Zoephel, A., Rasmussen, H., Morbidelli, L., Ahorn, H., Kunisada, K., Tontsch, U., Klenk, M., Yamauchi-Takihara, K., Ziche, M., Rofstad, E.K., Schweigerer, L. and Fotsis, T. (2002) 'N-myc oncogene overexpression down-regulates IL-6; evidence that IL-6 inhibits angiogenesis and suppresses neuroblastoma tumor growth', Oncogene, 21(22), pp. 3552-61.

He, X.M., Wikstrand, C.J., Friedman, H.S., Bigner, S.H., Pleasure, S., Trojanowski, J.Q. and Bigner, D.D. (1991) 'Differentiation characteristics of newly established medulloblastoma cell lines (D384 Med, D425 Med, and D458 Med) and their transplantable xenografts', Laboratory investigation; a journal of technical methods and pathology, 64(6), pp. 833-843.

Hedvat, M., Huszar, D., Herrmann, A., Gozgit, J.M., Schroeder, A., Sheehy, A., Buettner, R., Proia, D., Kowolik, C.M., Xin, H., Armstrong, B., Bebernitz, G., Weng, S., Wang, L., Ye, M., McEachern, K., Chen, H., Morosini, D., Bell, K., Alimzhanov, M., Ioannidis, S., McCoon, P., Cao, Z.A., Yu, H., Jove, R. and Zinda, M. (2009) 'The JAK2 Inhibitor, AZD1480, Potently Blocks Stat3 Signaling and Oncogenesis in Solid Tumors', Cancer cell, 16(6), pp. 487-497.

Henssen, A., Thor, T., Odersky, A., Heukamp, L., El-Hindy, N., Beckers, A., Speleman, F., Althoff, K., Schafers, S., Schramm, A., Sure, U., Fleischhack, G., Eggert, A. and Schulte, J.H. (2013) 'BET bromodomain protein inhibition is a therapeutic option for medulloblastoma', Oncotarget, 4(11), pp. 2080-95.

Herrera-Abreu, M.T., Palafox, M., Asghar, U., Rivas, M.A., Cutts, R.J., Garcia-Murillas, I., Pearson, A., Guzman, M., Rodriguez, O. and Grueso, J. (2016) 'Early adaptation and acquired resistance to CDK4/6 inhibition in estrogen receptor–positive breast cancer', Cancer research, 76(8), pp. 2301-2313.

Hill, Rebecca M., Kuijper, S., Lindsey, Janet C., Petrie, K., Schwalbe, Ed C., Barker, K., Boult, Jessica K., Williamson, D., Ahmad, Z., Hallsworth, A., Ryan, Sarra L., Poon, E., Robinson, Simon P., Ruddle, R., Raynaud, Florence I., Howell, L., Kwok, C., Joshi, A., Nicholson, Sarah L., Crosier, S., Ellison, David W., Wharton, Stephen B., Robson, K., Michalski, A., Hargrave, D., Jacques, Thomas S., Pizer, B., Bailey, S., Swartling, Fredrik J., Weiss, William A., Chesler, L. and Clifford, Steven C. (2015) 'Combined MYC and P53 Defects Emerge at Medulloblastoma Relapse and Define Rapidly Progressive, Therapeutically Targetable Disease', Cancer Cell, 27(1), pp. 72-84.

Hoffman, B. and Liebermann, D.A. (2008) 'Apoptotic signaling by c-MYC', Oncogene, 27(50), pp. 6462-72.

Höglund, A., Nilsson, L.M., Muralidharan, S.V., Hasvold, L.A., Merta, P., Rudelius, M., Nikolova, V., Keller, U. and Nilsson, J.A. (2011) 'Therapeutic implications for the induced levels of Chk1 in Myc-expressing cancer cells', Clinical Cancer Research, 17(22), pp. 7067-7079.

Holland, A.J. and Cleveland, D.W. (2012) 'Chromoanagenesis and cancer: mechanisms and consequences of localized, complex chromosomal rearrangements', Nat Med, 18(11), pp. 1630-8.

Hönnemann, J., Sanz-Moreno, A., Wolf, E., Eilers, M. and Elsässer, H.-P. (2012) 'Miz1 is a critical repressor of cdkn1a during skin tumorigenesis', PLoS One, 7(4), p. e34885.

Hooper, C.M., Hawes, S.M., Kees, U.R., Gottardo, N.G. and Dallas, P.B. (2014) 'Gene expression analyses of the spatio-temporal relationships of human medulloblastoma subgroups during early human neurogenesis', PLoS One, 9(11), p. e112909.

Horiuchi, D., Anderton, B. and Goga, A. (2014a) 'Taking on Challenging Targets: Making MYC Druggable', American Society of Clinical Oncology educational book / ASCO. American Society of Clinical Oncology. Meeting, pp. e497-e502.

Horiuchi, D., Anderton, B. and Goga, A. (2014b) American Society of Clinical Oncology educational book/ASCO. American Society of Clinical Oncology. Meeting. NIH Public Access.

Hossain, S.M., Sultana, N., Babar, S.M. and Haki, G.D. (2007) 'A new mathematical model for optimum production of neural stem cells in large-scale', Molecular and Cellular Toxicology, 3(2), pp. 77-84.

Hovestadt, V., Remke, M., Kool, M., Pietsch, T., Northcott, P.A., Fischer, R., Cavalli, F.M.G., Ramaswamy, V., Zapatka, M., Reifenberger, G., Rutkowski, S., Schick, M., Bewerunge-Hudler, M., Korshunov, A., Lichter, P., Taylor, M.D., Pfister, S.M. and Jones, D.T.W. (2013) 'Robust molecular subgrouping and copy-number profiling of medulloblastoma from small amounts of archival tumour material using high-density DNA methylation arrays', Acta Neuropathologica, 125(6), pp. 913-916.

Howarth, J.L., Lee, Y.B. and Uney, J.B. (2010) 'Using viral vectors as gene transfer tools (Cell Biology and Toxicology Special Issue: ETCS-UK 1 day meeting on genetic manipulation of cells)', Cell Biology and Toxicology, 26(1), pp. 1-20.

Huang, C.-H., Lujambio, A., Zuber, J., Tschaharganeh, D.F., Doran, M.G., Evans, M.J., Kitzing, T., Zhu, N., de Stanchina, E. and Sawyers, C.L. (2014) 'CDK9-mediated transcription elongation is required for MYC addiction in hepatocellular carcinoma', Genes & development, 28(16), pp. 1800-1814.

Huang, S.Y. and Yang, J.-Y. (2015) 'Targeting the Hedgehog Pathway in Pediatric Medulloblastoma', Cancers, 7(4), pp. 2110-2123.

Hummel, T.R., Wagner, L., Ahern, C., Fouladi, M., Reid, J.M., McGovern, R.M., Ames, M.M., Gilbertson, R.J., Horton, T. and Ingle, A.M. (2013) 'A pediatric phase 1 trial of vorinostat and temozolomide in relapsed or refractory primary brain or spinal cord tumors: a Children's Oncology Group phase 1 consortium study', Pediatric blood & cancer, 60(9), pp. 1452-1457.

Hwang, E.I. and Packer, R.J. (2013) 'Event-Free Survival of Children with Average-Risk Medulloblastoma: Treatment with Craniospinal Radiation Followed by Adjuvant Chemotherapy', in Pediatric Cancer, Volume 4. Springer, pp. 93-101.

Hwang, H.C. and Clurman, B.E. (2005) 'Cyclin E in normal and neoplastic cell cycles', Oncogene, 24(17), pp. 2776-86.

Iavarone, A. and Lasorella, A. (2014) 'Myc and differentiation: going against the current', EMBO Reports, 15(4), pp. 324-325.

Inghirami, G., Grignani, F., Sternas, L., Lombardi, L., Knowles, D.M. and Dalla-Favera, R. (1990) 'Down-regulation of LFA-1 adhesion receptors by C-myc oncogene in human B lymphoblastoid cells', Science, 250(4981), p. 682.

Ivanov, D.P., Coyle, B., Walker, D.A. and Grabowska, A.M. (2016) 'In vitro models of medulloblastoma: Choosing the right tool for the job', Journal of biotechnology, 236, pp. 10-25.

Jacobsen, P.F., Jenkyn, D.J. and Papadimitriou, J.M. (1985) 'Establishment of a human medulloblastoma cell line and its heterotransplantation into nude mice', Journal of Neuropathology & Experimental Neurology, 44(5), pp. 472-485.

Jafri, M.A., Ansari, S.A., Alqahtani, M.H. and Shay, J.W. (2016) 'Roles of telomeres and telomerase in cancer, and advances in telomerase-targeted therapies', Genome medicine, 8(1), p. 69.

Ji, H., Wu, G., Zhan, X., Nolan, A., Koh, C., De Marzo, A., Doan, H.M., Fan, J., Cheadle, C. and Fallahi, M. (2011) 'Cell-type independent MYC target genes reveal a primordial signature involved in biomass accumulation', PloS one, 6(10), p. e26057.

Jia, Y., Chen, L., Jia, Q., Dou, X., Xu, N. and Liao, D.J. (2016) 'The well-accepted notion that gene amplification contributes to increased expression still remains, after all these years, a reasonable but unproven assumption', Journal of Carcinogenesis, 15, p. 3.

Jolliffe, I.T. and Cadima, J. (2016) 'Principal component analysis: a review and recent developments', Phil. Trans. R. Soc. A, 374(2065), p. 20150202.

Jones, D.T., Jager, N., Kool, M., Zichner, T., Hutter, B., Sultan, M., Cho, Y.J., Pugh, T.J., Hovestadt, V., Stutz, A.M., Rausch, T., Warnatz, H.J., Ryzhova, M., Bender, S., Sturm, D., Pleier, S., Cin, H., Pfaff, E., Sieber, L., Wittmann, A., Remke, M., Witt, H., Hutter, S., Tzaridis, T., Weischenfeldt, J., Raeder, B., Avci, M., Amstislavskiy, V., Zapatka, M., Weber, U.D., Wang, Q., Lasitschka, B., Bartholomae, C.C., Schmidt, M., von Kalle, C., Ast, V., Lawerenz, C., Eils, J., Kabbe, R., Benes, V., van Sluis, P., Koster, J., Volckmann, R., Shih, D., Betts, M.J., Russell, R.B., Coco, S., Tonini, G.P., Schuller, U., Hans, V., Graf, N., Kim, Y.J., Monoranu, C., Roggendorf, W., Unterberg, A., Herold-Mende, C., Milde, T., Kulozik, A.E., von Deimling, A., Witt, O., Maass, E., Rossler, J., Ebinger, M., Schuhmann, M.U., Fruhwald, M.C., Hasselblatt, M., Jabado, N., Rutkowski, S., von Bueren, A.O., Williamson, D., Clifford, S.C., McCabe, M.G., Collins, V.P., Wolf, S., Wiemann, S., Lehrach, H., Brors, B., Scheurlen, W., Felsberg, J., Reifenberger, G., Northcott, P.A., Taylor, M.D., Meyerson, M., Pomeroy, S.L., Yaspo, M.L., Korbel, J.O., Korshunov, A., Eils, R., Pfister, S.M. and Lichter, P. (2012) 'Dissecting the genomic complexity underlying medulloblastoma', Nature, 488(7409), pp. 100-5.

Jung, P. and Hermeking, H. (2009) 'The c-MYC-AP4-p21 cascade', Cell Cycle, 8(7), pp. 982-9.

Karajannis, M.A. and Zagzag, D. (2015) Molecular Pathology of Nervous System Tumors. Springer.

Kautzmann, M.A., Kim, D.S., Felder-Schmittbuhl, M.P. and Swaroop, A. (2011) 'Combinatorial regulation of photoreceptor differentiation factor, neural retina leucine zipper gene NRL, revealed by in vivo promoter analysis', J Biol Chem, 286(32), pp. 28247-55.

Kawauchi, D., Robinson, G., Uziel, T., Gibson, P., Rehg, J., Gao, C., Finkelstein, D., Qu, C., Pounds, S., Ellison, D.W., Gilbertson, R.J. and Roussel, M.F. (2012) 'A mouse model of the most aggressive subgroup of human medulloblastoma', Cancer Cell, 21(2), pp. 168-80.

Kc, S., Cárcamo, J.M. and Golde, D.W. (2006) 'Antioxidants prevent oxidative DNA damage and cellular transformation elicited by the over-expression of c-MYC', Mutation Research/Fundamental and Molecular Mechanisms of Mutagenesis, 593(1–2), pp. 64-79.

Kiessling, A., Sperl, B., Hollis, A., Eick, D. and Berg, T. (2006) 'Selective inhibition of c-Myc/Max dimerization and DNA binding by small molecules', Chem Biol, 13(7), pp. 745-51.

Kijima, N. and Kanemura, Y. (2016) 'Molecular Classification of Medulloblastoma', Neurologia medico-chirurgica, 56(11), pp. 687-697.

Kim, S.K., Jung, W.H. and Koo, J.S. (2014) 'Differential expression of enzymes associated with serine/glycine metabolism in different breast cancer subtypes', PloS one, 9(6), p. e101004.

Kim, T.K. and Eberwine, J.H. (2010) 'Mammalian cell transfection: the present and the future', Analytical and bioanalytical chemistry, 397(8), pp. 3173-3178.

Kim, Y.H., Girard, L., Giacomini, C.P., Wang, P., Hernandez-Boussard, T., Tibshirani, R., Minna, J.D. and Pollack, J.R. (2006) 'Combined microarray analysis of small cell lung cancer reveals altered apoptotic balance and distinct expression signatures of MYC family gene amplification', Oncogene, 25(1), pp. 130-138.

Ko, H.R., Hwang, I., Ahn, S.Y., Chang, Y.S., Park, W.S. and Ahn, J.Y. (2017) 'Neuron-specific expression of p48 Ebp1 during murine brain development and its contribution to CNS axon regeneration', BMB Rep, 50(3), pp. 126-131.

Koh, C.M., Sabo, A. and Guccione, E. (2016) 'Targeting MYC in cancer therapy: RNA processing offers new opportunities', Bioessays, 38(3), pp. 266-75.

Kool, M., Jones, D.T., Jager, N., Northcott, P.A., Pugh, T.J., Hovestadt, V., Piro, R.M., Esparza, L.A., Markant, S.L., Remke, M., Milde, T., Bourdeaut, F., Ryzhova, M., Sturm, D., Pfaff, E., Stark, S., Hutter, S., Seker-Cin, H., Johann, P., Bender, S., Schmidt, C., Rausch, T., Shih, D., Reimand, J., Sieber, L., Wittmann, A., Linke, L., Witt, H., Weber, U.D., Zapatka, M., Konig, R., Beroukhim, R., Bergthold, G., van Sluis, P., Volckmann, R., Koster, J., Versteeg, R., Schmidt, S., Wolf, S., Lawerenz, C., Bartholomae, C.C., von Kalle, C., Unterberg, A., Herold-Mende, C., Hofer, S., Kulozik, A.E., von Deimling, A., Scheurlen, W., Felsberg, J., Reifenberger, G., Hasselblatt, M., Crawford, J.R., Grant, G.A., Jabado, N., Perry, A., Cowdrey, C., Croul, S., Zadeh, G., Korbel, J.O., Doz, F., Delattre, O., Bader, G.D., McCabe, M.G., Collins, V.P., Kieran, M.W., Cho, Y.J., Pomeroy, S.L., Witt, O., Brors, B., Taylor, M.D., Schuller, U., Korshunov, A., Eils, R., Wechsler-Reya, R.J., Lichter, P. and Pfister, S.M. (2014) 'Genome sequencing of SHH medulloblastoma predicts genotype-related response to smoothened inhibition', Cancer Cell, 25(3), pp. 393-405.

Kool, M., Korshunov, A., Remke, M., Jones, D.T., Schlanstein, M., Northcott, P.A., Cho, Y.J., Koster, J., Schouten-van Meeteren, A., van Vuurden, D., Clifford, S.C., Pietsch, T., von Bueren, A.O., Rutkowski, S., McCabe, M., Collins, V.P., Backlund, M.L., Haberler, C., Bourdeaut, F., Delattre, O., Doz, F., Ellison, D.W., Gilbertson, R.J., Pomeroy, S.L., Taylor, M.D., Lichter, P. and Pfister, S.M. (2012) 'Molecular subgroups of medulloblastoma: an international meta-analysis of transcriptome, genetic aberrations, and clinical data of WNT, SHH, Group 3, and Group 4 medulloblastomas', Acta Neuropathol, 123(4), pp. 473-84.

Kool, M., Koster, J., Bunt, J., Hasselt, N.E., Lakeman, A., van Sluis, P., Troost, D., Meeteren, N.S., Caron, H.N., Cloos, J., Mrsic, A., Ylstra, B., Grajkowska, W., Hartmann, W., Pietsch, T., Ellison, D., Clifford, S.C. and Versteeg, R. (2008) 'Integrated genomics identifies five medulloblastoma subtypes with distinct genetic profiles, pathway signatures and clinicopathological features', PLoS One, 3(8), p. e3088.

Korah, M.P., Esiashvili, N., Mazewski, C.M., Hudgins, R.J., Tighiouart, M., Janss, A.J., Schwaibold, F.P., Crocker, I.R., Curran, W.J., Jr. and Marcus, R.B., Jr. (2010) 'Incidence, risks, and sequelae of posterior fossa syndrome in pediatric medulloblastoma', Int J Radiat Oncol Biol Phys, 77(1), pp. 106-12.

Korbel, J.O. and Campbell, P.J. (2013) 'Criteria for inference of chromothripsis in cancer genomes', Cell, 152(6), pp. 1226-36.

Koschmann, C., Bloom, K., Upadhyaya, S., Geyer, J.R. and Leary, S.E. (2016) 'Survival after relapse of medulloblastoma', Journal of pediatric hematology/oncology, 38(4), pp. 269-273.

Kress, T.R., Sabo, A. and Amati, B. (2015) 'MYC: connecting selective transcriptional control to global RNA production', Nat Rev Cancer, 15(10), pp. 593-607.

Kurian, K.M., Watson, C.J. and Wyllie, A.H. (2000) 'Retroviral vectors', Molecular Pathology, 53(4), p. 173.

Kuzan-Fischer, C.M., Guerreiro Stucklin, A.S. and Taylor, M.D. (2017) 'Advances in Genomics Explain Medulloblastoma Behavior at the Bedside', Neurosurgery, 64(CN_suppl_1), pp. 21-26.

Lannering, B., Rutkowski, S., Doz, F., Pizer, B., Gustafsson, G., Navajas, A., Massimino, M., Reddingius, R., Benesch, M., Carrie, C., Taylor, R., Gandola, L., Bjork-Eriksson, T., Giralt, J., Oldenburger, F., Pietsch, T., Figarella-Branger, D., Robson, K., Forni, M., Clifford, S.C., Warmuth-Metz, M., von Hoff, K., Faldum, A., Mosseri, V. and Kortmann, R. (2012) 'Hyperfractionated versus conventional radiotherapy followed by chemotherapy in standard-risk medulloblastoma: results from the randomized multicenter HIT-SIOP PNET 4 trial', J Clin Oncol, 30(26), pp. 3187-93.

Laplante, M. and Sabatini, D.M. (2009) 'mTOR signaling at a glance', Journal of cell science, 122(20), pp. 3589-3594.

Le, A. and Dang, C.V. (2013) 'Studying Myc's role in metabolism regulation', The Myc Gene: Methods and Protocols, pp. 213-219.

Lee, E.Y.H.P. and Muller, W.J. (2010) 'Oncogenes and tumor suppressor genes', Cold Spring Harbor perspectives in biology, 2(10), p. a003236.
Leone, G., Sears, R., Huang, E., Rempel, R., Nuckolls, F., Park, C.H., Giangrande, P., Wu, L., Saavedra, H.I., Field, S.J., Thompson, M.A., Yang, H., Fujiwara, Y., Greenberg, M.E., Orkin, S., Smith, C. and Nevins, J.R. (2001) 'Myc requires distinct E2F activities to induce S phase and apoptosis', Mol Cell, 8(1), pp. 105-13.

Li, K.K., Lau, K.M. and Ng, H.K. (2013) 'Signaling pathway and molecular subgroups of medulloblastoma', Int J Clin Exp Pathol, 6(7), pp. 1211-22.

Liao, D.J. and Dickson, R.B. (2000) 'c-Myc in breast cancer', Endocr Relat Cancer, 7(3), pp. 143-64.

Lin, K.-I., Lin, Y. and Calame, K. (2000) 'Repression of c-myc Is Necessary but Not Sufficient for Terminal Differentiation of B Lymphocytes In Vitro', Molecular and Cellular Biology, 20(23), pp. 8684-8695.

Liu, Q., Thoreen, C., Wang, J., Sabatini, D. and Gray, N.S. (2009) 'mTOR mediated anti-cancer drug discovery', Drug Discovery Today: Therapeutic Strategies, 6(2), pp. 47-55.

Lo, A.W., Sabatier, L., Fouladi, B., Pottier, G., Ricoul, M. and Murnane, J.P. (2002) 'DNA amplification by breakage/fusion/bridge cycles initiated by spontaneous telomere loss in a human cancer cell line', Neoplasia, 4(6), pp. 531-8.

Lorenzin, F., Benary, U., Baluapuri, A., Walz, S., Jung, L.A., von Eyss, B., Kisker, C., Wolf, J., Eilers, M. and Wolf, E. (2016) 'Different promoter affinities account for specificity in MYC-dependent gene regulation', eLife, 5, p. e15161.

Louis, D.N., Ohgaki, H., Wiestler, O.D., Cavenee, W.K., Burger, P.C., Jouvet, A., Scheithauer, B.W. and Kleihues, P. (2007) 'The 2007 WHO classification of tumours of the central nervous system', Acta Neuropathol, 114(2), pp. 97-109.

Louis, D.N., Perry, A., Reifenberger, G., von Deimling, A., Figarella-Branger, D., Cavenee, W.K., Ohgaki, H., Wiestler, O.D., Kleihues, P. and Ellison, D.W. (2016a) 'The 2016 World Health Organization Classification of Tumors of the Central Nervous System: a summary', Acta Neuropathol, 131(6), pp. 803-20.

Louis, D.N., Perry, A., Reifenberger, G., Von Deimling, A., Figarella-Branger, D., Cavenee, W.K., Ohgaki, H., Wiestler, O.D., Kleihues, P. and Ellison, D.W. (2016b) 'The 2016 World Health Organization classification of tumors of the central nervous system: a summary', Acta neuropathologica, 131(6), pp. 803-820.

Louis, S.F., Vermolen, B.J., Garini, Y., Young, I.T., Guffei, A., Lichtensztejn, Z., Kuttler, F., Chuang, T.C.Y., Moshir, S. and Mougey, V. (2005) 'c-Myc induces chromosomal rearrangements through telomere and chromosome remodeling in the interphase nucleus', Proceedings of the National Academy of Sciences of the United States of America, 102(27), pp. 9613-9618.

Love, M.I., Huber, W. and Anders, S. (2014) 'Moderated estimation of fold change and dispersion for RNA-seq data with DESeq2', Genome Biol, 15(12), p. 550.

Maharaj, A.S.R., Saint-Geniez, M., Maldonado, A.E. and D’Amore, P.A. (2006) 'Vascular Endothelial Growth Factor Localization in the Adult', The American Journal of Pathology, 168(2), pp. 639-648.

Maier, T., Guell, M. and Serrano, L. (2009) 'Correlation of mRNA and protein in complex biological samples', FEBS Lett, 583(24), pp. 3966-73.

Manjunath, N., Haoquan, W., Sandesh, S. and Premlata, S. (2009) 'Lentiviral delivery of short hairpin RNAs', Advanced drug delivery reviews, 61(9), pp. 732-745.

Markley, J.L., Bruschweiler, R., Edison, A.S., Eghbalnia, H.R., Powers, R., Raftery, D. and Wishart, D.S. (2017) 'The future of NMR-based metabolomics', Curr Opin Biotechnol, 43, pp. 34-40.

Martin, T.A., Ye, L., Sanders, A.J., Lane, J. and Jiang, W.G. (2000) 'Cancer invasion and metastasis: molecular and cellular perspective'.

Martin, T.A., Ye, L., Sanders, A.J., Lane, J. and Jiang, W.G. (2013) 'Cancer invasion and metastasis: molecular and cellular perspective'.

Mascarin, M., Giugliano, F.M. and Coassin, E. (2015) 'Radiotherapy in Medulloblastoma', in Posterior Fossa Tumors in Children. Springer, pp. 363-380.

Masin, M., Vazquez, J., Rossi, S., Groeneveld, S., Samson, N., Schwalie, P.C., Deplancke, B., Frawley, L.E., Gouttenoire, J., Moradpour, D., Oliver, T.G. and Meylan, E. (2014) 'GLUT3 is induced during epithelial-mesenchymal transition and promotes tumor cell proliferation in non-small cell lung cancer', Cancer & Metabolism, 2, pp. 11-11.

Massie, B., Mullick, A., Lau, P.C.K. and Konishi, Y. (2010) 'Cumate-inducible expression system for eukaryotic cells'. Google Patents.

Massimino, M., Biassoni, V., Gandola, L., Garre, M.L., Gatta, G., Giangaspero, F., Poggi, G. and Rutkowski, S. (2016) 'Childhood medulloblastoma', Crit Rev Oncol Hematol, 105, pp. 35-51.

Masters, J.R.W. (2000) 'Human cancer cell lines: fact and fantasy', Nature reviews Molecular cell biology, 1(3), pp. 233-236.

Mathew, R., Karantza-Wadsworth, V. and White, E. (2007) 'Role of autophagy in cancer', Nature reviews. Cancer, 7(12), pp. 961-967.

Matsui, A., Ihara, T., Suda, H., Mikami, H. and Semba, K. 4 (2013) 'Gene amplification: mechanisms and involvement in cancer' BioMolecular Concepts. p. 567 6. Available at: http://www.degruyter.com/view/j/bmc.2013.4.issue-6/bmc-2013-0026/bmc-2013-0026.xml (Accessed: 2014-04-16t12:38:12.987+02:00).

Mazouzi, A., Velimezi, G. and Loizou, J.I. (2014) 'DNA replication stress: Causes, resolution and disease', Experimental Cell Research, 329(1), pp. 85-93.

McCabe, M.T., Ott, H.M., Ganji, G., Korenchuk, S., Thompson, C., Van Aller, G.S., Liu, Y., Graves, A.P., Della Pietra, A., 3rd, Diaz, E., LaFrance, L.V., Mellinger, M., Duquenne, C., Tian, X., Kruger, R.G., McHugh, C.F., Brandt, M., Miller, W.H., Dhanak, D., Verma, S.K., Tummino, P.J. and Creasy, C.L. (2012) 'EZH2 inhibition as a therapeutic strategy for lymphoma with EZH2-activating mutations', Nature, 492(7427), pp. 108-12.

McKeown, M.R. and Bradner, J.E. (2014) 'Therapeutic strategies to inhibit MYC', Cold Spring Harbor perspectives in medicine, 4(10), p. a014266.

Mendes-Pereira, A.M., Sims, D., Dexter, T., Fenwick, K., Assiotis, I., Kozarewa, I., Mitsopoulos, C., Hakas, J., Zvelebil, M. and Lord, C.J. (2012) 'Genome-wide functional screen identifies a compendium of genes affecting sensitivity to tamoxifen', Proceedings of the National Academy of Sciences, 109(8), pp. 2730-2735.

Menssen, A. and Hermeking, H. (2002) 'Characterization of the c-MYC-regulated transcriptome by SAGE: identification and analysis of c-MYC target genes', Proceedings of the National Academy of Sciences, 99(9), pp. 6274-6279.

Merten, O.-W., Hebben, M. and Bovolenta, C. (2016) 'Production of lentiviral vectors', Molecular Therapy-Methods & Clinical Development, 3, p. 16017.

Mertz, J.A., Conery, A.R., Bryant, B.M., Sandy, P., Balasubramanian, S., Mele, D.A., Bergeron, L. and Sims, R.J. (2011) 'Targeting MYC dependence in cancer by inhibiting BET bromodomains', Proceedings of the National Academy of Sciences, 108(40), pp. 16669-16674.

Meyer, N. and Penn, L.Z. (2008) 'Reflecting on 25 years with MYC', Nat Rev Cancer, 8(12), pp. 976-90.

Meyerson, M. and Pellman, D. (2011) 'Cancer genomes evolve by pulverizing single chromosomes', Cell, 144(1), pp. 9-10.

Michor, F., Iwasa, Y. and Nowak, M.A. (2004) 'Dynamics of cancer progression', Nature reviews cancer, 4(3), pp. 197-205.

Milde, T., Lodrini, M., Savelyeva, L., Korshunov, A., Kool, M., Brueckner, L.M., Antunes, A.S., Oehme, I., Pekrun, A., Pfister, S.M., Kulozik, A.E., Witt, O. and

Deubzer, H.E. (2012) 'HD-MB03 is a novel Group 3 medulloblastoma model demonstrating sensitivity to histone deacetylase inhibitor treatment', J Neurooncol, 110(3), pp. 335-48.

Miller, D.M., Thomas, S.D., Islam, A., Muench, D. and Sedoris, K. (2012) 'c-Myc and cancer metabolism', Clin Cancer Res, 18(20), pp. 5546-53.

Min, H.S., Lee, J.Y., Kim, S.K. and Park, S.H. (2013) 'Genetic grouping of medulloblastomas by representative markers in pathologic diagnosis', Transl Oncol, 6(3), pp. 265-72.

Moffat, J., Grueneberg, D.A., Yang, X., Kim, S.Y., Kloepfer, A.M., Hinkle, G., Piqani, B., Eisenhaure, T.M., Luo, B. and Grenier, J.K. (2006) 'A lentiviral RNAi library for human and mouse genes applied to an arrayed viral high-content screen', Cell, 124(6), pp. 1283-1298.

Mollaoglu, G., Guthrie, M.R., Böhm, S., Brägelmann, J., Can, I., Ballieu, P.M., Marx, A., George, J., Heinen, C. and Chalishazar, M.D. (2017) 'MYC drives progression of small cell lung cancer to a variant neuroendocrine subtype with vulnerability to aurora kinase inhibition', Cancer cell, 31(2), pp. 270-285.

Morfouace, M., Shelat, A., Jacus, M., Freeman, B.B., 3rd, Turner, D., Robinson, S., Zindy, F., Wang, Y.D., Finkelstein, D., Ayrault, O., Bihannic, L., Puget, S., Li, X.N., Olson, J.M., Robinson, G.W., Guy, R.K., Stewart, C.F., Gajjar, A. and Roussel, M.F. (2014) 'Pemetrexed and Gemcitabine as Combination Therapy for the Treatment of Group3 Medulloblastoma', Cancer Cell.

Mori, H., Ninomiya, K., Kino-oka, M., Shofuda, T., Islam, M.O., Yamasaki, M., Okano, H., Taya, M. and Kanemura, Y. (2006) 'Effect of neurosphere size on the growth rate of human neural stem/progenitor cells', J Neurosci Res, 84(8), pp. 1682-91.

Morrissy, A.S., Garzia, L., Shih, D.J., Zuyderduyn, S., Huang, X., Skowron, P., Remke, M., Cavalli, F.M., Ramaswamy, V. and Lindsay, P.E. (2016) 'Divergent clonal selection dominates medulloblastoma at recurrence', Nature, 529(7586), p. 351.

Mukherjee, K. and Storici, F. (2012) 'A mechanism of gene amplification driven by small DNA fragments', PLoS Genet, 8(12), p. e1003119.

Mullick, A., Xu, Y., Warren, R., Koutroumanis, M., Guilbault, C., Broussau, S., Malenfant, F., Bourget, L., Lamoureux, L., Lo, R., Caron, A.W., Pilotte, A. and Massie, B. (2006) 'The cumate gene-switch: a system for regulated expression in mammalian cells', BMC Biotechnol, 6, p. 43.

Munger, K., Pietenpol, J.A., Pittelkow, M.R., Holt, J.T. and Moses, H.L. (1992) 'Transforming growth factor beta 1 regulation of c-myc expression, pRB phosphorylation, and cell cycle progression in keratinocytes', Cell Growth Differ, 3(5), pp. 291-8.

Murga, M., Campaner, S., Lopez-Contreras, A.J., Toledo, L.I., Soria, R., Montana, M.F., Artista, L., Schleker, T., Guerra, C., Garcia, E., Barbacid, M., Hidalgo, M., Amati, B. and Fernandez-Capetillo, O. (2011a) 'Exploiting oncogene-induced replicative stress for the selective killing of Myc-driven tumors', Nat Struct Mol Biol, 18(12), pp. 1331-1335.

Murga, M., Campaner, S., Lopez-Contreras, A.J., Toledo, L.I., Soria, R., Montaña, M.F., Artista, L.D., Schleker, T., Guerra, C., Garcia, E., Barbacid, M., Hidalgo, M., Amati, B. and Fernandez-Capetillo, O. (2011b) 'Exploiting oncogene-induced replicative stress for the selective killing of Myc-driven tumors', Nature structural & molecular biology, 18(12), pp. 1331-1335.

Murnane, J.P. (2012) 'Telomere dysfunction and chromosome instability', Mutat Res, 730(1-2), pp. 28-36.

Muscal, J.A., Thompson, P.A., Horton, T.M., Ingle, A.M., Ahern, C.H., McGovern, R.M., Reid, J.M., Ames, M.M., Espinoza-Delgado, I. and Weigel, B.J. (2013) 'A phase I trial of vorinostat and bortezomib in children with refractory or recurrent solid tumors: a Children's Oncology Group phase I consortium study (ADVL0916)', Pediatric blood & cancer, 60(3), pp. 390-395.

Muz, B., de la Puente, P., Azab, F. and Azab, A.K. (2015) 'The role of hypoxia in cancer progression, angiogenesis, metastasis, and resistance to therapy', Hypoxia (Auckl), 3, pp. 83-92.

Naidoo, J. and Young, D. (2012) 'Gene regulation systems for gene therapy applications in the central nervous system', Neurology research international, 2012.
Nasi, S., Ciarapica, R., Jucker, R., Rosati, J. and Soucek, L. (2001) 'Making decisions through Myc', FEBS Letters, 490(3), pp. 153-162.

Nikitovic, M. and Golubicic, I. (2013) 'Treatment options for childhood medulloblastoma', Vojnosanit Pregl, 70(8), pp. 773-7.

Nilsson, J.A. and Cleveland, J.L. (2003) 'Myc pathways provoking cell suicide and cancer', Oncogene, 22(56), pp. 9007-21.

Niu, Z., Liu, H., Zhou, M., Wang, H., Liu, Y., Li, X., Xiong, W., Ma, J., Li, X. and Li, G. (2015) 'Knockdown of c-Myc inhibits cell proliferation by negatively regulating the Cdk/Rb/E2F pathway in nasopharyngeal carcinoma cells', Acta biochimica et biophysica Sinica, 47(3), pp. 183-191.

Noh, J.M., Kim, J., Cho, D.Y., Choi, D.H., Park, W. and Huh, S.J. (2015) 'Exome sequencing in a breast cancer family without BRCA mutation', Radiat Oncol J, 33(2), pp. 149-54.

Northcott, P.A., Dubuc, A.M., Pfister, S. and Taylor, M.D. (2012a) 'Molecular subgroups of medulloblastoma', Expert review of neurotherapeutics, 12(7), pp. 871-884.

Northcott, P.A., Jones, D.T., Kool, M., Robinson, G.W., Gilbertson, R.J., Cho, Y.J., Pomeroy, S.L., Korshunov, A., Lichter, P., Taylor, M.D. and Pfister, S.M. (2012b) 'Medulloblastomics: the end of the beginning', Nat Rev Cancer, 12(12), pp. 818-34.

Northcott, P.A., Korshunov, A., Witt, H., Hielscher, T., Eberhart, C.G., Mack, S., Bouffet, E., Clifford, S.C., Hawkins, C.E., French, P., Rutka, J.T., Pfister, S. and

Taylor, M.D. (2011) 'Medulloblastoma comprises four distinct molecular variants', J Clin Oncol, 29(11), pp. 1408-14.

Northcott, P.A., Shih, D.J., Remke, M., Cho, Y.J., Kool, M., Hawkins, C., Eberhart, C.G., Dubuc, A., Guettouche, T., Cardentey, Y., Bouffet, E., Pomeroy, S.L., Marra, M., Malkin, D., Rutka, J.T., Korshunov, A., Pfister, S. and Taylor, M.D. (2012c) 'Rapid, reliable, and reproducible molecular sub-grouping of clinical medulloblastoma samples', Acta Neuropathol, 123(4), pp. 615-26.

O'Donnell, K.A., Yu, D., Zeller, K.I., Kim, J.-w., Racke, F., Thomas-Tikhonenko, A. and Dang, C.V. (2006) 'Activation of transferrin receptor 1 by c-Myc enhances cellular proliferation and tumorigenesis', Molecular and cellular biology, 26(6), pp. 2373-2386.

O’Keefe, E.P. (2013) 'siRNAs and shRNAs: Tools for protein knockdown by gene silencing', Word Lab.

Otsuka, K. and Ochiya, T. (2014) 'Genetic networks lead and follow tumor development: microRNA regulation of cell cycle and apoptosis in the p53 pathways', BioMed research international, 2014.

Packer, R.J., Gajjar, A., Vezina, G., Rorke-Adams, L., Burger, P.C., Robertson, P.L., Bayer, L., LaFond, D., Donahue, B.R., Marymont, M.H., Muraszko, K., Langston, J. and Sposto, R. (2006) 'Phase III study of craniospinal radiation therapy followed by adjuvant chemotherapy for newly diagnosed average-risk medulloblastoma', J Clin Oncol, 24(25), pp. 4202-8.

Pei, Y., Liu, K.-W., Wang, J., Garancher, A., Tao, R., Esparza, L.A., Maier, D.L., Udaka, Y.T., Murad, N. and Morrissy, S. (2016) 'HDAC and PI3K antagonists cooperate to inhibit growth of MYC-driven medulloblastoma', Cancer cell, 29(3), pp. 311-323.

Pei, Y., Moore, C.E., Wang, J., Tewari, A.K., Eroshkin, A., Cho, Y.J., Witt, H., Korshunov, A., Read, T.A., Sun, J.L., Schmitt, E.M., Miller, C.R., Buckley, A.F., McLendon, R.E., Westbrook, T.F., Northcott, P.A., Taylor, M.D., Pfister, S.M., Febbo, P.G. and Wechsler-Reya, R.J. (2012) 'An animal model of MYC-driven medulloblastoma', Cancer Cell, 21(2), pp. 155-67.

Pelengaris, S. and Khan, M. (2003) 'The many faces of c-MYC', Arch Biochem Biophys, 416(2), pp. 129-36.

Pelengaris, S., Khan, M. and Evan, G. (2002) 'c-MYC: more than just a matter of life and death', Nat Rev Cancer, 2(10), pp. 764-76.

Pfister, S.M., Korshunov, A., Kool, M., Hasselblatt, M., Eberhart, C. and Taylor, M.D. (2010) 'Molecular diagnostics of CNS embryonal tumors', Acta Neuropathol, 120(5), pp. 553-66.

Piatt, J.H., Jr. (2004) 'Recognizing neurosurgical conditions in the pediatrician's office', Pediatr Clin North Am, 51(2), pp. 237-70.

Pierotti, M.A., Sozzi, G. and Croce, C.M. (2003) 'Mechanisms of oncogene activation', Kufe DW, Pollock RE, Weichselbaum RR, and et al. Holland-Frei Cancer Medicine. 6th.

Pizer, B. and Clifford, S. (2008) 'Medulloblastoma: new insights into biology and treatment', Arch Dis Child Educ Pract Ed, 93(5), pp. 137-44.

Pizer, B., Donachie, P.H., Robinson, K., Taylor, R.E., Michalski, A., Punt, J., Ellison, D.W. and Picton, S. (2011) 'Treatment of recurrent central nervous system primitive neuroectodermal tumours in children and adolescents: results of a Children's Cancer and Leukaemia Group study', Eur J Cancer, 47(9), pp. 1389-97.

Pizer, B.L. and Clifford, S.C. (2009) 'The potential impact of tumour biology on improved clinical practice for medulloblastoma: progress towards biologically driven clinical trials', British Journal of Neurosurgery, 23(4), pp. 364-375.

Podar, K. and Anderson, K.C. (2010) 'A therapeutic role for targeting c-Myc/Hif-1-dependent signaling pathways', Cell cycle (Georgetown, Tex.), 9(9), pp. 1722-1728.

Pomeroy, S.L., Tamayo, P., Gaasenbeek, M., Sturla, L.M., Angelo, M., McLaughlin, M.E., Kim, J.Y., Goumnerova, L.C., Black, P.M., Lau, C., Allen, J.C., Zagzag, D., Olson, J.M., Curran, T., Wetmore, C., Biegel, J.A., Poggio, T., Mukherjee, S., Rifkin, R., Califano, A., Stolovitzky, G., Louis, D.N., Mesirov, J.P., Lander, E.S. and Golub, T.R. (2002) 'Prediction of central nervous system embryonal tumour outcome based on gene expression', Nature, 415(6870), pp. 436-42.

Poole, C.J. and van Riggelen, J. (2017) 'MYC—Master Regulator of the Cancer Epigenome and Transcriptome', Genes, 8(5), p. 142.

Pourdehnad, M., Truitt, M.L., Siddiqi, I.N., Ducker, G.S., Shokat, K.M. and Ruggero, D. (2013) 'Myc and mTOR converge on a common node in protein synthesis control that confers synthetic lethality in Myc-driven cancers', Proceedings of the National Academy of Sciences, 110(29), pp. 11988-11993.

Pushparaj, P.N., Aarthi, J.J., Manikandan, J. and Kumar, S.D. (2008) 'siRNA, miRNA, and shRNA: in vivo applications', Journal of dental research, 87(11), pp. 992-1003.

Rabinowitz, J.D., Purdy, J.G., Vastag, L., Shenk, T. and Koyuncu, E. (2011) 'Metabolomics in drug target discovery', Cold Spring Harb Symp Quant Biol, 76, pp. 235-46.

Rady, B., Chen, Y., Vaca, P., Wang, Q., Wang, Y., Salmon, P. and Oberholzer, J. (2013) 'Overexpression of E2F3 promotes proliferation of functional human beta cells without induction of apoptosis', Cell Cycle, 12(16), pp. 2691-702.

Raffel, C. (2004) 'Medulloblastoma: molecular genetics and animal models', Neoplasia, 6(4), pp. 310-22.

Ramaswamy, V., Remke, M., Bouffet, E., Bailey, S., Clifford, S.C., Doz, F., Kool, M., Dufour, C., Vassal, G. and Milde, T. (2016) 'Risk stratification of childhood medulloblastoma in the molecular era: the current consensus', Acta neuropathologica, 131(6), pp. 821-831.

Ramaswamy, V., Remke, M., Bouffet, E., Faria, C.C., Perreault, S., Cho, Y.-J., Shih, D.J., Luu, B., Dubuc, A.M. and Northcott, P.A. (2013) 'Recurrence patterns across medulloblastoma subgroups: an integrated clinical and molecular analysis', The lancet oncology, 14(12), pp. 1200-1207.

Ramesh, T., Lee, S.-H., Lee, C.-S., Kwon, Y.-W. and Cho, H.-J. (2009) 'Somatic Cell Dedifferentiation/Reprogramming for Regenerative Medicine', International Journal of Stem Cells, 2(1), pp. 18-27.

Rao, D.D., Vorhies, J.S., Senzer, N. and Nemunaitis, J. (2009) 'siRNA vs. shRNA: similarities and differences', Advanced drug delivery reviews, 61(9), pp. 746-759.

Rausch, T., Jones, D.T., Zapatka, M., Stutz, A.M., Zichner, T., Weischenfeldt, J., Jager, N., Remke, M., Shih, D., Northcott, P.A., Pfaff, E., Tica, J., Wang, Q., Massimi, L., Witt, H., Bender, S., Pleier, S., Cin, H., Hawkins, C., Beck, C., von Deimling, A., Hans, V., Brors, B., Eils, R., Scheurlen, W., Blake, J., Benes, V., Kulozik, A.E., Witt, O., Martin, D., Zhang, C., Porat, R., Merino, D.M., Wasserman, J., Jabado, N., Fontebasso, A., Bullinger, L., Rucker, F.G., Dohner, K., Dohner, H., Koster, J., Molenaar, J.J., Versteeg, R., Kool, M., Tabori, U., Malkin, D., Korshunov, A., Taylor, M.D., Lichter, P., Pfister, S.M. and Korbel, J.O. (2012) 'Genome sequencing of pediatric medulloblastoma links catastrophic DNA rearrangements with TP53 mutations', Cell, 148(1-2), pp. 59-71.

Reka, A.K., Kuick, R., Kurapati, H., Standiford, T.J., Omenn, G.S. and Keshamouni, V.G. (2011) 'Identifying inhibitors of epithelial-mesenchymal transition by connectivity map-based systems approach', J Thorac Oncol, 6(11), pp. 1784-92.

Rice, H., Bryant, S., Handley, C. and Hall, M. (2014) 'The Chemist', The Chemist, p. 15.
Riss, T.L., Moravec, R.A., Niles, A.L., Duellman, S., Benink, H.A., Worzella, T.J. and Minor, L. (2016) 'Cell viability assays'.

Rivlin, N., Brosh, R., Oren, M. and Rotter, V. (2011) 'Mutations in the p53 Tumor Suppressor Gene: Important Milestones at the Various Steps of Tumorigenesis', Genes & Cancer, 2(4), pp. 466-474.

Robinson, G., Parker, M., Kranenburg, T.A., Lu, C., Chen, X., Ding, L., Phoenix, T.N., Hedlund, E., Wei, L., Zhu, X., Chalhoub, N., Baker, S.J., Huether, R., Kriwacki, R., Curley, N., Thiruvenkatam, R., Wang, J., Wu, G., Rusch, M., Hong, X., Becksfort, J., Gupta, P., Ma, J., Easton, J., Vadodaria, B., Onar-Thomas, A., Lin, T., Li, S., Pounds, S., Paugh, S., Zhao, D., Kawauchi, D., Roussel, M.F., Finkelstein, D., Ellison, D.W., Lau, C.C., Bouffet, E., Hassall, T., Gururangan, S., Cohn, R., Fulton, R.S., Fulton, L.L., Dooling, D.J., Ochoa, K., Gajjar, A., Mardis, E.R., Wilson, R.K., Downing, J.R., Zhang, J. and Gilbertson, R.J. (2012) 'Novel mutations target distinct subgroups of medulloblastoma', Nature, 488(7409), pp. 43-8.

Rodrik-Outmezguine, V.S., Okaniwa, M., Yao, Z., Novotny, C.J., McWhirter, C., Banaji, A., Won, H., Wong, W., Berger, M. and de Stanchina, E. (2016) 'Overcoming mTOR resistance mutations with a new-generation mTOR inhibitor', Nature, 534(7606), pp. 272-276.

Rogers, H., Miller, S., Lowe, J., Brundler, M., Coyle, B. and Grundy, R. (2009) 'An investigation of WNT pathway activation and association with survival in central nervous system primitive neuroectodermal tumours (CNS PNET)', British journal of cancer, 100(8), p. 1292.

Rohban, S. and Campaner, S. (2015) 'Myc induced replicative stress response: How to cope with it and exploit it', Biochimica et Biophysica Acta (BBA) - Gene Regulatory Mechanisms, 1849(5), pp. 517-524.

Roney, I.J., Rudner, A.D., Couture, J.-F. and Kærn, M. (2016) 'Improvement of the reverse tetracycline transactivator by single amino acid substitutions that reduce leaky target gene expression to undetectable levels', Scientific reports, 6, p. 27697.

Roohi, A. and Hojjat-Farsangi, M. (2017) 'Recent advances in targeting mTOR signaling pathway using small molecule inhibitors', Journal of drug targeting, 25(3), pp. 189-201.

Roussel, M.F. and Hatten, M.E. (2011) 'Cerebellum development and medulloblastoma', Curr Top Dev Biol, 94, pp. 235-82.

Roussel, M.F. and Robinson, G.W. (2013) 'Role of MYC in Medulloblastoma', Cold Spring Harb Perspect Med, 3(11).

Ruan, K., Song, G. and Ouyang, G. (2009) 'Role of hypoxia in the hallmarks of human cancer', J Cell Biochem, 107(6), pp. 1053-62.

Ruggiero, A., Rizzo, D., Attina, G., Lazzareschi, I., Mastrangelo, S., Maurizi, P., Migliorati, R., Bertolini, P., Pastore, M., Colosimo, C. and Riccardi, R. (2010) 'Phase I study of temozolomide combined with oral etoposide in children with recurrent or progressive medulloblastoma', Eur J Cancer, 46(16), pp. 2943-9.

Runge, M.S. and Patterson, C. (2007) Principles of molecular cardiology. Springer Science & Business Media.

Ryan, K.M. and Birnie, G.D. (1996) 'Myc oncogenes: the enigmatic family', Biochem J, 314 (Pt 3), pp. 713-21.

Sabnis, H.S., Somasagara, R.R. and Bunting, K.D. (2017) 'Targeting MYC Dependence by Metabolic Inhibitors in Cancer', Genes, 8(4), p. 114.

Sakuma, T., Barry, M.A. and Ikeda, Y. (2012) 'Lentiviral vectors: basic to translational', Biochemical Journal, 443(3), pp. 603-618.

Samano, A.K., Ohshima-Hosoyama, S., Whitney, T.G., Prajapati, S.I., Kilcoyne, A., Taniguchi, E., Morgan, W.W., Nelon, L.D., Lin, A.L., Togao, O., Jung, I., Rubin, B.P., Nowak, B.M., Duong, T.Q. and Keller, C. (2010) 'Functional evaluation of therapeutic response for a mouse model of medulloblastoma', Transgenic Res, 19(5), pp. 829-40.

Santarius, T., Shipley, J., Brewer, D., Stratton, M.R. and Cooper, C.S. (2010) 'A census of amplified and overexpressed human cancer genes', Nat Rev Cancer, 10(1), pp. 59-64.

Scala, F., Brighenti, E., Govoni, M., Imbrogno, E., Fornari, F., Treré, D., Montanaro, L. and Derenzini, M. (2016) 'Direct relationship between the level of p53 stabilization induced by rRNA synthesis-inhibiting drugs and the cell ribosome biogenesis rate', Oncogene, 35(8), pp. 977-989.

Schipor, S., Vladoiu, S., Baciu, A.E., Niculescu, A.M., Caragheorgheopol, A., Iancu, I., Plesa, A., Popescu, A.I., Manda, D. and Scientific, A. (2016) 'A COMPARATIVE ANALYSIS OF THREE METHODS USED FOR RNA QUANTITATION', Romanian Reports in Physics, 68(3), pp. 1178-1188.

Schlosser, I., Hölzel, M., Mürnseer, M., Burtscher, H., Weidle, U.H. and Eick, D. (2003) 'A role for c-Myc in the regulation of ribosomal RNA processing', Nucleic acids research, 31(21), pp. 6148-6156.

Schröder, L.B.W. and McDonald, K.L. (2015) 'CDK4/6 Inhibitor PD0332991 in Glioblastoma Treatment: Does It Have a Future?', Frontiers in Oncology, 5, p. 259.

Schroeder, K. and Gururangan, S. (2014) 'Molecular variants and mutations in medulloblastoma', Pharmgenomics Pers Med, 7, pp. 43-51.

Schuhmacher, M., Kohlhuber, F., Hölzel, M., Kaiser, C., Burtscher, H., Jarsch, M., Bornkamm, G.W., Laux, G., Polack, A. and Weidle, U.H. (2001) 'The transcriptional program of a human B cell line in response to Myc', Nucleic acids research, 29(2), pp. 397-406.

Schwalbe, E.C., Lindsey, J.C., Straughton, D., Hogg, T.L., Cole, M., Megahed, H., Ryan, S.L., Lusher, M.E., Taylor, M.D., Gilbertson, R.J., Ellison, D.W., Bailey, S. and Clifford, S.C. (2011) 'Rapid diagnosis of medulloblastoma molecular subgroups', Clin Cancer Res, 17(7), pp. 1883-94.

Schwalbe, E.C., Williamson, D., Lindsey, J.C., Hamilton, D., Ryan, S.L., Megahed, H., Garami, M., Hauser, P., Dembowska-Baginska, B. and Perek, D. (2013a) 'DNA methylation profiling of medulloblastoma allows robust subclassification and improved outcome prediction using formalin-fixed biopsies', Acta neuropathologica, 125(3), pp. 359-371.

Schwalbe, E.C., Williamson, D., Lindsey, J.C., Hamilton, D., Ryan, S.L., Megahed, H., Garami, M., Hauser, P., Dembowska-Baginska, B., Perek, D., Northcott, P.A., Taylor, M.D., Taylor, R.E., Ellison, D.W., Bailey, S. and Clifford, S.C. (2013b) 'DNA methylation profiling of medulloblastoma allows robust subclassification and improved outcome prediction using formalin-fixed biopsies', Acta Neuropathol, 125(3), pp. 359-71.

Sedlacek, H., Czech, J., Naik, R., Kaur, G., Worland, P., Losiewicz, M., Parker, B., Carlson, B., Smith, A. and Senderowicz, A. (1996) 'Flavopiridol (L86 8275; NSC 649890), a new kinase inhibitor for tumor therapy', International journal of oncology, 9(6), pp. 1143-1168.

Semenza, G.L. (2003) 'Targeting HIF-1 for cancer therapy', Nat Rev Cancer, 3(10), pp. 721-32.

Sengupta, S., Krummel, D.P. and Pomeroy, S. (2017) 'The evolution of medulloblastoma therapy to personalized medicine', F1000Research, 6.

Shammas, M.A. (2011) 'Telomeres, lifestyle, cancer, and aging', Current Opinion in Clinical Nutrition and Metabolic Care, 14(1), pp. 28-34.

Sharpe, L.J. and Brown, A.J. (2013) 'Controlling cholesterol synthesis beyond 3-hydroxy-3-methylglutaryl-CoA reductase (HMGCR)', J Biol Chem, 288(26), pp. 18707-15.

Shaw, A. and Cornetta, K. (2014) 'Design and potential of non-integrating lentiviral vectors', Biomedicines, 2(1), pp. 14-35.

Shaw, G., Morse, S., Ararat, M. and Graham, F.L. (2002) 'Preferential transformation of human neuronal cells by human adenoviruses and the origin of HEK 293 cells', The FASEB Journal, 16(8), pp. 869-871.

Shay, J.W. and Wright, W.E. (2011) 'Role of telomeres and telomerase in cancer', Seminars in Cancer Biology, 21(6), pp. 349-353.

Shirisha Rani, G., Pattipati, S., Begum, M.R. and Naveen Kumar, M. (2013) 'Multiple odontogenic keratocysts indicating Gorlin-Goltz syndrome', international journal of stomatology & occlusion medicine, 6(2), pp. 77-81.

Shroff, E.H., Eberlin, L.S., Dang, V.M., Gouw, A.M., Gabay, M., Adam, S.J., Bellovin, D.I., Tran, P.T., Philbrick, W.M. and Garcia-Ocana, A. (2015) 'MYC oncogene overexpression drives renal cell carcinoma in a mouse model through glutamine metabolism', Proceedings of the National Academy of Sciences, 112(21), pp. 6539-6544.

Singh, A.K., Lopez-Araujo, A. and Katabathina, V.S. (2014) 'Gorlin Syndrome', J Pediatr.
Slotkin, E.K., Patwardhan, P.P., Vasudeva, S.D., de Stanchina, E., Tap, W.D. and Schwartz, G.K. (2015) 'MLN0128, an ATP-competitive mTOR kinase inhibitor with potent in vitro and in vivo antitumor activity, as potential therapy for bone and soft-tissue sarcoma', Molecular cancer therapeutics, 14(2), pp. 395-406.

Smith, A.P., Verrecchia, A., Faga, G., Doni, M., Perna, D., Martinato, F., Guccione, E. and Amati, B. (2009) 'A positive role for Myc in TGFbeta-induced Snail transcription and epithelial-to-mesenchymal transition', Oncogene, 28(3), pp. 422-30.

Soneson, C. and Delorenzi, M. (2013) 'A comparison of methods for differential expression analysis of RNA-seq data', BMC bioinformatics, 14(1), p. 91.

Squillace, R.M., Miller, D., Cookson, M., Wardwell, S.D., Moran, L., Clapham, D., Wang, F., Clackson, T. and Rivera, V.M. (2011) 'Antitumor activity of ridaforolimus and potential cell-cycle determinants of sensitivity in sarcoma and endometrial cancer models', Mol Cancer Ther, 10(10), pp. 1959-68.

Staal, J.A., San Lau, L., Zhang, H., Ingram, W.J., Hallahan, A.R., Northcott, P.A., Pfister, S.M., Wechsler-Reya, R.J., Rusert, J.M. and Taylor, M.D. (2015) 'Proteomic profiling of high risk medulloblastoma reveals functional biology', Oncotarget, 6(16), p. 14584.

Stearns, D., Chaudhry, A., Abel, T.W., Burger, P.C., Dang, C.V. and Eberhart, C.G. (2006) 'c-myc overexpression causes anaplasia in medulloblastoma', Cancer Res, 66(2), pp. 673-81.

Steller, E.J., Raats, D.A., Koster, J., Rutten, B., Govaert, K.M., Emmink, B.L., Snoeren, N., van Hooff, S.R., Holstege, F.C., Maas, C., Borel Rinkes, I.H. and Kranenburg, O. (2013) 'PDGFRB promotes liver metastasis formation of mesenchymal-like colorectal tumor cells', Neoplasia, 15(2), pp. 204-17.

Su, W.-C., Hsu, S.-F., Lee, Y.-Y., Jeng, K.-S. and Lai, M.M.C. (2015) 'A nucleolar protein, ribosomal RNA processing 1 homolog B (RRP1B), enhances the recruitment of cellular mRNA in influenza virus transcription', Journal of virology, 89(22), pp. 11245-11255.

Sun, L. and Gao, P. (2017) 'Small molecules remain on target for c-Myc', eLife, 6, p. e22915.

Suzuki, D.T. and Griffiths, A.J.F. (1976) An introduction to genetic analysis. WH Freeman and Company.

Swartling, F.J., Grimmer, M.R., Hackett, C.S., Northcott, P.A., Fan, Q.W., Goldenberg, D.D., Lau, J., Masic, S., Nguyen, K., Yakovenko, S., Zhe, X.N., Gilmer, H.C., Collins, R., Nagaoka, M., Phillips, J.J., Jenkins, R.B., Tihan, T., Vandenberg, S.R., James, C.D., Tanaka, K., Taylor, M.D., Weiss, W.A. and Chesler, L. (2010) 'Pleiotropic role for MYCN in medulloblastoma', Genes Dev, 24(10), pp. 1059-72.

Tabori, U., Baskin, B., Shago, M., Alon, N., Taylor, M.D., Ray, P.N., Bouffet, E., Malkin, D. and Hawkins, C. (2010) 'Universal poor survival in children with medulloblastoma harboring somatic TP53 mutations', J Clin Oncol, 28(8), pp. 1345-50.

Tan, J. and Yu, Q. (2013) 'Molecular mechanisms of tumor resistance to PI3K-mTOR-targeted therapy', Chinese journal of cancer, 32(7), p. 376.

Tansey, W.P. (2014) 'Mammalian MYC proteins and cancer', New Journal of Science, 2014.

Tarbell, N.J., Friedman, H., Polkinghorn, W.R., Yock, T., Zhou, T., Chen, Z., Burger, P., Barnes, P. and Kun, L. (2013) 'High-risk medulloblastoma: a pediatric oncology group randomized trial of chemotherapy before or after radiation therapy (POG 9031)', J Clin Oncol, 31(23), pp. 2936-41.

Tarrado-Castellarnau, M., de Atauri, P., Tarragó-Celada, J., Perarnau, J., Yuneva, M., Thomson, T.M. and Cascante, M. (2017) 'De novo MYC addiction as an adaptive response of cancer cells to CDK4/6 inhibition', Molecular Systems Biology, 13(10), p. 940.

Taxman, D.J., Moore, C.B., Guthrie, E.H. and Huang, M.T.-H. (2010) 'Short hairpin RNA (shRNA): design, delivery, and assessment of gene knockdown', RNA Therapeutics: Function, Design, and Delivery, pp. 139-156.

Taylor, M.D., Northcott, P.A., Korshunov, A., Remke, M., Cho, Y.J., Clifford, S.C., Eberhart, C.G., Parsons, D.W., Rutkowski, S., Gajjar, A., Ellison, D.W., Lichter, P., Gilbertson, R.J., Pomeroy, S.L., Kool, M. and Pfister, S.M. (2012) 'Molecular subgroups of medulloblastoma: the current consensus', Acta Neuropathol, 123(4), pp. 465-72.

Taylor, R.E., Bailey, C.C., Robinson, K., Weston, C.L., Ellison, D., Ironside, J., Lucraft, H., Gilbertson, R., Tait, D.M., Walker, D.A., Pizer, B.L., Imeson, J. and Lashford, L.S. (2003) 'Results of a randomized study of preradiation chemotherapy versus radiotherapy alone for nonmetastatic medulloblastoma: The International Society of Paediatric Oncology/United Kingdom Children's Cancer Study Group PNET-3 Study', J Clin Oncol, 21(8), pp. 1581-91.

Taylor, R.E., Bailey, C.C., Robinson, K.J., Weston, C.L., Ellison, D., Ironside, J., Lucraft, H., Gilbertson, R., Tait, D.M., Saran, F., Walker, D.A., Pizer, B.L. and Lashford, L.S. (2004) 'Impact of radiotherapy parameters on outcome in the International Society of Paediatric Oncology/United Kingdom Children's Cancer Study Group PNET-3 study of preradiotherapy chemotherapy for M0-M1 medulloblastoma', Int J Radiat Oncol Biol Phys, 58(4), pp. 1184-93.

Taylor, R.E., Howman, A.J., Wheatley, K., Brogden, E.E., Large, B., Gibson, M.J., Robson, K., Mitra, D., Saran, F., Michalski, A. and Pizer, B.L. (2014) 'Hyperfractionated Accelerated Radiotherapy (HART) with maintenance chemotherapy for metastatic (M1-3) Medulloblastoma - A safety/feasibility study', Radiother Oncol.

Thompson, M.C., Fuller, C., Hogg, T.L., Dalton, J., Finkelstein, D., Lau, C.C., Chintagumpala, M., Adesina, A., Ashley, D.M., Kellie, S.J., Taylor, M.D., Curran, T., Gajjar, A. and Gilbertson, R.J. (2006) 'Genomics identifies medulloblastoma subgroups that are enriched for specific genetic alterations', J Clin Oncol, 24(12), pp. 1924-31.

Tomás, H.A., Rodrigues, A.F., Alves, P.M. and Coroadinha, A.S. (2013) Lentiviral gene therapy vectors: challenges and future directions. Open Source, InTech.

Toniatti, C., Bujard, H., Cortese, R. and Ciliberto, G. (2004) 'Gene therapy progress and prospects: transcription regulatory systems', Gene therapy, 11(8), pp. 649-657.

Toyoshima, M., Howie, H.L., Imakura, M., Walsh, R.M., Annis, J.E., Chang, A.N., Frazier, J., Chau, B.N., Loboda, A., Linsley, P.S., Cleary, M.A., Park, J.R. and Grandori, C. (2012) 'Functional genomics identifies therapeutic targets for MYC-driven cancer', Proc Natl Acad Sci U S A, 109(24), pp. 9545-50.

Valovka, T., Schonfeld, M., Raffeiner, P., Breuker, K., Dunzendorfer-Matt, T., Hartl, M. and Bister, K. (2013) 'Transcriptional control of DNA replication licensing by Myc', Sci Rep, 3, p. 3444.

van Riggelen, J., Yetil, A. and Felsher, D.W. (2010) 'MYC as a regulator of ribosome biogenesis and protein synthesis', Nat Rev Cancer, 10(4), pp. 301-9.

Vaughan, L.S., Cullis, E., Barker, K., Jamin, Y., Robinson, S., Maira, S.-M. and Chesler, L. (2010) 'NVP-BEZ235 a dual PI3K/mTOR inhibitor destabilises Mycn in vitro and is growth inhibitory in the TH-MYCN murine neuroblastoma model'. AACR.

Velez, A.M.A. and Howard, M.S. (2015) 'Tumor-suppressor Genes, Cell Cycle Regulatory Checkpoints, and the Skin', North American Journal of Medical Sciences, 7(5), pp. 176-188.

Venkataraman, S., Alimova, I., Balakrishnan, I., Harris, P., Birks, D.K., Griesinger, A., Amani, V., Cristiano, B., Remke, M., Taylor, M.D., Handler, M., Foreman, N.K. and Vibhakar, R. (2014) 'Inhibition of BRD4 attenuates tumor cell self-renewal and suppresses stem cell signaling in MYC driven medulloblastoma', Oncotarget, 5(9), pp. 2355-71.

Verdine, G.L. and Walensky, L.D. (2007) 'The challenge of drugging undruggable targets in cancer: lessons learned from targeting BCL-2 family members', Clin Cancer Res, 13(24), pp. 7264-70.

Verlooy, J., Mosseri, V., Bracard, S., Tubiana, A.L., Kalifa, C., Pichon, F., Frappaz, D., Chastagner, P., Pagnier, A. and Bertozzi, A.I. (2006) 'Treatment of high risk medulloblastomas in children above the age of 3 years: a SFOP study', European journal of cancer, 42(17), pp. 3004-3014.

Vervoorts, J., Lüscher-Firzlaff, J. and Lüscher, B. (2006) 'The ins and outs of MYC regulation by posttranslational mechanisms', Journal of Biological Chemistry, 281(46), pp. 34725-34729.

Vogel, C. and Marcotte, E.M. (2012) 'Insights into the regulation of protein abundance from proteomic and transcriptomic analyses', Nat Rev Genet, 13(4), pp. 227-32.

von Bueren, A.O., Oehler, C., Shalaby, T., von Hoff, K., Pruschy, M., Seifert, B., Gerber, N.U., Warmuth-Metz, M., Stearns, D. and Eberhart, C.G. (2011) 'c-MYC expression sensitizes medulloblastoma cells to radio-and chemotherapy and has no impact on response in medulloblastoma patients', BMC cancer, 11(1), p. 74.

von Bueren, A.O., Shalaby, T., Oehler-Janne, C., Arnold, L., Stearns, D., Eberhart, C.G., Arcaro, A., Pruschy, M. and Grotzer, M.A. (2009) 'RNA interference-mediated c-MYC inhibition prevents cell growth and decreases sensitivity to radio- and chemotherapy in childhood medulloblastoma cells', BMC Cancer, 9, p. 10.

Wadhwa, E. and Nicolaides, T. (2016) 'Bromodomain inhibitor review: Bromodomain and extra-terminal family protein inhibitors as a potential new therapy in central nervous system tumors', Cureus, 8(5).

Waikel, R.L., Kawachi, Y., Waikel, P.A., Wang, X.-J. and Roop, D.R. (2001) 'Deregulated expression of c-Myc depletes epidermal stem cells', Nature genetics, 28(2), pp. 165-168.

Walter, W. and Stein, U. (2000) 'Viral vectors for gene transfer a review of their use in the treatment of human disease', Drugs, 60, pp. 249-71.

Wang, S., Jiang, B., Zhang, T., Liu, L., Wang, Y., Wang, Y., Chen, X., Lin, H., Zhou, L., Xia, Y., Chen, L., Yang, C., Xiong, Y., Ye, D. and Guan, K.-L. (2015) 'Insulin and mTOR Pathway Regulate HDAC3-Mediated Deacetylation and Activation of PGK1', PLoS Biology, 13(9), p. e1002243.

Wang, S.W. and Sun, Y.M. (2014) 'The IL-6/JAK/STAT3 pathway: potential therapeutic strategies in treating colorectal cancer (Review)', Int J Oncol, 44(4), pp. 1032-40.

Wang, X., Cunningham, M., Zhang, X., Tokarz, S., Laraway, B., Troxell, M. and Sears, R.C. (2011) 'Phosphorylation regulates c-Myc's oncogenic activity in the mammary gland', Cancer research, 71(3), pp. 925-936.

Wang, Y.-h., Liu, S., Zhang, G., Zhou, C.-q., Zhu, H.-x., Zhou, X.-b., Quan, L.-p., Bai, J.-f. and Xu, N.-z. (2005) 'Knockdown of c-Myc expression by RNAi inhibits MCF-7 breast tumor cells growth in vitro and in vivo', Breast Cancer Research, 7(2), p. R220.

Wang, Z., Gerstein, M. and Snyder, M. (2009) 'RNA-Seq: a revolutionary tool for transcriptomics', Nature reviews genetics, 10(1), pp. 57-63.

Weinstein, I.B. and Joe, A. (2008) 'Oncogene addiction', Cancer Res, 68(9), pp. 3077-80; discussion 3080.

Wetmore, C., Herington, D., Lin, T., Onar-Thomas, A., Gajjar, A. and Merchant, T.E. (2014) 'Reirradiation of recurrent medulloblastoma: does clinical benefit outweigh risk for toxicity?', Cancer, 120(23), pp. 3731-3737.

Whitehead, K.A., Langer, R. and Anderson, D.G. (2009) 'Knocking down barriers: advances in siRNA delivery', Nature reviews Drug discovery, 8(2), pp. 129-138.

Whitfield, J.R., Beaulieu, M.-E. and Soucek, L. (2017) 'Strategies to inhibit Myc and their clinical applicability', Frontiers in cell and developmental biology, 5, p. 10.

Wiederschain, D., Wee, S., Chen, L., Loo, A., Yang, G., Huang, A., Chen, Y., Caponigro, G., Yao, Y.M., Lengauer, C., Sellers, W.R. and Benson, J.D. (2009) 'Single-vector inducible lentiviral RNAi system for oncology target validation', Cell Cycle, 8(3), pp. 498-504.

Wiegering, A., Uthe, F.W., Jamieson, T., Ruoss, Y., Hüttenrauch, M., Küspert, M., Pfann, C., Nixon, C., Herold, S. and Walz, S. (2015) 'Targeting translation initiation bypasses signaling crosstalk mechanisms that maintain high MYC levels in colorectal cancer', Cancer discovery, 5(7), pp. 768-781.

Wilson, W.R. and Hay, M.P. (2011) 'Targeting hypoxia in cancer therapy', Nat Rev Cancer, 11(6), pp. 393-410.

Wolfer, A., Wittner, B.S., Irimia, D., Flavin, R.J., Lupien, M., Gunawardane, R.N., Meyer, C.A., Lightcap, E.S., Tamayo, P. and Mesirov, J.P. (2010) 'MYC regulation of a “poor-prognosis” metastatic cancer cell state', Proceedings of the National Academy of Sciences, 107(8), pp. 3698-3703.

Xiang, Y., Stine, Z.E., Xia, J., Lu, Y., O'Connor, R.S., Altman, B.J., Hsieh, A.L., Gouw, A.M., Thomas, A.G., Gao, P., Sun, L., Song, L., Yan, B., Slusher, B.S., Zhuo, J., Ooi, L.L., Lee, C.G., Mancuso, A., McCallion, A.S., Le, A., Milone, M.C., Rayport, S., Felsher, D.W. and Dang, C.V. (2015a) 'Targeted inhibition of tumor-specific glutaminase diminishes cell-autonomous tumorigenesis', J Clin Invest, 125(6), pp. 2293-306.

Xiang, Y., Stine, Z.E., Xia, J., Lu, Y., O’Connor, R.S., Altman, B.J., Hsieh, A.L., Gouw, A.M., Thomas, A.G. and Gao, P. (2015b) 'Targeted inhibition of tumor-specific glutaminase diminishes cell-autonomous tumorigenesis', The Journal of clinical investigation, 125(6), p. 2293.

Xiao, D., Yue, M., Su, H., Ren, P., Jiang, J., Li, F., Hu, Y., Du, H., Liu, H. and Qing, G. (2016) 'Polo-like Kinase-1 Regulates Myc Stabilization and Activates a Feedforward Circuit Promoting Tumor Cell Survival', Mol Cell, 64(3), pp. 493-506.

Xie, C.M., Wei, W. and Sun, Y. (2013) 'Role of SKP1-CUL1-F-box-protein (SCF) E3 ubiquitin ligases in skin cancer', J Genet Genomics, 40(3), pp. 97-106.

Xie, J., Wang, X. and Proud, C.G. (2016) 'mTOR inhibitors in cancer therapy', F1000Research, 5.

Yang, D., Liu, H., Goga, A., Kim, S., Yuneva, M. and Bishop, J.M. (2010) 'Therapeutic potential of a synthetic lethal interaction between the MYC proto-oncogene and inhibition of aurora-B kinase', Proceedings of the National Academy of Sciences, 107(31), pp. 13836-13841.

Yang, G., Kramer, M.G., Fernandez-Ruiz, V., Kawa, M.P., Huang, X., Liu, Z., Prieto, J. and Qian, C. (2015) 'Development of endothelial-specific single inducible lentiviral vectors for genetic engineering of endothelial progenitor cells', Scientific reports, 5.

Yao, H. and Rahman, I. (2012) 'Role of histone deacetylase 2 in epigenetics and cellular senescence: implications in lung inflammaging and COPD', Am J Physiol Lung Cell Mol Physiol, 303(7), pp. L557-66.

Yaron, A. and Zheng, B. (2007) 'Navigating their way to the clinic: emerging roles for axon guidance molecules in neurological disorders and injury', Dev Neurobiol, 67(9), pp. 1216-31.

Yin, X., Giap, C., Lazo, J.S. and Prochownik, E.V. (2003) 'Low molecular weight inhibitors of Myc–Max interaction and function', Oncogene, 22(40), pp. 6151-6159.

Yoo, K.H. and Hennighausen, L. (2012) 'EZH2 methyltransferase and H3K27 methylation in breast cancer', Int J Biol Sci, 8(1), pp. 59-65.

Younas, A. (2011) 'Medulloblastoma in a case of migraine-like headache with head tilt: a case report', Grand Rounds, 11.

Yu, D., Cozma, D., Park, A. and Thomas-Tikhonenko, A. (2005) 'Functional validation of genes implicated in lymphomagenesis: an in vivo selection assay using a Myc-induced B-cell tumor', Annals of the New York Academy of Sciences, 1059(1), pp. 145-159.

Yu, L.-J., Wu, M.-L., Li, H., Chen, X.-Y., Wang, Q., Sun, Y., Kong, Q.-Y. and Liu, J. (2008) 'Inhibition of STAT3 Expression and Signaling in Resveratrol-Differentiated Medulloblastoma Cells', Neoplasia (New York, N.Y.), 10(7), pp. 736-744.

Yu, T., Tang, B. and Sun, X. (2017) 'Development of Inhibitors Targeting Hypoxia-Inducible Factor 1 and 2 for Cancer Therapy', Yonsei Med J, 58(3), pp. 489-496.

Zarogoulidis, P., Lampaki, S., Turner, J.F., Huang, H., Kakolyris, S., Syrigos, K. and Zarogoulidis, K. (2014) 'mTOR pathway: A current, up-to-date mini-review (Review)', Oncology Letters, 8(6), pp. 2367-2370.

Zaytseva, Y.Y., Valentino, J.D., Gulhati, P. and Evers, B.M. (2012) 'mTOR inhibitors in cancer therapy', Cancer letters, 319(1), pp. 1-7.

Zhang, G., Ueberheide, B.M., Waldemarson, S., Myung, S., Molloy, K., Eriksson, J., Chait, B.T., Neubert, T.A. and Fenyö, D. (2010) 'Protein Quantitation Using Mass Spectrometry', Methods in molecular biology (Clifton, N.J.), 673, pp. 211-222.

Zhang, L., Huang, G., Li, X., Zhang, Y., Jiang, Y., Shen, J., Liu, J., Wang, Q., Zhu, J., Feng, X., Dong, J. and Qian, C. (2013) 'Hypoxia induces epithelial-mesenchymal transition via activation of SNAI1 by hypoxia-inducible factor -1alpha in hepatocellular carcinoma', BMC Cancer, 13, p. 108.

Zhang, P., Li, H., Wu, M.L., Chen, X.Y., Kong, Q.Y., Wang, X.W., Sun, Y., Wen, S. and Liu, J. (2006) 'c-Myc downregulation: a critical molecular event in resveratrol-induced cell cycle arrest and apoptosis of human medulloblastoma cells', J Neurooncol, 80(2), pp. 123-31.

Zhang, W.C., Shyh-Chang, N., Yang, H., Rai, A., Umashankar, S., Ma, S., Soh, B.S., Sun, L.L., Tai, B.C., Nga, M.E., Bhakoo, K.K., Jayapal, S.R., Nichane, M., Yu, Q., Ahmed, D.A., Tan, C., Sing, W.P., Tam, J., Thirugananam, A., Noghabi, M.S., Pang, Y.H., Ang, H.S., Mitchell, W., Robson, P., Kaldis, P., Soo, R.A., Swarup, S., Lim, E.H. and Lim, B. (2012) 'Glycine decarboxylase activity drives non-small cell lung cancer tumor-initiating cells and tumorigenesis', Cell, 148(1-2), pp. 259-72.

Zinzalla, G. (2016) 'Targeting MYC: is it getting any easier?'. Future Science.
Zirath, H., Frenzel, A., Oliynyk, G., Segerström, L., Westermark, U.K., Larsson, K., Persson, M.M., Hultenby, K., Lehtiö, J. and Einvik, C. (2013) 'MYC inhibition induces metabolic changes leading to accumulation of lipid droplets in tumor cells', Proceedings of the National Academy of Sciences, 110(25), pp. 10258-10263.

Zuber, J., Shi, J., Wang, E., Rappaport, A.R., Herrmann, H., Sison, E.A., Magoon, D., Qi, J., Blatt, K. and Wunderlich, M. (2011) 'RNAi screen identifies Brd4 as a therapeutic target in acute myeloid leukaemia', Nature, 478(7370), pp. 524-528.